HYDRODYNAMICS AND MINERAL BENEFICIATION EFFICIENCY OF IONIC MICROBUBBLE

RAJEEV PARMAR

HYDRODYNAMICS AND MINERAL BENEFICIATION EFFICIENCY OF IONIC MICROBUBBLE

THESIS

Submitted in Partial Fulfillment of the Requirements for the Degree of

Doctor of Philosophy
in
Engineering
by

Rajeev Parmar

Roll No. 11610710

Under the supervision of

Dr. Subrata Kumar Majumder

DEPARTMENT OF CHEMICAL ENGINEERING
INDIAN INSTITUTE OF TECHNOLOGY GUWAHATI
GUWAHATI-781039, INDIA

March, 2016

Dedicated to my family

INDIAN INSTITUTE OF TECHNOLOGY GUWAHATI
GUWAHATI - 781039, ASSAM, INDIA

DEPARTMENT OF CHEMICAL ENGINEERING

CERTIFICATE

This is to certify that the thesis entitled "***Hydrodynamics and Mineral Beneficiation Efficiency of Ionic Microbubble***" submitted by **Rajeev Parmar** in fulfillment of the requirement of the *Degree of Doctor of Philosophy in Engineering*, is a record of bonafide research work carried out by him, in the Department of Chemical Engineering, Indian Institute of Technology, Guwahati, under my guidance and supervision. The work documented in this thesis has not been submitted to any other University or Institute for the award of any degree or diploma. In my opinion, the thesis has reached the standard fulfilling the requirements of the Ph. D. degree as prescribed in the regulations of this institute.

Dr. Subrata Kumar Majumder
Associate Professor
Department of chemical Engineering
Indian institute of Technology Guwahati
Guwahati-781039, India.

ACKNOWLEDGEMENTS

I would like to express my gratitude to all those who helped me in different ways in completing this research work within the time span of four years, directly or indirectly. First and foremost, I would like to express my deep felt gratitude to my supervisor, **Dr. Subrata Kumar Majumder** for providing me continuous inspiration and guidance throughout the entire course of work. In addition, his philosophical guidance has built up a momentum inside me. His uncompromising approach to complete the experimental part, data analysis, writing manuscripts as well as thesis within the stipulated time period helped me a lot in completing my research work. The numerous brain storming sessions during the project meetings with him were very useful in enriching my analytical power. I also remain indebted for his understanding, support and caring during the times when I was really down and depressed due to personal problems. I also thank almighty for making me to feel fortunate to work under his great stewardship.

I wish to acknowledge my respectful thanks to **Dr. V.S. Mohalkar**, former HOD and **Prof. Bishnupada Mandal** present HOD, Department of Chemical Engineering, for extending all the necessary facilities for carrying-out my research work. I am also grateful to all the professors in the department for their sincere cooperation.

I must also thank my doctoral committee members **Dr. Chandan Das, Dr. Rajesh Kumar Upadhyay** of the Department of Chemical Engineering and **Dr. Pankaj Biswas** of the Department of Mechanical Engineering, for their valuable suggestions and contribution towards my research work.

I wish to thank all the non-teaching staff of our department for the help received from them.

I would like to thank my co-researchers and friends Mr. Sivaiah (Late), Mr. Anil Kumar, Mr. Bharath Kumar, Mr. Fahad M.K, Mr. Arindam and Mr. Medithi Vikas for their enormous help and support during research work.

I am thankful to my friends Mr. Biney Deogam, Mr. Devendra Kumar Maravi, Mr. Santhosh Shettihalli, Mr. Sujoy Bose, Mr. Ashish Kumar Thokchom, Mr. Sarede Yadav, Mr. Sankar Chakma, Mr. Jay Bhasarkar and Mr. Abhishek Shukla for their companion in this journey and have also for their indirect help that was rendered in the completion of my work.

I would also like to thank my family who have not only supported me in the completion of my Ph.D. but also have stood by me throughout my life. They have patiently supported me at all instances in my research work.

I am indebted to my wife Seema whose constant encouragement, suggestion, patience and motivation, made me to achieve this endeavor in a peaceful and cheerful manner. She transformed all the odds into reality.

Date:

Place:

Rajeev Parmar

CURRICULUM VITAE

Name **RAJEEV PARMAR**

Date of birth **31-05-1986**

Education Qualifications:

Degree	University/Institute	Year of Passing
Bachelor of Engineering in Chemical Engineering	Ujjain Engineering College, Ujjain	2009
Master of Technology in Petroleum Refinery Engineering	Indian Institute of Technology, Guwahati	2011
Research Scholar in Chemical Engineering	Indian Institute of Technology, Guwahati	Since 2011

Awards Scholarships and Recognitions:

MHRD Govt. of India scholarship for Ph.D from July 2011 to June 2015.

MHRD Govt. of India scholarship for M.Tech. from August 2009 to June 2011.

Awarded second Prize in computer project during the year 2002-2003.

Awarded third prize in relay race during the year 2000-2001.

Qualified Gate-2009 and secured all India rank 438 in Chemical Engineering.

Parmar, R., Majumder, S.K., 2013. Microbubble generation and microbubble-aided transport process intensification-A state-of-the-art report. Chemical Engineering and Processing 64, 79-97, has been included in top 20 most downloaded article of Chemical Engineering and Processing.

A. Research Papers in Journal:

- Parmar, R., Majumder, S.K., 2016. Mineral beneficiation by ionic microbubble in continuous plant prototype: Efficiency and its analysis by kinetic model. Chemical Engineering Science 142, 42-54.
- Parmar, R., Majumder, S.K., 2015. Dispersion characteristics of ionic microbubble suspension in continuous plant prototype developed for mineral beneficiation. Chemical Engineering and Processing 95, 43-53.
- Parmar, R., Majumder, S.K., 2015. Terminal rise velocity, size distribution and stability of microbubble suspension. Asia-Pacific Journal of Chemical Engineering 10, 450-465.
- Parmar, R., Majumder, S.K., 2015. Flotation of fine particles from binary mixture by ionic microbubbles. Chemexpress 8, 133-137.
- Parmar, R., Majumder, S.K., 2015. Lifetime of microbubble an interpretation. Chemexpress 9, 46-54.
- Parmar, R., Majumder, S.K., 2014. Hydrodynamics of microbubble suspension flow in Pipes. Industrial and Engineering Chemistry Research 53, 3689-3701.
- Parmar, R., Majumder, S.K., 2013. Microbubble generation and microbubble-aided transport process intensification-A state-of-the-art report. Chemical Engineering and Processing 64, 79-97.
- Parmar, R., Majumder, S.K., 2013. A stochastic analysis of liquid mixing in bubble column. American Journal of Fluid Dynamics 3, 75-79.

B. Book Chapter:

- Parmar, R., Majumder, S.K., 2013. Chapter-9 Flow behaviour of microbubble-liquid mixture in pipe, in: Sonawane, S., Setty, Y.P., Sapavatu, S.N. (Eds.), Chemical and Bioprocess Engineering: Trends and Developments, Apple Academic Press, Taylor and Francis Group, USA, 91-100.

C. Research Papers in Conferences:

- Parmar, R. Majumder, S.K. Aluminium oxide recovery by using microbubble flotation, International Conference on New Frontiers in Chemical, Energy and Environmental Engineering (INCEEE), National Institute of Technology, Warangal-506 004, Telangana, India,. 20-21 March, 2015.
- Parmar, R., Majumder, S.K. Flow behaviour of microbubble-liquid mixture in pipe. International conference on Chemical and bioprocess Engineering, NIT Warangal, Telangana, India, 16-17 November, 2014.
- Parmar, R., Majumder, S.K. Recovery of fine particle by using ionic microbubble flotation. National symposium-cum-workshop on NER coals and minerals: Issues, challenges and opportunities, CSIR-North East Institute of Science and Technology, Jorhat, Assam, India, 30-31 October, 2014.
- Parmar, R., Sivaiah, M., Majumder, S.K. Energy efficiency of gas-liquid-solid mixing in a plunging liquid jet slurry bubble column. International Conference on Power and Energy, North Eastern Regional Institute of Science and Technology, Nirjuli, Arunachal Pradesh, India, 28-29 December, 2012.

ABSTRACT

Microbubble aided flotation has been widely employed in the various fields for the process intensification. They have been used for recovery of proteins, recovery of microorganism, removal of heavy metal ions from water, removal of dye and pigment. So an interest was felt to study the stability, rheology, dispersion characteristics of microbubble suspension in order to use them for the mineral beneficiation.

Based on the present status of research, this work was undertaken with the following objectives:

- ✓ Study the hydrodynamics such as rheology, pressure drop and friction factor of microbubble-suspension flow. Development of mechanistic model to analyze the interfacial stress of microbubble suspension flow considering the bubble formation, drag at interface and loss of energy due to wettability.
- ✓ Study the terminal rise velocity, microbubble size distribution and stability of microbubble. Development of correlations to interpret the bubble size and stability of microbubble.
- ✓ Investigation of the dispersion characteristic of ionic microbubble suspension in continuous plant prototype. Development of phenomenological model with consideration of liquid circulation to analyze the dispersion coefficient of the microbubble suspension.
- ✓ Study the mineral beneficiation by ionic microbubble in continuous plant prototype. Development of phenomenological kinetic model based on mixing, collision, attachment and detachment mechanisms of fine particles.

In the present study, experiments have been conducted to study the hydrodynamics and mineral beneficiation efficiency of microbubble suspension flow. The first attempt was made to explore the stability characteristics of microbubble. The stability of microbubble suspension was analyzed by drainage curve method and by electrical conductance method. The stability of microbubble dispersion can be evaluated in terms of its half-life, which is the time taken to drain half of initial liquid volume. Freshly prepared microbubbles were transferred to the measuring cylinder (0.03 m i.d.) and the volume of the drained liquid below the dispersion was measured at various times. Experimental results revealed that the stability of the microbubble can be significantly enhanced by increasing surfactant concentration. The half-life of SDS microbubbles increased from 72 s to 444 s as the SDS concentration increased from 5 ppm to 3000 ppm. For CTAB, the half-life of microbubbles increased from 101 s to 475 s as the CTAB concentration increased from 5 ppm to 500 ppm. In case of Tween-20, the half-life of microbubbles increased from 71 s to 364 s as the Tween concentration increased from 5 ppm to 100 ppm. From drainage curve analysis, it was observed that the liquid drainage curves of the microbubble dispersions followed the same trend for all kind of surfactants. Microbubble drainage process found to occur in three distinct phases.

Extensive experimental studies have been carried out to investigate the effect of physicochemical properties of phases on the size distribution and motion of rising microbubble. Liquid containing dispersed microbubbles was delivered from the microbubble generator in a short span of time to a transparent graduated glass cylinder (0.03 m i.d.). Immediately, the cloud of microbubbles in the suspension starts rising due to buoyancy, leaving a clear liquid interface. The terminal rise velocity of microbubble was determined by the rising trajectories of microbubble. The motion of rising microbubble was found to be significantly affected by physicochemical properties of liquid and gas phase. In the present study three methods were used to calculate the

size of microbubble. At low viscosity, the microbubble size was found to be dependent on surface tension of liquid. The microbubble size decreased from 52 μm to 25 μm as the surface tension deceased from 72 mN/m to 57 mN/m. The bubble size distribution of microbubble suspension for different concentrations was best fitted to Weibull distribution.

Next an attempt has been made to predict the gas holdup and rheological characteristics of microbubble in pipe. The gas holdup of system estimated by the electrical conductance method. The rheological characteristic of microbubble suspension flow was determined by the pressures drop across the pipe. The results reveals that the microbubble suspensions behave as a shear-thinning non-Newtonian liquid. An increase in surfactant concentration caused a decrease in shear stress and effective viscosity with shear rate. The drag coefficient and friction factor found to be decreased inversely with the Reynolds number. The results suggested that the presence of microbubbles can significantly reduce the frictional resistance. A mechanistic model has been developed to analyze the interfacial stress of microbubble suspension flow in a pipe by considering bubble formation, drag at the interface and loss of energy due to wettability. A correlation between the intensity factor of interfacial stress and the friction factor based on energy loss due to wettability has been developed. The functional form of the correlation appears to predict the hydrodynamics satisfactorily for the flow of a microbubble suspension in a pipe.

Extensive experimental studies have been carried out to measure the dispersion characteristics of microbubble suspension in continuous plant prototype developed for mineral beneficiation. The effects of different operating variables and physiochemical properties of liquid on the dispersion of microbubble suspension were also examined. It was observed that the dispersion coefficient increased with increase in surfactant concentrations. The value of dispersion coefficient increased from 10.9×10^{-2} m^2/s to 12.41×10^{-2} m^2/s as the SDS concentration increase from 0 ppm to 15

ppm at fixed circulation velocity. For CTAB, value of dispersion coefficient increased from 11.10× 10^{-2} m^2/s to 12.10 × 10^{-2} m^2/s as the CTAB concentration increase from 34 ppm to 100 ppm. In case of Tween 20 dispersion coefficient increased from 11.3 × 10^{-2} m^2/s to 12.21 × 10^{-2} m^2/s as the Tween concentration increase from 0 ppm to 15 ppm at fixed circulation velocity. The value of dispersion coefficient decreased with increasing SCMC concentration. The effect of physicochemical properties of liquid on dispersion coefficient due to liquid circulation was also analyzed. A phenomenological model with consideration of liquid circulation was developed to analyze the dispersion coefficient of the microbubble suspension due to circulation. Generalized correlations for dispersion coefficient and the time to reach uniform dispersion were also developed based on the physicochemical properties of microbubble suspension.

Next an attempt has been made to investigate the mineral beneficiation by ionic microbubble in continuous plant prototype. The present study showed that fine particles can be significantly recovered by using microbubbles. The results revealed that the charge on the surface of microbubble is highly promising in separating opposite charged particles. The recovery of mineral particle was found to be dependent on surfactant concentration, size of microbubble and particles, zeta potential of microbubble, nature of surface potential of bubble and microbubble-particle mixture circulation velocity. It was also observed that the separation efficiency of microbubble increased with increase in mixture circulation velocity. The addition of surfactant in the mixture intensified the recovery efficiency. The recovery of ZnO and Al_2O_3 particles was maximum with CTAB. A maximum recovery of approximately 84 % and 72 % was obtained for ZnO and Al_2O_3 particle respectively by using CTAB. In case of CuO particles, the SDS and Tween-20 were found to be more effective than CTAB. For CuO particles, maximum recovery of approximately 78 % was obtained by using SDS. A flotation model that includes the contributions from the efficiencies

of collision, attachment and stability between particles and microbubbles was used to calculate the flotation rate constants. It was observed that rate constant is significantly influenced by the physicochemical properties of the liquid and particles. The flotation rate constant was also analyzed based on the mixing phenomena in the column.

CONTENTS

Page No.

Page No.

LIST OF FIGURES

LIST OF TABLES

CHAPTER-1

BACKGROUND AND FORMULATION OF WORK

This chapter presents a summary of the properties and the components of the microbubble. The application of microbubbles in different fields of engineering are enunciated. Various types of microbubble generators and their operating principles have been explained. The various aspects that affects the microbubble flotation are also discussed. The scope and significance of research in this field are explained. The research formulation based on the scope is highlighted.

1.1 Background of the Study

Over the last few decades, technology is changing day by day. Technologies are getting much deeper and smaller, thereby enhancing the efficiency and capacity. In every field, research has gone to higher level by exploring new areas. In chemical engineering, bubbles play an important role in various unit operations. In recent studies, it has been reported that smaller bubbles give rise to larger interfacial area, which motivates the introduction of processes aided with microbubbles (Tsuge, 2014). In the present scenario microbubbles has got much popularity as it is being used in many chemical, biochemical, metallurgical and petrochemical industries to increase the efficiency of the process (Devatine et al., 2007; Koichi and Yasuyuki, 2007; Weber and Agblevor, 2005; Xiaohui et al., 2011). The important characteristics, properties and applications of microbubbles are described in the following sections.

1.1.1 Characteristics of Microbubbles

1.1.1.1 Definition

In the field of fluid physics, bubble having diameter of hundred micrometer or less is considered as microbubble whereas in the studies of physiological activity, bubble of diameter 10-40 µm is considered as microbubble (Tsuge, 2010). Li et al. (2009) defined microbubble as a bubble of diameter several tens of micrometers and has many characteristics different from common millibubble of diameter of the order of millimeter. Ishii et al. (2005) defined microbubble as a bubble having diameter ranging from several tens of micrometer to several hundreds of nanometer. Some researchers defined microbubble as tiny bubble, whose diameter is less than several hundred micrometers (Kawahara et al., 2009). It is seen that researchers have not yet reached conformity on the definition of microbubble. However, in general a bubble can be considered as microbubble if its size range 1-100 µm (Kurup and Naik, 2010). In the present work, bubbles having the diameter in the range of 1-100 µm are considered as microbubbles.

1.1.1.2 Components of Microbubble

Microbubbles have three main components such as gas phase, shell material enclosing the gas phase and liquid as shown in Figure 1.1 (Khuntia et al., 2012; Sirsi, and Borden, 2009).

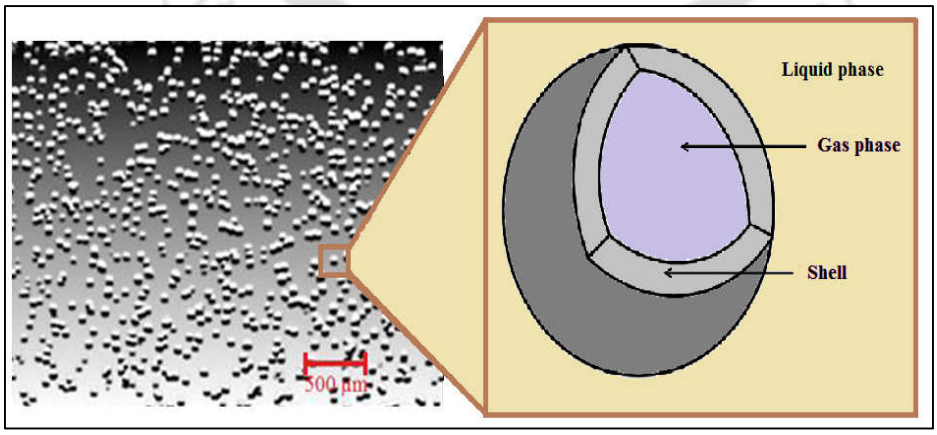

Figure 1.1: Components of a microbubble.

The gas phase comprises of a single gas or combination of gases. The combination of gases are generally used for two particular reasons, first is to create differentials in partial pressure and second is to generate gas osmotic pressures which stabilize the bubbles. In case of combinations of gases one gas is called primary or first gas and the other one is known as gas osmotic agent. Gas which is less permeable through the bubble surface than the modifier is preferred as gas osmotic agent (Ernest et al., 2005). The gas osmotic agent is either a gas at room temperature or liquid so long as it has a sufficient partial pressure or vapor pressure at the temperature of use to provide the desired osmotic effect (Kurup and Naik, 2010). Air and nitrogen are examples of primary gas. Sulphur hexafluoride is an example of osmotic gas agent. The gas phase is enclosed by shell material. Diffusion of gas from microbubble and the mechanical properties of microbubble depend on the shell material (Azmin et al., 2012). The shell plays a vital role in encapsulation of molecules. If the elasticity of shell material is more, the acoustic energy it can withstand before bursting or breakup is high, which increases the residence time of the bubble (Prajapati and Agrawal, 2012). The external liquid surrounding the shell in which the bubble resides can be same as of shell material, or it can be surfactant or foaming agent depending upon the operations.

1.1.2 Properties of Microbubble

The properties of microbubbles can significantly affect the transport process. The physicochemical properties of microbubbles are of interest in ionic microbubble flotation as these properties have been shown to affect the mechanism of attachment of bubbles to surfaces (Liu et al., 2010; Yi-jun et al., 2009). The internal pressure of bubble depends on surface tension and diameter of bubble. The internal pressure of bubble increases on decreasing the bubble diameter. Decreasing the bubble diameter increases the partial pressure of the dissolving gas which increases the gas dissolution (Agarwal et al., 2011). The Young-Laplace equation relates the difference in pressure

between inside and outside surrounding liquid (ΔP) with bubble diameter (d_{mb}) and surface tension (σ) as:

$$\Delta P = \frac{4\sigma}{d_{mb}} \tag{1.1}$$

The ratio of area to volume of a sphere is inversely proportional to its diameter. Microbubbles due to its small diameter hold high interfacial area. Microbubbles have high gas dissolution rate. When the bubble reaches to its size micro to nano, the rate of its dissolution increases because the surface area and internal pressure of bubble increase and rising velocity decreases (Tsuge, 2010). Due to this high pressure inside the bubble, gas inside the microbubbles tends to diffuse outside from a region of high pressure to a low pressure of surrounding. As a consequence of this, the microbubbles shrink and finally collapse. This causes high mass transfer rate of gas microbubble to the surrounding liquid (Ohnari, 2007). Microbubbles behave almost like spherical bubbles and sometime like solid spheres where the flow at the gas liquid boundary is free. Recently most of the studies have shown that the rise velocity of microbubble (U_b) follows the Stokes' law (Haapala et al., 2010; Kelsall et al., 1996; Parkinson and Ralston, 2010; Takahashi, 2005; Stokes, 1851).

$$U_b = \frac{\rho_l g d_{mb}^{\ 2}}{18\mu_l} \tag{1.2}$$

Reynolds number based on the terminal rise velocity of microbubbles is very less (approximately $Re \leq 1$), due to its small size. The microbubble can reduce the fluid resistance on the wall of the channel by reducing the friction coefficient (Kodama, 2007; Serizawa et al., 2005). The coefficient of friction decreases with increasing in volume fraction of microbubbles. The physical properties of water are altered by bubbling microbubbles in water. The electrical conductivity, viscosity and surface tension of liquid changes on bubbling with microbubbles. The breakdown of hydrogen

bonds between water molecules and ionization of compounds present in the water are the main factors causing these changes (Himuro, 2007).

1.1.3 Zeta potential

The liquid layer surrounding the microbubble exists as two parts as shown in Figure 1.2: (i) an inner region (stern layer) where ions are strongly bound and (ii) an outer (diffuse) region where they are weakly associated (Hunter, 1989). There is a notational boundary inside which the ions and particles form a stable entity inside the diffuse layer. When the particle moves (e.g. due to gravity), ions within the boundary move it. Those ions beyond this boundary reside with the bulk dispersant (Lyklema, 2000). The electrical potential of the slipping plane (as shown in Figure 1.2) is the zeta potential and the amount of ions and their valence in the plane determine the value of zeta potential (Hasegawa et al., 2008). The most widely used technique for measuring zeta potentials is electrophoresis. Electrophoresis is the motion of dispersed particles relative to a fluid under the influence of a spatially uniform electric field (Okada and Akagn, 1987). This electrokinetic phenomenon was observed for the first time in 1807 by Ferdinand Frederic Reuss (Moscow State University), who noticed that the application of a constant electric field caused clay particles dispersed in water to migrate (Dukhin and Derjaguin, 1974; Hunter, 1989; Lyklema, 2000). In order to obtain the zeta potential an electric field is applied across a sample, which induces charged particles to move. The direction and velocity (electrophoretic mobility) of the particles depends on the applied field (Wierserna et al., 1966). The velocity of a particle in an electric field is dependent on: the strength of the electric field; the dielectric constant of the liquid the viscosity of the liquid; the zeta potential (Oliveira and Rubio, 2011). Particles in suspension having a large negative potential tend to repel each other. But if the particles have low zeta potential, then there will be no forces to avoid the particle to come closer (Lyklema, 2000). The

zeta potential of bubbles is an important property which determines the interactions of bubbles with other materials such as oil droplets, solid particles, etc.

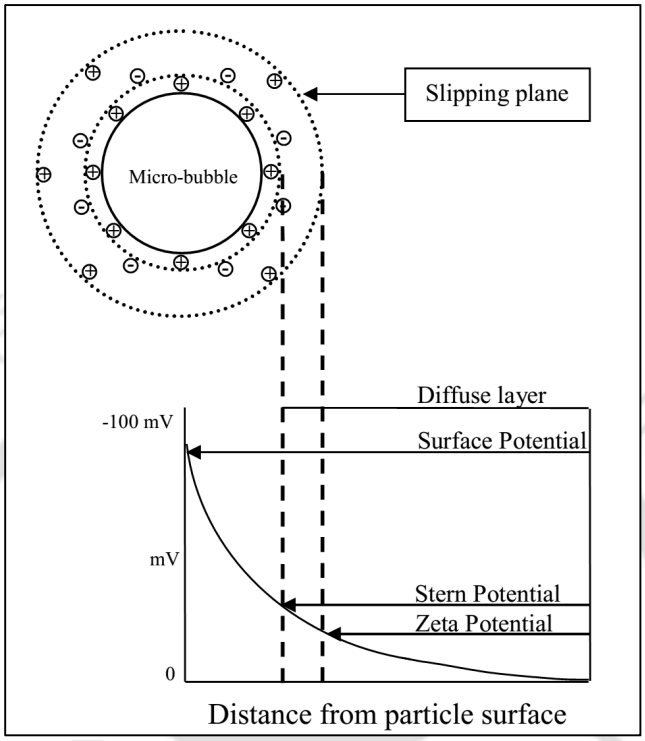

Figure 1.2: Schematic representation of zeta potential (Lyklema, 2000).

The zeta potential is determined by the Smoluchowski equation (Eq. (1.3)) (Takahashi, 2005)

$$\zeta = \mu m'/\in \qquad (1.3)$$

where ζ is the zeta potential (V), m' is the mobility (m^2/sV) and ϵ is permittivity of liquid ($s^2C^2/kg^1.m^3$).

The important characteristics of zeta potential of microbubble are as follows:

(i) The addition of the electrolytes such as NaCl and $MgCl_2$ cause a reduction in the magnitude of negative zeta potential value to less negative value (Lyklema, 2000).

(ii) The zeta potential of microbubble in a solution is affected by the addition of alcohol (Methanol, 2-propanol and butanol) in the solution. The negative zeta potential value

reduces to less negative as the concentration of alcohol in the liquid increases (Lyklema, 2000).

(iii) There is no change of zeta potential with bubble diameter (Hasegawa et al., 2008).

(iv) The zeta potential of microbubble in water is negative (Oliveira and Rubio, 2011).

(v) The zeta potential of microbubble is affected by pH. The negative value decreases as the pH increases from 2 to 7. The highest negative value is about - 25 mV near pH = 7. (Han and Dockko, 1998).

1.1.4 Rheological behaviour

Rheological properties of microbubble reflect the creation and stability of microbubble suspensions. These properties may be very different from those of their constituent fluids. Microbubbles suspension shows non-Newtonian behavior (Shams et al., 2014). The viscosity of microbubbles generally decreases with increase in shear stress (Shen et al., 2008). For non-Newtonian fluid, the most common model which relates the wall shear stress (τ_w), wall shear rate (γ_w) and apparent shear rate (γ_a) is power law model which is described as:

$$\tau_w = \mu_e \gamma_a = K \gamma_w^n \tag{1.4}$$

The apparent shear rate and wall shear rate are related as:

$$\gamma_w = \left(\frac{3n+1}{4n} \right) \gamma_a \tag{1.5}$$

The wall shear stress (τ_w) and apparent shear rate (γ_a) are experimentally determined from volumetric flow rate (Q) and pressure drop (ΔP) according to the relations (Enzendorfer et al., 1995)

$$\tau_w = \frac{D_h \Delta P}{4Z} \tag{1.6}$$

$$\gamma_a = \frac{32Q}{\pi D_h^3} \tag{1.7}$$

1.2 Applications of Microbubbles

Over the last few decades, microbubbles have drawn great attention due to their wide applications in many fields of science and technology. Microbubble finds application in both engineering and medical fields. Some of their important applications are:

1.2.1 Mass Transfer Enhancement

Microbubbles offers high surface area per unit volume than the conventional bubbles which helps to intensify the mass transfer processes at low cost. The application of the microbubble in aerobic fermentation was investigated by Kaster et al. (1990). They reported that the large specific interfacial area provided by the microbubbles has resulted in 30% high mass transfer rate. Bredwell and Worden (1998) also investigated the mass transfer characteristic of microbubbles. They reported that mass transfer characteristic of microbubbles is 6 fold higher than conventional bubbles. Ago et al. (2005) measured the volumetric mass transfer coefficient for carbon dioxide microbubbles. They observed an increase in the volumetric mass transfer coefficient by several times compared with the conventional bubbling technique. A similar kind of observation was reported by Nakano et al. (2005), who compared the volumetric mass transfer coefficients of oxygen in water by the microbubble and air-stone dissolution method. Chu et al. (2007) studied ozonation of synthetic waste water containing azo dye ($C_6H_{21}N_5O_{19}S_64Na$) by using microbubble and conventional bubble. The authors observed from their experimental results that the total mass transfer coefficient is 1.8 times higher and pseudo-first order rate constant is 3.2-3.6 times higher

in microbubble system as compared to conventional bubble. The microbubbling technique is now the accepted practice in wine manufacturing (Devatine et al., 2007). Microbubble ozonation has widely used in water treatment process. It utilizes ozone characteristic as a strong oxidant. Chu et al. (2008) reported that the COD removal efficiency of ozone microbubble is 20% higher than the conventional bubble.

The mass transfer coefficient for ozonation with microbubbles is 2.45 times higher than that of conventional bubbles (Karamah et al., 2010). Ozone microbubbles provides an alternate way for disinfection against fungi and bacteria (Kobayashi et al., 2011). Kobayashi et al. (2009) have also investigated the ability of CO_2 microbubbles to inactivate Escherichia coli suspended in a saline solution. A significant reduction in the bacterial population occurred with microbubble-aided CO_2 treatment. Microbubble have also used for degradation of methyl orange using short-wavelength ultraviolet light beam with oxygen microbubbles. It was reported that the decolourization reaction constant in microbubble system is 2.1 times higher than conventional bubbles system (Tasaki et al., 2009). The high mass transfer coefficients in liquid–liquid micro dispersion systems, due to their very high interfacial areas and very short mass transfer diffusion distances make them ideal for the development of an efficient extraction process. Tan et al. (2011) studied the hydrogen peroxide extraction process by using microbubbles. The author reported that Murphee efficiency can be reached higher than 90% using microbubble agitated extraction. Bang et al. (2011) studied the precipitation of calcium carbonate by carbon dioxide microbubbles. They observed that higher conversion efficiency of carbon dioxide to carbonate minerals was achieved with microbubble system. Al-Mashhadani et al. (2012) also reported that the absorption efficiency of CO_2 microbubbles is 29% higher that fine bubbles. Recently Ying et al. (2013) reported that microbubble can improve the mass transfer coefficient by more than 30% compared to fine-bubble.

1.2.2 Water Purification

In the recent years, more and more attention has been given to the potential applications of the microbubbles for water treatment due to their ability to generate highly reactive free radicals without the use of any toxic chemical. Subramaniam et al. (1990) were one of the first to use microbubbles for clarifying industrial effluents. They applied microbubbles to clarify palm oil mill effluent, suspensions of microalgae and suspensions of three inorganic minerals. Microbubbles have been proven to be a new environmental friendly technique for oxidation of organic compounds, water disinfection and fouling control. Microbubbles have also employed to remove the impurities like methyl orange and methylene blue dye from water (Basu and Malpani, 2001). Hashim and Gupta (1998) used microbubble separate fine fibers from a lean slurry of cellulosic pulp. Evidence shows that nitrogen microbubble can be applied for water and wastewater treatment, fermentation, brewing as well for human waste treatment. Michelsen et al. (1988) have developed a microbubble-based biodegradation system for treating hazardous wastes. The microbubbles were stabilized by surfactants. They reported that microbubble dispersion proved to be superior to the sparged air-water injections. Approximately 25% of oxygen present in the microbubbles increased dissolved oxygen, as anaerobic groundwater flowed through the treatment zone.

Microbubble have been found to catalyze chemical reactions, and enhance the detoxification efficiency, thereby improving the efficiency of chemical treatment of water. (Agarwal et al., 2011; Yamasaki et al., 2009). Microbubble have also been used for degradation of various organic compounds, such as alachlor, p-nitrophenol, rhodamine B and decolorization of dye effluent stream (Agarwal et al., 2011). Generation of highly reactive free radicals associated with the collapsing microbubble provides great potential for water disinfection. Lab-scale study suggests

that the cost of hydrodynamic cavitation for water disinfection giver better results than conventional chlorination and ozonation (Jyoti and Pandit, 2001). It is also observed from the literature that the total organic content reduction by ozone microbubble under strong acidic conditions was much higher than other conventional methods. Wastewaters released from the textile and dye manufacturing industries are heavily colored, a major part of which is non-biodegradable in nature. Ozonation has been used by various researchers for the removal of color (Khuntia et al., 2012; Shu and Huang, 1995; Wang et al., 2003). Ozonation of a mixture of benzene, toluene, ethylbenzene and xylenes with microbubble also provides better results (Walker et al., 2001). The effectiveness of air microbubbles in applications such as decolorization can be enhanced by the use of ultraviolet irradiation. The degradation of methyl orange using short-wavelength ultraviolet light beam with oxygen microbubbles has provided a new alternative for water treatment (Tasaki et al., 2009). Shibata et al. (2011) also employed ultraviolet light with oxygen microbubble to decolorization of methylene blue solution. Microbubble also helped to enhance the removal of soluble organics from simulated seawater.

1.2.3 Drag Reduction

Microbubble injection into the boundary layer on a solid surface is one of the most promising methods for the reduction of skin friction. Madavan et al. (1985) was the first to report that microbubble can be used for reduction of friction during fluid flow. Fontaine and Deutsch (1992) studied the influence of the type of gas on the reduction of skin friction drag by microbubble injection. They selected 5 different gases which covers a wide range of density and solubility (air, argon, carbon dioxide, helium and sulfa-hexafluoride). A maximum drag reduction of 25%- 30% was reported by them. The authors observed similar reduction of skin friction for all the gases.

Later on Kato et al. (1999) examined the effect of microbubbles on the structure of turbulence in a turbulent boundary layer. The authors reported that injecting microbubbles is an effective way of reducing the friction resistance. They also reported that with increasing the void fraction, the turbulence intensity in the buffer layer first increased, then reached to a peak and then decreased. Ships play a major role in marine transportation. They are very large and move very slowly. They are especially suited to microbubbles. Kodama et al. (2000) performed their experiment to study the applicability of microbubbles to reduce skin friction in ships and observed that skin friction can be reduced up to 40% with microbubbles. Yasuhiro and Kato (2002) examined the effect of microbubble diameter and size distribution on frictional resistance reduction. They reported that the frictional resistance reduction increased with increasing mean void ratio and microbubble diameter does not affect the frictional resistance reduction. Wu et al. (2008) studied the microbubble drag reduction in a channel flow by using the Taguchi method. The authors tried to search out optimum parametric levels for stout design of microbubble drag reduction in a turbulent channel flow. Air injection, air jet area and microbubble size were the three controllable factors analyzed in their study. Based on their analysis model the drag reduction by microbubble can be obtained up to 21.6%. Tsai et al. (2011) derived boundary mixture model to visualize the performance of microbubble drag reduction technique for a flat plate having porous material microbubble system. The maximum drag reduction effect of microbubble in water tunnel and towing tank were 80% and 30% respectively. They conducted test in water tunnel and towing tank.

1.2.4 Oil Separation

Produced water generated at the oil exploration sites contains a large amount of oil. The oil components may be either dissolved in the water or present as a dispersed phase. The oil may have

aliphatic, aromatic, phenolic and fatty acid component. Microbubble flotation is used to separate oil from water. In the microbubble-aided flotation of oil from wastewater, the oil droplets adhere to the surface of the bubbles, rise upward and collect at the surface of water. A frothy layer of oil is formed on the surface of microbubbles, which is skimmed off. Smaller microbubbles have high effectivity in separating oil from water, which results in a drier froth and a very low skim volume (Khuntia et al., 2012). Leung (1988) developed a technique for the use of microbubbles in the conventional hot water process in the primary flotation to recover bitumen. In his process, stream of microbubbles was injected into the aqueous slurry formed in the hot water process. This injection was followed after the conditioning step and prior to the introduction of the slurry into the flotation/settling step. Thoma et al. (1999) have used microbubbles within the size range 60-100 μm to treat simulated produced waters that contained paraffins (e.g., octane and decane) and aromatic compounds (i.e., benzene, toluene and ethylbenzene). Microbubble are also effective in removing various volatile and semi-volatile materials dissolved in wastewater (Valsaraj et al. 1991). Microbubbles has also been employed for separating oil from synthetic oily wastewater, which was produced by emulsifying low concentrations of oil in water with a nonionic surfactant. Gotoh et al. (2006) have examined the removal of oil from oil-polluted soil by air microbubbles. They reported that the separation of oil from high-concentration oil-in-water emulsion was significantly enhanced by microbubble injection and approximately 70-80 % of the oil can be removad microbubbles flotation. Deng et al. (2011) developed a T-tube dynamic state flotation device. They have reported that their device can reduce oil concentration from 38 to 12 g.m ^{3}. Xiaohui et al. (2011) also developed a new oil removal technique by microbubble floatation for water treatment on offshore oil platform. The author reported that the more than 50% of oil content can be reduced by method.

1.2.5 Fine Particle Separation

A large amount of valuable minerals are thrown away today as fines and ultrafines because of inadequate technology to process them economically. Treatment of fine particles is a challenging problem in the raw material processing units. Its solution is required in both production and effluent treatment unit (Rousseau, 1987). Flotation is the most significant beneficiation method in this regard. However, going to finer size ranges, flotation faces problems, because the bubble–particle collision probability decreases with decreasing particle size (Weber and Paddock, 1983). In the present scenario, significant interest is uprising in developing new methods and in improving old ones for the recovery of fines. Microbubble flotation is the latest technique of separating fine suspended particles. This method utilizes ionic or charged microbubbles for separating opposite charge particles. During the flotation, as the particles come nearer to the ionic microbubbles, it collides with the bubble. After colliding with microbubble, the particle attaches the bubble surface due to electrostatic interaction and forms a stable particle–bubble aggregate, which can be separated by a skimming device. The schematic representation of the interaction is shown in Figure 1.3.

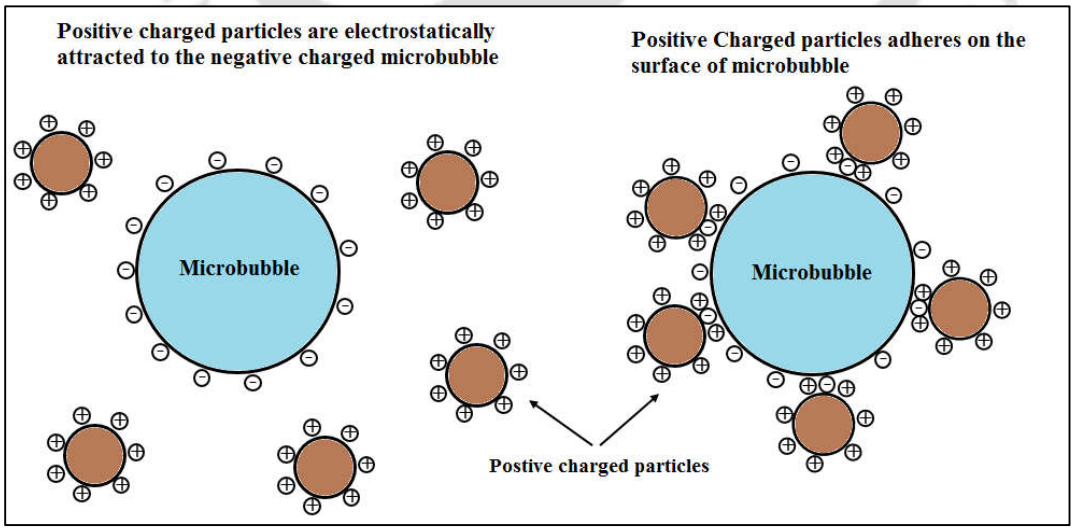

Figure 1.3: Schematic representation of interaction between microbubble and particles.

Microbubble flotation is advantageous over the other conventional method as it does not prone to electrode corrosion, scaling and production of objectionable gases, which may arise in case of electroflotation. It is also effective in separation of ultrafines particles which cannot be separated by precipitate flotation and conventional ionic flotation (Matis and Mavros, 1991; Rahman et al., 2014). The separation efficiency of ionic microbubble flotation is also be considered to higher than the dissolved air and induced air flotation due to an additional electrostatic force between the microbubble and the particle (Rahman et al., 2014). Caballero et al. (1989) were the first to using microbubbles in mineral processing and particle separation. They applied microbubbles in coflotation and solvent sublation processes. In their coflotation of Cu with $Fe(OH)_3$ and HTAB, up to 95% of the separation recovery was achieved in less than 1 min.

The separation and pre-concentration of heavy metals using microbubbles in connection with co-flotation processes were carried out by Cabezón et al. (1994). They reported over 90% recovery for the elements (Cu, Co, Cd, and Ni). Cilliers and Bradshaw (1996) carried comparative experiments of conventional batch flotation and microbubble flotation. Their results indicated that microbubble flotation system may be applied for the selective recovery of finely ground minerals, which was then investigated by Waters et al. (2008). Waters et al. (2008) separated fine particles of copper oxide from silica using microbubble. Koichi and Yasuyuki (2007) used microbubble floatation column to separate fine carbon particle. The authors observed that anionic surfactant can entrap carbon particle most efficiently. Yi-jun et al. (2009) also reported that microbubble flotation is highly efficient for separation of fine nickel and copper ores than the conventional floatation.

1.3 Different Aspects of Microbubble Flotation for Fine Separation

Microbubble flotation is a three-phase separation process for fine particle based on the difference in hydrophobicity and surface charge of the solids and microbubbles. For a better understanding of microbubble flotation, many aspects of microbubble flotation have to be considered. The most important aspects can be grouped as follows (Nguyen, 2007)

(i) ***Engineering aspects***: The major engineering aspects are microbubble generation, particle and bubble dispersion, and design of unit.

(ii) ***Physical aspects***: The important physical aspects that can significantly affect the ionic microbubble flotation are microbubble properties, particle hydrophobicity and floatability, hydrodynamics of microbubble flow, bubble–particle interactions, microbubble stability and flotation kinetics.

(iii) ***Chemical aspects***: The chemical aspects that affects the microbubble flotation are surface chemistry of microbubble and mineral particles, chemistry of flotation reagents, mineral–reagent interactions and ionic strength of microbubble.

1.3.1 Engineering Aspects

1.3.1.1 Dispersion Characteristics of Microbubble

For flotation operating between the plug-flow and perfect mixing regimes, the recovery depends on the particle and microbubble dispersion in the cell. For efficient capture to occur between a microbubble and a particle they must undergo a sufficient closed encounter. The encounter process is mainly governed by the hydrodynamics and mixing characteristics. Mixing of the phases affects both the particle-bubble collision and detachment and hence affects the overall performance of the flotation process (Schubert, 2008).

1.3.1.2 Design of Unit

The modeling and design of a three-phase reactor requires the knowledge of several hydrodynamic (e.g., flow regime, pressure drop, holdups of various phases, etc.) and transport (e.g., degree of backmixing in each phase, gas-liquid, liquid solid mass transfer, fluid-reactor wall heat transfer, etc.) parameters (Shah, 1979). During the past decade, extensive research efforts have been made in order to improve our knowledge in these areas (Shah et al., 1982). Advancement on flotation technology has come about through the application of new theories (i.e. adsorption mechanism, electrochemical control) novel flotation reagents, various alternative flotation technique and so on. In the last decay new horizons have been opened for this process in chemical technology, particularly in its use as a selective separation technique. The design of a flotation column where separation would be carried out on a commercial scale would depend on multiple aspects of chemical engineering (Mathis, 1995). The design and efficient operation of ionic flotation column also require knowledge of what is happening inside the column: how much time is allowed for the particles to mix with the microbubble? Are there any dead spaces, where mixture gets trapped, or any bypassing, with either air or pulp leaving the column too soon? All these are cases of malfunctioning results non-ideal flow and lead to poor performance of the unit (Matis and Mavros, 1991).

1.3.1.3 Microbubble Generation

Microbubbles can be generated by number of ways. Researchers had made several efforts to develop a generator which can produce microbubbles with a minimal power requirement. A brief description of different microbubble generation methods are as follows:

1.3.1.3.1 Methods based on the Mechanics of Flowing Fluid

The mechanics of flowing liquid is used to create the microbubbles. Some of the important methods for microbubble generation under this category have been described in the following section:

(i) ***Spherical body in a flowing tube***: Microbubbles can be generated by introducing pressurized water in a pipe having spherical body in the core region. The spherical body increases the velocity of liquid in the pipe, due to which pressure reduces and creates automatic suction of gas in liquid, results in generation of microbubbles of approximately 50 µm (Sadatomi, 2003).

(ii) ***Rotary liquid flow type***: In this method, pressurized water is pumped to create a rotary type of flow of liquid which sequentially causes a reduction in pressure in its central axial part. Gas is automatically induced to the reduced pressure area. The air-liquid mixture then develops microbubbles of approximately 63 µm, due to high smashed and shears (Koichi and Yasuyuki, 2007). Ohnari (2006) developed a cylindrical microbubble generator by this principle. The liquid flow rate can be up to 12 litres per hour and the rotary speed of the gas-liquid mixture can have 300-600 revolution per sec. The 63.

(iii) ***Static mixture type***: The smashing of flow in a static mixture with a swirl pattern can produce fine bubbles. The gas-liquid flow is channelized into a swirl pattern by guided vanes. The smashing of flow is done by two mushroom shaped projections. This type of microbubble generator generates microbubbles having size ranges from 5 to 50 µm at maximum rate of 1500 l/min (Uematsu, 2006).

(iv) ***Venturi type***: In this method, gas and liquid are passed simultaneously through the venturi tube to generate microbubble. It is composed of an inlet section, a tubular part,

a throat and a tapered out flow section. Pressurised fluid is introduced in the tabular part through the inlet section. The throat of venturi-system accelerates the two phase fluid, due to which the pressure in this part decreases. Because of decrease in pressure cavitation occurs in the system which generates microbubbles (Fujiwara, 2006). Yoshida et al. (2008) used this method to generate microbubble having diameter of approximately 70 μm.

(v) ***Ejector type***: Ejector uses the venturi effect of a converging-diverging nozzle to convert the pressure energy of a motive fluid to velocity energy which creates a low pressure zone that draws in and entrains a suction gas. After passing through the throat of the injector, the gas-liquid mixer expands and the velocity is reduced. The shearing of gas-liquid mixture in turbulent flow creates the microbubbles of diameter less than 58 μm (Nakatake et al., 2007; Chu et al., 2008).

(vi) ***Multi fluid mixture device***: Sadatomi and kawahara (2008) invented a new device which can generate microbubbles as well as mists. They used orifice and porous pipe instead of spherical body and small drilled holes. When pressurized water enters in the generator, the velocity of water increases due to the presence of orifice, from the principle of energy conservation, the pressure at a little downstream of the orifice becomes negative, this creates automatic suction air in water from porous pipe, which results in generation of microbubble.

(vii) ***Pressurized dissolution type***: In this method air is allowed to dissolve in water by applying a pressure of about 3-4 atm and water is flushed through a nozzle inside the water pool. Because of reduction in pressure the supersaturated air is released into expelled water in the form of microbubbles of approximately 52 μm (Tsuge, 2010).

1.3.1.3.2 Methods without Accompanying Liquid Flow

These methods of microbubble generation has only gas phase in motion, and the blowing gas used to generate microbubbles. Some of the methods for microbubble generation with gas phase in motion are rotary gas flow type, porous mullet ceramics technique, porous membrane type, etc. (Kukizaki et al., 2004; Okada et al., 2010; Onoe et al., 2002). Some of low power generation methods are also used to generate microbubble such as are flow focusing technique, microchannel technique, ultrasonic systems, micro-bubbler technique, etc. (Gañán-Calvo and Gordillo, 2001; Lee et al., 2005; Makuta et al., 2006; Yasuno et al., 2004). Microbubbles can also be generated by some other techniques such as by applying electric field, from porous plates, by spinning disk and by electrohydrodynamic atomization (Burns et al., 1997; Farook et al., 2007; Fujikawa et al., 2003; Weber and Agblevor, 2005). More details of all the method are published by us (Parmar and Majumder, 2013).

1.3.2 Physical Aspects of Ionic Microbubble Flotation

The important physical aspects of microbubble flotation are discussed in the following section:

1.3.2.1 Particle Hydrophobicity and Floatability

The mineral flotation is based on reducing the surface free energy of the species to be floated, using certain kind of chemical reagents. Surface properties of particles and air bubbles can be described in terms of particle surface hydrophobicity and surface forces. The surface hydrophobicity is usually measured by the contact angle against water, surfactant solutions, or other liquids. Contact angle describes the ability of mineral particles to displace water and to attach to bubbles (Fuerstenau et al. 2007; Nguyen, 2007).

1.3.2.2 Bubble–Particle Interactions

Bubble–particle interaction during flotation comprises of collision, attachment and detachment (Phan et al., 2003). The bubble–particle interaction is controlled by a number of forces, including the surface and hydrodynamic forces (Anfruns and Kitchener, 1986; Schulze, 1989). All the interactions among atoms, ions, and molecules constituting the particle, bubble and intervening liquid film give a force acting between the bubble and particle surfaces, known as the surface force. The hydrodynamic forces are due to the resistance of liquid films between the surfaces (Dai et al., 1999). The main surface forces affecting the bubble–particle interaction are van der Waals force, hydrophobic force and electrostatic double-layer force (Dai et al., 2000; Edzwald, 1995; Verrelli et al., 2011). The van der Waals force may be due to the dipolar interactions among atoms and molecules. The electrostatic forces acting between particles and microbubbles can be calculated from their zeta potentials. An electrostatic double-layer force is due to the interaction between diffuse layers of electrolytes concentrated at the electrically charged surfaces of particles and bubbles (Miettinen et al., 2010; Ralston et al., 1999). The hydrophobic effect is the observed tendency of nonpolar substances to aggregate in aqueous solution and exclude water molecules. Surface forces and hydrodynamic forces are function of the separation distance between the bubble and the particle surfaces the mobility of the bubble surface and the hydrophobicity of the solid surface (Liang et al. 2007; Yoon, 2000).

1.3.2.3 Microbubble Stability

Microbubble dispersion stability is a desirable characteristic in separation processes. The gas inside the microbubbles tends to diffuse outside. As a consequence of this, the microbubbles shrinks. Therefore microbubble stability plays important role in determining mineral flotation recovery and selectivity. In microbubble dispersions liquid drainage rate is the principle parameter

determining stability because no perceptible breakdown of bubbles takes place prior to the majority of liquid being drained from dispersion (Borden et al., 2012).

1.3.2.4 Hydrodynamics of Microbubble Flow

The interactions between particles and microbubbles are strongly influenced by the hydrodynamics of microbubble flow (Dia et al., 1998; Trahar and Warren, 1976). The motions of particles is different in magnitude and direction (Schubert and Bischofberger, 1978). Because of the momentum exchange, a particle that finds itself in the proximity of rising microbubble in flotation system experiences different kinds of forces. The first force is due to liquid acceleration required to suspend the particle and disperse the microbubble (Schubert, 2008). The hydrodynamic drag force and other forces due to surface interaction between the particle and microbubble is also affected by hydrodynamics of microbubble flow. (Serizawa et al., 2003; Yamaguchi et al., 2001a; Yamaguchi et al., 2001b)

1.3.2.5 Flotation Kinetics

To determine the theoretical rate of flotation of mineral in a column, it is necessary to make use of simplified model of the system, which ignores unimportant variables while retaining essential features (Sutherland, 1948; Zhang, 1989). A large number of effort has been made to mathematically model the flotation separation process (Bloom and Heindel, 1997; Fichera and Chudacek, 1992). Despite the differences in design of flotation device almost all flotation column operate on similar principles: (i) aeration, where air bubbles are introduced into the system; (ii) mixing, where bubbles and particles are intimately mixed to maximize bubble–particle interaction; and (iii) separation, where bubbles and bubble–particle aggregates are allowed to separate from the bulk mixture and skimmed away (Bloom and Heindel, 2003; Tuteja et al., 1994). Experimental observations of the flotation process have shown that it can be linked to a chemical reactor and be

described by an ordinary differential equation (Finch and Dobby, 1990; Wills and Munn, 2005). The efficiency can be modelled from the first principle and the collision, attachment, and detachment interactions between bubbles and particles (Ahmed and Jameson, 1989; Duan et al., 2003; Sutherland, 1948).

1.3.3 Chemical Aspects of Microbubble Flotation

1.3.3.1 Surface Chemistry of Minerals in Water

Selective recovery is driven by the chemistry of the surface of the mineral. The mineral particle–bubble attachment and its ensuing stability are governed by the balance of hydrophobic/hydrophilic species on the particle surface (Fuerstenau et al., 2007). Generally the mineral surface have two surface characteristics such as polar and non-polar surface characteristics. The majority of particles have strong covalent or ionic surface bonding and exhibit high free energy at their polar surface. The surfaces of these minerals react strongly with polar water molecules, rendering the minerals naturally hydrophilic in varying degrees. Ionic microbubble flotation is the most efficient flotation for such types of particle. The particle and bubble surfaces are electrostatically charged in water, forming the electrical double layers. The diffuse layers of the double layers on the particle and bubble surfaces overlap at close approach, giving a repulsive or attractive force. Although the actual double-layer interactions between the particle and microbubble act in limited distance (Fuerstenau et al., 2007; Nguyen, 2007). Several mineral surfaces, such as graphite, coal, sulfur, talc and molybdenite, are not readily wetted by water. These minerals are composed of covalent molecules held together by nonpolar forces which produce special crystal lattice structures with nonpolar surfaces. The nonpolar surfaces are

hydrophobic for which does not easily attach to the water dipoles. Ionic microbubble flotation may not be as effective in these mineral because of nonpolar surface forces (Fuerstenau et al., 2007).

1.3.3.2 Chemistry of Flotation Reagents

Several organic and inorganic reagents are used in flotation for controlling the characteristics of interfaces. According to their functionality, flotation reagents are classified into collectors, regulators and frothers (Nguyen, 2007). Collectors adsorb at the solid–liquid interface, making the surface of required minerals water-repellent. The collectors increases the contact angle so that bubbles adheres to the particle surface, aiding bubble–particle attachment. Generally collectors can be classified as ionising collectors and non-ionising collectors (Khoshdast and Sam, 2011; Wills and Munn, 2005). The non-ionizing collectors cannot chemically adsorb to the mineral surface due to absence of polar functional groups (examples are kerosene, transformer oil, synthetic hydrocarbon oils, etc.). These compounds are hydrocarbon liquids of petroleum origin and their adsorption is due to the intermolecular van der Waals forces. The collectors are primarily used in the flotation of naturally hydrophobic minerals which have insufficient hydrophobicity for the strong and fast attachment to bubbles (Nguyen, 2007; Wills and Munn, 2005). The ionizing collectors are widely used in flotation and can be conveniently divided into cationic (examples are fatty amines, ether amines, etc.) and anionic collectors (examples are organic acids, soap, xanthates, etc.). Another important chemical that is widely used in flotation is frothers. Frothers (also known as surfactants) are water-soluble organic reagents that preferentially adsorb at the gas–liquid interface. They are added to stabilize the bubble formation in the pulp phase, to create a reasonably stable bubble to allow selective drainage from the froth of entrained gangue, and to increase flotation kinetics. The choice of frothers in ionic microbubble depends on the nature of charge of particle. If the particle to be separated is anionic, cationic surfactant or frothers should

be used to create the ionic microbubble. The ionic strength of microbubble is a key parameter in ionic microbubble flotation. The magnitude of charge on the surface of microbubble is governed by the surfactant concentration (Yoon and Yordan, 1986). The presence of dissolved inorganic salts inhibits the flotation, because collector ions function as counter ions in the double layer (Lyklema, 2000).

1.4 Knowledge Gap

It is clear from the literature, that microbubble possess a great potential to separate fine suspended particles. In order to explore this technology into a larger or commercial scale, it is very essential to understand the complexity of the process (Jauregi and Dermiki, 2010; Spigno et al., 2010). The hydrodynamics of microbubble, stability of microbubble and dispersion phenomena are the main parameter which can significantly affect the microbubble particle-interaction. Although these parameter has not got considerable attention. The microbubble size, produced in a liquid by pressurizing the gas or by shearing action of gas-liquid mixture, depends on the physical properties of liquid. Modifying the surface tension of liquid can not only shift the bubble size distribution, it also influences the stability of microbubble. But no significant studies are available in literature that can correlate the size distribution and life time of microbubble with concentration of surface tension modifier. There is no such quantitative research available in literature that can completely demonstrate the effect of different gas on microbubble hydrodynamics. Efforts are required to completely analyze the complex mechanism of drainage of microbubble, in order to expose this technology at large scale. The potential of microbubbles to separate fine particle are also limited to few particles systems. The mixing behavior of microbubble suspension is also not explored in

literature. To achieve technical feasibility of microbubble suspension flow and microbubble aided mineral separation by flotation, a detailed study on the dispersion characteristics of microbubble suspension is also required. The present work is formulated based on those scope which is given as follows:

1.5 Formulation of the Work

In view of the importance of ionic microbubble flotation, present research has been undertaken for a systematic study of various aspects of ionic microbubble flotation to separate fines. The term "ionic microbubble" is used in the present work because microbubble carries charge over it. Based on the background on the possibility of the work in microbubble aided floatation processes, the following work is proposed for the present research:

1.5.1 Microbubble Generation and Stability of Microbubble

Microbubble requires three states of matter to persist for a useful time frame: a gas core, a liquid medium, and a viscoelastic stabilizing shell. The stability and dynamics of a microbubble depend on the properties of all three components. The stability of microbubble is very important aspect in order to use them for fine separation. The transport process associated with microbubble is significantly affected by the microbubble stability. Thus it becomes very essential to study the stability characteristics of microbubbles. In the present work, the stability of microbubble dispersion is analyzed by the drainage mechanism. The stability of microbubble dispersions is also examined by using its electrical properties. Correlations are also developed to interpret the half-life and drainage mechanism of microbubble. The details of work is described in chapter 2.

1.5.2 Rise Velocity and Size Distribution of Microbubble

The collection of particles by rising air bubbles in flotation can be predicted by determining the motion of particles in the path of the bubble rise (Reay and Ratcliff, 1973). The flotation rate also depends on the bubble surface area flux which is inversely proportional to bubble size (Laskowski et al., 2003). The particle recovery depends not only on the solids content of the pulp and the hydraulic regimes in the column, but also on the size, the bubble population and distribution of the bubbles (Lee and Lee, 2002). So the bubble size is an important variable in a flotation process (Tao, 2005). To optimize the flotation process on the basis of surface area flux, it is essential to know the microbubble size, its distribution along with the knowledge of the microbubble rise velocity. This work, hence, intended to examine the microbubble size and its distribution of microbubbles. The effect of physicochemical properties of liquid and gas on motion of microbubble is also enunciate. Correlations are also develop to interpret the size and distribution of microbubble based on its physicochemical properties of liquid. The details of the work is presented in chapter 3.

1.5.3 Hydrodynamics of Microbubble Flow

The microbubble-particle interaction is highly affected by the hydrodynamics and the phenomena associated with microbubble suspension flow. In applications of microbubbles, the microbubbles are pumped through columns, pipes, etc. Therefore the studies on the flow behavior of microbubble suspensions flow, pressure drop, hydrodynamics drag, friction and rheology of microbubble suspension flow is required in this regard. Present work investigates the hydrodynamic characteristics of the flow of a microbubble suspension in a surfactant solution through a pipe. A mechanistic model has been developed to analyze the interfacial stress of microbubble suspension

flow in a pipe by considering bubble formation, drag at the interface, and loss of energy due to wettability. A correlation between the intensity factor of interfacial stress and the friction factor based on energy loss due to wettability has been developed, which are described in details in chapter 4.

1.5.4 Dispersion Characteristic of Ionic Microbubble

The particle-bubble collision is affected by intensity of mixing in the device. The mixing process is affected by all three phases present in a column. However, most attention has been paid to the liquid phase. It is suggested, that the solids and liquid axial dispersion coefficient are equal for fine particles having mean diameters less than 150 μm (Mavros, 1993). Therefore in the present research, the dispersion characteristic of ionic microbubble suspension in continuous plant prototype developed for mineral beneficiation has been investigated. The effects of different operating variables and physiochemical properties of liquid on the dispersion of ionic microbubble suspension are examined. A phenomenological model with consideration of liquid circulation was developed to analyze the dispersion coefficient of the microbubble suspension due to circulation. Generalized correlations for dispersion coefficient and the time to reach uniform dispersion are also developed based on the physicochemical properties of microbubble suspension. The details of the work is presented in chapter 5.

1.5.5 Fine Particle Separation by Ionic Microbubble

Fine separation is one of the most important application of ionic microbubble (Jauregi et al., 1997). Industrial applications of flotation moved much faster than scientific understanding of the phenomena involved. It is recognized that the size of the bubbles and its surface potential has an influence on the efficiency of the flotation process (Ahmadi et al., 2014). This work, hence,

intended to explore the separation characteristics of ionic microbubble for fine particle separation. The effects of different operating variables and physicochemical properties of liquid on the separation characteristics of ionic microbubble are enunciated. A phenomenological kinetic model based on collision, attachment and detachment mechanisms of fine particle is developed to analyze the flotation characteristics of the ionic microbubbles. An analysis of particle recovery based on the mixing of phenomena of microbubble dispersion is also presented. Generalized correlations for flotation rate constant and induction time are also developed based on the physicochemical properties of microbubble particle mixture. The details is enunciated in chapter 6.

Notations

d_{mb}	Bubble diameter (m)
D_h	Hydraulic diameter (m)
g	Acceleration due to gravity (m^2/s)
K	Consistency of fluid ($Pa.s^n$)
L	Length of test section (m)
m'	Mobility of bubble ($m^2/s.V$)
n	Flow behavior index (-)
ΔP	Hydrostatic pressure drop (N/m^2)
Q	Volumetric flow rate (m^3/s)
U_b	Bubble rise velocity (m/s)

Greek letters

μ_l	Viscosity of liquid phase (kg/m.s)
σ	Surface tension (N/m)

ζ	Zeta potential (V)
ϵ	Permittivity ($s^2.C^2/Kg.m^3$)
τ_w	Wall Shear stress (Pa)
γ_w	Wall shear rate (1/s)
γ_a	Apparent shear rate (1/s)

CHAPTER-2

GENERATION OF MICROBUBBLE AND ITS STABILITY

This chapter presents the details of the microbubble generation method and stability of microbubble. The stability of microbubble is examined by the drainage mechanism and by using its electrical properties. The effects of surfactants and its concentrations on microbubble stability are enunciated. Correlations have been developed to interpret the half-life and drainage mechanism of microbubble.

2.1 Introduction

Microbubble generation remains a subject of interest over the past few decades. Researchers had made several efforts to develop a generator that can generate continuous microbubbles with minimal power requirement. Zimmerman et al. (2008) categorized three ways of generating microbubbles. The first class utilizes the compression of air stream to dissolve air into liquid, which is subsequently released through a specially designed nozzle system, to nucleate small bubbles as potentially microbubbles, based on the cavitation principle. These bubbles subsequently grow into much bigger bubbles through the fast dissolution of the supersaturated liquid. Pressurized dissolution method is one of the example of this class. The second category uses power of ultrasound to induce cavitation locally at points of extreme rarefaction in the standing ultrasonic waves (Makuta et al., 2006; Xu et al., 2008). The third class uses an air stream delivered under low offset pressure and airs to break off the bubbles due to an additional feature, whether it be mechanical vibration, or flow focusing or fluidic oscillation. By the present time, many kinds of generators are developed, but most of them were too small for the practical usages (Tsuge, 2014).

Considering their industrial usages, the microbubble must be stable to use them in the practical sites. The stability of microbubble is another aspect which is highly focused for their practical usage. It has been reported that microbubble produced in water and surfactant solutions have a narrow and reproducible size distribution, exhibits high stability, separates easily from the bulk liquid phase (Johnson and Wangersky, 1987; Wan et al., 2001). A gas bubble in a liquid-gas solution will grow or shrink by diffusion according to the solution of oversaturated or undersaturated. The resulting motion of the bubble boundary introduces a transport term in the diffusion equation which makes it very difficult to obtain an analytic solution.

Epstein and Plesset (1950) were the first, who investigated the stability of bubble based on its dissolution mechanism. Later on the dissolution process of gas bubbles has been investigated by many researchers both experimentally and theoretically (Clift et al., 1978). D'arrigo and Imae (1992) reported that lipid-coated, microbubbles of 1-5 μm diameter were stable in an air-saturated aqueous solution up to one year. Soetanto et al. (1997) demonstrated that coated microbubbles dissolved much more slowly in a degassed medium than an air microbubble with no shell. The longevity of surfactant coated microbubbles can be optimized by using the appropriate molar ratio of constituent surfactants (Singhal et al., 1993). Wang et al. (1996) suggested three possible mechanisms for microbubble stabilization including reduction in surface tension, surface hardening, and resistance to gas transport. Although their experimental evidence lacks to determine which mechanism dominates. Borden and Longo (2002) observed that the gas permeation resistance is the significant factor in controlling the stability of microbubbles. Duncan and Needham (2004) described the effects of surface tension on bubble dissolution by the Epstein–Plesset model. Andreatta et al. (2006) reported that surfactant can increase the stability of microbubble. Kwan and Borden (2010) also observed the enhancement of microbubble stability.

Some researchers tried to increase the microbubble stability by surface encapsulation (Katiyar et al., 2009; Katiyar and Sarkar, 2010). Generally three process parameters such as surfactant, electrolyte and pH have significant effects on microbubble stability. Surfactants can inhibit gas transport through an interface, and can significantly affect the stability of bubble, but on increasing the electrolyte concentration a contrary effect on the stability was observed (Feng et al., 2009; Yan et al., 2005). The effects of pH on microbubble stability have been inconsistent and no conclusive results can be drawn (Jauregi et al., 1997; Subramaniam et al., 1990).

From the above literature review it is seen that the stability of microbubble can be enhanced by using surfactant. However, no informative study is available in literature that can completely demonstrate the effect of concentration and type of surfactants on microbubble stability. The purpose of present study is to analyze the effect of surfactant concentrations and its type, on the stability of microbubble produced by pressurized dissolution method.

2.2 Experimental Procedure

2.2.1 Microbubble Generation by Pressurized Dissolution Method

In the present work microbubble is generated based on the principal of pressurized dissolution method. The photo graph of the microbubble generator is shown in Figure 2.1(a) and the schematic representation of pressurized dissolution method is shown in Figure 2.1(b). In this method, mixture of gas and liquid are mixed and transport to pressure vessel, where the gas is dissolved at the saturation concentration. A pressure of about 3–4 atm is built up in the chamber by adjusting the outlet flow rate. The water with saturated air is released to low atmospheric pressure. Microbubble

are produced by flashing this saturated liquid through microbubble output control valve, into the expelled liquid.

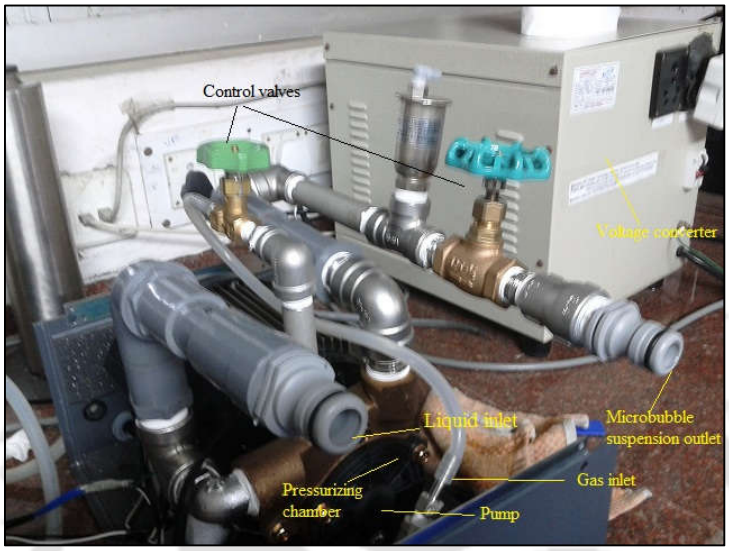

Figure 2.1(a): Photograph of microbubble generator.

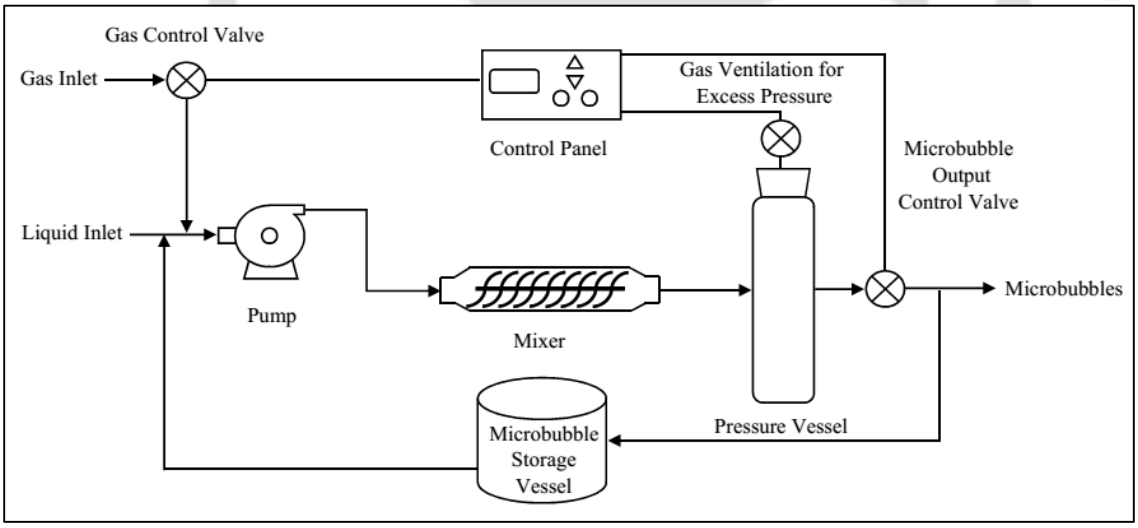

Figure 2.1(b): Schematic representation of the microbubble generation technique.

The pressurized dissolution method is superior to the other methods from the point of view of producing fine bubbles (Maeda et al., 2015). The void fraction of microbubbles generated by the

pressurized dissolution method is determined by the concentration of dissolved gas which depends on the pressure at the dissolution section. The pressure at the dissolution section can be varied either by manually or automatically to produce microbubble within the range of 1-100 µm. The density of microbubble generated by pressurized dissolution method is also higher than other methods. A typical snapshot of the microbubbles (after refinement by with Adobe Photoshop 5.5 software) taken by a high-resolution camera (Model-PCO Pixelfly-USB, resolution 1360 ×1024, 19 fps; PCO Ltd., Kelheim, Germany) is shown in Figure 2.2. The details of bubble size distribution is explained in chapter 3.

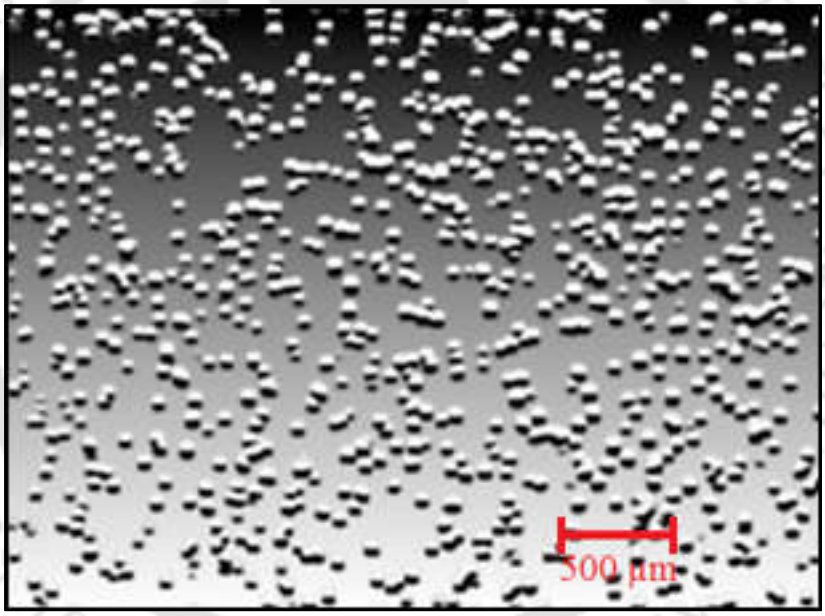

Figure 2.2: Typical snapshot of microbubble without surfactant.

2.2.2 Stability Measurement by the Drainage Curve Method

Generally three fundamental bubble-collapsing mechanisms control the stability of aqueous foam (Jacobi et al., 1956; Myers, 1991; Yan et al., 2005). They are: the rapid hydrodynamic drainage of liquid between bubbles; conglutination between two bubbles; and lamellar rupture, whereby the

bubbles coalesce or collapse. Conglutination is a mechanism where the larger bubbles to expand at the expense of the smaller bubbles by coalescence. It has been reasoned that since no detectable breakdown of bubbles takes place prior to the majority of liquid being drained from the dispersion, the liquid drainage rate is the principle parameter to determine microbubble stability (Sebba, 1971; Sebba, 1987). The stability of microbubble dispersion can be evaluated in terms of its half-life, which is the time taken to drain half of initial liquid volume. The half-life method is the most commonly used to measure the microbubble stability and is simply estimated using a measuring cylinder (Feng et al., 2009). Freshly prepared microbubbles were transferred to the measuring cylinder and the volume of the drained liquid below the dispersion was measured with time as shown by schematic diagram in Figure 2.3. After production, the suspension was transferred by a pump to a 100 ml measuring cylinder in order to study microbubble drainage rate by measuring electrical conductivity and visual observation of change of phase interface.

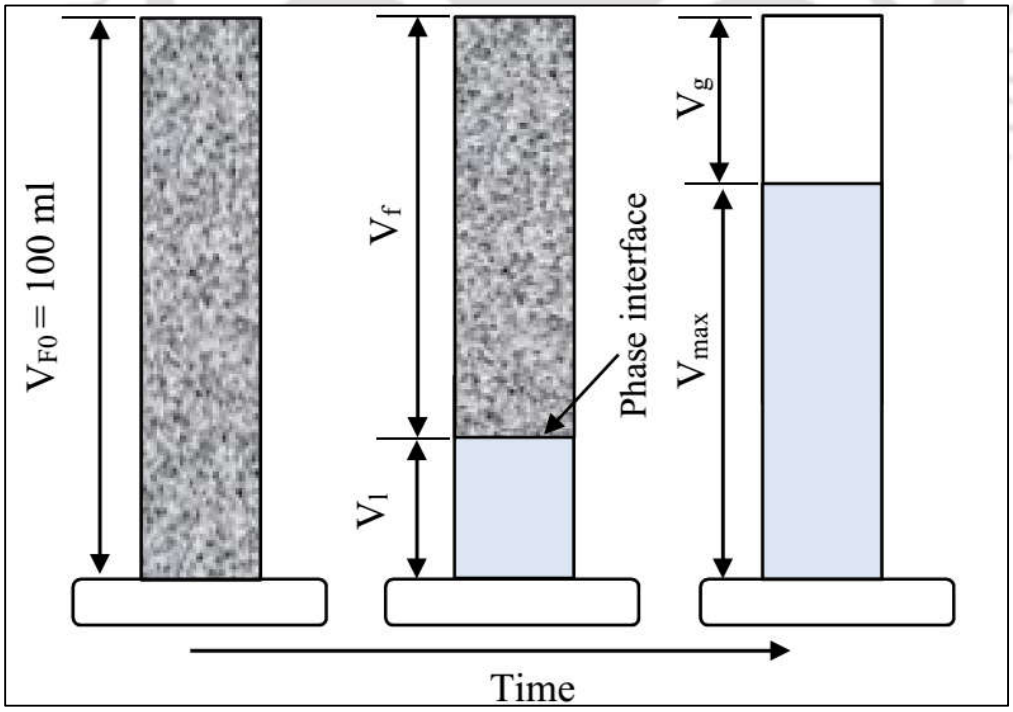

Figure 2.3: Schematic representation of microbubble drainage.

Volumes of the drained liquid (V_l) and dispersion phase (V_f) were recorded with time. The final volume of drained liquid (V_{max}) was recorded after the dispersion phase had completely disappear. Each test was replicated five times by repeating the above procedure. The gas volume fraction of the microbubbles provided a measure of the amount of gas entrained in the microbubble dispersion and was expressed as the ratio of the gas volume (100 ml V_{max}) to the total volume of the dispersion (100 ml). According to Sebba (1985), the stability of the microbubble dispersion was quantified as the time taken for half the liquid to drain from the dispersion, i.e., the half-life ($T_{1/2}$). The liquid drainage volume (V_l) was plotted against time and the time corresponding to the half of the final drained liquid (1/2 V_{max}) was identified from the graph as shown in Figure 2.4.

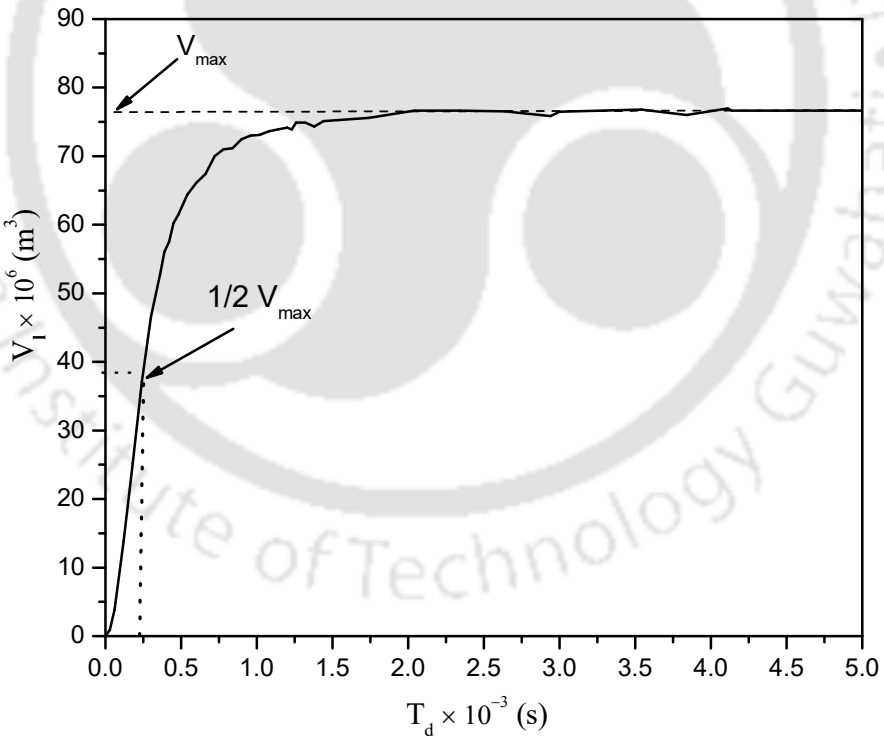

Figure 2.4: Typical outline to estimate the half-life of microbubble dispersion.

2.2.3 Stability Measurement by the Electrical Conductivity Method

Electrical conductivity (EC) of drained liquid was measured using conductivity probe (Model: VSI-04 ATC Deluxe, VSI Electronics Pvt. Ltd., Chandigarh, India). EC of drained liquid was measured integrally. For integrally measurement, the position of probe was fixed at the bottom of the cylinder and the EC readings were recorded versus time. The EC readings were calibrated by pure water every often. EC of clear solution for all samples were 0.5 ±1 (μs/m) before adding surfactant. The advantage of using electrical conductivity, rather than conventional volume method, is in choosing a more sensitive parameter when studying the microbubble suspension stability. It also gives better insight in distinguishing different drainage stages and transforming moment in microbubble morphology.

2.3 Physical Properties of the System

In the present work, aqueous solutions of sodium dodecyl sulphate (SDS), cetyl trimethyl ammonium bromide (CTAB) and Tween-20 were used as liquid phase whereas air was used as gas phase. The densities of the solutions were measured with a specific gravity bottle. The surface tension was measured by tensiometer (model K9-MK1, Kruss GmbH, Hamburg, Germany). The viscosity of the solutions were measured by rheometer (model Haake Rheostress 1, Thermo Electron Co. Germany). All the experiments in the present work were carried out at 25° C. The physical properties of gas and liquid phase are given in Table 2.1.

Table 2.1: Physical properties of system measured at 25 ± 1 ºC.

Type of Fluid	Concentration in water (ppm)	Density (kg/m^3)	Surface tension (mN/m)	Viscosity (mPa·s)
Water	0	999.68	71.20	1.050
SDS-1	5	999.69	68.00	1.112
SDS-2	10	999.69	64.70	1.230
SDS-3	15	999.70	62.50	1.301
SDS-4	20	999.71	62.50	1.310
SDS-5	50	999.73	61.00	1.315
SDS-6	100	999.78	59.00	1.318
SDS-7	500	1000.18	56.60	1.321
SDS-8	1000	1000.68	46.70	1.322
SDS-9	2364.5	1002.05	37.49	1.329
SDS-10	3000	1002.98	37.51	1.333
CTAB-1	5	999.685	66.14	1.110
CTAB-2	10	999.69	65.37	1.221
CTAB-3	20	999.70	63.87	1.250
CTAB-4	50	999.73	59.62	1.291
CTAB-5	100	999.78	53.33	1.293
CTAB-6	200	999.88	43.75	1.310
CTAB-7	328.005	1000.01	37.32	1.312
CTAB-8	500	1000.18	38.12	1.313
Tween-20-1	5	999.69	70.00	1.115
Tween-20-2	10	999.76	69.27	1.200
Tween-20-3	20	999.79	67.22	1.311
Tween-20-4	34	999.81	65.21	1.318
Tween-20-5	50	999.89	61.55	1.323
Tween-20-6	69	999.92	60.22	1.325
Tween-20-7	100	1000.15	53.70	1.330
Air	-	1.18	-	0.018

2.4 Results and Discussion

2.4.1. Kinetics of Stability of Microbubble

The profile obtained in the present work for volume of drained liquid is very similar to the curve reported by Yan et al. (2005). Figure 2.5 shows the drainage process for SDS. The drainage process

for CTAB and Tween-20 are shown in Figures 2.6 and 2.7 respectively. The figures shows that drainage mechanism have the same trend independent of concentrations and surfactant types. But, drained liquid (V_l) and drainage time (T_d) are affected by surfactant type and concentration. Higher concentrations result in decreasing drained liquid. This is due to smaller bubbles in the suspension produced by higher surfactant concentrations. The drainage time was recorded for higher concentrations up to critical micelle concentration (CMC) because of saturated absorption capacity on microbubble surface. The least stable microbubble dispersions in these series of tests were generated when the smallest amount of surfactant, i.e. ~5 ppm SDS is used. As it is known, it is not possible to produce any microbubble in the pure water, so a minimum concentration of surfactant is essential for microbubble formation. Therefore it is logical to expect that the least microbubbles dispersions are generated in lowest concentration of surfactant. However, beyond a threshold concentration, size and stability of microbubbles should not depend on concentration if only surfactant is used in the microbubbles generator. The formation of dense froth starts at concentration above 20 ppm. There are two important key addresses in literature for stability of microbubbles. Firstly, the most stable microbubbles are produced when the concentration of surfactant is equal to CMC (Moshkelani and Amiri, 2008). Secondly the stability of microbubbles decreases when the concentration of surfactant is higher than CMC (Yan et al., 2005). The observation is consistent with findings from other studies (Yan et al., 2005). Comparing CTAB and SDS drainage curves it reveals that, more V_l and T_d are observed for CTAB. This can be related to their molecular structure. Longer alkyl group of CTAB lowers CMC and increase V_l. Increasing in hydrophobic chain length, results in more intercohesive forces that make microbubble dispersion more stable and consequently increase drainage time (Rosen, 1989). The most stable microbubble suspension was produced at CMC concentration.

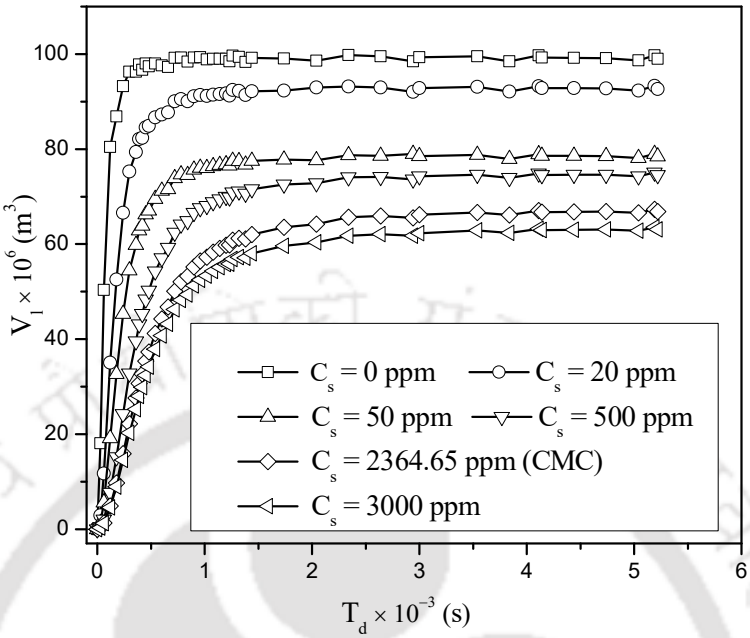

Figure 2.5: Variation of drained liquid volume in SDS solution during drainage process.

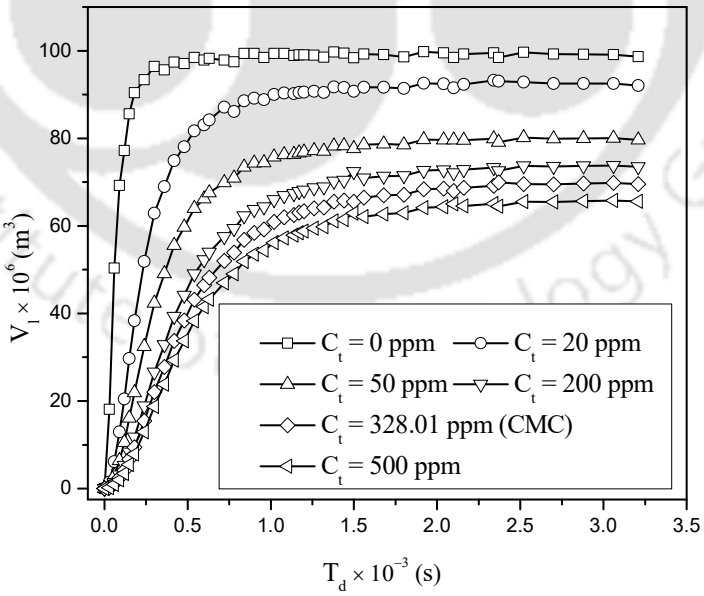

Figure 2.6: Variation of drained liquid volume in CTAB solution during drainage process.

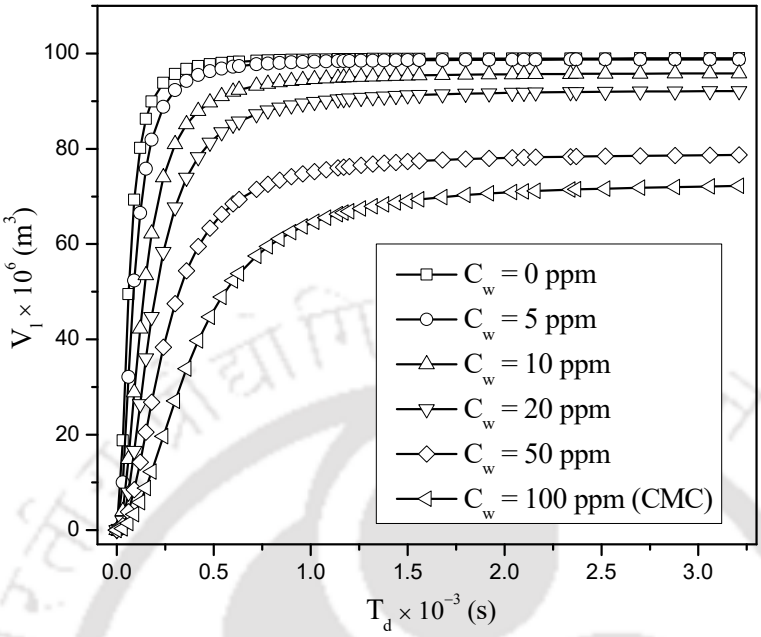

Figure 2.7: Variation of drained liquid volume in Tween-20 solution during drainage process.

2.4.2 Modeling for Liquid Drainage

Distinct drainage models have been presented in the literature to describe the drainage from bubble dispersion (Amiri and Woodburn, 1990; Germick et al., 1994; Wang and Narsimhan, 2004; Yan et al., 2005). However, these models do not appear to apply to the microbubble dispersion due to the observations that dispersion resembles emulsion and demonstrates different drainage behaviors to conventional foams. Amiri and Woodburn (1990) developed the equation based on Stokes' law. This equation describes a drainage profile similar to an exponentially decreasing profile for conventional foams, and so fails to address the "S"-shaped drainage curve of typical microbubble dispersion. The other equation proposed by Yan et al. (2005) fits well to the "S"-shaped drainage profile, although its conceptual model appears to be incomplete as it describes a two-stage drainage process that is similar to the drainage mechanisms proposed for conventional wet foams (Indrawati

and Narsimhan, 2008; Koehler et al., 2000). As per present experimental observation, the drainage data follows the "S"-shaped pattern. So the equation proposed by Yan et al. (2005) was considered to be a better candidate since it exhibit an "S"-shaped profile which is expressed as

$$V_t = V_{\max} \frac{T_d^q}{T_{1/2}^q + T_d^q} \tag{2.1}$$

where V_t and $V_{\max}$ are the volume of drained liquid at time T_d and the final drained liquid volume respectively, $T_{1/2}$ is the half-life for liquid drainage and q describes the sigmoid character of the drainage curve. The model by Yan et al. (2005) was fitted to the present experimental values. Figure 2.8 shows the difference between the experimental and the fitted values for microbubble dispersion created from 50 ppm surfactant of SDS.

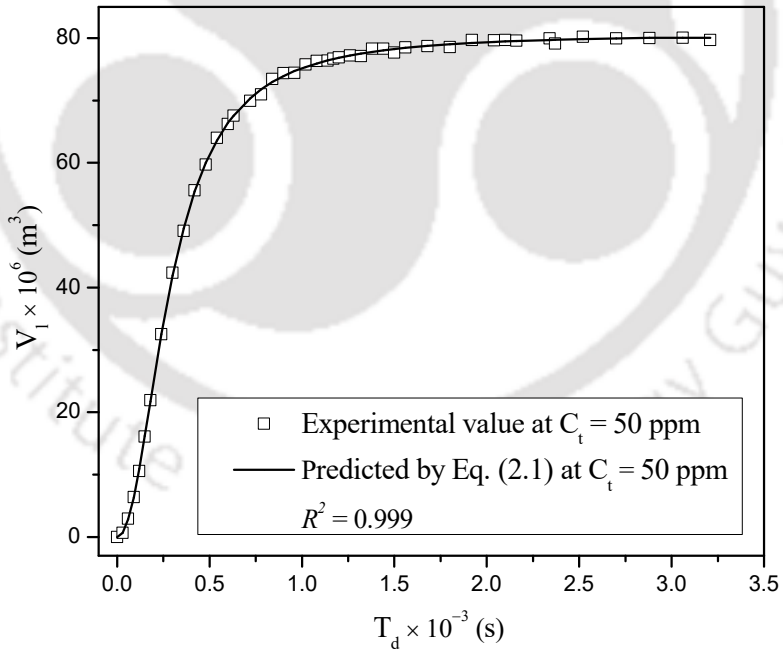

Figure 2.8: Comparison of experimental liquid drainage data with model at 50 ppm CTAB concentration.

The model estimates well the drainage of liquid from SDS or CTAB microbubble dispersions (V_{max} and fitted half-life $T_{1/2}$) used in this study. This is clearly shown in the residuals plot (in Figure 2.9) that the model is well fitted to the experimental data with the residuals of the model less than 0.5.

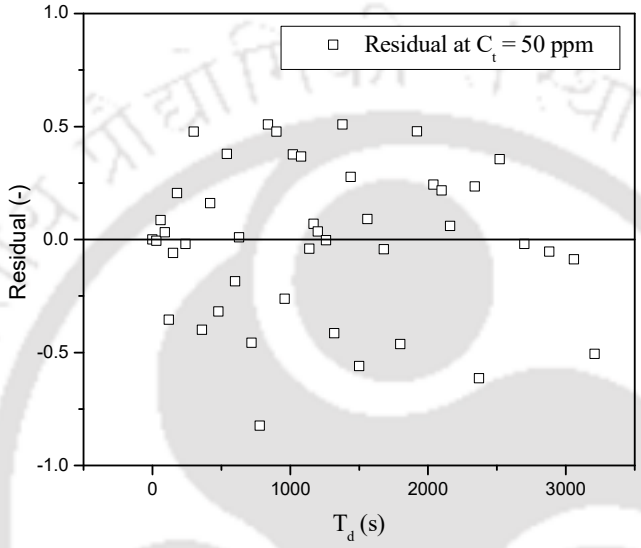

Figure 2.9: Residual plot of model equation.

The half-life and drained liquid volume values of the experimental data and model output are summarized in Table 2.2 and 2.3. The half-life of the microbubble was found to be strongly dependent on the concentration of surfactant and the type of surfactant. The half-life of microbubble dispersion can be correlated with the surfactant concentration as

$$T_{1/2} = 58.129\ln(C_s) - 20.707 \qquad 0 < C_s \leq 3000 \text{ ppm} \qquad (2.2)$$

$$T_{1/2} = 81.413\ln(C_t) - 29.37 \qquad 0 < C_t \leq 500 \text{ ppm} \qquad (2.3)$$

$$T_{1/2} = 97.765\ln(C_w) - 85.6 \qquad 0 < C_w \leq 100 \text{ ppm} \qquad (2.4)$$

where C_s, C_t and C_w are the concentrations of surfactants SDS, CTAB and Tween-20 respectively in ppm. The correlation coefficients for the above correlations were found to be 0.999, 0.998 and 0.989 respectively. Since the correlation coefficients are closer to 1, it shows that the model is well suited. The values of q in the model were found to depend mainly on the surfactant concentration. From the trend of the experimental results and output from the model it can be concluded that microbubble drainage process is a constant acceleration mechanism due to enlargement while rising to the interface. By differentiation of the fitted model equation with time, drainage rate can be easily calculated. Figure 2.10 shows a typical variation of drainage rate (R_d) of microbubble dispersion with drainage time. The complete drainage process occurs in three phases. In the first phase the drainage rate increases rapidly with time, while in the second phase, the drainage rate sharply decreases with time and finally in the third phase the rate of drainage becomes relatively small. The drainage mechanism in the first phase is a combination of liquid flow due to gravity through the plateau boarder and the upward creaming of microbubbles. In the first phase, the microbubbles size changes with time, due to disproportionation, whereby gas diffuses from the smaller bubbles into larger bubbles. As more liquid drains away, the average microbubble size increases, which increases the liquid drainage. Up to the end of first phase, microbubble size sufficiently increases. At this stage, the microbubble dispersion starts losing its colloidal character due to bubble expansion, which starts the second phase. In this phase, the governing drainage mechanism is gravity-driven liquid flow. The size of microbubble may increase up to three times during the expansion process (Frumkin and Levich, 1947). Up to the beginning of third phase 90 % of liquid in the dispersed phase removes from the dispersion. In this phase the drainage rate is very less due to small fraction of microbubble remains in the dispersion. At this stage the bigger microbubbles in the dispersion completely drains and few small microbubble remain in the

dispersion, which causes a very slow drainage. Table 2.4 shows the maximum drainage rates for various surfactants and concentrations.

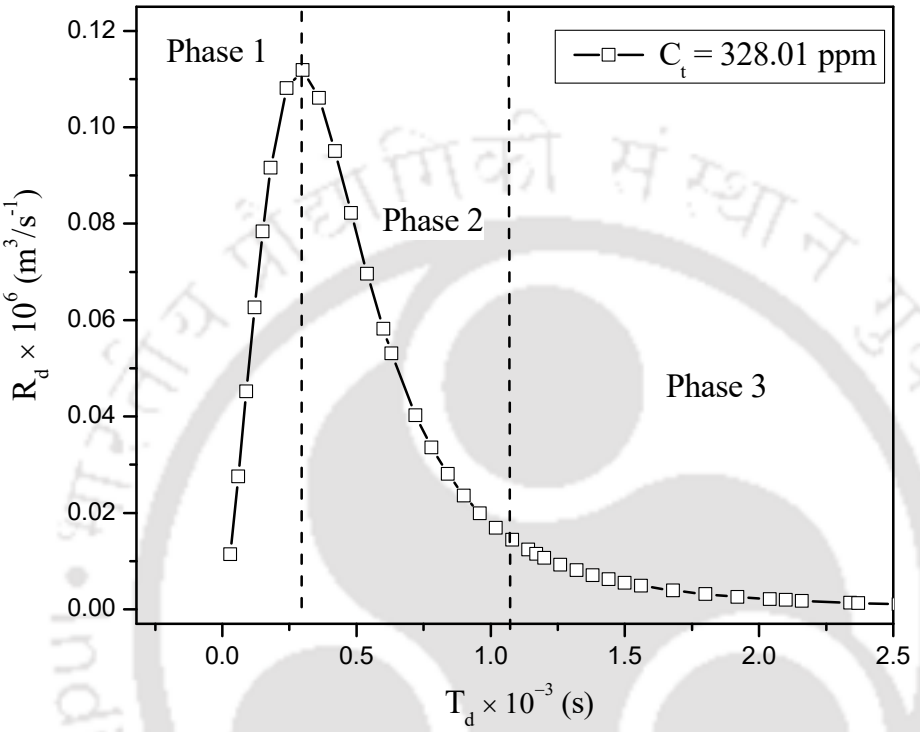

Figure 2.10: Variation of drainage rate of microbubble dispersion with time.

Table 2.2: Comparison of observed and fitted half-life and drained liquid volume for SDS.

Surfactant	Concentration (ppm)	Experimental data		Model output		
		$T_{1/2}$	V_{max}	$T_{1/2}$	V_{max}	q
SDS	5	60	99.00	60.38	99.17	2.03
	10	70	99.01	70.96	99.34	1.97
	20	112	96.19	113.20	96.51	2.06
	50	157	92.63	154.29	92.97	2.09
	100	210	78.43	207.77	78.74	2.11
	500	335	74.53	74.91	340.69	2.10
	1000	375	72.58	72.98	380.38	2.07
	2364.65 (CMC)	418	66.84	67.40	430.49	2.01
	3000	435	63.06	63.65	444.25	1.97

Table 2.3: Comparison of observed and fitted half-life and drained liquid for C_t and C_w.

Surfactant	Concentration (ppm)	Experimental data		Model output		
		$T_{1/2}$	V_{max}	$T_{1/2}$	V_{max}	q
CTAB	5	60	98.60	99.27	60.38	2.07
	10	100	95.71	96.54	101.46	2.15
	20	157	92.06	93.00	158.37	2.11
	50	214	79.66	80.67	214.73	2.17
	100	284	77.54	78.63	289.24	2.11
	200	342	73.50	74.95	344.83	2.11
	328.01 (CMC)	397	69.53	71.13	401.99	2.10
	500	434	65.58	67.29	442.47	2.10
Tween-20	5	85	98.80	86.00	98.00	2.17
	10	137	95.95	134.50	97.00	2.06
	20	190	92.34	185.50	93.65	2.10
	50	250	79.04	247.00	80.06	2.10
	100 (CMC)	380	73.04	386.00	74.12	2.13

Table 2.4: Maximum drainage rates for various surfactants and concentrations.

Surfactant	Concentration (ppm)	Maximum drainage rate × 10^{-6} (m^3/s)
SDS	5	1.052
	10	0.854
	20	0.555
	50	0.379
	100	0.252
	500	0.202
	1000	0.144
	2364.65 (CMC)	0.127
	3000	0.106
CTAB	5	0.663
	10	0.417
	20	0.299
	50	0.196
	100	0.158
	200	0.128
	328.01 (CMC)	0.111
	500	0.098
Tween-20	5	0.758
	10	0.470
	20	0.330
	50	0.210
	100 (CMC)	0.120

2.4.3 Stability based on Electrical Conductivity

From the observation of change of electrical conductivity (EC) the drainage can be divided into four phases which are shown in Figure 2.11. The first stage is an absorption phase in which EC decreases for short period (disengagement time) and no drainage occurs. Adding surfactant to the clear solution raised EC, but in the case of microbubble clear solution, the increase in EC is extremely sharp for the same surfactant concentration. Furthermore the solution without microbubble shows greater EC than that of clear solution at the same time of intervals. This fact depicts that diffusion of surfactant into microbubble-free solution is completely different when drainage is involved. Since drainage rate diminishes as it progresses, it can be concluded that at macroscopic phase, the drainage rate reaches zero. Therefore when considering drainage rate, dominant stages are macroscopic and bubble. It is believed that in this phase, bulk ions absorb to the surface of microbubbles and reduce EC. The macroscopic drainage phase started with an increase in EC of microbubble clear solution. It continued sharply, and finished in less than ~5 minutes. At this phase, bulk liquid started flowing down because of gravity force. EC and drainage rate reached their maximum values and microbubbles maintained their spherical shapes. In the third phase, namely bubble phase, drainage took less than 10 minutes to complete. Smaller bubbles merged into larger bubbles under influence of Laplace pressure. The last phase (microscopic phase), bubbles change morphology to polyhedral foam. It is extremely sluggish to complete (about 1-3 hours), because of lamella and plateau border drainage. Therefore EC and drainage rate variations were negligible. An interesting point about microscopic phase is EC fluctuations at the end of the phase which is devoted to surfactant molecules migration to the gas-liquid surface. The variations of electrical conductivity in clear solution for different concentrations and surfactants are shown in Figures 2.12 and 2.13.

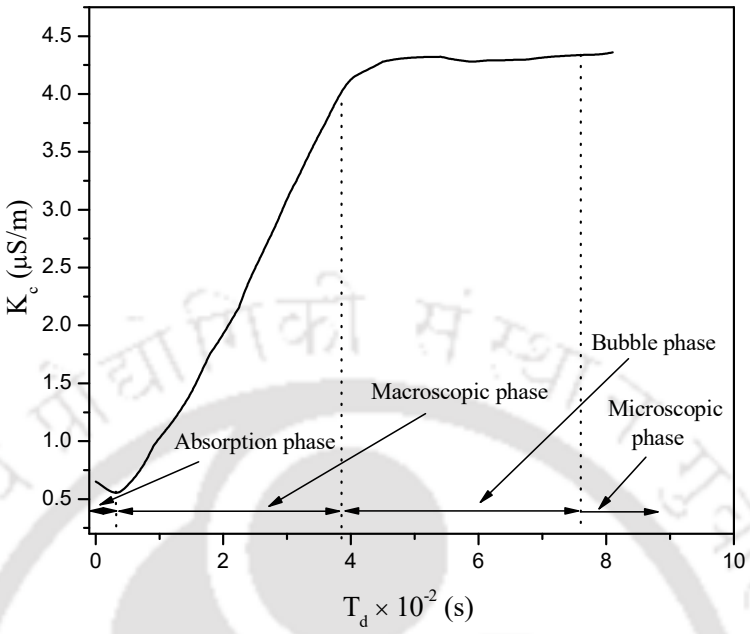

Figure 2.11: Four phases of drainage process in microbubble dispersion.

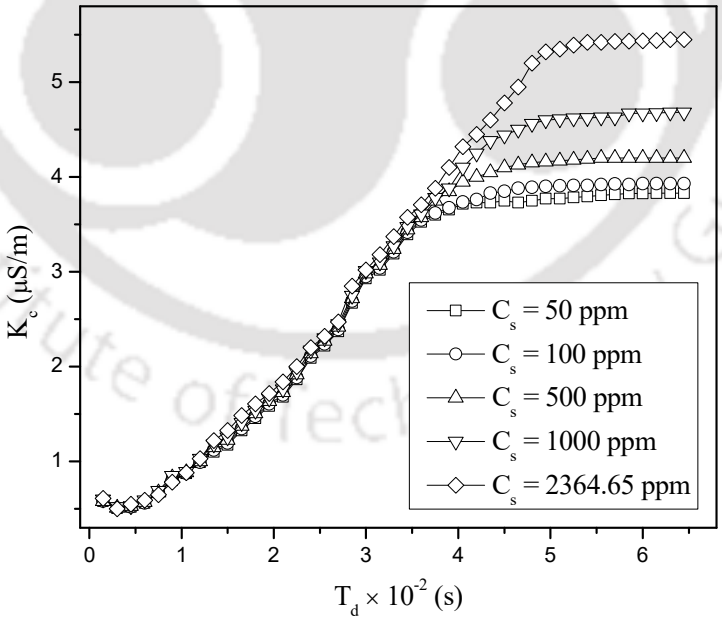

Figure 2.12: Variation of electrical conductivity of microbubble dispersion with time for SDS.

However in the present work, for Tween-20 no significant change in electrical conductivity of liquid was observed within the experimental range. The microbubbles merged into larger bubbles under influence of Laplace pressure and finally disappears from the suspension. After their complete drainage only clear liquid remains without microbubble. The electrical property of microbubble-free liquid does not change with time. So the electrical conductivity of the microbubble remains unchanged after certain time.

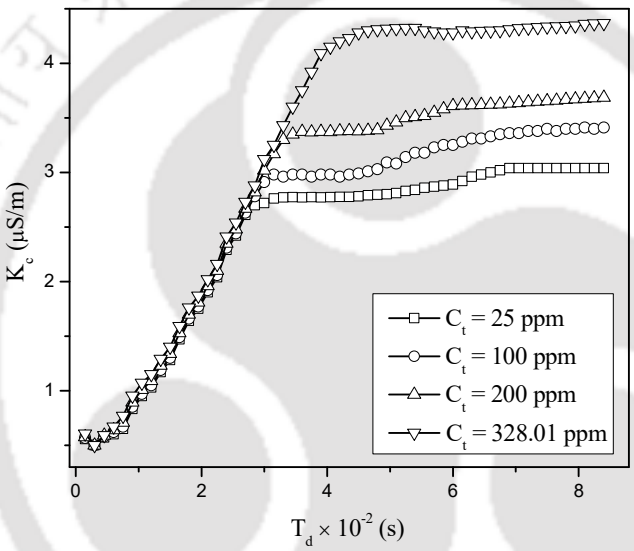

Figure 2.13: Variation of electrical conductivity of microbubble dispersion with time for CTAB.

2.4.4 Modeling for Electrical Conductivity

Electrical properties of the suspension can well characterize the microbubble suspension. Conventional volume measurements could not be an informative indicator for drainage process of microbubble suspension as it would be bound to large errors. As per present experimental data, the EC of microbubble suspension can be mathematically expressed as

$$K_c = \frac{A_1 - A_2}{1 + e^{(T_d - \lambda)/\delta}} + A_2 \qquad (2.5)$$

where A_1 and A_2 represent the initial and final values of conductivity (K_c). The parameter λ and δ are constants and depends on type and concentration of surfactant in the liquid. The parameter λ and δ can be expressed as

$$\lambda = 0.0138C_s - 3\times10^{-6}C_s^2 + 241.36 \qquad 0 < C_s \leq 2364.65 \qquad (2.6)$$

$$\lambda = 0.0105C_t + 5\times10^{-4}C_t^2 + 214.36 \qquad 0 < C_t \leq 328.01 \qquad (2.7)$$

$$\delta = 0.0229C_s - 3\times10^{-6}C_s^2 + 61.925 \qquad 0 < C_s \leq 2364.65 \qquad (2.8)$$

$$\delta = 0.1805C_t - 4\times10^{-4}C_t^2 + 55.298 \qquad 0 < C_t \leq 328.01 \qquad (2.9)$$

Figure 2.14 shows a typical comparison of EC data of microbubble suspension with model equation at 328.01 ppm CTAB concentration.

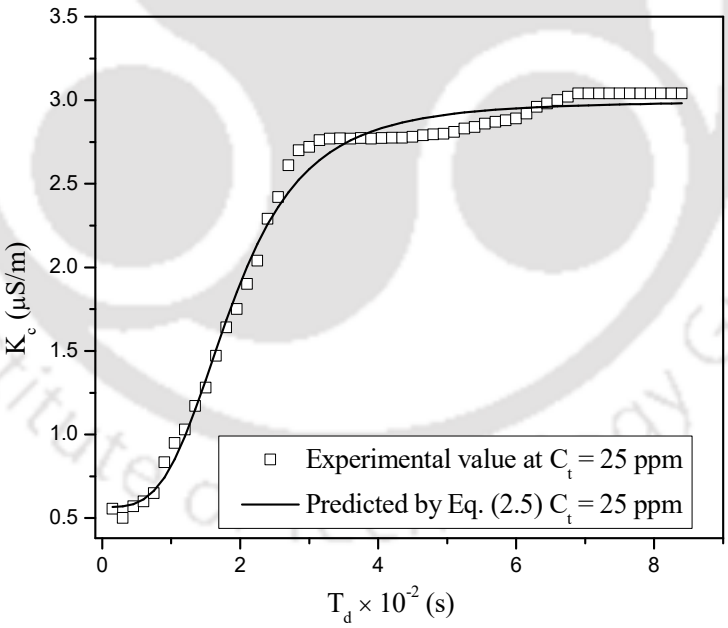

Figure 2.14: Parity plot of predicted and experimental value of EC.

It is clear from the figure that the proposed model can well predict the conductivity of microbubble dispersion.

2.5 Conclusion

In the present work, the effects of surfactants and their concentrations on stability of microbubble, generated by pressurized dissolution method are investigated. From drainage curve analysis it is clear that the stability of the microbubble can be enhanced by increasing surfactant concentration. The liquid drainage curves of the microbubble dispersions followed the same trend for all kind of surfactants. Microbubble drainage process found to occur in three distinct phases. In the first phase the drainage rate increased rapidly with time, while in the second phase, the drainage rate sharply decreased with time and finally in the third phase, it became relatively small. The microbubble half-life increased with surfactant concentration. The lifetimes of microbubble was also correlated with the surfactant concentration. It was found that both drainage and electrical conductance methods can estimate well the stability of microbubble.

Notations

$A_{1,2}$	Parameter defined in Eq. (2.5) (-)
C_s	Concentration of SDS (ppm)
C_t	Concentration of CTAB (ppm)
C_w	Concentration of Tween-20 (ppm)
K_c	Electrical conductivity (μS/m)
q	Parameter defined in Eq. (2.1) (-)
R_d	Drainage rate (m^3/s)
t	Time (s)
T	Temperature (°K)
T_d	Drainage time (s)

V_l	Drained liquid Volumes (m^3)
V_f	Dispersion phase Volumes (m^3)
V_{max}	Final volume of drained liquid (m^3)
$T_{l/2}$	Half Life (s)

Greek letters

λ	Parameter defined in Eqs. (2.6) and (2.7) (-)
δ	Parameter defined in Eqs. (2.8) and (2.9) (-)

CHAPTER-3

TERMINAL RISE VELOCITY AND SIZE DISTRIBUTION OF MICROBUBBLE

In the previous chapter, effects of surfactants on the stability of microbubble have been reported. This chapter deals with the investigation of terminal rise velocity and size distribution of microbubble in different liquid medium. The effect of physicochemical properties of liquid and gas phases on the rise velocity of microbubble are enunciated. The size of microbubble produced by the pressurized dissolution method is also compared with three different methods. A Correlation has been developed to interpret the bubble size distribution of microbubble.

3.1 Introduction

Bubble plays vital role in various chemical, petrochemical, mining and food industries. The formation of gas bubbles and their subsequent rise due to buoyancy are very important fundamental phenomena that contributes significantly to the hydrodynamics in gas-liquid reactors. The rise of bubble, driven by buoyancy, commonly occurs in natural and industrial processes. The rise of a bubble in dispersion can also be associated with possible coalescence and dispersion followed by its disengagement from the system. Understanding the interactions between rising bubbles is not only important for scientific interests but also for industrial applications. The transport processes such as heat transfer, mass transfer, mixing etc. occurring in the multiphase device are highly affected by the motion and properties of bubbles (Clift et al., 2005). The movement of bubble in the liquid affects the flow regime and residence time in the device and hence affects the yield and efficiency (López et al., 2013). It is also acknowledged that the residence time of the gaseous phase is an important parameter for design of an equipment (Shah et al., 1982). For a given equipment, the contact time of the phases can

be calculated only if the rise velocity of bubble is known. The drag force on the bubble is responsible for the dissipation of inertial and viscous energy which depends on the bubble rise velocity (Stewart, 1969). The motion of rising microbubble is not only affected by the inertial and viscous force acting on the bubble, electrostatic field around the bubble can also affect its motion (Kelsall et al., 1996). The rise velocity of microbubbles showed a perfect agreement with theoretical correlation, but as the size of bubble increased the discrepancy also increased (Duineveld, 1995). Takahashi (2005) reported that the rise velocity of swarm of microbubbles in distilled water was close to the value calculated from Stokes' law. Parkinson and Ralston (2010) estimated the rise velocity of single microbubble (15–120 μm diameter) under buoyancy force in an aqueous electrolyte. They observed a reversible effect of transition in bubble boundary condition from full-slip to no-slip condition which depends on pH, ionic strength, and film thickness. Haapala et al. (2010) studied the rise velocity of microbubbles in papermaking process waters. Their experimental results showed that suspension viscosity, surface tension and solids content can significantly affect the kinetics of microbubbles. Recently Jung et al. (2014) development a tracking x-ray microtomography to visualizes rising microbubbles in 4-D by counterbalancing their rise. Measurement of number concentration and size distribution of microbubble is also essential for all aspects of its practical implementation. It has been found that the size distribution of microbubbles is unaffected to changes in shell composition (Dicker et al., 2013). Different methods have been proposed to measure bubble size, but imaging methods have been the most used ones (Moruzzi and Reali, 2010). Han et al. (2002) developed a new method to measure the bubble size, using commercially available batch-type and on-line particle counters. Light scattering method are also used to estimate the mean bubble size of microbubble (Aslan et al., 2006; Couto et al., 2009).

From the literature it is found that studies regarding the microbubble rise velocity and its size distribution have increased but there are knowledge gaps in this regards. The microbubble size,

produced in a liquid by sparging gas or by shearing action of gas-liquid mixture, depends on the physical properties of liquid. Modifying the surface tension of liquid can not only shift the bubble size distribution, it also influences the motion of microbubble. But no significant studies are available in literature that can correlate the size distribution of microbubble with concentration of surface tension modifier. There is no such quantitative research available in literature that can completely demonstrate the effect of different gases on microbubble hydrodynamics. In the present chapter the hydrodynamic parameters such as bubble size distribution and rise velocity of microbubble in various liquids are reported. The factors affecting the size distribution and microbubble rise velocity are also enunciated.

3.2 Theoretical Background

The need to understand the phenomenon associated with multiphase flows has inspired the development of numerous techniques over the last decade that can specify the shape and volume of bubbles with improved accuracy and high-speed. The most used methods to determine bubble size are high-speed photography, electrical impedance tomography, capillary suction probes, optical probes and capacitance probes (Vazquez et al., 2005).

3.2.1 Terminal rise velocity

The terminal bubble rise velocity in stagnant liquid is mainly governed by the buoyancy force and the drag force experienced by the bubble. The existence of wakes if any behind the bubbles can affect the motion of bubble. Tsuge and Hibino (1972) reported that wake effect influences the bubble rise velocity in the diameter range 5×10^{-3} to 9×10^{-3} m whereas Marks (1973) observed no influence of wake for air bubbles in water for diameter less than 1200 µm. Generally three main theoretical approaches are available in literature to calculate the rise velocity of bubbles, namely force balance approach, dimensional analysis and the wave analogy approach (Kulkarni and Joshi, 2005). In force balance approach the terminal velocity

is calculated from the balance of buoyancy and drag force. Under this approach, it is assumed that the bubbles are perfectly spherical, no internal circulation within the bubble and no slip exist at the boundary. The most illustrative solutions are observed in creeping and potential flow, when the bubbles are small and viscous force dominates (Harper, 1972). The wave analogy is proposed by Mendelson (1967) to predict the rise velocity, based on the assumption that behaviour of rising bubbles is strikingly similar to the behaviour of surface waves propagated over deep water. However the wave analogy presents best results when the bubble size is less than 5×10^{-4} m. Later on Lehrer (1976) modified the wave theory by stating that during the rise of bubble, potential energy of bubble is converted into kinetic energy and finally it is dissipated by the wakes. Fan and Tsuchiya (1990) developed a correlation to determine the terminal rise velocity of bubble applicable for pure and contaminated system. If the equivalent radius of bubble is smaller than 100 μm, the shape of bubble remains almost spherical and the bubble behaves like a solid sphere and if the equivalent radius of bubble increases, a change in bubble shape from spherical to ellipsoidal to spherical cap can occur. The radius at which these transitions occur depends on the physicochemical properties of the liquid (Haberman and Morton, 1953). When the size of bubble reaches to micron level, i.e. Reynolds number approaches to zero, bubbles can be considered as a rigid spherical body. Thus the terminal rise velocity of microbubble (U_b) can be described by Stokes' law (Takahashi, 2005). Stokes (Stokes, 1851) expressed the terminal rise velocity of bubble in a viscous liquid at low Reynolds number as

$$U_b = \frac{d_{mb}^2 g\left(\rho_l - \rho_g\right)}{18\mu_l} \tag{3.1}$$

where g is acceleration due to gravity. ρ_l and ρ_g represent the densities of liquid and gas respectively. d_{mb} denotes diameter of microbubble.

3.3 Experimental Procedure

3.3.1 Estimation of Bubble Size Distribution and Rise Velocity

In the present work laser diffraction technique, photo graphic and gas disengagement techniques were used to calculate the microbubble size. The laser diffraction method delivers rapid bubble size distributions over millimeter, micrometer and nanometer ranges. A typical bubble size distribution measured by particle size analyzer (Model-APA 2000, Malvern Instruments Ltd., Malvern, UK) is shown in Figure 3.1.

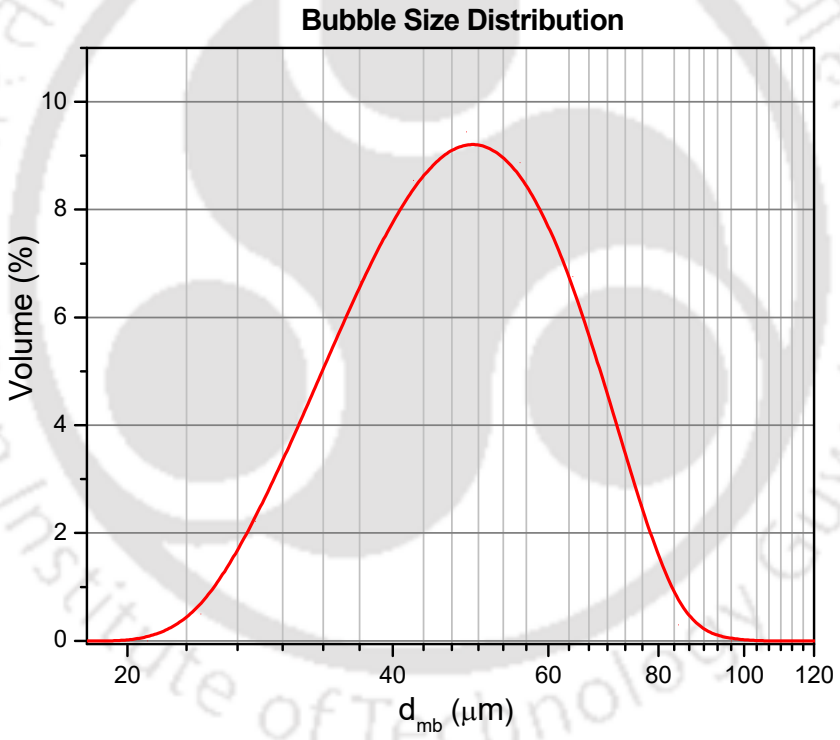

Figure 3.1: Typical microbubble size distribution in water without surfactant.

Freshly prepared microbubbles were transferred to the measuring chamber of the particle size analyser which containing a viscous liquid, to avoid easy escape of microbubbles. Laser diffraction measures particle size distributions by measuring the angular variation in intensity of light scattered as a laser beam passes through a dispersed microbubble sample. Large

particles scatter light at small angles relative to the laser beam and small particles scatter light at large angles. The angular scattering intensity data is then analyzed to calculate the size of the particles responsible for creating the scattering pattern, using the Mie theory of light scattering. The particle size is reported as a volume equivalent sphere diameter (Stojanović et al., 2012). The size of microbubble was also determined by using photographic method. The schematic representation of bubble size measurement by photographic method is shown in Figure 3.2. Microbubbles from the microbubble generator were filled in a glass cell. The principle of method of microbubble generation is described in Chapter 2.

A CCD camera (Model-PCO Pixelfly-USB,PCO Ltd Germany) having a resolution of 1360 ×1024 pixels in conjunction with a macro zoom lens (Navitar) was used to capture the images of microbubbles inside the cell. The images were recorded with a frame rate of 19 frames per second and stored in a computer. The digital photographs were further processed and enhanced by using Image Processing Software (Image J 1.48v). The size of the bubble was estimated by the same software and a total 300-400 bubbles were examined to determine the size. A typical snapshot of the microbubble at 15 ppm SDS is shown in Figure 3.3.

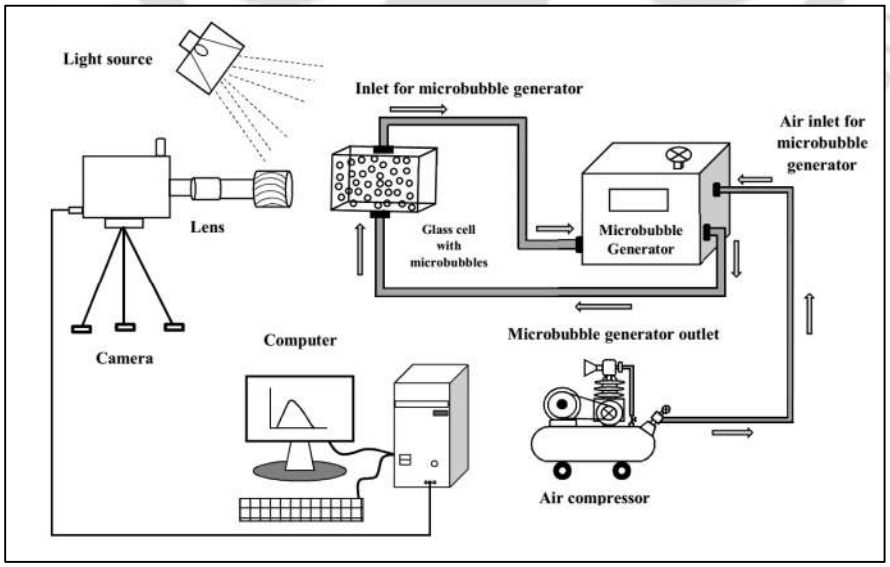

Figure 3.2: Schematic representation of bubble size measurement by photographic method.

The mean bubble diameter was considered and calculated as Sauter mean bubble diameter. The Sauter mean bubble diameter of microbubble (D_{vs}) is defined as the volume-to-surface mean bubble diameter and it is calculated by (Majumder et al., 2006)

$$D_{vs} = \frac{\sum_{i=1}^{N} N_i D_{bi}^3}{\sum_{i=1}^{N} N_i D_{bi}^2} \tag{3.2}$$

where N_i is the number of bubbles of diameter D_{bi}.

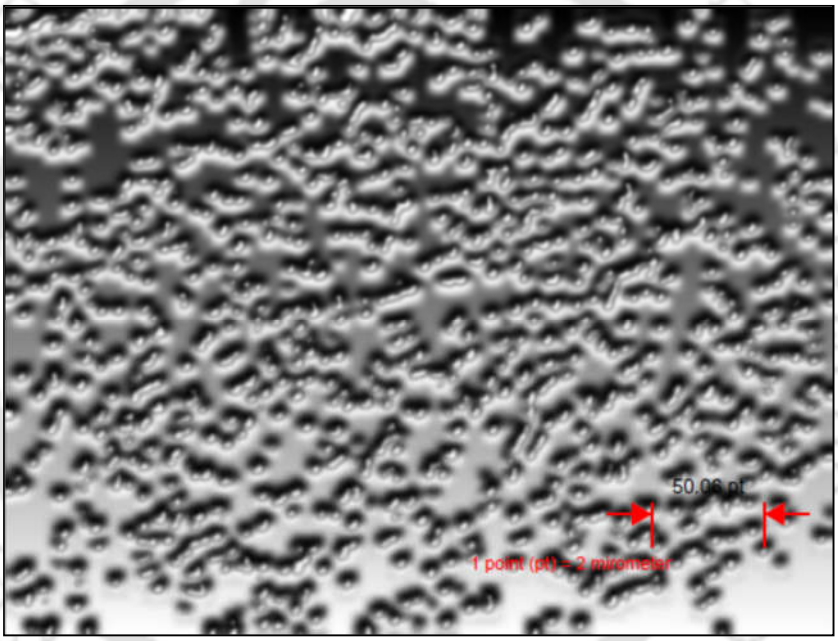

Figure 3.3. Typical snapshot of microbubbles at 15 ppm SDS.

Jauregi et al. (2000) and Amiri and Woodburn (1990) used gas disengagement method to determine the size of microbubble. The same principle is also used in the present work to determine the bubble size. The two main assumptions in this method are (i) microbubble are monosized and spherical and (ii) there is no coalescence and breakup of microbubbles in the suspension. Liquid containing dispersed microbubbles was delivered from the microbubble generator in a short span of time to a transparent graduated glass cylinder (0.03 m i.d.).

Immediately the cloud of microbubbles in the suspension starts rising due to buoyancy, leaving a clear liquid interface as shown in Figure 3.4(a). The rising trajectories of the microbubbles were recorded by a high definition camera (Sony DSC-HX10V). The camera was placed approximately 0.20 m away from the glass cylinder wall on a tripod stand and the background of the glass cylinder was made black for clear vision of the bubble cloud (Figure 3.4(b)).

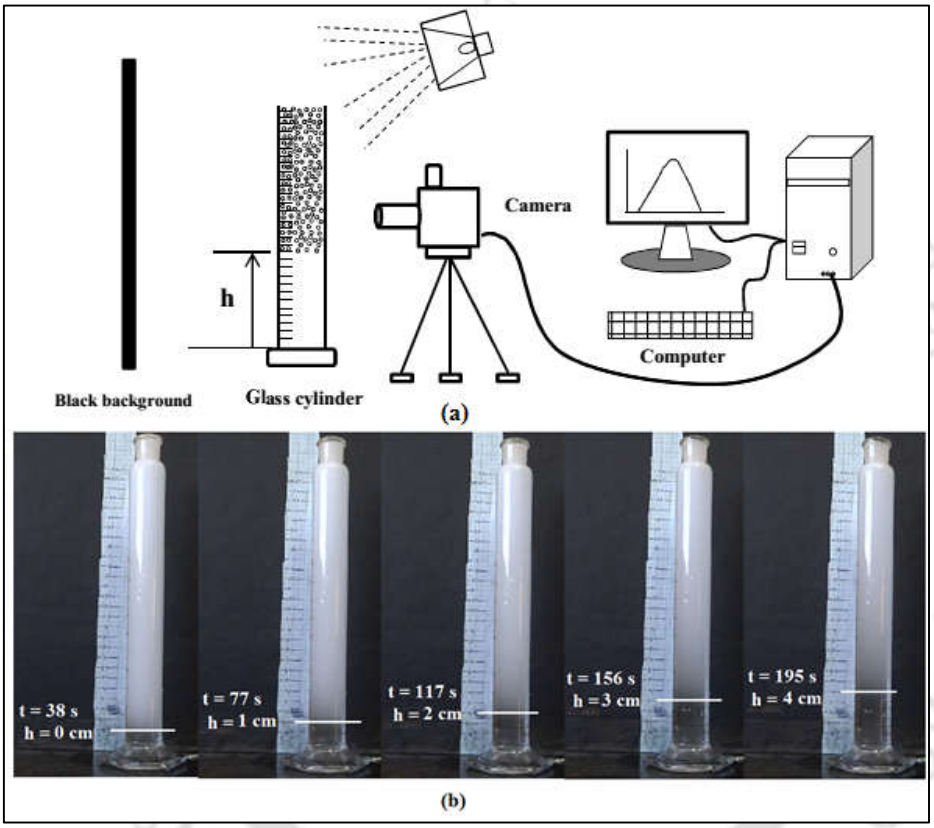

Figure 3.4: (a) Schematic diagram of rise velocity measurement; (b) Experimental photograph of estimation of bubble rise velocity.

The motion of microbubble rising in a stagnant liquid is well described by Stokes' law (Takahashi, 2005). If it is assumed that there is no coalescence and breakup of microbubble, then diameter of the microbubble rising in a stagnant liquid can be calculated by

$$d_{mb} = \sqrt{\frac{18\,\mu_l U_b}{g\left(\rho_l - \rho_g\right)}} \tag{3.3}$$

The rise velocity of the microbubbles can be easily calculated from the distance moved by swarm of microbubbles between two label on the scale and the time interval taken between those labels as per Eq. (3.4).

$$U_b = \frac{h_2 - h_1}{t_2 - t_1} \tag{3.4}$$

where h_1 and h_2 are position of swarm of bubbles at time t_1 and t_2 respectively.

3.4 Physical Properties of the System

In the present work, aqueous solutions of sodium dodecyl sulphate (SDS), cetyl trimethyl ammonium bromide (CTAB), Tween-20, sodium carboxymethyl cellulose (SCMC) and glycerol were used as liquid phase whereas air, nitrogen and carbon dioxide were used as gas phase. All the experiments in the present work were carried out at 25° C. Each test was repeated five times by repeating the above procedure. The physical properties of SDS, CTAB and Tween-20 has been reported in Table 2.1. The physical properties of SCMC, glycerol and gases are given in Table 3.1.

Table 3.1: Physical properties of system measured at 25 ± 1 ºC.

Type of Fluid	Concentration in water*	Density (kg/m^3)	Surface tension (mN/m)	Viscosity (mPa·s)
SCMC-1	0.25	1000.08	78.40	2.650
SCMC-2	0.50	1000.65	74.25	4.220
SCMC-3	0.75	1000.72	71.91	5.910
SCMC-4	1.00	1000.94	70.30	7.020
Glycerol-1	5	1020.864	66.01	1.200
Glycerol-2	10	1039.14	63.00	1.450
Glycerol-3	15	1057.82	60.00	1.800
Glycerol-4	20	1068.33	57.02	2.000
Air	-	1.18	-	0.018
Nitrogen	-	1.14	-	0.017
Carbon dioxide	-	1.78	-	0.015

* The units are in kg/m^3 for SCMC; in wt % for Glycerol

3.5 Results and Discussion

3.5.1 Effect of Physicochemical Properties of Liquid on Size Distribution of Microbubble

Bubble populations have significant impact on the hydrodynamics as well as heat and mass transfer characteristics of two-phase flow. The bubble size distribution of microbubbles obtained from image analysis with different surfactant concentrations is shown in Figure 3.5. The average size of microbubble without surfactant is approximately 52 μm. Addition of surfactant in water alters the interfacial surface tension. It was observed that the microbubble size decreased with increase in surfactant concentration. Surfactant lowers the surface energy of the gas-liquid interface and thus create smaller bubble. SDS is a strong surfactant, even low concentrations of SDS in the liquid are capable of reducing bubble sizes.

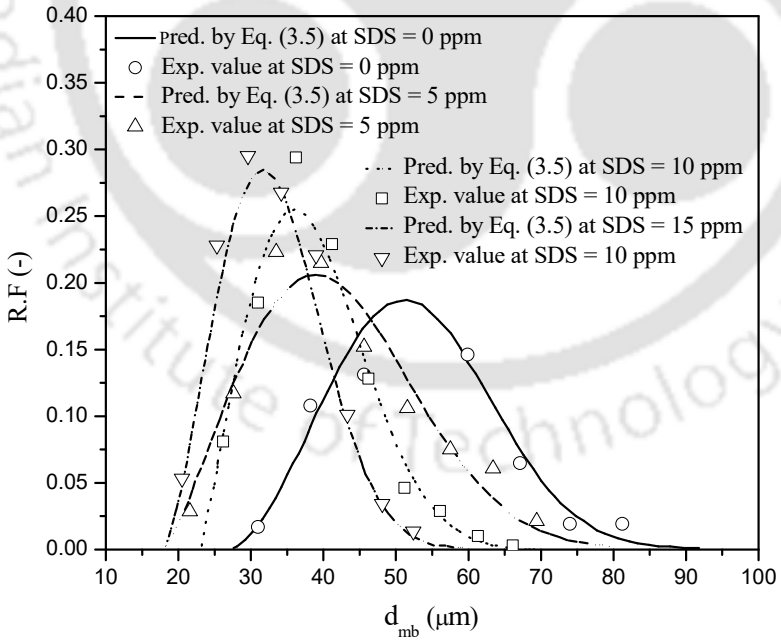

Figure 3.5: Bubble size distribution for microbubble by photographic method at different surfactant concentration.

The population of microbubble also increased with increasing surfactant concentration. Coalescence of smaller bubbles also reduced with increasing the surfactant concentration. Couto et al. (2009) also analysed the microbubble size distribution and reported a decrease in bubble size with addition of surfactants (Flotigam and sodium oleate). In the present work the obtained bubble size distribution data was analysed by using STAT::FIT software. It was observed that Weibull distribution function describes the microbubble size distribution with least error in all sets of data. Typical results for the goodness of fit for the different distributions are given in Appendix-II. A typical bubble size distribution with the experimental data for 10 ppm surfactant concentration is shown in Figure 3.6.

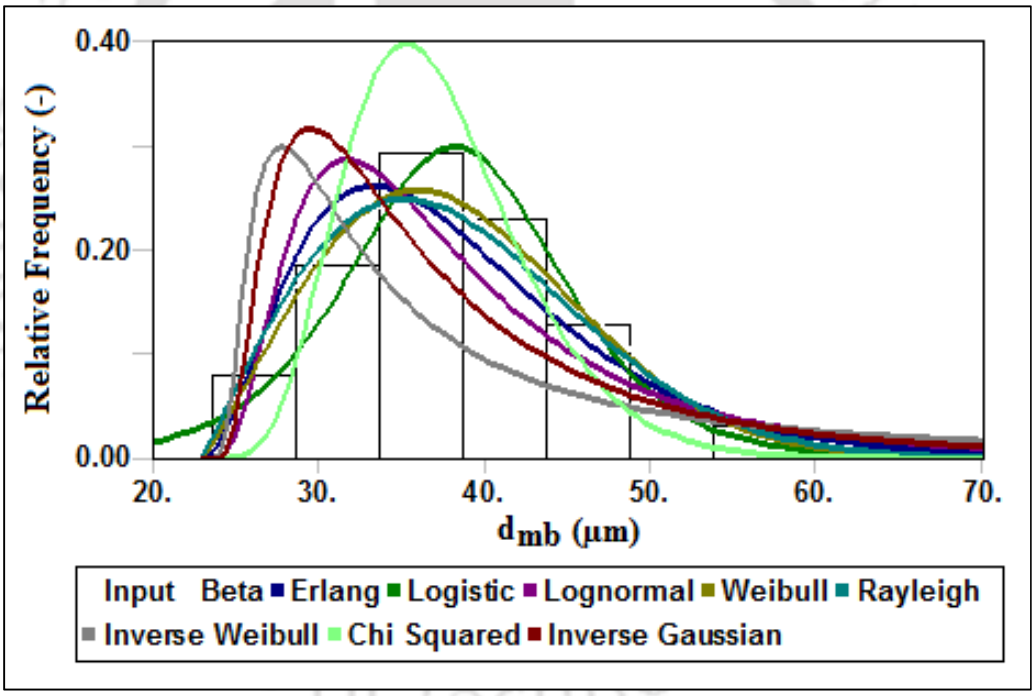

Figure 3.6: Bubble size distribution of microbubble with 10 ppm SDS concentration.

The bubble size distribution as per Weibull distribution can be expressed as

$$f(d_{mb}) = \frac{\Omega}{\psi}\left(\frac{d_{mb}-\chi}{\psi}\right)^{\Omega-1} \exp\left[-\left(\frac{d_{mb}-\chi}{\psi}\right)^{\Omega}\right] \qquad (3.5)$$

where the parameter Ω, ψ and χ found to be dependent on the surface tension (σ) of the liquid and can be correlated with the surface tension as

$$\Omega = 6.0\times10^{-5}\sigma^{-3.809} \quad R^2 = 0.9928 \tag{3.6}$$

$$\psi = 1.0\times10^{10}\sigma^{7.4334} \quad R^2 = 0.9434 \tag{3.7}$$

$$\chi = 1.19\times10^{4}\sigma^{2..342} \quad R^2 = 0.979 \tag{3.8}$$

It was observed that the microbubble size distribution becomes narrow with increase in glycerol concentration (C_g) as shown in Figure 3.7. The bubble size distribution of microbubble is highly affected by properties of gas and liquid.

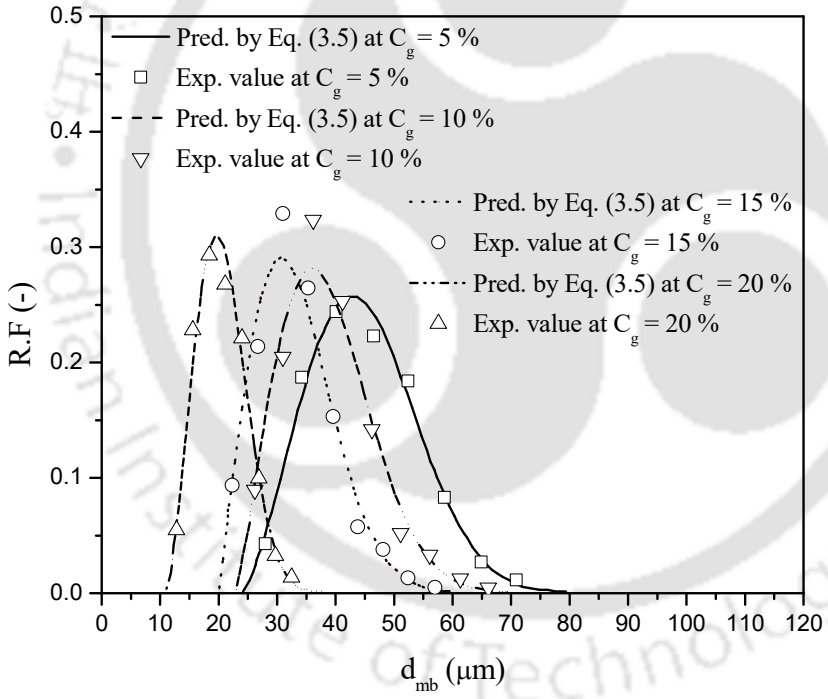

Figure 3.7: Effect of glycerol on bubble size distribution of microbubble.

Viscosity and surface tension are two important parameters that may change the size of microbubble. An increase in viscosity of liquid may weaken the liquid turbulence intensity inside the microbubble generator and decrease the degree of mixing, causing increase in bubble

size. But in the present experiment, the viscosity of glycerol solution does not change significantly. Hence the reduction of bubble size in glycerol solution was mainly caused by the reduction in surface tension. A generalised correlation to predict the microbubble size obtained from particle size analyzer with surface tension is developed and can be expressed as

$$d_{mb} = 0.4258\sigma^{3.406} \qquad 57 \leq \sigma \leq 72 \text{ mN/m} \qquad (3.9)$$

The dependency of microbubble size obtained from different methods on surface tension in different liquids is shown in Figure 3.8.

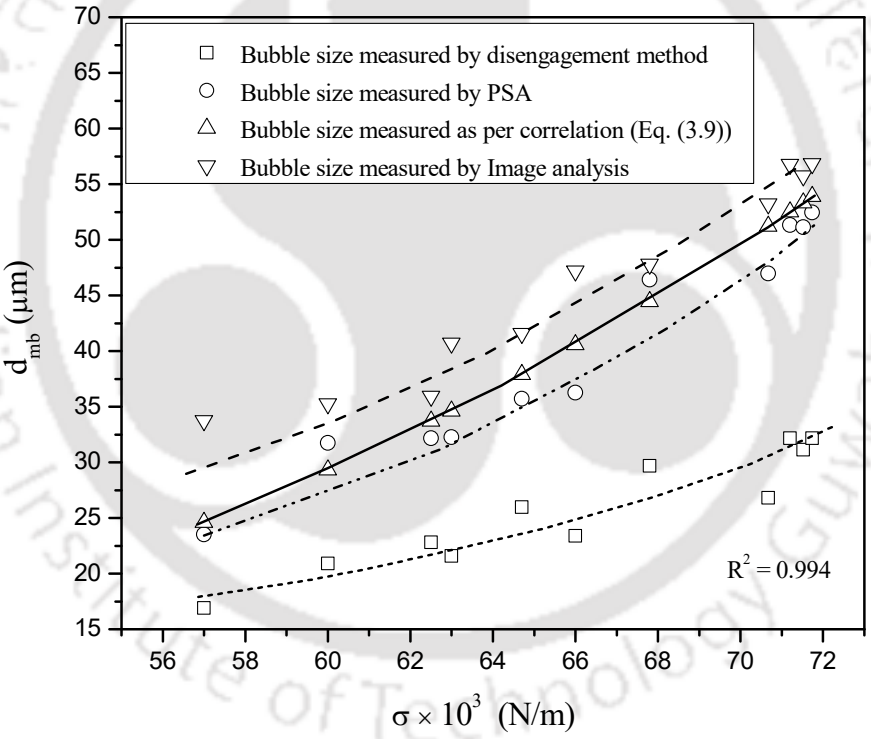

Figure 3.8: Comparison of microbubble size obtained from different methods in different liquids.

It is clear that within the low range of viscosity the microbubble size totally depends on gas liquid interfacial tension. The microbubble size determined by the particle size analyzer can be

considered as the most accurate among all the three methods. As light scattering technique usually gives more precise results for bubble less than 0.1 mm diameter. The probability of error with the diffraction technique is less. It is seen that the bubble size predicted by image analyses are found to be higher than the laser particle size analyzer. In the present work it has been observed that the bubble size predicted by analysis of image is approximately 15 % more than predicted by particle size analyzer. The accuracy of photographic method decreases as the bubble size reduces (Mohammadi and Sharp, 2013). The results of photographic process rely on the wall curvature, parallax bubble count, etc. (Majumder et al., 2006). Therefore the bubble size measured by photographic method is higher than particle size analyzer. The standard uncertainty of measuring the bubble diameter was in the range of 4.15×10^{-7}–6.5×10^{-7}. It is also observed from the Figure 3.8 that the bubble size measured by disengagement method is least out of these three methods. The microbubble size measured by disengagement method is nearly 30 % less than those measured by particle size analyzer. The bigger microbubbles rise at faster rate as compared to smaller bubble. The bubble size calculated by Stokes' equation where the rise velocity of microbubble is estimated by the disengagement method (as shown in Figure 3.4(b)), which accounts only for smaller bubble as the larger bubble rise early in the suspension. Therefore the disengagement method gives microbubble size lower than that the actual value. The average size of microbubble produced by the microbubble generator is predicted by (Evans et al., 1992)

$$d_{mb} = \phi \frac{\sigma^{0.6}}{P_{in}^{0.4} \rho_l^{0.2}} \tag{3.10}$$

where ϕ is a constant and P_{in} is the power input per unit volume. The power input per unit volume is equal to the product of microbubble suspension velocity, acceleration due to gravity and density of suspension that comes from microbubble generator outlet (Chisti and Moo-Young, 1988). The stability of microbubble depends on the parameter ϕ. The parameter ϕ

resembles with critical Weber number, reported by Hinze (1955) for bubble breakup in viscous shear flow. The author reported that the value is 1.18 for conventional bubbles. Sevik and Park (1973) found a value of 1.24 for critical Weber number in their system. Ryskin and Leal (1984) observed a functional dependency of critical Weber number with Reynolds number. They found values of critical Weber number in the range of 0.95-2.76. The stability of bubble in the turbulent mixing depends on the Weber number. Up to a certain Weber number the bubbles remain stable, and bubbles will split once a critical value is reached. In the present study, the microbubble are stable and the parameter ϕ was found to be 0.125 to 0.165 which is less than all critical weber number reported by various investigators.

3.5.2 Effect of Addition of SCMC on Rise Velocity of Microbubble

The effects of SCMC concentration on terminal rise velocity of microbubble with different gases is shown in Figure 3.9.

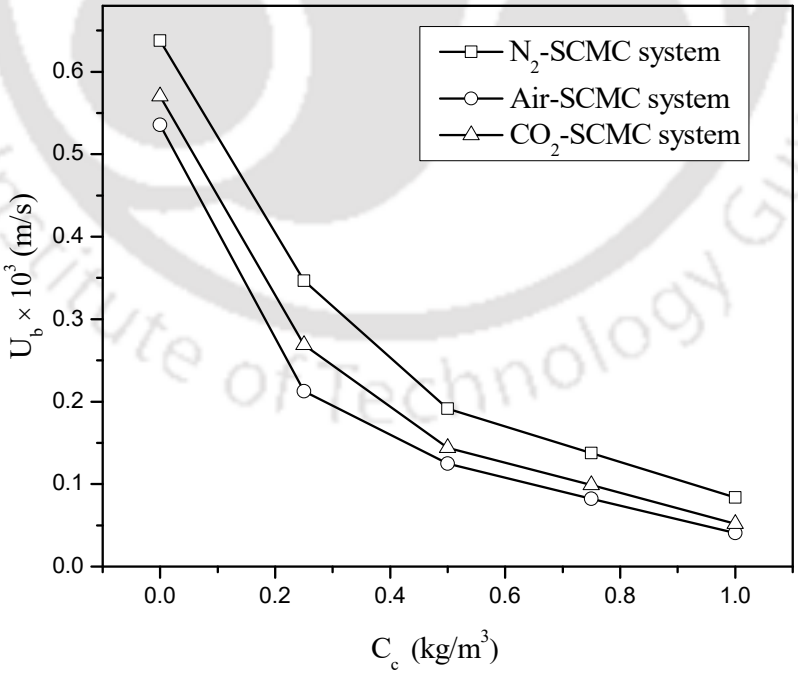

Figure 3.9: Variation of microbubble terminal rise velocity with SCMC concentration.

It is observed that the microbubble rise velocity for all the gases decreases with increase in concentration of SCMC. The rise velocity of bubble in a still liquid is mainly governed by the buoyancy force, weight and drag force. The rise velocity is a function of gas density, viscosity of liquid and bubble size (as per Stokes' law). The decrease in microbubble size is also one of the factor which may be contributed by increase in concentration or change in interfacial tension. However in the present experimental range, the surface tension of SCMC solution changes slightly. Another possible mechanism can be attributed from the fact that the viscosity of solution significantly increases with increase in concentration of SCMC, which probably increases the drag force experienced by the microbubble, due to which the rise velocity decreases. Garabedian (1957) reported that bubble rise velocity strongly depends on viscosity and decreases with increasing viscosity. A similar observation is reported by Margaritis et al. (1999) and Tzounakos et al. (2004). The increase in apparent viscosity was attributed to the main cause of the decrease in velocity. Theoretically the order of rise velocity for the gases for same concentration of SCMC in liquid is $U_{b\text{-}Nitrogen} > U_{b\text{-}Air} > U_{b\text{-}carbondioxide}$. However experimentally it is observed that the CO_2 microbubble shows a higher rise velocity than air microbubble. This may be due to the higher solubility of CO_2 as compared to air. The dissolution of CO_2 in water is also complicated as it forms carbonic acid with water. However such chemical reaction is not observed in case of air and nitrogen (Parkinson et al., 2008). Another clarification for the higher rise velocity of CO_2 is the reduction of viscosity of the liquid at the interface (Caw and Wylie, 1961). Parkinson et al. (2010) observed an enhancement in rise velocity of CO_2 microbubbles in water in the microbubble range 10–100 μm. They reported that the presence of diffusion boundary layer was responsible for the enhancement.

3.5.3 Effect of Addition of Surfactants on Rise Velocity of Microbubble

The effect of surfactants on microbubble rise velocity is shown in Figure 3.10. It is observed that for all the surfactants microbubble rise velocity reduces as the surfactant concentration

increases in water. The increase in surfactant in water reduces its surface energy. The density of liquid does not change significantly by addition of surfactant in the liquid. The reduction of surface energy causes a production of smaller microbubble by microbubble generator. Accumulation of surfactant molecules at the surface may also cause to the decrease in velocity. When a bubble moves in a liquid, the surfactant molecules present at interface are rapidly absorbed and swept to the rear of the gas-liquid interface, leaving frontal region relatively uncontaminated, which causes an additional shear on trailing pole of the bubble due to concentration gradient. This shear retards the motion of bubble due to which microbubble rise velocity decreases.

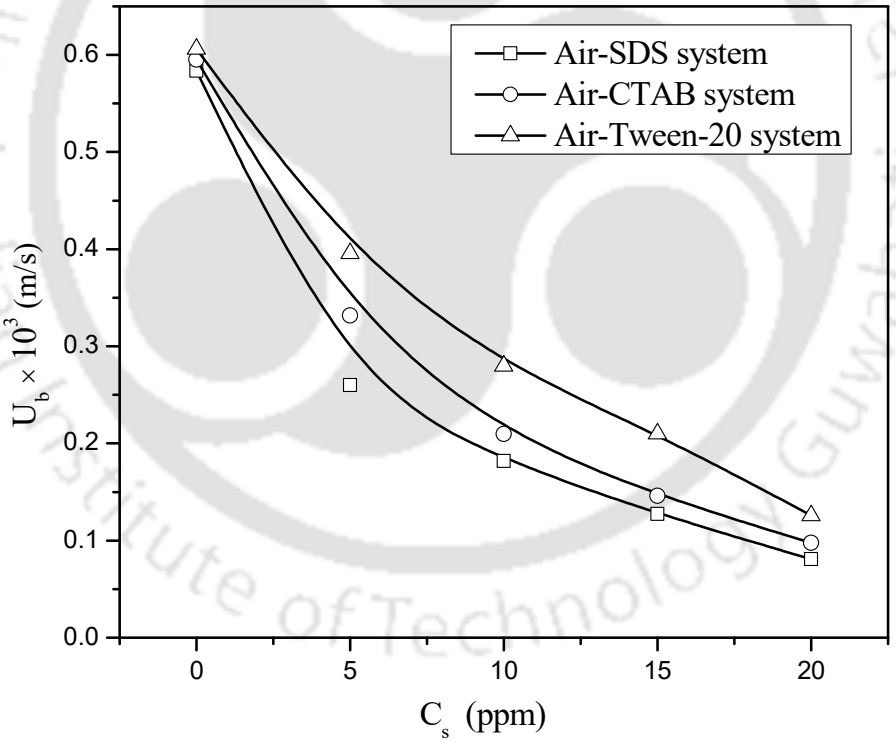

Figure 3.10: Variation of microbubble rise velocity with surfactants concentration.

Frumkin and Levich (1947) also reported that presence of surfactant at the interface causes an additional tangential stress tending to retard the motion of bubbles. Fuerstenau and Wayman

(1958) examined the retardation of rise velocity of bubbles in presence of surfactant, however the author explained that retardation is caused by reductions in internal circulation and boundary slip. The circulation becomes considerable whenever skin friction becomes leading surface force (Hughes and Gilliland, 1952). The internal circulation of gas inside the bubble depends on the accumulation of surfactant at the interface. Surfactant tends to reduce internal motion of bubble by rendering at the interface (Scheid et al., 1999).

3.5.4. Effect of addition of Glycerol on Terminal Velocity of Microbubble

The hydrodynamic drag experienced by the bubble significantly increases with increase in viscosity and density of liquid. The addition of glycerol in water increases the density as well as viscosity of solution. The effect of glycerol concentration on terminal microbubble rise velocity is shown in Figure 3.11.

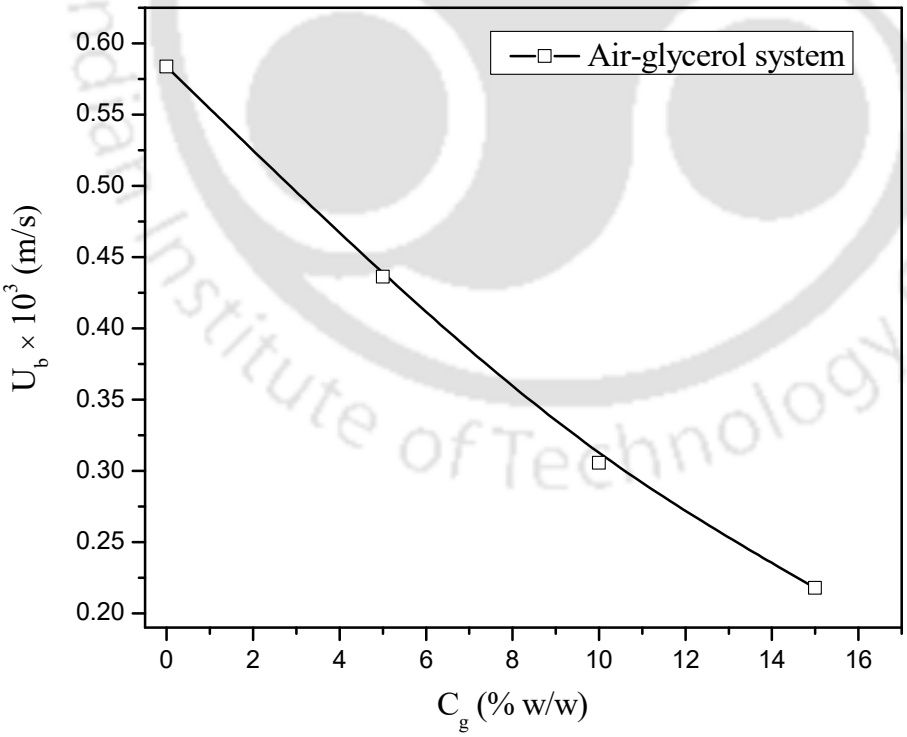

Figure 3.11: Variation of microbubble rise velocity with glycerol concentration.

A reduction in the rise velocity is seen on addition of glycerol in water. Glycerol is completely soluble in water and it is strongly adsorbed at the interface. As a consequence, the surface tension or surface energy of gas-liquid interface decreases and viscosity of the solution increases. Increase in viscosity increases the hydrodynamic drag and decrease in surface tension reduces the microbubble size. Both the factors reduce terminal rise velocity of microbubble. Many investigators reported the reduction of terminal velocity in presence of alcohol. Peeble and Garber (1953) undertook a detailed examination of terminal rise velocity of air bubbles in different organic liquids. Addition of alcohol not only decreases the bubble rise velocity, it also reduces the coalescence tendency of the bubble (Levich, 1962). In the present work it is found that the microbubble size is a function of surface tension wielding in gas-liquid interface. Decrease in surface tension reduced the bubble size. Addition of alcohol reduces the surface tension, which ultimately reduces bubble size. At the liquid side of the gas-liquid interface the glycerol molecules form a monolayer whose stability depends on concentration. The molecules of glycerol points with their hydrophilic group into the liquid, and with their hydrophobic part into the gas phase. On account of this orientation, the liquid surface around gas bubbles is electrically charged. The microbubble surface polarization produces repulsive forces when two microbubbles come close to each other. Thus they increase stability by inhibiting the coalescence. The trend of the curve obtained in the present study is similar to that reported by Jamialahmadi and Müller-Steinhagen (1992). The addition of alcohol, reducing the bubble size, increases the bubble stability and the effect becomes more pronounced as the molecular weight of the solvent increases (Jamialahmadi and Steinhagen, 1990). The free rise velocity decreases with increasing viscosity with the possibility of reduction of the interfacial motion due to viscous force (Rodrigue et al., 1996).

3.6 Conclusion

In the present work, the microbubble size distribution in different liquids have been studied. The effects of liquid and gas properties on the microbubble rise velocity are also investigated. The bubble size distribution of microbubble suspension for different concentrations was fitted to Weibull distribution. The motion of rising microbubble was found to be significantly affected by physicochemical properties of system. The microbubble size estimated by disengagement method was lower than that predicted by particle size analyzer, while the image analysis predicted bubble size higher than the particle size analyzer. At low viscosity, the microbubble size was found to be dependent on surface tension of liquid. The experimental results shows that increase in surface tension, viscosity and density of the liquid decreases the terminal rise velocity of microbubble. The terminal rise velocity of carbon dioxide microbubble was found to be higher than air and lower than nitrogen microbubble.

Notations

C_c	Concentration of SCMC (kg/m^3)
C_s	Concentration of SDS (ppm)
C_w	Concentration of Tween-20 (ppm)
C_t	Concentration of CTAB (ppm)
C_g	Concentration of glycerol (wt %)
d_{mb}	Microbubble diameter (m)
D_{sv}	Sauter mean bubble diameter (m)
$f(d_{mb})$	Bubble distribution function (-)
g	Acceleration due to gravity (m^2/s)
$h_{1\text{-}2}$	Position of microbubble (m)

N_i	Number of bubble in i^{th} class (-)
P_{in}	Power input per unit liquid volume (kg/s^2)
$R.F$	Relative frequency (-)
U_b	Bubble rise velocity (m/s)

Greek letters

μ_l	Viscosity of liquid (kg/m.s)
ρ_l	Density of liquid (kg/m^3)
ρ_g	Density of gas (kg/m^3)
σ	Surface tension (N/m)
Ω	Parameter defined in Eq. (3.6) (-)
ψ	Parameter defined in Eq. (3.7) (-)
χ	Parameter defined in Eq. (3.8) (-)
ϕ	Parameter defined in Eq. (3.10) (-)

CHAPTER-4

FLOW CHARACTERISTICS OF MICROBUBBLE

In the previous chapter investigations of the effects of physicochemical properties of liquids on terminal rise velocity and microbubble size distribution have been reported. This chapter reports the flow characteristics of microbubble suspensions. A mechanistic model has been developed to analyze the interfacial stress of microbubble suspension flow in pipe by considering the bubble formation, drag at interface and loss of energy due to wettability. Correlations have been developed to interpret the gas holdup, friction factor and drag coefficient of microbubble suspension flow.

4.1 Introduction

Dispersed microbubble flow has received a considerable attention in the last two decades. It has become an important research area due to its wide range of applications and its effect on many processes to enhance the efficiency of devices. The hydrodynamic characteristics of microbubble are the main process parameters of dispersed microbubble flow process, as designing of the unit mainly rely on them. The size of micro bubbles is smaller than micro turbulent scale. It is therefore expected that the bubbles with diameter smaller than the micro turbulent scale may exhibit different behaviors from those shown by ordinary sized bubbles, specifically in the way of hydrodynamic interactions with the flow and thus the two-phase flow structures may be changed. Yamaguchi et al. (2001a) was among the pioneer investigators who examined the hydrodynamic behaviour of dispersed microbubbles. They examined the microbubble behaviour associated with the flow pattern, when the fluid enters a rotating pipe section from a stationary pipe. The authors observed a unique flow pattern by the bubble

assembly in the rotating flow field. The work was further extended by Yamaguchi et al. (2001b). The authors provided a numerical simulation for microdispersed bubbly flow in a suddenly expanded rotating section. The most important phenomena of dispersed microbubble flow is that the two-phase flow becomes laminarized by injecting micro bubbles. The flow laminarization can takes place even at low gas holdup of 0.2% (Serizawa et al., 2003). The gas holdup of microbubble flow is significantly affected by the surfactant concentration. Addition of surfactant in the microbubble suspension can significantly enhance the gas holdup. However, no qualitative information is available in literature to correlate the gas holdup of microbubble with surfactant concentration (Aslan et al., 2006).

The local liquid velocity in dispersed microbubble flow follows nearly a 1/7-power law at high Reynolds numbers in turbulent flow and a little bit flattened profile in radial direction at lower Reynolds numbers in near laminar flow (Serizawa et al., 2003). Microbubbles suspended in liquid undergo various phenomena for mathematical formulation. Complicated interactions like collisions and coalescences between adjacent bubbles, interactions between bubbles and the pipe wall, and transfiguration of bubbles affect the local conditions of the flow field, causing fluctuations in static pressure and in velocity (Kawara et al., 2007). In most of the applications of microbubble suspension, the microbubble is pumped through columns, pipes or fittings or the applications executed by the effects of microbubble flow behaviour in the devices. However it is difficult to transport large flowrates of microbubble suspensions through these pipes as the flow rheology completely differs from the single phase flow (Deshpande and Barigou, 2001). Larmignat et al. (2008) studied the rheology of two phase mixture having bubble diameter in the range 10 to 100 μm and gas holdup in the range 0.6-0.75. They reported that rheology of two phase mixture is affected by surfactant concentration in the mixture and not affected by pipe shape and hydraulic diameter. Tseng et al. (2006) studied the rheological behavior of two phase mixture in mini-channel having porosity in the range of 0.64-0.70. They

reported that the fluid behaves as a shear-thinning under experimental condition. Other researches on rheology, are mainly focused on the rheological properties of gas-liquid mixture having high gas holdup or porosity (Briceño and Joseph, 2003; Calvert and Nezhati, 1986; Enzendorfer et al., 1995; Khan and Armstrong, 1986; Kraynik and Hansen, 1987; Raza and Marsden, 1967). However the rheological behavior of gas-liquid mixture of high gas holdup may differ from that of gas-liquid mixture of low gas holdup. Shen et al. (2008) studied the rheological behaviour of concentrated monodispersed food emulsifier-coated microbubble suspensions. They observed that the viscosity of the system decreased as the shear stress increased, indicating that microbubble suspension is shear-thinning in nature. Several studied reported reduction of friction factor in microbubble flow as compared to single phase flow (Kodama et al., 2000; Madavan et al., 1984). The drag reduction by microbubble suspension is found to be affected by gas holdup and curvature of pipes (Shatat et al., 2009; Wu et al., 2008) while the types of gas and bubble diameter do not affect friction reduction (Fontaine and Deutsch, 1992; Moriguchi and Kato, 2002; Shen et al., 2006). Kato et al. (1998) reported that bubble smaller than certain diameters, can only effect on friction of microbubble induced flow. Recently Haapala et al. (2010) studied the hydrodynamic drag of microbubbles in papermaking process.

From the above literature review it is observed that reliable correlations are available for predicting the pressure drop, gas holdup and the rheological behaviors of flow containing dispersed microbubbles, but information on the effect of surfactant concentration on dispersed microbubble flow and modeling is rare. To achieve technical feasibility of the microbubble flow behaviour, a detailed study of transport phenomena of dispersed microbubbles is required. In the present study with vision of engineering importance as well as scientific attentiveness, the rheological behaviors of flow containing dispersed microbubbles in pipe with different concentrations of surfactant have been investigated. A mechanistic model has been developed

to analyze the interfacial stress of microbubble suspension flow in a pipe by considering bubble formation, drag at the interface, and loss of energy due to wettability. Correlations between the intensity factor of interfacial stress and the friction factor based on energy loss due to wettability are also developed. The functional form of the correlation appears to predict the hydrodynamics satisfactorily for the flow of a microbubble suspension in a pipe.

4.2 Theoretical Background

4.2.1 Properties of Microbubble Suspension Flow

Microbubble suspensions behave as non-Newtonian shear-thinning (pseudoplastic) fluids (Shen et al., 2008). For pseudoplastic fluids, the most common model relating the wall shear stress (τ_w), wall shear rate (γ_w) and apparent shear rate (γ_a) is a power-law model, given by

$$\tau_w = \mu_e \gamma_a = K \gamma_w^n \tag{4.1}$$

where n is the flow behaviour index and K is the flow consistency index. The apparent shear rate and wall shear rate are related as

$$\gamma_w = \left(\frac{3n+1}{4n} \right) \gamma_a \tag{4.2}$$

The wall shear stress (τ_w) and apparent shear rate (γ_a) were experimentally determined from volumetric flow rate (Q) and pressure drop (ΔP) according to the relations (Enzendorfer et al., 1995)

$$\tau_w = \frac{D_h \Delta P}{4Z} \tag{4.3}$$

$$\gamma_a = \frac{32Q}{\pi D_h^3} \tag{4.4}$$

4.2.2 Analysis of Interfacial Shear Stress in Microbubble Suspension Flow

The fluid dynamics of a microbubble-liquid mixture flow through a pipe is described in this section using an internal flow model. The dynamic interaction of the phases is taken into account in modeling the flow by introducing the rate of energy dissipation. The mechanical energy balance is used to calculate the pressure drop which can be regarded as either the force per unit cross sectional area required to overcome frictional forces or the energy dissipation per unit volume. The model is presented with the following assumptions:

(i) The flow is steady and isothermal with uniform gas holdup.

(ii) Acceleration effect is negligible due to the absence of interphase mass transfer.

(iii) Uniform frictional loss is assumed throughout the pipe.

The mechanical energy balance equation for the microbubble-liquid mixture is given by

$$\Delta P_{l-mb} A_t U_m - E = 0 \tag{4.5}$$

where $\Delta P_{l\text{-}mb}$ is the frictional pressure drop in liquid microbubble suspension, U_m is the velocity of mixture and A_t is the cross sectional area of the pipe.

In Eq. (4.5), the first term is energy due to liquid-microbubble flow pressure (N.m/s) and second term (E) represents the energy dissipation per unit mixture volume due to friction between the microbubble wall and the liquid (E_l) and due to the wettability between the liquid and the pipe wall (E_w). Then, Eq. (4.5) can be represented as

$$\Delta P_{l-mb} = E / U_m A_t \tag{4.6}$$

The energy dissipation (E_l) at the microbubble-liquid surface occurs as a result of the drag force exerted by the liquid on the microbubble surface (Majumder et al., 2007). Equation (4.7)

describes the amount of energy (E_l) irreversibly converted into thermal energy due to friction. The total energy dissipation can be calculated from the product of the force exerted by the liquid on a single bubble (F_d), the liquid velocity, and the bubble population, which can be represented as

$$E_l = F_d(U_{sl}/\varepsilon_l)N_b = C_m \frac{1}{4}\pi d_{mb}^2 \frac{1}{2}\rho_l (U_{sl}/\varepsilon_l)^2 (U_{sl}/\varepsilon_l)N_b \quad (4.7)$$

where C_m is the hydrodynamic drag coefficient of microbubble flow in the fluid, ε_l is the liquid holup, d_{mb} is the bubble diameter, and ρ_l is the density of the liquid. The bubble population (N_b) can be calculated as

$$N_b = \frac{L(1-\varepsilon_l)A_t}{(1/6)\pi d_{mb}^3} \quad (4.8)$$

The rate of energy loss due to the wettability of the liquid with the surface of the pipe wall is the summation of the energy loss due to wettability between the liquid and the surface of the column wall and the energy loss due to the wettability between the liquid and the surface of the bubble. This can be represented as

$$E_w = \frac{\pi d_t U_{sl}\sigma_{lw}}{\varepsilon_l} + \frac{U_{sl}\sigma_{l-mb}}{a\varepsilon_l} \quad (4.9)$$

where a is the specific interfacial area of bubble and liquid, σ_{lw} is the interfacial surface tension at the boundaries between the liquid and the wall and $\sigma_{l\text{-}mb}$ is the surface tension between liquid and microbubble. The specific interfacial area of bubble can be calculated from liquid holdup and bubble diameter (Deckwer, 1992)

$$a = \frac{6(1-\varepsilon_l)}{d_{mb}} \quad (4.10)$$

Wettability is the affinity of a solid matrix for aqueous phases. It is normally quantified by the value of the contact angle. A contact angle of $\theta < \pi/2$ indicates that the solid is wetted by the liquid whereas $\theta > \pi$ indicates non-wetting conditions. The limits θ equals to *0* and π defines complete wetting and complete non-wetting, respectively. The energy loss due to the wetting of the liquid depends on the dynamic contact angle between liquid and solid wall. The dynamic contact angle (θ) is approximately equal to $Ca^{1/3}$, where Ca is the capillary number which is defined as (Cubaud and Ho, 2004)

$$Ca = \frac{\mu_e U_{sl}}{\varepsilon_l \sigma_l} \tag{4.11}$$

The surface tension between the liquid and the solid wall (σ_{ls}) can be calculated from Young's equation as

$$\sigma_l \cos\theta = \sigma_{lw} \tag{4.12}$$

Here, σ_l represents the force needed to stretch an interface by a unit distance. According to the present study, the contact angle is less than 90º within a range of liquid velocity and the range of the capillary number is 0.011 to 0.032. Therefore Eq. (4.6) can be written as

$$\Delta P_{l-mb} = \left[\frac{1}{U_m A_t}\right]\left[(3/4)C_m \rho_l U_{sl}^3 A_t \frac{1-\varepsilon_l}{\varepsilon_l^3}\frac{L}{d_{mb}} + \frac{\pi d_t U_{sl}\sigma_{lw}}{\varepsilon_l} + \frac{U_{sl}\sigma_{l-mb}}{a\varepsilon_l}\right] \tag{4.13}$$

From the experiments the total pressure drop can be obtained as the frictional pressure drop due to liquid flow in the absence of a vertical hydrostatic pressure drop, which can then be expressed as

$$\Delta P_{l-mb} = \Delta P_{fl} = \left[\frac{1}{U_m A_t}\right]\left[(3/4)C_m \rho_l U_{sl}^3 A_t \frac{1-\varepsilon_l}{\varepsilon_l^3}\frac{L}{d_{mb}} + \frac{\pi d_t U_{sl}\sigma_{lw}}{\varepsilon_l} + \frac{U_{sl}\sigma_{l-mb}}{a\varepsilon_l}\right] \tag{4.14}$$

To determine the frictional losses due to liquid flow in the pipe, a model can be formulated on the basis of the following assumptions:

(i) The friction factor for the liquid phase is a constant multiple, α′, of that for a single liquid phase without bubbles taking place in the pipe.

(ii) The area of contact of the liquid phase with the wall is α″ times that of the flow of a single phase without bubbles in the pipe (Majumder et al., 2007).

From these assumptions, a simple overall momentum balance for liquid phase can be represented as

$$\frac{\Delta P_{fl}(Cross\,sectional\ area)_{l-mb}}{\Delta P_{fl0}(Cross\,sectional\ area)_{l0}} = \frac{(Wall\ \ shear\ stress)_{l-mb}}{(Wall\ \ shear\ stress)_{l0}} \times \frac{(Area\ of\ contact\ with\ wall)_{l-mb}}{(Area\ of\ contact\ with\ wall)_{l0}} \quad (4.15)$$

which implies

$$\frac{\Delta P_{fl} A_t \varepsilon_l}{\Delta P_{fl0} A_t} = \frac{(0.5 f \rho_l U_{sl}^2)_{l-mb}}{(0.5 f \rho_l U_{sl}^2)_{l0}} \times \frac{(Areaof\ contactwithwall)_{l-mb}}{(Areaof\ contactwithwall)_{l0}}$$
$$= \frac{f_{l-mb}}{f_{l0}} \cdot \frac{(U_{sl}^2)_{l-mb}}{(U_{sl}^2)_{l0}} \times \frac{(Areaof\ contactwithwall)_{l-mb}}{(Areaof\ contactwithwall)_{l0}} = \alpha_l' \cdot \frac{1}{\varepsilon_l^{\,2}} \cdot \alpha_l'' = \frac{\alpha_l}{\varepsilon_l^{\,2}} \quad (4.16)$$

which implies

$$\Delta P_{fl} = \frac{\alpha_l \Delta P_{fl0}}{\varepsilon_l^{\,3}} \quad (4.17)$$

which becomes

$$\alpha_l = \frac{\Delta P_{fl} \varepsilon_l^{\,3}}{\Delta P_{fl0}} = \frac{\Delta P_{l-mb} \varepsilon_l^{\,3}}{\Delta P_{fl0}} \quad (4.18)$$

where the subscripts *l0* refers to liquid single phase, *l-mb* refers to liquid-microbubble wall, *sl* refers to liquid superficial, $(U_{sl})_{l-mb}$ equals to $(U_{sl})_{l0}/\varepsilon_l$, α_l equals to $\alpha_l'\alpha_l''$ and cross-sectional

area for the flow of liquid is equal to ε_l times the cross-sectional area of the pipe. α_l' is defined as f_{l-mb}/f_{l0} and α_l'' is defined as $(\text{area of contact})_{l-mb}/(\text{area of contact})_{l0}$. The value of α_l'' is equal to the specific interfacial area in test section of the pipe. The parameter α_l is an intensity factor which signifies intensity of interfacial shear stress. ΔP_{fl0} is the frictional pressure drop due to liquid when only liquid phase flows through the pipe. The single liquid phase frictional pressure drop is calculated using Fanning's equation:

$$\Delta P_{fl0} = 2 f_{l0}\ \rho_l U_{sl}^2 L / d_t \tag{4.19}$$

The friction factor is calculated as

$$f_{l0} = \frac{16}{\text{Re}} \qquad \text{for laminar flow} \tag{4.20}$$

$$f_{l0} = \frac{0.079}{n^5 (\text{Re})^{\frac{2.63}{10.5^n}}} \qquad \text{for turbulent flow} \tag{4.21}$$

where *Re* is the Reynolds number for non-Newtonian fluid flow, which can be represented as (Chhabra and Richardson, 1999)

$$\text{Re} = \frac{d_t^n U_{sl}^{2-n} \rho}{8^{n-1} K} \left(\frac{4n}{3n+1} \right)^n \tag{4.22}$$

For transition flow, the friction factor *f* can be deduced from the generalized pressure loss equation (Desouky and EL-Emam, 1989)

$$f_{l0} = 0.125 \left[n^{\sqrt{n}} \left(0.0112 + \text{Re}^{-0.3185} \right) \right] \tag{4.23}$$

Substituting the Eq. (4.17) for ΔP_{fl} into Eq. (4.14), one gets

$$\frac{\alpha_l \Delta P_{fl0}}{\varepsilon_l^3} = \left[\frac{1}{U_m A_t} \right] \left[(3/4) C_m \rho_l U_{sl}^3 A_t \frac{1-\varepsilon_l}{\varepsilon_l^3} \frac{L}{d_{mb}} + \frac{\pi d_t U_{sl} \sigma_{lw}}{\varepsilon_l} + \frac{U_{sl} \sigma_{l-mb}}{a \varepsilon_l} \right] \tag{4.24}$$

This gives the hydrodynamic drag coefficient as

$$C_m = \frac{4}{3}\left[\frac{\alpha_l \Delta P_{fl0} U_m A_t}{\varepsilon_l^3} - \left(\frac{\pi d_t U_{sl} \sigma_{lw}}{\varepsilon_l} + \frac{U_{sl}\sigma_{l-mb}}{a\varepsilon_l}\right)\right]\left[\frac{\varepsilon_l^3 d_{mb}}{(1-\varepsilon_l)\rho_l U_{sl}^3 A_t L}\right] \quad (4.25)$$

In Eq. (4.18), except α_l, all parameters are known. Using the experimental pressure drop, the corresponding values of α_l can be calculated from Eq. (4.18). Once the value of α_l is calculated, the drag coefficient of microbubble flow can be calculated from Eq. (4.25). From the definition of α_l, one can calculate the friction factor, $f_{l\text{-}mb}$ in the straight pipe as

$$f_{l-mb} = \frac{\alpha_l f_{l0}}{\alpha_l''} \quad (4.26)$$

The average liquid-microbubble interfacial shear stress (τ_i) is expressed as

$$\tau_i = 0.5(f_{l-mb}\rho_l U_{sl}^2)/\varepsilon_l^{\,2} = 0.5\left(\frac{\alpha_l f_{l0}}{\alpha_l''}\rho_l U_{sl}^2\right)/\varepsilon_l^{\,2} \quad (4.27)$$

If there is a slip at the interface, then Eq. (4.27) can be expressed as

$$\tau_i = \frac{1}{2}(f_{l-mb}\rho_m (U_{sl} - U_{is})^2/\varepsilon_l^{\,2} \quad (4.28)$$

where U_{is} is slip velocity.

4.3 Experimental Setup and Procedure

4.3.1 Estimation of Pressure Drop

The experimental setup to study pressure drop characteristics is shown in Figure 4.1. It consists mainly of a tank, a pump, a microbubble generator, a pressure transducer with a data logger system (Model-3002 U1- PD2; Integrated Electrolife System, Kolkata, India), one rotameter,

valves, a thermometer and a test section. Pressure drop was measured in straight horizontal pipes having diameters of 3×10^{-3}, 6×10^{-3}, 8×10^{-3}, and 1×10^{-2} m, respectively.

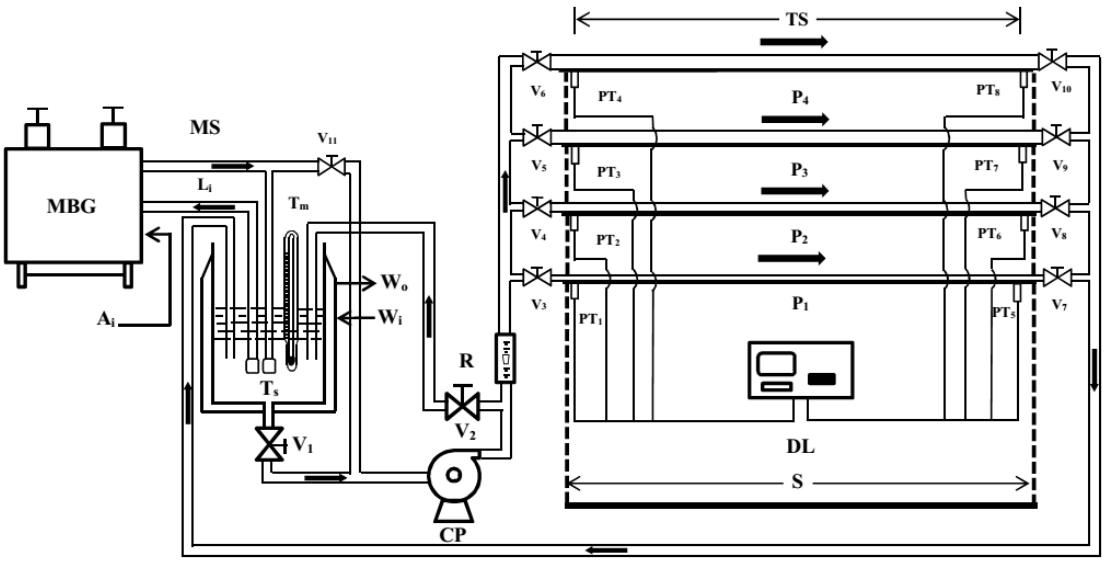

Figure 4.1: Schematic representation of experimental setup for pressure drop. Legend: A_i: Air Inlet; CP: Pump; DL: Data logger unit; L_i: Liquid inlet; MBG: Microbubble Generator; MS: Microbubble suspension; $P_{1\text{-}4}$: Pipes (i.d. 0.003 m, 0.006 m, 0.008 m and 0.010 m); R: Rotameter; S: Self angle support; $PT_{1\text{-}8}$: Pressure transducers; TS: Test section; T_s: Microbubble suspension tank with cooling jacket; T_m: Thermometer; $V_{1\text{-}11}$: Flow control valve; W_i: Water inlet; W_o: Water outlet.

The distance between the two pressure transducers was taken as 2.4 m for each pipe based on the condition L/d > 50 for fully developed ow. The test section was designed well to minimize losses due to contraction and expansion. The rotameter and pressure transducers were calibrated well to minimize the experimental error. Microbubbles were generated in a tank with a volume of 5×10^{-2} m^3 by the microbubble generator. The volumetric ow rate of uid owing through the pipe was measured by the rotameter and controlled by a ow control valve. The test uid containing dispersed microbubbles was transported from the tank to the test section by a pump (ow rate range of 0 6×10^{-4} (m^3/s). The pressure transducer with a data logger

was used to measure the pressure drop along the length. Each experiment was performed repeatedly and allowed to run for 5 min to attain steady-state conditions.

4.3.2 Estimation of Gas Holdup

Gas holdup is defined as the volume fraction of the gas phase occupied by bubbles. The gas holdup in a microbubble column can be measured by the phase isolation method (Karamah et al., 2010; Kawahara et al., 2009). The gas holdup in microbubble-aided aeration systems can be measured by

$$\varepsilon_g = \left(1 - \frac{\rho_m}{\rho_w}\right) \tag{4.29}$$

where ε_g is the gas holup, ρ_m and ρ_w are densities of the gas-liquid mixture and water respectively. In case of microbubble aided systems, the volume of liquid before and after bubbling does not change remarkably. Therefore the accuracy of the phase isolation method decreases as the bubble size and liquid volume under test is very less. In the present study, the gas holdup was measured by the electrical conductivity method. Maxwell (1892) reported that the effective conductivity of a dispersion ($K_{l\text{-}d}$) is related to the volume fraction (ε_d) of a dispersed nonconductive phase by

$$k_{l-d} = k_l\left(\frac{1-\varepsilon_d}{1+0.5\varepsilon_d}\right) \tag{4.30}$$

Gas holdup can be calculated based on this principle as

$$\varepsilon_g = \left(\frac{k_l - k_{l-g}}{k_l + 0.5k_{l-g}}\right) \tag{4.31}$$

where k_l and $k_{l\text{-}g}$ are the electrical conductivities of the liquid and liquid-gas mixture respectively. The electrical conductivities of the liquid and liquid-gas mixture were measured

by digital conductivity meter (Model: VSI-04 ATC Deluxe, VSI Electronics Pvt. Ltd., Chandigarh, India). A schematic diagram of the apparatus used for gas holdup measurements is shown in Figure 4.2. The cell in the conductivity meter was an adaptation of a section of the "ideal" cell consisting of two infinite and parallel plate electrodes (Kasper, 1940). The electrical conductance provided by the electrodes is described by the equation

$$K_l = \kappa \frac{A}{L_e} \tag{4.32}$$

where K_l is the electrical conductance (inverse of resistance); κ is the electrical conductivity and A and L_e are the area (m^2) and separation (m) of the electrodes respectively. A/L_e is referred to as the cell constant. Such a cell has been used to measure effective conductivities of dispersions (Achwal and Stepanek, 1975; Dhanuka and Stepanek, 1978; Marchese et al., 1992; Turner, 1976). Alternating current (ac) of sufficiently high frequency (about 1000 Hz) and low voltage (~1.5 V) was used to avoid polarization of the electrodes.

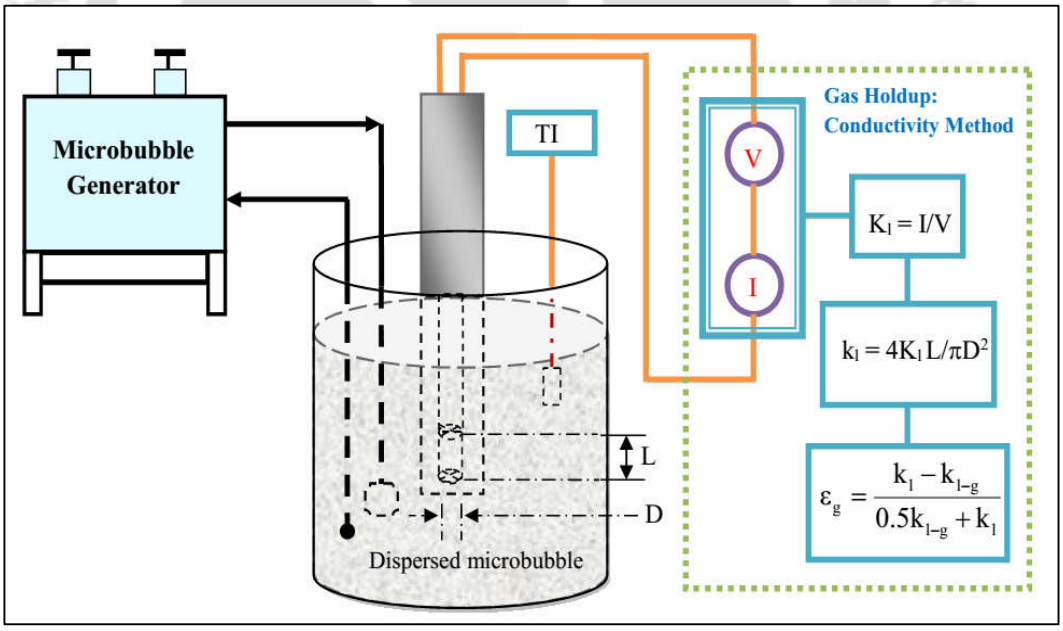

Figure 4.2: Schematic representation of gas holdup measurement.

4.3.3 Physical Properties of the System

In the present work, aqueous solutions of sodium dodecyl sulphate (SDS), cetyl trimethyl ammonium bromide (CTAB) and Tween-20 were used as liquid phase whereas air was used as gas phase. The densities of the solutions were measured with a specific gravity bottle. The surface tension was measured by tensiometer (model K9-MK1, Kruss GmbH, Hamburg, Germany). All the experiments in the present work were carried out at 25° C. Each test was replicated five times by repeating the above procedure and the average of them was taken as final reading. The physical properties of gas and liquid phase are shown in Table 2.1. Moreover, the viscosities of these fluids can increase or decrease due to changes in the rate of shear, which again is subject to the nature of the fluid. Unlike Newtonian fluids, non-Newtonian fluids are defined as materials that do not conform to a direct proportionality between shear stress and shear rate (Chhabra and Richardson, 1999). The effective viscosity of the liquid flowing through the pipe was calculated according to the equation

$$\mu_e = K\left(\frac{3n+1}{4n}\right)^n\left(\frac{8U_{sl}}{d_t}\right)^{n-1} \tag{4.33}$$

where μ_e is the effective viscosity of the suspension, n is flow behavior index, K is the flow consistency index, U_{sl} is the velocity of the microbubble suspension and d_t is diameter of the pipe.

4.4 Results and Discussion

4.4.1 Variation of Gas Holdup

The effect of surface tension of liquid on gas holdup is shown in Figure 4.3. It can be seen that surfactant strongly enhanced the gas holdup. When the gas-liquid mixture was introduced into the mixing chamber of the generator, a high shearing and smashing occurred between the two

phases. The addition of surfactant lowered the surface tension of the liquid, as a result of which the interface between the phases was easily stretched. This led to the easy formation of new surface area between the phases, which caused an increase in gas bubbles per unit volume and ultimately increased the gas holdup.

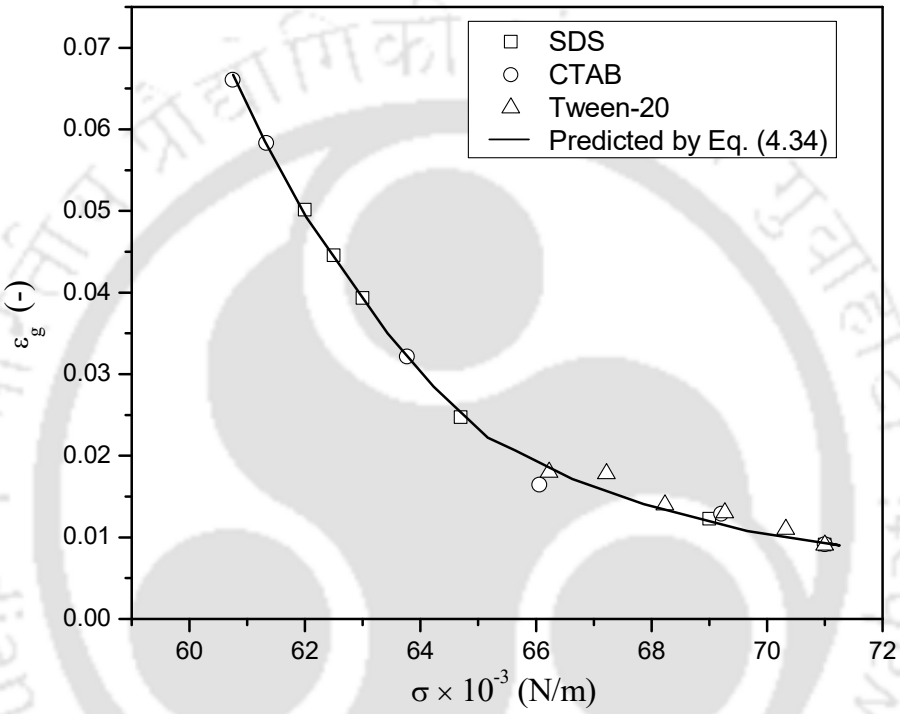

Figure 4.3: Variation of gas holdup with liquid surface tension.

Pallapothu and Al Taweel, (2012) also reported an increase in gas holdup for microbubble-induced an internal loop reactor with surfactant concentration. Other studies in conventional systems also reported an increase in gas holdup in the presence of surfactants (Dargar and Macchi, 2006; Oels et al., 1978; Sajjadi et al., 2010; Schügerl et al., 1977). Anastasiou et al. (2010) used three different types of surfactants in their study and observed that the surfactants significantly enhanced gas holdup. The gas holdup profile was found to satisfy the following correlations developed on the basis of the present experimental data

$$\varepsilon_g = 7\times10^{-4}\sigma^2 - 9.88\times10^{-2}\sigma + 3.45 \quad if\ 59 \le \sigma \le 71\ (\text{mN/m}) \tag{4.34}$$

4.4.2 Shear Stress in Microbubble Suspension Flow

The shear stress for water increases linearly with shear rate. Microbubble suspensions exhibit the power-law behavior of a pseudoplastic non-Newtonian fluid. The shear stress verses shear rate behaviors of single-phase water and microbubble suspensions for different surfactants are shown in Figures 4.4, 4.5 and 4.6.

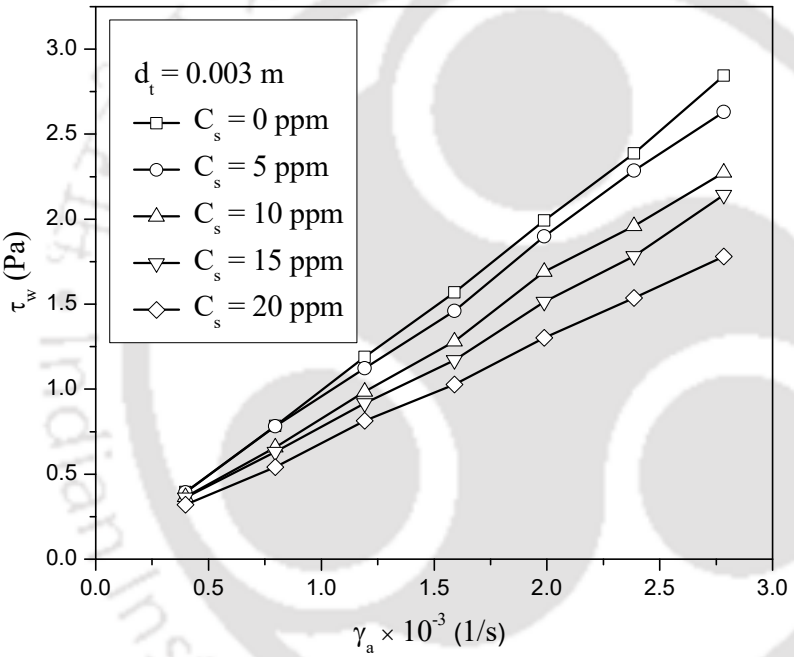

Figure 4.4: Variation of shear stress with shear rate for SDS microbubble suspension.

The non-Newtonian nature of the microbubble suspensions was found to be dependent on surfactants concentration in the suspension. An increase in the concentration of surfactant in water increased its non-Newtonian behavior. An increase in surfactant concentration significantly decreases the surface tension, which causes a reduction in bubble size and increases in the bubble population and gas holdup (Moraveji et al., 2012). However, it is

difficult to correlate the bubble size with the rheological properties of the fluid (Llewellin et al., 2002; Rust and Manga, 2002).

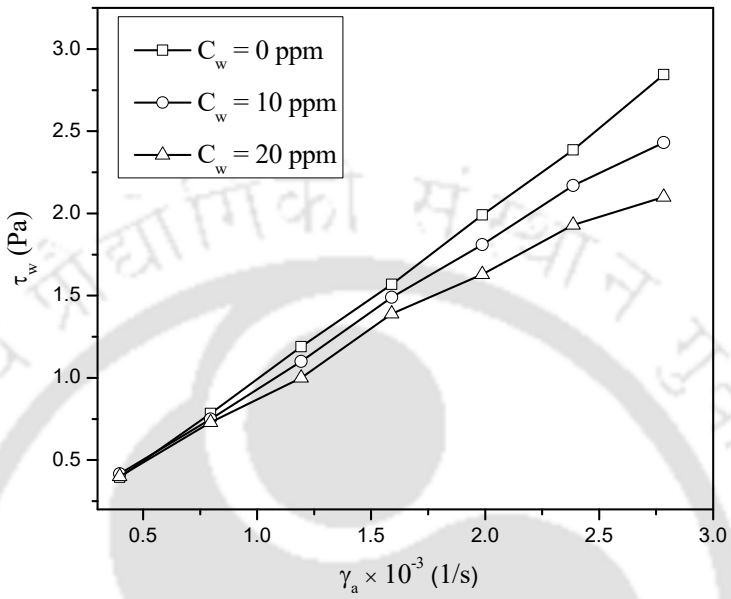

Figure 4.5: Variation of shear stress with shear rate for Tween-20 microbubble suspension.

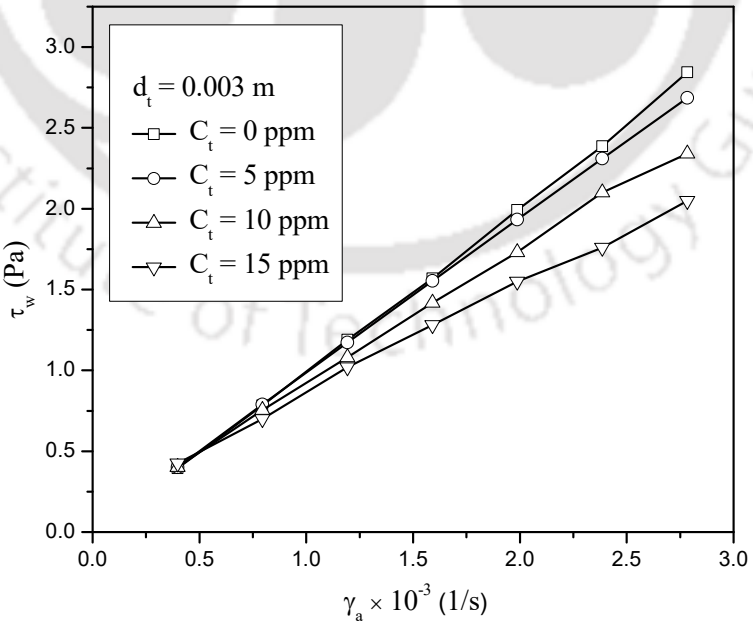

Figure 4.6: Variation of shear stress with shear rate for CTAB microbubble suspension.

The increase in gas holdup decreases the density of the fluid mixture, so that the momentum flux in the direction of the flow decreases and causes the fluid flow behavior to change. The extent of non-Newtonian behavior, however, largely depends on the physicochemical properties of the fluid. The values of the flow behavior index in all of the pipes for microbubble suspensions were found to be less than 1. It was observed that microbubble suspensions with high surfactant concentrations had the lowest of flow behavior indexes, which demonstrates the high degree of non-Newtonian behavior. However, a general trend for the flow consistency index in all of the pipes was not observed. Shen et al. (2008) observed the shear-thinning nature of microbubble suspensions. The shear-thinning nature of microfoam has also been reported in the literature (Calvert and Nezhati, 1986; Larmignat et al., 2008; Tseng et al., 2006). However, they observed an increase in shear stress with surfactant concentration and concluded that this contradiction arises as a result of an increase in the effective viscosity of the fluid with shear rate. This might be due to the Marangoni effect. When there is a temperature gradient around the bubble, a nonuniform steady-state distribution of surface active species along the interface is created. The surface tension gradient leads to tangential stress at the bubble interface, which drives the bubble toward a warmer region or a low-surface tension region (Takahashi et al., 1999). The phenomenon is known as the Marangoni effect. This effect is prominent in microbubble systems, if a temperature gradient is provided. In the present study, experiments were performed under isothermal conditions, so the temperature gradient around the bubbles was negligible. The minimum bubble diameter for this effect is around 10 μm (Takahashi et al., 1999). From the present experimental data, it was found that the range of microbubble size was 30-50 μm, which was 3-5 times higher than the minimum value. Therefore, in the present study, it was assumed that the Marangoni effect was negligible. The variation of the effective viscosity of microbubble suspensions with shear rate is shown in Figure 4.7. The effective

viscosity of the microbubble suspension in pipe flow decreased with increasing shear rate, which resulted in the shear-thinning nature of the microbubble suspension. The rates of decrease of the effective viscosity with shear rate were also different for all of the microbubble suspensions. On increasing the concentration of surfactant in the suspensions, the effective viscosity decreased more rapidly.

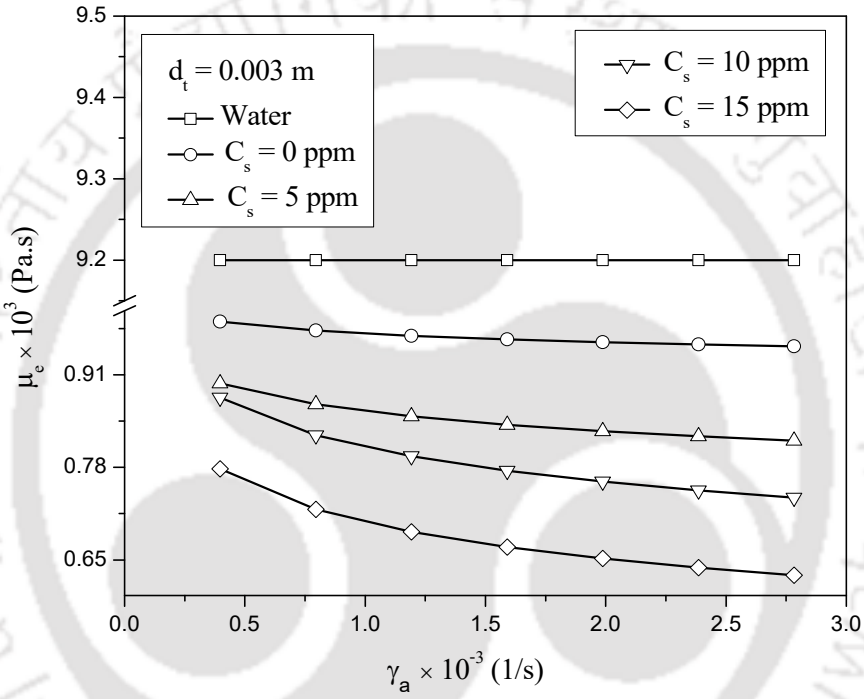

Figure 4.7: Variation of effective viscosity with apparent shear rate for a microbubble suspension.

The addition of surfactant decreased the surface tension, which increased the gas holdup and decreased the bubble size. The pressure between the inlet and outlet generally decreased as the gas holdup increased, as a result of which the shear stress decreased. The decrease in shear stress could cause the effective viscosity to decrease. Shen et al. (2008) observed a decrease in the viscosity of microbubble suspensions with apparent shear rate. Tseng et al. (2006) also

reported a decrease in effective viscosity with apparent shear rate in microfoams having bubble diameters in the range of 10-100 μm.

4.4.3 Wall Friction Factor

The frictional pressure drop is caused by the resistance to the flow of fluid. The main factors of resistance to fluid flow are changes in kinetic energy through the pipe and fluid viscosity. Figure 4.8 shows the variation of the frictional pressure drop across the test section with Reynolds number based on the pipe diameter.

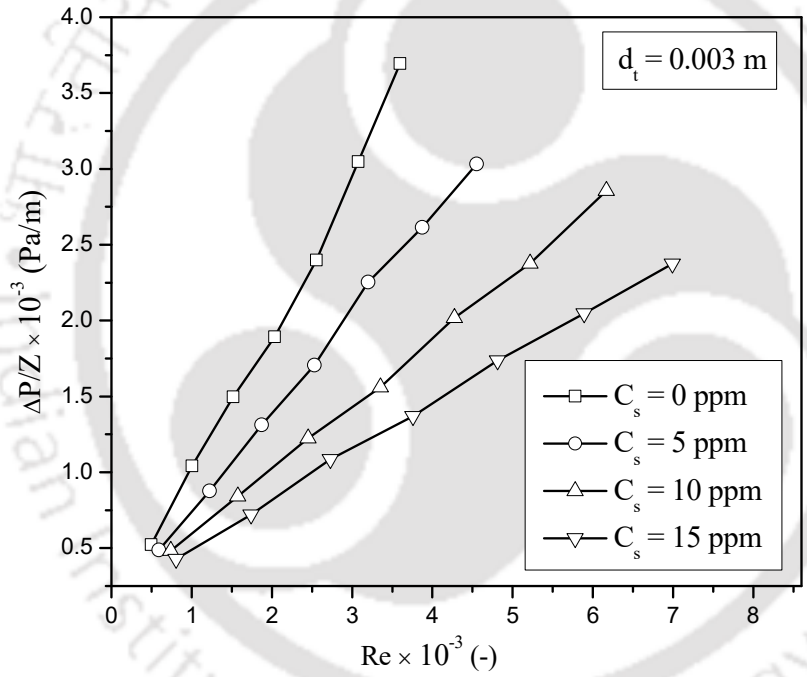

Figure 4.8: Variation of friction pressure drop with Reynolds number.

It can be seen that the frictional pressure drop per unit length increased with increasing Reynolds number and decreased with increasing concentration of surfactant in the suspension. An increase in the Reynolds number enhances the kinetic energy of the fluid flowing. The increase in kinetic energy raises the interfacial shear stress in the pipe, which results in an increase in pressure drop. The increase in surfactant concentration leads to increases in the

bubble population, which decreases the liquid holdup in the suspension, causing a reduction in the momentum of the fluid flowing in the pipe, as a result of which the pressure drop decreases. The variation in the friction factor with Reynolds number based on the pipe is shown in Figure 4.9. It was observed that friction factor decreased with increasing Reynolds number based on pipe diameter. The viscous force decreased with increasing Reynolds number because the viscosity of the suspension decreased as a result of the shear thinning nature of the fluid. This caused a reduction of the friction factor with Reynolds number.

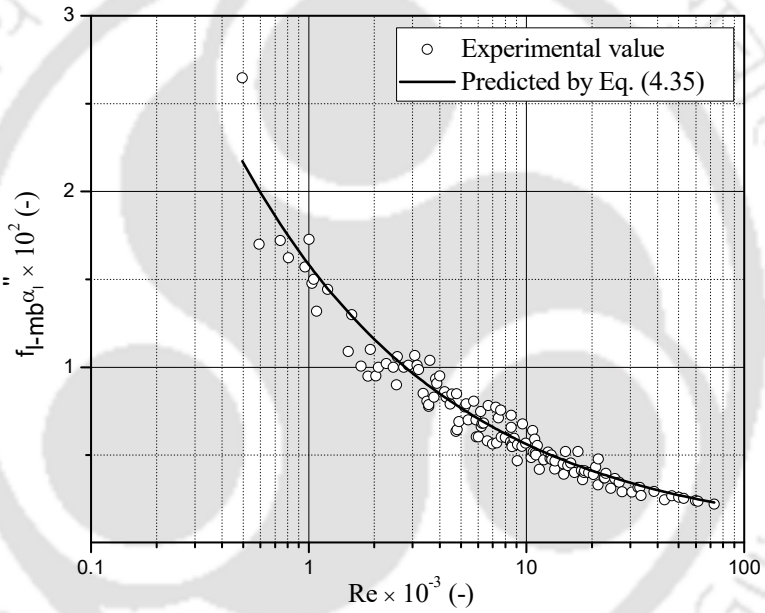

Figure 4.9: Friction factor as a function of Reynolds number.

The dependency of the friction factor on the Reynolds number can be presented by developing a correlation based on the present experimental data as

$$f_{l-mb} = \frac{1.5398}{\alpha_l'' \, \mathrm{Re}^{0.454}} \tag{4.35}$$

A more generalized correlation of friction factor with the other independent variables can be represented as

$$f_{l-mb} = 0.3958(1+C_s)^{-0.0277}\left(\frac{d_t}{d_{mb}}\right)^{-0.0439}(\mathrm{Re})^{-0.4359}\left(\alpha_l''\right)^{-1} \quad (4.36)$$

The correlation coefficient and standard error of the correlation are found to be 0.998 and 0.097.

4.4.4 Friction Factor in Microbubble Suspension Flow based on Energy Loss due to Wettability

The wetting effect of the solid-liquid surface during the flow of fluid is a matter of concern because some amount of energy is lost due to the wettability. The extent of wettability is determined by an equilibrium between adhesive and cohesive forces. Surface tension, fluid velocity, and gas holdup are important factors upon which the wettability of liquid in two-phase flow depends. The variation of the friction factor with energy losses due to wettability at different surface is shown in Figure 4.10.

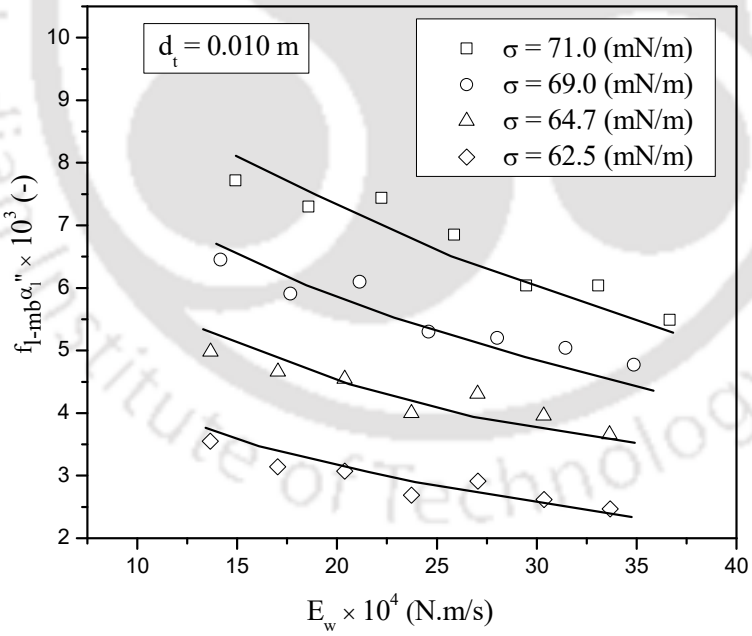

Figure 4.10: Variations of the friction factor with energy loss due to wettability at different surfactant concentrations.

It can be seen that the friction factor decreased with increasing energy loss due to wettability for a specific wetted area, whereas the friction factor increased with wetted area at fixed energy dissipation due to wettability. Higher surfactant concentrations in the suspensions led to a decrease in the surface tension and an increase in the gas holdup. Both of these factors decreased the energy loss due to wettability because of capillary action of the flowing fluid in the pipe.

The friction factor due to wettability can be expressed as

$$f_{l-mb}\alpha_l^{''} = pE_w^q \tag{4.37}$$

where the parameter p and q are define as

$$p\times10^4 = -0.175\sigma^2 + 23.5\sigma - 77.7, \quad R^2 = 0.979 \tag{4.38}$$

$$q = 5.2\times10^{-3}\sigma^2 - 0.676\sigma + 22.46, \quad R^2 = 0.996 \tag{4.39}$$

4.4.5 Hydrodynamic Drag Coefficient in Microbubble Suspension Flow

The drag coefficient derived for the system includes the hydrodynamic drag on the microbubbles and the pipe wall. Drag on the bubble depends on the surface area of bubble (bubble size), fluid velocity, fluid density, and so on. Changing surfactant concentrations changes bubble size, which affects the drag force experienced by bubble. Similarly, changing the pipe diameter changes the fluid velocity in the pipe, which ultimately changes the drag coefficient. The effect of the Reynolds number on the drag coefficients is shown in Figure 4.11. At low Reynolds number, the viscous forces in the pipe are high. As the Reynolds number increases, the momentum energy of the fluid increases. Because of the shear-thinning behavior of the fluid, the effective viscosity decreases with increasing inertia of the fluid. Hence, the magnitude of the drag force decreases with decreasing viscosity of the fluid. Consequently, the drag coefficient decreases with increasing Reynolds number. It was also observed that

microbubble suspensions having low surface tension resulted in low drag coefficients. This might be due to the reduction of the size of the microbubbles upon the addition of surfactants.

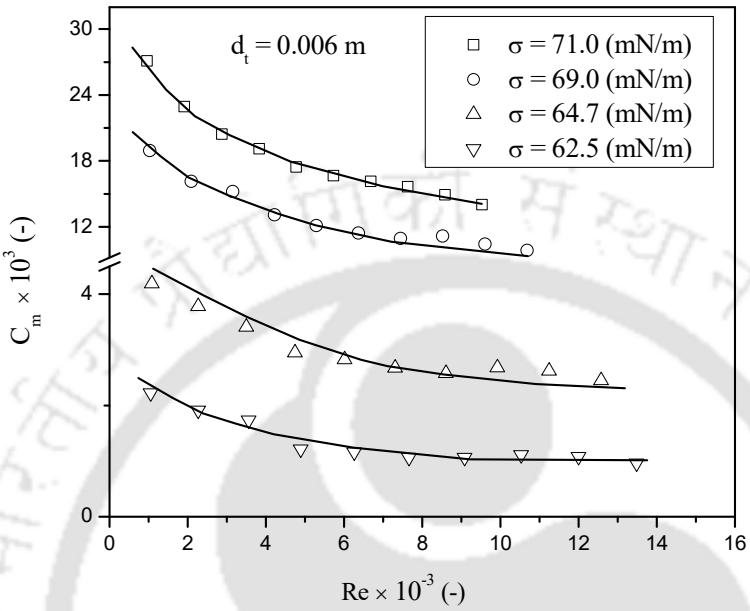

Figure 4.11: Variations of the drag coefficient with Reynolds number at different surfactant concentrations.

A correlation by dimensional analysis was developed to interpret the drag coefficient based on the present experimental data with other independent variable as follows

$$C_m = 1.0639 \times 10^{22} \left(\frac{Z}{d_{mb}}\right)^{-4.11} \left(\frac{d_t}{d_{mb}}\right)^{-1.517} (We_b)^{0.2694} (\mathrm{Re})^{-0.796} \tag{4.40}$$

where We_b is the Weber number defined as

$$We_b = \frac{\rho_l U_{sl}^2 d_{mb}}{\sigma} \tag{4.41}$$

The correlation coefficient and standard error of Eq. (4.40) were found to be 0.987 and 0.163 respectively. The details of the calculation for the regression are shown in Appendix-I. The goodness of fit of the correlation proposed for the drag coefficient (C_m) with the experimental value is shown in Figure 4.12. The correlation proposed was developed on the basis of the

dynamic variable: microbubble suspension velocity; the geometric variable: pipe diameter; and the physicochemical properties of the system: viscosity density, and surface tension. It was found that the developed correlation is in good agreement within the ranges of variables

$4.68\times10^{4} \le \frac{Z}{d_{mb}} \le 7.47\times10^{4}$, $58.51 \le \frac{d_t}{d_{mb}} \le 311.46$, $1.06\times10^{-2} \le We_b \le 4.68$ and

$4.95\times10^{2} \le \mathrm{Re} \le 7.28\times10^{4}$.

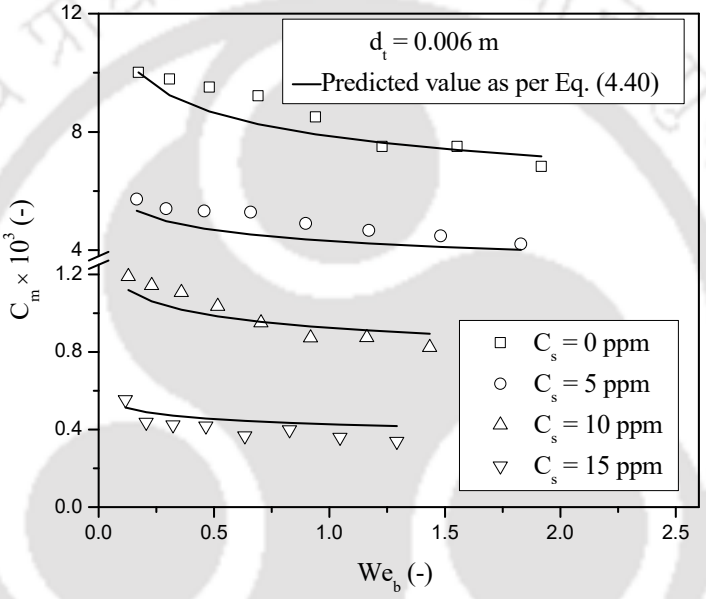

Figure 4.12: Variations of the drag coefficient with Weber number at different surfactant concentrations.

4.5 Conclusion

The present study mainly focuses on the rheological study of microbubble suspension in horizontal pipe and the development of model based on wetting effect of microbubble suspensions. From the present experiments it was found that the effective viscosity of the microbubble suspensions decrease with apparent shear rate, indicating that microbubble

suspensions behave as shear-thinning non-Newtonian fluids. An increase in surfactant concentration caused a decrease in shear stress and effective viscosity with shear rate. The friction factor was found to decrease inversely with the Reynolds number to the power of 0.45, whereas it decreased without the microbubble suspension with a power of 0.25. The results suggested that the presence of microbubbles reduces the frictional resistance. The friction factor was found to decrease with increasing wettability. As the fluid velocity increased, frictional loses decreased at the specific wetted surface area. Surfactant concentration in the suspension plays an important role in increasing the gas holdup and decreasing the energy loss due to wettability. The drag coefficient was found to decrease with increasing Reynolds number, as well as with increasing surfactant concentration in the suspension.

Notations

a Specific interfacial area (1/m)

A Area of electrode (m^2)

A_t Pipe cross-sectional area (m^2)

C_s Concentration of SDS (ppm)

C_w Concentration of Tween-20 (ppm)

C_t Concentration of CTAB (ppm)

C_m Drag coefficient of microbubble mixture (-)

C_a Capillary number $(\mu_{eff} U_{sl})/(\varepsilon\sigma_l)$ (-)

d_t Pipe diameter (m)

d_{mb} Bubble diameter (m)

D Diameter of electrode (m)

D_h Hydraulic diameter (-)

E_l Energy dispersion per unit volume of test section (N.m/s)

F_d Drag force (N)

E_l Energy dispersion per unit length in pipe (N.m/s)

E_w Energy loss due to wettability (N.m/s)

$f_{l\text{-}mb}$ Friction factor of liquid-microbubble system (-)

f_{lo} Friction factor of single liquid system (-)

g Gravitational acceleration (m/s^2)

K Consistency of fluid ($Pa.s^n$)

K_l Conductance of liquid (S)

k_l Electrical conductivity of liquid (S/m)

$k_{l\text{-}g}$ Electrical conductivity of liquid-gas mixture (S/m)

$k_{l\text{-}d}$ Electrical conductivity of dispersion (S/m)

L Length of test section (m)

L_e Separation of the electrodes (m)

MS Microbubble suspension (-)

n Flow behavior index (-)

N_b Number of bubbles (-)

p Parameter defined in Eq. (4.38) (-)

$P_{l\text{-}mb}$ Liquid-micobubble suspension pressure (N/m^2)

$P_{fl\text{-}mb}$ Frictional pressure due to liquid-microbubble flow (N/m^2)

P_{flo} Frictional pressure due to single liquid-phase (N/m^2)

q Parameter defined in Eq. (4.39) (-)

Q Volumetric flow rate (m^3/s)

Re Non-Newtonian liquid Reynolds number ($\frac{d_t^n V_{sl}^{2-n} \rho}{8^{n-1} K}\left(\frac{4n}{3n+1}\right)^n$) (-)

U_{is} Interfacial slip velocity (m/s)

U_{sl} Superficial liquid velocity (m/s)

U_m Gas-liquid mixture velocity (m/s)

We_b Weber number ($\rho_l U_{sl}^2 d_{mb} / \sigma$) (-)

Z Length of test section (m)

Greek letters

α_l Parameter defined in Eq. (4.18) (-)

ε_g Gas holdup (-)

ε_l Liquid holdup (-)

ε_d Dispersed non-conducting phase holdup (-)

κ	Electrical conductivity (S/m)
μ_e	Effective viscosity (kg/m.s)
μ_l	Viscosity of liquid (kg/m.s)
ρ_l	Density of liquid (kg/m^3)
ρ_m	Density of gas-liquid mixture (kg/m^3)
ρ_w	Density of water (kg/m^3)
σ	Surface tension (N/m)
$\sigma_{l\text{-}mb}$	Surface tension between liquid and microbubble (N/m)
σ_{lw}	Surface tension between at the boundary between liquid and pipe wall (N/m)
τ_i	Interfacial shear stress (N/m^2)
τ_w	Wall Shear stress (Pa)
γ_w	Wall shear rate (1/s)
γ_a	Apparent shear rate (1/s)
ΔP	Pressure drop (N/m^2)
θ	Liquid-wall contact angle (radian)

Subscripts

b	Bubble
f	Frictional
g	Gas phase

i	Interfacial
l	Liquid Phase
l-mb	Liquid-Microbubble
l-w	Liquid-Wall
p	Pipe
s	Superficial
w	Wettability
0	Single

CHAPTER-5

DISPERSION CHARACTERISTICS OF MICROBUBBLE SUSPENSION IN CONTINUOUS PLANT PROTOTYPE

This chapter is about the investigation of the dispersion characteristic of ionic microbubble suspension in continuous plant prototype developed for mineral beneficiation. The effects of different operating variables and physicochemical properties of liquid on the dispersion of ionic microbubble suspension are reported. A phenomenological model with consideration of liquid circulation is developed to analyze the dispersion coefficient of the microbubble suspension due to circulation. Generalized correlations for dispersion coefficient and mixing time are developed based on the physicochemical properties of microbubble suspension are also enunciated in this chapter.

5.1 Introduction

Mixing of phases are widely encountered in process industry in various processes involving physical and chemical changes. Mixing is a central feature of many processes in the pharmaceutical, paper, plastics, ceramics and mineral processing industries (Harnby et al., 1992). The mixing process in column are conventionally divided into two parts. The first is the macromixing, which gives information about the retention times of the elementary volumes. The second part is micromixing which describes the communication between the elementary volumes. Micro mixing includes all aspects of mixing not defined by residence-time distribution (Shah, 1979). The gas-liquid-solid mixing inside flotation column directly affects

the column performance. The contact of the gas with the solid-liquid phase effectively brings into contact the phases, allowing for collisions and eventual adhesion of the hydrophobic particles on the rising gas bubbles. It is obvious that, although a certain amount of turbulence is necessary to achieve the required contact, too much turbulence and mixing may result in the disruption of the particle-bubble bonds and their detachment, reducing the process efficiency (Mavros, 1996). Significant research has been published during the past three decades on the effects of backmixing on flow reactor performance. The two extreme ideal cases of a column are the complete mixing where perfect backmixing is achieved and a plug flow reactor where backmixing is negligible. The performance of a column in between these two ideal cases can be characterized by various existing models viz. dispersion model, cell model, multistage dispersion model, back-flow model and dispersion-back-flow model (Szeri et al., 1976).

Even though the mass transfer and hydrodynamics properties of microbubbles have been discussed in the literature, still there is a significant knowledge gap on dispersion mechanism of flow of microbubble suspension. To achieve technical feasibility of microbubble suspension flow and microbubble aided mineral separation by flotation, a detailed study on the dispersion characteristics of microbubble suspension are required. To the best of our knowledge, a single study by Bredwell and Worden (1998) is available in literature in which a brief description of liquid axial dispersion coefficient of microbubble is illustrated. Thus in the present chapter an attempt has been made to explore the dispersion characteristic and mixing time of microbubble suspension of recirculation system in a continuous plant prototype, which has not been reported till date. The aim of this chapter is to study the phenomenon of dispersion associated with microbubble-suspension flow to aid in mineral beneficiation. The results of this dispersion phenomenon is incorporated to the degree of separation of fine particle by microbubble flotation in the chapter 6.

5.2 Theoretical Background

5.2.1 Dispersion Coefficient of Microbubble Suspension

Residence time distribution of material is one of the globally acceptable technique to estimate the dispersion coefficient. Normally for the measurement of residence time distribution the tracer technique is used which involves the injection of tracer material at some location in the column and the concentration of the column is detected as a function of time at one or more downstream positions. The tracer input may be step, impulse, imperfect pulse, sinusoidal (Kramers et al., 1958) and step decrease in concentration (Bennett and Goodridge, 1970). But majority of literature studies have used impulse input. Proper precaution should be taken to inject the tracer carefully to ensure good pulse injection. Flow maldistribution have significant effects on the residence time distribution. Other factors such as reactor channeling dead zones, by passing on the residence time distribution are undesired for proper residence time distribution. The non-uniform velocity and method of injection and detection can also affect the nature of residence time distribution curve. The position of detection probe can also affect the curve (Shah, 1979). The design and scale-up of bubble column reactors generally depend on the quantification of three main phenomena: (i) heat and mass transfer characteristics; (ii) chemical kinetics of the reacting system and (iii) dispersion characteristics. The physical and chemical processes more or less depend on the dispersion characteristic of the phases. Dispersion reduces the degree of non-uniformity or gradient of a property in a system such as concentration, viscosity, temperature etc. It is achieved when an element or material to be mixed moves from a region to another either by molecular diffusion or by agitation, to gain a uniformity in concentration (Shah, 1979). The axial dispersion model is widely accepted model for the determination of dispersion characteristics and is thus used in the present work. This model is based on the concept that dispersion process in the column follows a random,

diffusion-like eddy movement superimposed on a plug flow (Majumder et al., 2005). As per axial dispersion model, the concentration of tracer in the column at any position Z can be written as:

$$\frac{\partial C}{\partial t} = E_z \frac{\partial^2 C}{\partial Z^2} - U_c \frac{\partial C}{\partial Z} \tag{5.1}$$

Here U_c is microbubble suspension circulation velocity, E_z is the axial dispersion coefficient (m^2/sec), C is concentration of tracer. In the circulation region, the dispersion follows a different patterns from the continuous non-circulating region. The dispersion of the tracer in the circulation region are mainly caused by the differences in velocity of the different streamlines and the differences in length of the various circulation loops inside the device. The dispersion of the circulating stream appears to be conceivable by the average circulation time and a coefficient, which characterizes the dispersion during the circulation. Consider a device of infinite length wherein a certain amount of longitudinal dispersion is occurred and the response are recorded at the positions $Z = L, 2L, 3L...jL$ for a tracer injected at $Z = 0$ and $t = 0$ as shown in Figure 5.1.

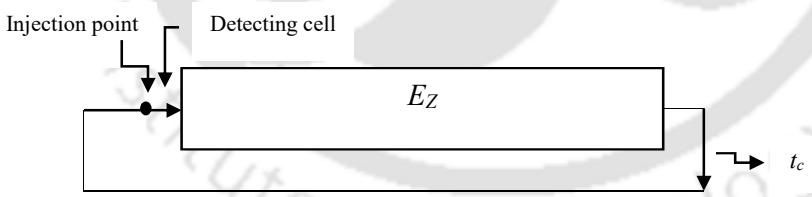

Figure 5.1: Column with dispersion and complete recirculation.

The concentration profile at the distance $Z = jL$, downstream from the point of injection is then expressed by (Voncken et al., 1964)

$$C = \frac{Q_t L}{2V\sqrt{\pi E_z t}} \exp\left[\frac{-(jL - U_c t)^2}{4E_z t}\right] \tag{5.2}$$

where Q_t is the amount of tracer injected and V denotes the volume of a section between $Z = jL$ and $Z = (j\text{-}1)L$. Eq. (5.2) gives the response of a tracer, injected at $Z = 0 = L$ in the device of characteristic length L with complete recirculation and detected at the same place. The characteristic length L represents the length of the average circulation streamline. The time required for a fluid element to flow with the average velocity once around the average circulation loop is called circulation time (t_c). Hence $t_c = L/U_c$. As the dispersion proceeds, the tracer fluid is evenly distributed in the device. This runs continuously without a supply of liquid from outside. The analytical solution of Eq. (5.2) for the normalized response curve is given as (Voncken et al., 1964)

$$\frac{C}{C_\infty} = \sqrt{\frac{Bo}{4\pi\theta}} \sum_{j=1}^{\infty} \exp\left[-\frac{Bo}{4\theta}(j-\theta)^2 \right] \tag{5.3}$$

where the concentration of the tracer at infinite time (C_∞) is equal to the ratio of the amount of tracer injected to the volume of column (Q_t/V). The symbols θ and Bo denote dimensionless time and dimensionless number (Bodenstein number) which are expressed respectively as

$$\theta = \frac{t}{t_c} \tag{5.4}$$

$$Bo = \frac{LU_c}{E_z} \tag{5.5}$$

The dispersion coefficient (E_z) is then estimated as from Eq. (5.5) after fitting the Eq. (5.3) with experimental data.

5.2.2 Mixing Time of Microbubble Suspension

Mixing time is an index of dispersion for the closed circulation. It is defined as the time required to reach a predefined level of homogeneity after a tracer is added to it. Pulse technique is most common method for the estimation of mixing time. However the results obtained by this

method depends on the injection position and the desired degree of homogeneity (Hadjiev et al., 2006; Kawase and Moo-Young, 1989).

5.3 Experimental Setup and Procedure

5.3.1 Experimental Setup

The schematic of the plant prototype in which the experiments were carried out is shown in Figure 5.1.

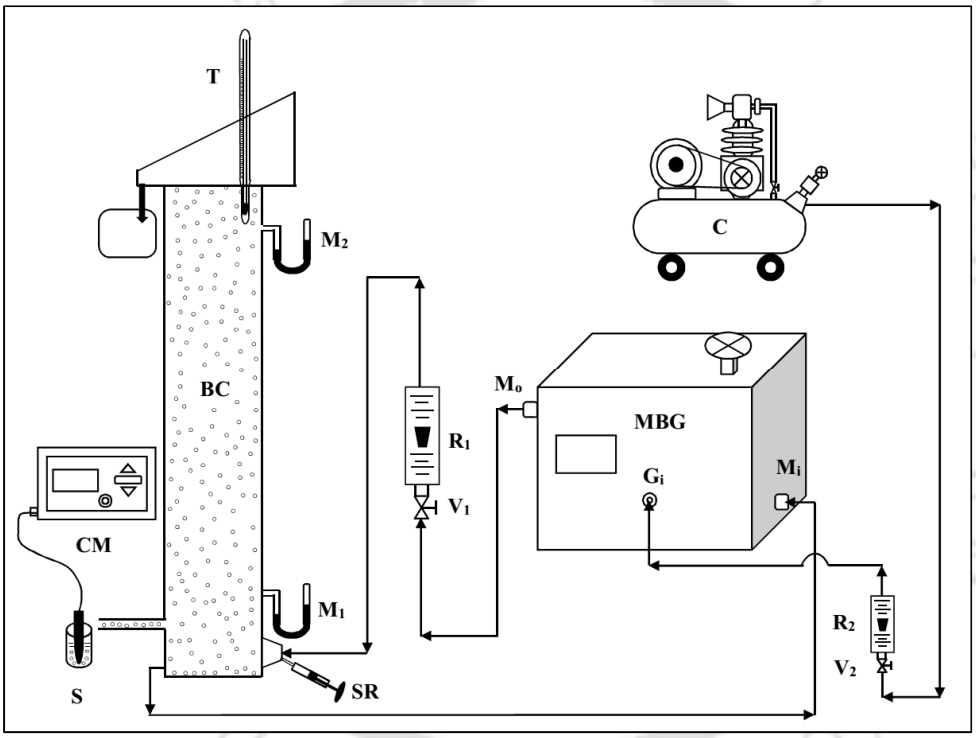

Figure 5.2: Schematic diagram of plant prototype. Legend: - BC: Bubble column; C: Air compressor; CM: Conductivity meter; MBG: Microbubble generator; M_o: Microbubble generator output; M_i: Microbubble generator input; M_1, M_2: Manometers; R_1, R_2: Rotameters; S: Suspension sample; SR: Syringe; T: Thermometer; V_1, V_2: Control valves

It consists of a microbubble generator, a gas compressor and other accessories such as rotameters, control valves, conductivity meter, thermometer and test tubes for collecting

samples. The column was 0.60 m high and having internal diameter 0.20 m. Both inlet and outlet of the column were at the lower end through which microbubble generator was connected. The air used to create microbubbles was supplied from a compressor controlled by a valve. The liquid flow rate was measured using rotameters from which the flow was maintained by using control valves. In the present study the mixing characteristics of microbubble suspension is estimated by tracer technique. This method involves the injection of a tracer at one location in the column and then detection of its concentration at downstream position. After attaining steady-state, 3 ml of sodium chloride solution of strength 3.0 M was injected from the bottom of the column as a tracer. The injection was carried out as quickly and smoothly as possible by a syringe. The variation of tracer concentration with time was measured by conductivity probe (Model: VSI-04 ATC Deluxe, VSI Electronics Pvt. Ltd., Chandigarh, India). The conductivity probe was mounted at the same place (0.05 m above the bottom of the column) where the tracer was injected. The experiments were conducted at six different suspension circulation velocities (U_c) in the range of 0.24 to 0.36 m/s. The circulation velocity in the column is determined by $Q_{sp}/(A_c/2)$ where Q_{sp} is the suspension volumetric flowrate measured by rotameter and A_c is the column cross-sectional area. The suspension circulation velocity is taken on the basis of half of cross-sectional area of column, assuming that the microbubble suspension flows through half of column cross-section and recirculates. In the present work the microbubble generator and the column is considered as a closed loop because inlet and outlet both of the MBG are connected to the same bubble column. The microbubble sucked the liquid from the column and discharge to the bubble column. The closed circulation loop describes circulation in the column as well as MBG. To minimize the error five runs were performed and the average of three was taken as a final reading. In the present work, aqueous solutions of sodium dodecyl sulphate (SDS), cetyl trimethyl ammonium

bromide (CTAB) and Tween-20 were used as liquid phase and air was used as a gas phase. The physicochemical properties of the liquids and gas phases are shown in Table 2.1.

5.3.2 Calibration of Conductivity Meter

A digital conductivity meter is used in the present work. The range of this conductivity meter was about 0- 999 micro Siemens per meter (μ S.m-1). For the calibration of the conductivity meter the conductivity of different known samples of NaCl in microbubble suspension were noted. From the conductivity and concentration data, a linear correlation of conductivity with concentration was made for calibration. Since in the present work surfactants and SCMC solutions were used. So for each gas-liquid system the conductivity meter was calibrated. The concentration of tracer in the solutions as a function of conductivity, can be represented as

$$C_{sc} = aK_c - b \tag{5.6}$$

where K_c is conductivity of solution (mS/cm), the values of parameters a and b for different suspensions are given in Table 5.1.

Table 5.1: Calibration parameters for the systems measured at 25 ± 1 ºC.

System	Parameter, a	Parameter, b
microbubble	0.1887	0.0526
SDS-5 ppm + microbubble	0.3399	0.0646
SDS-10 ppm + microbubble	0.3492	0.0707
SDS-15 ppm + microbubble	0.3603	0.0724
CTAB-5 ppm + microbubble	0.3439	0.0686
CTAB-10 ppm + microbubble	0.3582	0.0712
CTAB-15 ppm + microbubble	0.3743	0.0784
Tween-20-34 ppm + microbubble	0.1895	0.0523
Tween-20-69 ppm + microbubble	0.1908	0.0529
Tween-20-100 ppm + microbubble	0.1935	0.0533
CMC-0.25 kg/m^3 + microbubble	0.3313	0.0809
CMC-0.50 kg/m^3 + microbubble	0.3416	0.0905
CMC-0.75 kg/m^3 + microbubble	0.3550	0.1189
CMC-1.00 kg/m^3 + microbubble	0.3664	0.1280

5.3.3 Effective Viscosity of Microbubble Suspension

Microbubble suspension is a time-independent non-Newtonian pseudo-plastic fluid (Tseng et al., 2006). Its rheology is described by Ostwald–De Waele model or Power law model as described by in Chapter 4. The effective viscosity of microbubble suspension (μ_e) is defined as the ratio of the shear stress at the wall to the average shear rate at the boundary which was calculated by

$$\mu_e = k\left(\frac{3n+1}{n}\right)^n\left(\frac{8U_c}{d_c}\right)^{n-1} \tag{5.7}$$

where n is the flow behaviour index and K is the flow consistency index. U_c is microbubble suspension circulating velocity and d_c is the diameter. The values of n and K are calculated experimentally in a horizontal pipe from the wall shear stress (τ) and the apparent shear rate (γ_a). The wall shear stress and apparent shear rate can be calculated from the volumetric flow rate of microbubble suspension (Q) and pressure drop (ΔP) in the pipe which is discussed in chapter 4.

5.3.4 Estimation of Mixing Time

In the present work, the mixing time is noted when the concentration of tracer reaches to 98% of equilibrium concentration value. Figure 5.3 represents a typical outline to estimate the mixing time from the C/C_∞ vs time plot for three different circulation velocities of microbubble suspension. In the figure, time t_1 corresponds to the mixing time of microbubble suspension at circulation velocity equals to 0.36 m/s, while the time t_3 corresponds to the mixing time of microbubble suspension at suspension circulation velocity equals to 0.24 m/s. The microbubble generator is placed very close to the column. In this regard it is to be noted that the complete

length of MBG loop is approximately 0.3 m and its residence time is less than 5 seconds. So the mixing time in MBG loop is negligible compared to that in microbubble column.

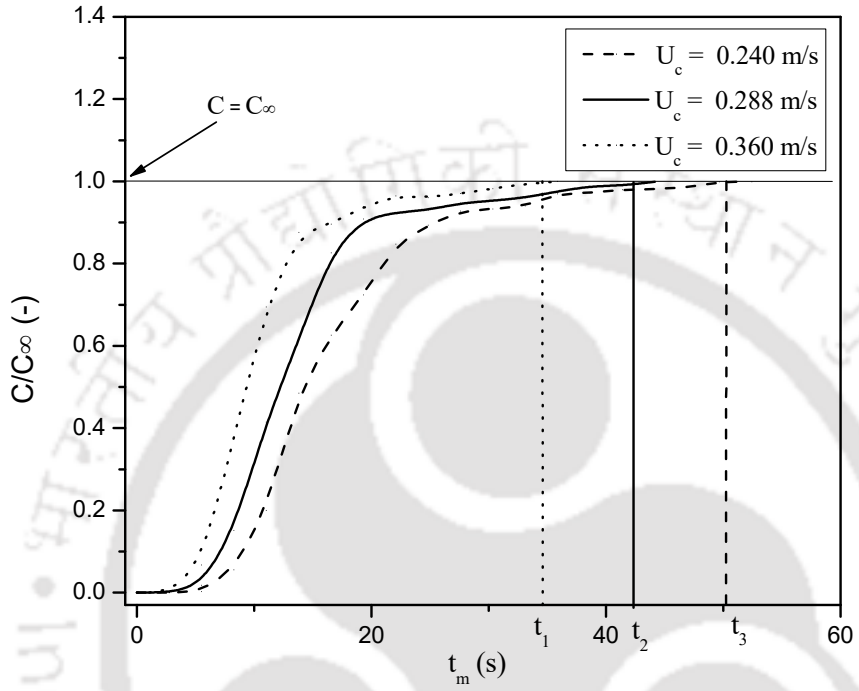

Figure 5.3: Outline to estimate the mixing time for microbubble suspension at different circulation velocities.

5.3.5 Estimation of Dispersion Coefficient

In the present work the value of dispersion coefficient is calculated from the Bodenstein number (as per Eq. (5.5)). The overall value of Bodenstein number was estimated by best fitting the experimental data with the Eq. (5.3). Figure 5.4 shows a typical comparison of experimental and theoretical values for *Bo* as a fitting parameter.

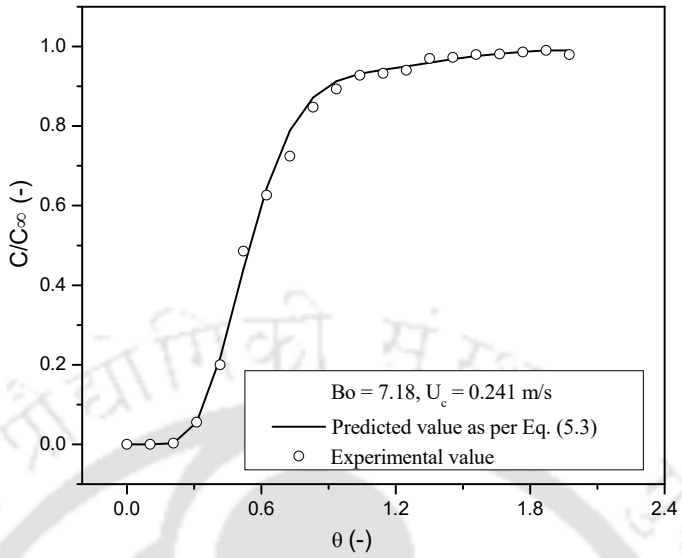

Figure 5.4: C/C_∞ vs θ curve for microbubble suspension: experimental and predicted.

5.4 Results and Discussion

5.4.1 Effect of Phase Velocities on Dispersion Coefficient

The axial dispersion coefficient in two-phase flow depends on many parameters such as gas flow rate, liquid flow rate, diameter of column and physicochemical properties of the system. The effect of microbubble suspension circulation velocity on its dispersion coefficient is shown in Figure 5.5. It was observed that dispersion coefficient increased with increasing circulation velocity. The motion of microbubble suspension are strongly affected by the turbulence in the system. As the turbulence increases, a rapid momentum exchange occurs between the phases, which causes an agitation in the column and the fluid tends to deviate from plug flow. The dispersion characteristic of tracer depends on the kinetic energy of the fluid flow. At low suspension rate the circulation in the device is weak. At higher suspension circulation velocity, the kinetic energy of the system significantly increases, which enhances the turbulence of the

gas-liquid mixture in the column. As a consequence of this gas-liquid interaction, backmixing and fluid circulation inside the column increases. This enhances the dispersion in the column.

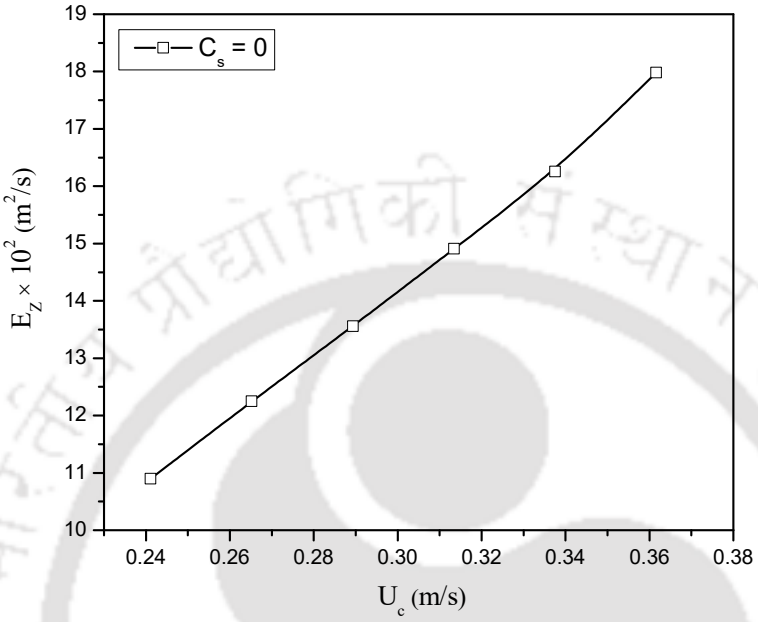

Figure 5.5: Variation of dispersion coefficient with microbubble suspension circulation velocity.

In case of larger bubbles, dispersion is affected by the size of bubbles. The transport of fluid by means of eddies; diffusion and convection are three core phenomena which causes the dispersion in a column. However the size of eddies and wakes produced by a microbubble are insignificant as compared to the conventional bubbles. So the intensity of dispersion in case of microbubble suspension is mainly governed by the turbulence and liquid circulation in a loop.

5.4.2 Effect of Suspension Properties on Dispersion Coefficient

Liquid phase dispersion is significantly affected by liquid properties. The effect of concentration of SCMC on dispersion coefficient of microbubble suspension is shown in Figure 5.6. It was observed that at constant suspension circulation velocity, dispersion coefficient of microbubble suspension decreased with increasing the SCMC concentration in

liquid. The viscosity of the microbubble suspension increases considerably with increasing the SCMC concentration. For a fixed suspension circulation velocity, an increase in viscosity of a liquid reduces the circulation inside the column. This is due to frictional resistance to flow. At higher viscosity the drag force acting on the layers of microbubble suspension also increases.

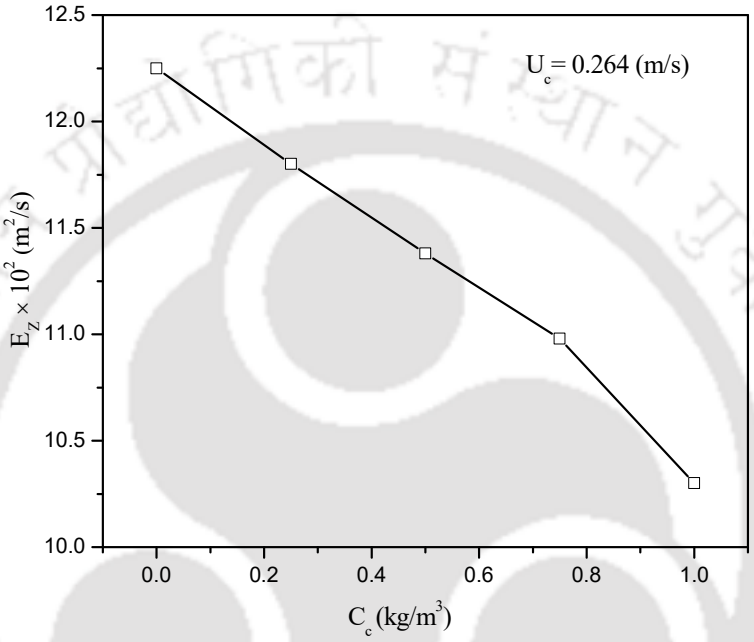

Figure 5.6: Variation of dispersion coefficient with SCMC concentration.

The energy of system decreases because of the dissipation of energy due to viscous stresses. Hence the dispersion coefficient of the system decreases. Yet, to the best of our knowledge there is no definitive correlation available in literature that can correlate the dispersion coefficient with viscosity or the diameter of the bubble. Pilhofer et al. (1978), Hikita and Kikukawa (1974) and Kelkar and Shah (1985) also observed a dependency of dispersion coefficient on the liquid phase properties. Their experimental results showed that increase in viscosity of liquid decreases the dispersion. Rice et al. (1981) observed a system dependency of dispersion phenomena. However Cova (1974) and Aoyama et al. (1968) claimed that viscosity has no influence on dispersion coefficient for conventional bubbles. The effect of

surfactants on the dispersion characteristic of microbubble suspensions is shown in Figures 5.7, 5.8 and 5.9. For all the three surfactants, it was observed that the dispersion coefficient increased with increasing surfactant concentration in the liquid. Addition of surfactant in the liquid lowers the interfacial tension between the gas and the liquid causing production of smaller microbubble from microbubble generator. Increase in the surfactant concentration results in increase in population of microbubble while apparent viscosity decreases. So at high surfactant concentration kinetic energy of the system is higher, due to reduction in viscosity. A populated microbubbles, increase the interactions among them, results more turbulence of gas liquid mixture in the column, which significantly enhance the dispersion coefficient. Further, Rice et al. (1981) reported that the small bubbles can carry more water in the form of wakes and hence create a higher backmixing.

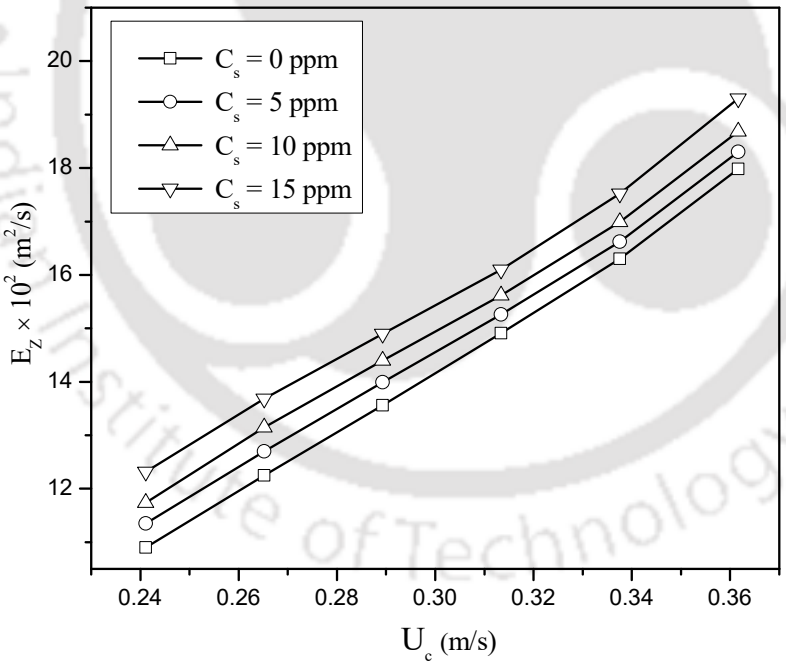

Figure 5.7: Variation of dispersion coefficient of microbubble suspension with SDS concentration.

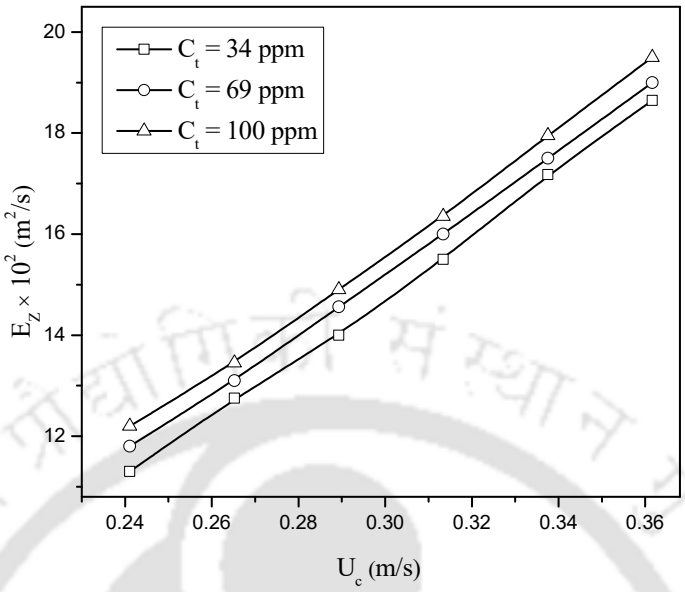

Figure 5.8: Variation of dispersion coefficient of microbubble suspension with CTAB concentration.

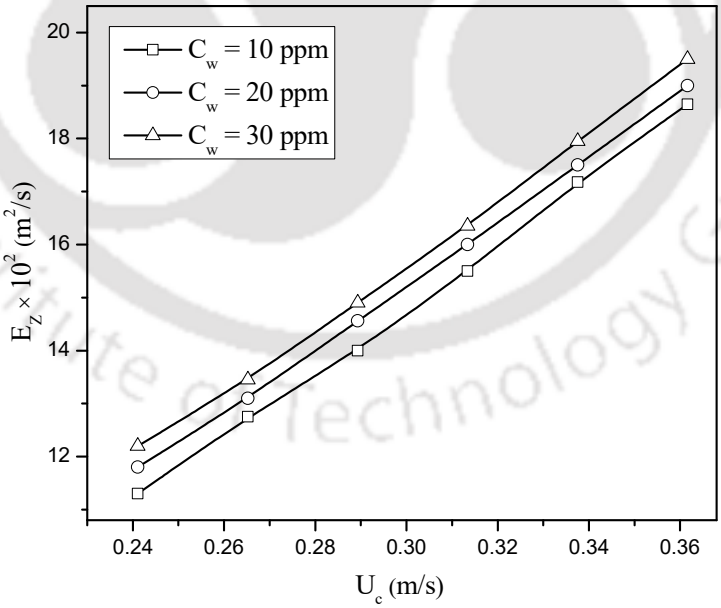

Figure 5.9: Variation of dispersion coefficient of microbubble suspension with Tween concentration.

From the present work, it was found that the axial dispersion coefficient of microbubble suspension is a function of different operating variables such as suspension circulation velocity, density, viscosity etc. Based on the present experimental data, the axial dispersion coefficient has been correlated in terms of the dimensionless groups of Reynolds number, Froude number and Weber number by the dimensional analysis. The correlation was made by fitting present experimental data with the help of multiple regression analysis by Microsoft Excel 2013, which can be expressed as

$$\frac{E_z}{U_c L} = 7.84\times10^{-3}\,\mathrm{Re}_n^{\,0.079} We^{0.264} Fr^{-0.209} \qquad (5.8)$$

The correlation coefficient and standard error of Eq. (5.8) were found to be 0.989 and 0.031 respectively. The parity plot of the correlation proposed for the dispersion number $(E_z/(U_cL))$ with the experimental value is shown in Figure 5.10. It was found that the developed correlation fitted well within the ranges: $35.04\times10^2 \le Re_n \le 68.86\times10^3$, $1.48\times10^2 \le We \le 5.72\times10^2$ and $2.96\times10^{-2} \le Fr \le 6.67\times10^{-2}$.

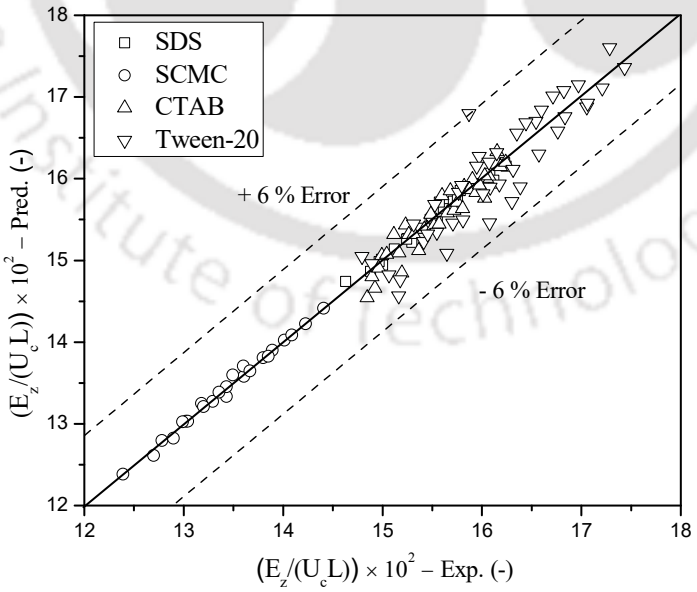

Figure 5.10: Parity plot of experimental and predicted values of dispersion number.

5.4.3 Effect of Circulation Velocity of Suspension on Mixing Time

The performance of bubble column depends on the intensity of dispersion of the gas and liquid phase. A lot of extensive efforts have been recently devoted to understand the dispersion characteristics. Mixing time represents the time for the tracer to reach the final equilibrium of homogeneity (Buwa and Ranade, 2003). Figure 5.11 shows the effect of suspension circulation velocity on mixing time of liquid in microbubble suspension without surfactant in the present device. It was observed that the mixing time decreased with increasing circulation velocity. An increase in suspension circulation velocity increases fluid circulation and backmixing in the column. The dispersion of tracer also increased with the suspension circulation velocity and caused an increase in dispersion in the column.

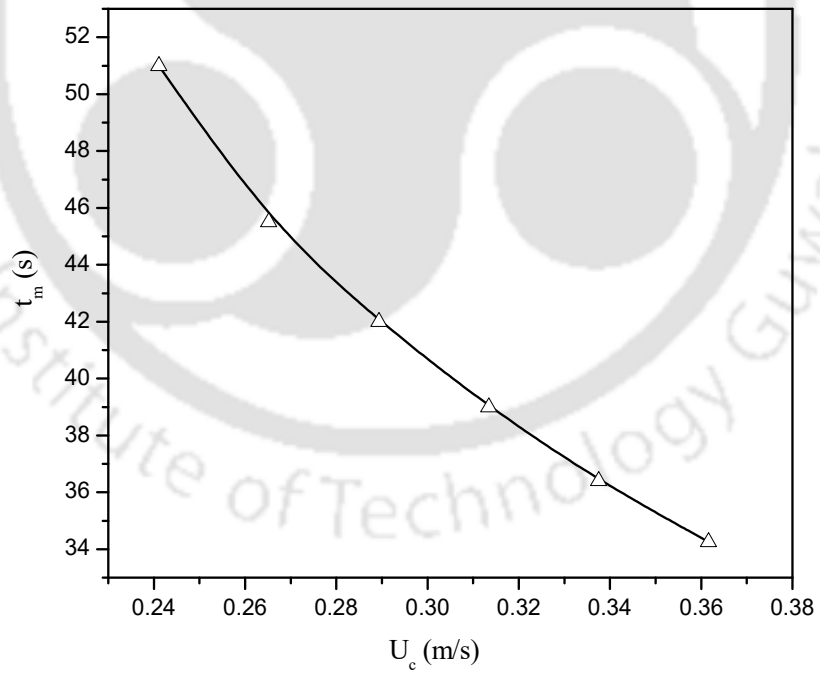

Figure 5.11: Variation of mixing time with microbubble suspension circulation velocity for suspension without surfactant.

5.4.4 Effect of Microbubble Suspension Properties on Mixing Time

The effect of SCMC on mixing time is shown in Figure 5.12. It is seen that for fixed circulation velocity the mixing time of microbubble suspension increases with increase in SCMC concentration. The viscosity of liquid increases with increasing the concentration of SCMC. The movement of microbubbles are restricted by increasing viscosity of liquid. The retarding force on the slow moving microbubbles increases with increase in viscosity of the solution. The circulation of suspension decreases as the frictional resistance between fluid and wall increases. Therefore the dispersion decreases and the mixing time of the liquid increases. For the surfactants solution, it was observed that mixing time decreased with increase in surfactant concentration. A typical variation of mixing time of SDS microbubble suspension with liquid circulation velocity shown in Figure 5.13.

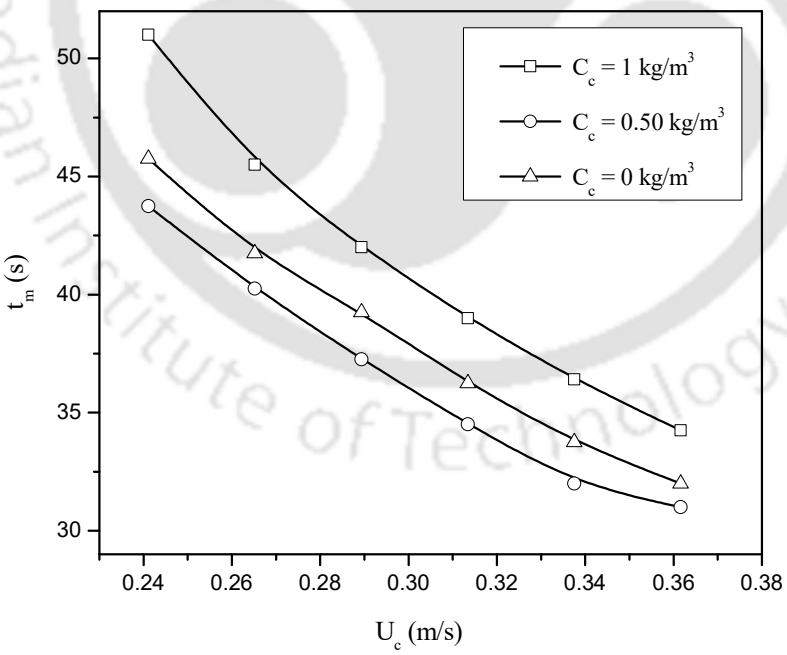

Figure 5.12: Variation of mixing time with SCMC concentrations.

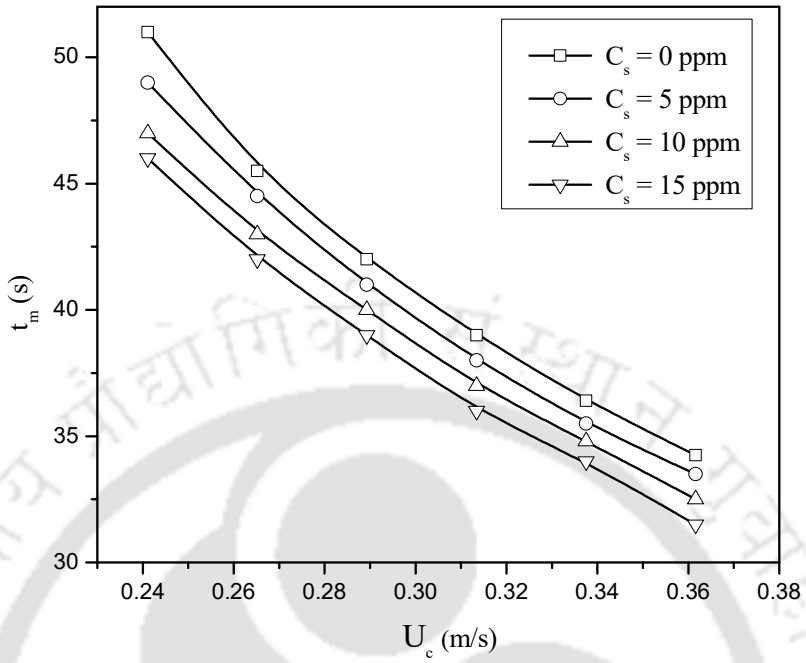

Figure 5.13: Variation of mixing time with SDS concentrations.

Addition of surface additive agents increases the dispersion. This is due to less energy dissipation to get the same degree of circulation and turbulence in the system for dispersion. This helps the fluid elements to disperse at a faster rate. Hence the increase in liquid circulation reduces the mixing time of the microbubble suspension. The mixing time of suspension based on its circulation velocity and physical properties can be correlation as

$$\frac{t_m U_c}{D_c} = 0.034 Bo^{1.104} \mathrm{Re}_n^{0.113} We^{0.515} Fr^{-0.419} \qquad (5.9)$$

The correlation coefficient and standard of Eq. (5.9) are 0.978 and 0.021 respectively. The parity of plots for the comparison of experimental and predicted values of mixing time of microbubble suspension is shown in Figure 5.14. It is clear that proposed correlation can predict mixing time well within the ranges $6.0 \le Bo \le 8.07$, $50.04\times10^2 \le Re_n \le 68.86\times10^3$, $1.48\times10^2 \le We \le 5.72\times10^2$ and $2.96\times10^{-2} \le Fr \le 6.67\times10^{-2}$.

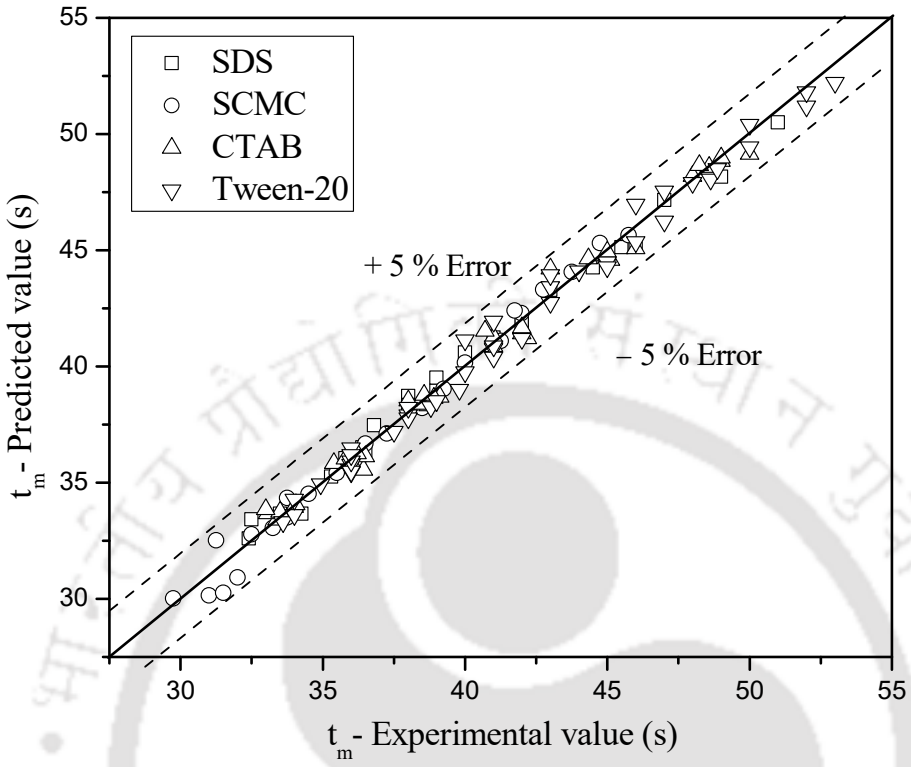

Figure 5.14: Parity of experimental and predicted values of mixing time.

5.4.5 Model Development to Interpret the Intensity of Dispersion

Literature on liquid dispersion has revealed that dispersion of liquid is caused by the convective liquid recirculation (Burns and Rice, 1997; Joshi and Sharma, 1979). However these mechanisms are expected to become more significant at higher flow rates (Kumar et al., 1994; Wilkinson et al., 1993). For complete liquid recirculation, the dispersion is affected by the liquid recirculation inside the device. In order to determine the influence of liquid recirculation, a simple mechanistic model is developed based on combined effect of both turbulence and liquid circulation. In the present system the suspension flows as shown in Figure 5.15. The reversal of the velocity occurs at the top of the column. The circulation velocity is significantly affected by the dynamic variables like microbubble suspension flowrate and the physical

properties of the suspension. At the interface of upstream and downstream flowing suspension, the microbubble suspension circulation velocity is almost zero.

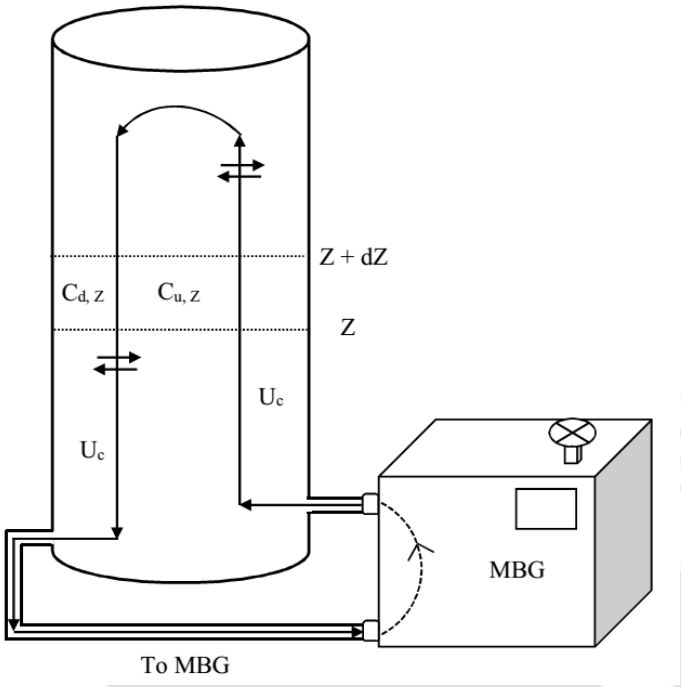

Figure 5.15: Schematic diagram of microbubble suspension circulation.

The suspension flows with the wide distribution of velocities over the cross-section of the column. This distribution may depend upon the geometry, circulation pattern and operating conditions of bubble column. In the present study it is assumed that there a uniform circulation in each operating conditions in the column. Due to this variation of velocity in upstream and downstream suspensions, a radial interaction occurs between the suspensions and there is an exchange of some amount of liquid with each other. This exchange is denoted by a parameter λ and the dispersion in both the up and the downward flowing section is represented by parameter E. A mass balance of tracer at any position Z for the upstream suspension can be written as

$$A_u\left(\frac{\partial C_u}{\partial t}\right)_z = A_u E\left(\frac{\partial^2 C_u}{\partial Z^2}\right)_z - A_u U_c\left(\frac{\partial C_u}{\partial Z}\right)_z - \lambda S\left(C_{u,z} - C_{d,z}\right) \qquad (5.10)$$

Similarly the mass balance of tracer for the downstream suspension is

$$A_d\left(\frac{\partial C_d}{\partial t}\right)_z = A_d E\left(\frac{\partial^2 C_d}{\partial Z^2}\right)_z + A_d U_c\left(\frac{\partial C_d}{\partial Z}\right)_z + \lambda S\left(C_{u,z} - C_{d,z}\right) \tag{5.11}$$

If the interaction between the upstream and downstream suspension is high, the concentration difference ($C_{u,z} - C_{d,z}$) will be relatively small. It is assumed that the upcoming area and downcoming area of flow are equal to half of the area of column, i.e. $A_u \approx A_d = 0.5A_c$. Then the circumference between the upcoming and downstream fluid (S) will be equals $\pi D_c/\sqrt{2}$. Incorporating all these assumption in Eq. (5.10) and (5.11) and adding them, one gets

$$\left(\frac{\partial\left(C_u + C_d\right)}{\partial t}\right)_z = E\left(\frac{\partial^2\left(C_u + C_d\right)}{\partial Z^2}\right)_z - U_c\left(\frac{\partial\left(C_u - C_d\right)}{\partial Z}\right)_z \tag{5.12}$$

By substituting $C_u + C_d = 2\overline{C}$, Eq. (5.12) becomes

$$\left(\frac{\partial\left(\overline{C}\right)}{\partial t}\right)_z = E\left(\frac{\partial^2 \overline{C}}{\partial Z^2}\right)_z - \frac{U_c}{2}\left(\frac{\partial\left(C_u - C_d\right)}{\partial Z}\right)_z \tag{5.13}$$

Now subtracting Eq. (5.10) from Eq. (5.11) and rearranging, it leads to

$$2\lambda S(C_{u,z} - C_{d,z}) = A_d E\left(\frac{\partial^2\left(C_u - C_d\right)}{\partial Z^2}\right)_z - A_d U_c\left(\frac{\partial\left(C_u + C_d\right)}{\partial Z}\right)_z - A_d\left(\frac{\partial\left(C_u - C_d\right)}{\partial t}\right)_z \tag{5.14}$$

Since the concentration difference (C_u - C_d) is very small, it may be assumed that all the terms on the right-hand side of Eq. (5.14) containing C_d - C_u are negligible and $C_u + C_d = 2\overline{C}$.

Hence Eq. (5.14) can be expressed as

$$2\lambda S(C_{u,z} - C_{d,z}) = -2A_d U_c\left(\frac{\partial\left(\overline{C}\right)}{\partial Z}\right)_z \tag{5.15}$$

The Eq. (5.15) after differentiating with respect to Z can be expressed as

$$\left(\frac{\partial\left(C_u - C_d\right)}{\partial Z}\right)_z = -\frac{A_c U_c}{2\lambda S}\left(\frac{\partial^2 \overline{C}}{\partial Z^2}\right) \tag{5.16}$$

Now from Eq. (5.16) and Eq. (5.13), one gets

$$\left(\frac{\partial\left(\overline{C}\right)}{\partial t}\right)_z = \left(E + \frac{U_c^2 D_c \sqrt{2}}{16\lambda}\right)\left(\frac{\partial^2 \overline{C}}{\partial Z^2}\right) \tag{5.17}$$

Eq. (5.17) is similar to the one dimensional axial dispersion model and the coefficient of dispersion can be written as

$$E_z = E + E_c = E + \frac{\delta}{\lambda} \tag{5.18}$$

where the parameter E_z is overall dispersion coefficient, E represents dispersion due to liquid turbulence and the parameter E_c denotes dispersion due to liquid circulation, which can be expressed as

$$E_c = \frac{U_c^2 D_c \sqrt{2}}{16\lambda} = \frac{\delta}{\lambda} \tag{5.19}$$

where the parameter δ is defined as

$$\delta = \frac{U_c^2 D_c \sqrt{2}}{16} \tag{5.20}$$

The values of the liquid exchange parameter (λ) and dispersion due to liquid turbulence (E) for different experimental conditions can be calculated from the Eq. (5.18) by plotting overall dispersion coefficient (E_z) versus δ from the experimental data. The intercept of the plot represents dispersion coefficient E. The liquid exchange parameter (λ) can be calculated as

$$\lambda = \left[\text{slope of equation (5.18)}\right]^{-1} \tag{5.21}$$

5.4.6 Interpretation on Dispersion due to Suspension Circulation

It was observed that the dispersion coefficient due to liquid circulation increased with increasing suspension circulation velocity. The magnitude of dispersion is proportional to average liquid circulation and superficial liquid velocity (Joshi and Sharma, 1979). At high liquid velocity more turbulences exists in the column. The liquid circulation rate in the column increases with increase in microbubble suspension circulation velocity. Figure 5.16 shows a typical variation of dispersion coefficient due to liquid circulation with SDS concentration. It can be seen that the dispersion coefficient due to liquid circulation is affected by SDS concentration. At high surfactant concentration, the dispersion coefficient due to liquid circulation is higher. Microbubble suspension behave as a non-Newtonian fluid, whose apparent viscosity decreases with fluid velocity. So at high surfactant concentration, the apparent viscosity of the suspension decreases with increase in circulation rate, which decreases the energy dissipation between the suspension layers. Therefore the dispersion coefficient due to liquid circulation increases with SDS concentration. Based on present experimental data, the functionality of E_c with suspension circulation velocity for SDS microbubble suspensions can be expressed as

$$E_c = pU_c^q \tag{5.22}$$

where the parameter p depends on the concentration of SDS in the microbubble suspension (C_s) and can be correlated as

$$p = 0.9 + 10.20 \times 10^{-3} C_s - 7 \times 10^{-5} C_s^2 \tag{5.23}$$

while the value of parameter q is found to be 2.

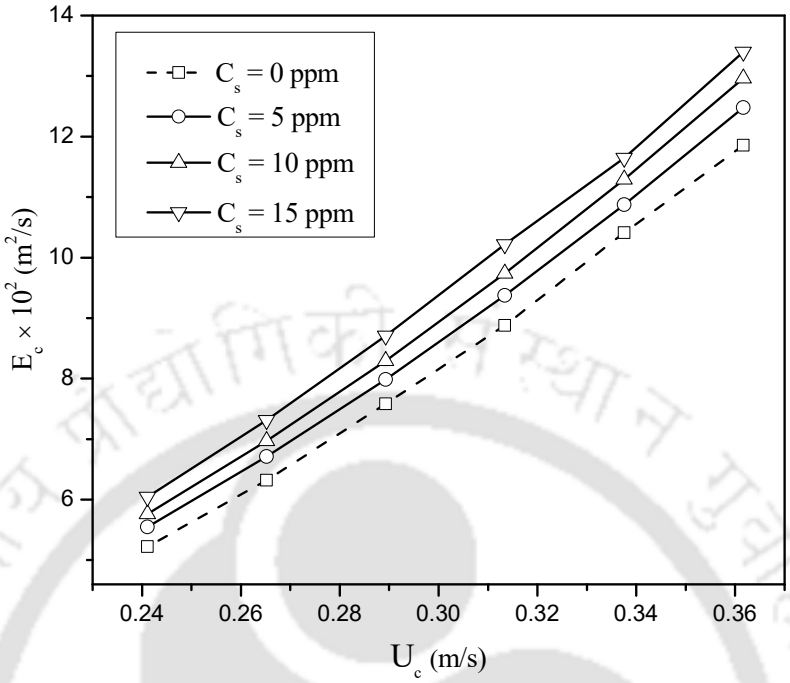

Figure 5.16: Variation of dispersion coefficient due to circulation with microbubble suspension circulation velocity in SDS solution.

The effect of SCMC on the dispersion coefficient due to liquid circulation is shown in Figure 5.17. It was observed that the dispersion coefficient due to circulation decreased with increasing SCMC concentration. The energy dissipation rate between the layers of microbubble suspension depends on the apparent viscosity of suspension. The energy dissipation rate increases with increase in liquid viscosity. This causes reduction in the liquid circulation of the microbubble suspension. Therefore the dispersion coefficient due to circulation decreases with addition of SCMC in the liquid. The functionality of dispersion coefficient due to circulation with the SCMC concentration can be expressed as

$$E_c = \alpha U_c^2 \tag{5.24}$$

The proportionality constant (α) of Eq. (5.24) is correlated with the concentration of SCMC as

$$\alpha = 0.9 - 0.184C_c - 0.104C_c^2 \quad (5.25)$$

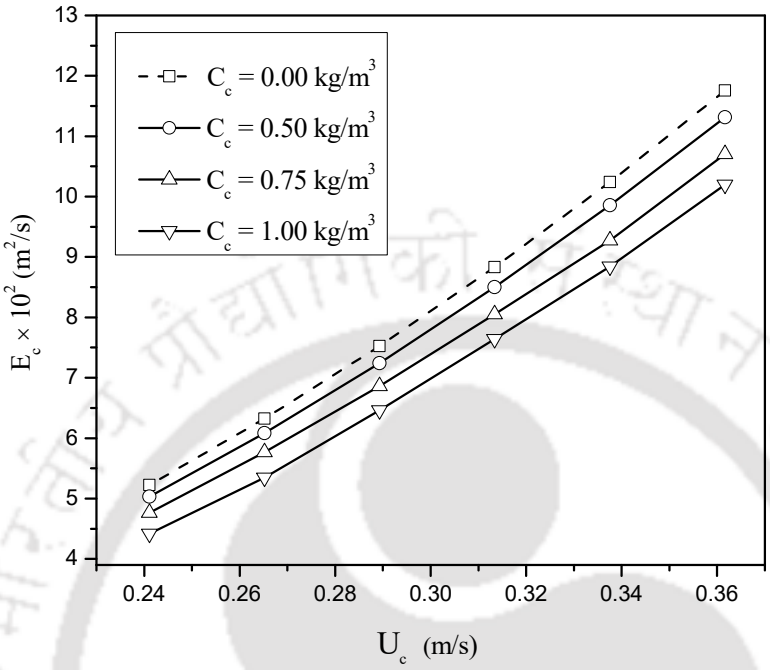

Figure 5.17: Variation of dispersion coefficient due to circulation with microbubble suspension circulation velocity in SCMC solution.

5.4.7 Interpretation of Exchange Factor (λ)

The liquid exchange factor is significantly affected by the operating variables. It was observed that for all three surfactants the liquid exchange factor decreased with increasing surfactant concentration in the suspension. A typical variation of liquid exchange factor with SDS concentration is shown in Figure 5.18. The liquid exchange factor depends on distribution of velocity in the column. At high circulation velocity, the column gets agitated and the velocity distribution in the column changes. At high circulation velocity, the radial distribution of velocity decreases. This causes the reduction in the liquid exchange factor. However a reverse effect was observed in case of SCMC microbubble suspensions as shown in Figure 5.19.

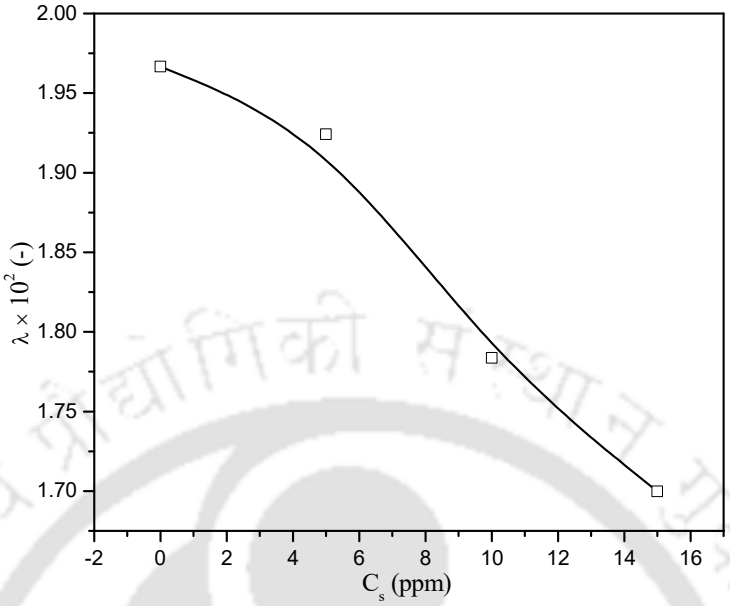

Figure 5.18: Variation of liquid exchange factor with SDS concentration.

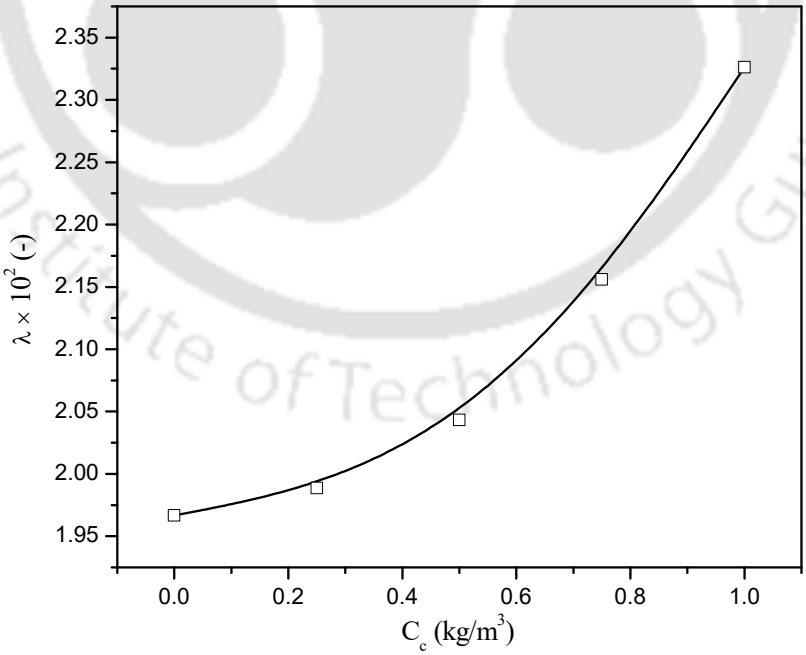

Figure 5.19: Variation of liquid exchange factor with SCMC concentration.

Increase in concentration of SCMC increases the viscosity of the suspension. This causes a reduction in turbulence in the column and change in velocity distribution. Due to increase in radial velocity the exchange between liquid layers increases. From the present experiment it is seen that the liquid exchange factor satisfies the functionality with SDS concentration as

$$\lambda = 19.7 \times 10^{-3} - 1 \times 10^{-4} C_s - 4 \times 10^{-6} C_s^2 \quad (5.26)$$

Similarly for SCMC concentration the liquid exchange factor can be expressed as

$$\lambda = 19.7 \times 10^{-3} + 5 \times 10^{-4} C_c + 4 \times 10^{-3} C_c^2 \quad (5.27)$$

A high liquid exchange will not contribute a high dispersion unless a sufficient turbulence and circulation are in the system. Similarly, if there is high liquid circulation inside the column and there is no exchange between the liquid ($\lambda = 0$), high circulation rate will not contribute to high dispersion. So both circulations and exchange of liquid are required for dispersion phenomenon.

5.5 Conclusion

The present chapter mainly emphasis on the estimation of intensity of mixing of microbubble suspensions in a vertical bubble column. The dispersion of liquid due to liquid circulation inside microbubble suspension is also analysed. From the present work it was found that the intensity of dispersion of microbubble suspension depends on the operating variables and the physicochemical properties of system. It was also observed that the mixing time of microbubble depends on the circulation velocity and properties of suspension. The mixing time of microbubble suspension decreased with increasing suspension circulation velocity and surfactants concentration, while the mixing time increases with increase in SCMC

concentration. The dispersion coefficient due to liquid circulation of the suspension found to be dependent on the phase velocity, surfactant concentrations and SCMC concentration in the suspension. The dispersion coefficient due to liquid circulation of the suspension increased with increasing suspension circulation velocity. The magnitude of dispersion coefficient due to liquid circulation decreased with increasing the SCMC concentration in the suspension, while with increasing the surfactant concentration its value found to be increased. The liquid exchange factor λ depends on the physicochemical properties of suspension. It was found that increase in turbulence of the phases increases the kinetic energy of the system and decreases the velocity characteristic factor.

Notations

A_c	Column cross-sectional area (m^2)
C	Tracer concentration (Kg/m^3)
C_u	Tracer concentration in upstream suspension (Kg/m^3)
C_d	Tracer concentration in downstream suspension (Kg/m^3)
$\overline{C}$	Average concentration (Kg/m^3)
C_s	Concentration of surfactant (ppm)
C_c	Concentration of SCMC (kg/m^3)
C_{sc}	Concentration of salt (kg/m^3)
C_∞	Equilibrium tracer concentration (Kg/m^3)
D_c	Column diameter (m)
d_b	Microbubble diameter (m)
E_z	Overall liquid dispersion coefficient (m^2/s)
E	Dispersion coefficient due to turbulence (m^2/s)
E_c	Dispersion coefficient due to circulation (m^2/sec)

g	Acceleration due to gravity (m^2/sec)
K	Consistency of fluid ($Pa.s^n$)
K_c	Conductivity (μS/m)
L	Characteristic length (m)
L_p	Length of pipe (m)
n	Flow behavior index (-)
ΔP	Pressure drop (N/m^2)
p	Parameter defined in Eq. (5.23)
Q	Microbubble suspension flow rate (m^3/s)
Q_t	Amount of tracer injected (kg)
q	Constant in Eq. (5.22)
S	Circumference between upstream and downstream microbubble flow (m)
U_c	Suspension circulation velocity (m/s)
t	Time (s)
t_m	Mixing time (s)
Z	Location in vertical axis (m)

Greek letters

μ_e	Effective viscosity (kg/m.s)
ρ_m	Density of suspension (kg/m^3)
λ	Liquid exchange factor (m/s)
δ	Parameter defined in Eq. (5.20)
α	Parameter defined in Eq. (5.25)
Θ	Dimensionless time (-)
τ	Wall shear stress (N/m^2)
γ_a	Apparent shear rate (s^{-1})

σ	Surface tension (N/m)

Dimensionless groups

Bo	Bodenstein number ($(U_c L/E_Z)$ (-)
Fr	Froude number (U_c^2/gL) (-)
Re_n	Non-Newtonian liquid Reynolds number ($\frac{D_c^n U_c^{2-n}\rho}{8^{n-1}K}\left(\frac{4n}{3n+1}\right)^n$) (-)
We	Weber number $\rho_m U_c^2 L/\sigma$ (-)

Subscripts

e	Effective
d	Downstream flow
m	Mixture
p	Pipe
t	Tracer
u	Upstream flow

CHAPTER-6

MINERAL BENEFICIATION BY IONIC MICROBUBBLE

The performance of ionic microbubble for fine particle separation is investigated and reported in this Chapter. The effects of different operating variables and physicochemical properties of liquid on the separation characteristics of ionic microbubble are examined. A phenomenological kinetic model based on collision, attachment and detachment mechanisms of fine particle is developed to analyze the flotation characteristics of the ionic microbubbles. Generalized correlations for flotation rate constant and induction time are also developed based on the physicochemical properties of microbubble-particle mixture. The recovery of particles based on the mixing phenomena is also enunciated.

6.1 Introduction

Separation of fine particles is widely encountered in mineral industries. A large sum of operating expenditures of mineral industries are associated with separation of mineral processes. Therefore the influence of separation process technology on the profitability is high in mineral industries (Rousseau, 1987). Flotation is most common means of separating the valuable components in this regard. Flotation is beneficial not only to mineral separation, a large variety of chemical species such as ions, molecules, microorganisms, oil droplets etc. are also separated by this method. They

can either be separated from one another or concentrated from solution (Al-Shamrani et al., 2002; Gaudin et al., 1960; Matis and Mavros, 1991). The coarse particles are easily separated by the conventional flotation method but when the size of mineral particle is in micrometer range, it is very difficult to separate it. The poor recovery of fine mineral by flotation is mainly due to the low probability of bubble–particle collision, which decreases with decreasing particle size (Weber and Paddock, 1983). Conventional flotation (Conventional flotation is the floatation using millibubbles. The bubble size in conventional flotation is generally of the order of 0.5 mm (Waters et al., 2008)) are inefficient in encountering collision and attachment of fine particles and bubbles. For the recovery of fine mineral particles, the flotation cell should have fine bubbles or microbubbles suitable to catch these particles (Trahar and Warren, 1976). Microbubbles have been extensively used in the mineral and liquid effluent treatment, and especially for the flotation of particles having size less than 100 μm (Solari and Gochin, 1992). The charge on the surface of microbubble helps it, to become a propitious tool for the fine mineral separation (Han and Dockko, 1998). According to Jauregi et al. (1997) the potential applications of microbubbles can be grouped into four main zones: (i) flotation for the removal of biological and non-biological products; (ii) protein recovery; (iii) enhancement of oxygen mass transfer; and (iv) bioremediation. Microbubble aided flotation has been widely employed in the various fields for the process intensification. They have been used for recovery of proteins (Amiri and Valsaraj, 2004; Jarudilokkul et al., 2004; Jauregi et al., 1997; Noble et al., 1998), recovery of microorganism (Hanotu et al., 2012), removal of heavy metal ions from water (Ciriello et al., 1982), removal of dye and pigment (Alves et al., 2006; Roy et al., 1992). Cilliers and Bradshaw (1996) used microbubble to recovery of fine pyrites. Shen and Wheelock, (2000) reported that approximately 85% recovery of fine coal particles can be achieved by using microbubbles. The recovery of fines can be increased up to 95% using

microbubbles with proper chemical agents (Han and Dockko, 1998). Separation can further be enhanced by using ultrasound with the microbubble (Shibata et al., 2008). Mechanical modification has also been done to improve this technology for mineral beneficiation (Yi-jun et al., 2009). Microbubble-aided flotation not only increases the recovery it also reduces the frother consumption (Ahmadi et al., 2014). The electrical double layer interactions and the particle and bubble charge can affect the rate of recovery for fine particles. The electrostatic interactions present between charged microbubble and particles of opposite charge may be a governing force for separation. Fuda and Jauregi (2006) carried out a detailed study to observe the mechanism of separation of proteins by ionic microbubbles. They concluded that electrostatic interactions were the driving force for the separation. Waters et al. (2008) also used ionic microbubble to separate fine binary mixture of mineral. They found that surface charge of microbubble can be changed by using surfactants. They compared the results obtained with conventional flotation method and observed that ionic microbubble has high recovery over conventional flotation. Recently, Johnson et al. (2009) reported that repulsive long-range interactions are responsible for the selective attachment of mineral particles to microbubbles in a charge-dependent manner.

It is very clear from the literature that, the ionic microbubble has a potential to intensify recovery in mining industries. When considering the industrial applications of ionic microbubble in mineral separation, it is important to evaluate the benefits of ionic microbubble based on scientific principles, from an academic standpoint and to compare microbubble flotation technology with existing technology both in terms of its functional quality and effectiveness. Thus it becomes very important to examine the effect of physicochemical properties of liquid and mineral particle based on mechanism of ionic microbubble flotation. The present chapter is aimed to study the potential

of ionic microbubble for the separation of binary fine particle by flotation. Furthermore, the effects of surfactants on the recovery of fine particle are also analyzed.

6.2 Experimental Setup and Procedure

6.2.1 Materials

In the present study three mineral particle mixtures such as (i) zinc oxide (ZnO) and silica (SiO_2) (ii) Copper oxide (CuO) and silica (iii) Aluminum oxide (Al_2O_3) and silica were used to study the separation characteristics of ionic microbubble. The surfactants cetyltrimethylammonium bromide (CTAB), sodium dodecyl sulfate (SDS) and Polysorbate 20 (Tween-20) were used to form ionic microbubble. The concentrations of CTAB and SDS were varied from 5 ppm to 35 ppm. The concentration of Tween-20 was varied from 17 ppm to 207 ppm. Preliminary tests carried out on the stability of ionic microbubble (which has been discussed in Chapter 3) showed that 5 ppm of CTAB and SDS each was sufficient to ensure the dispersion without break down when being pumped. In case of Tween-20, concentration 17 ppm was sufficient to produce stable microbubble. All the chemicals used in the present work had a purity of > 98% and were purchased from Merck Chemicals (India). The effective viscosity of particle-microbubble mixture was calculated as per the procedure discussed in Chapter 4. All the experiments in the present chapter were carried out at 25±1° C. The physical properties of liquid phase are listed in Table 6.1.

6.2.2 Experimental Setup

The schematic of the plant prototype in which the experiments were carried out is shown in Figure 6.1. The experimental system includes a flotation column, a microbubble generator, a gas compressor and other accessories such as rotameters, control valves, thermometer, etc. The

separation system is composed of the microbubble flotation column. The flotation column was made of plexiglass having an internal diameter of 0.2 m and a height of 0.6 m.

Table 6.1: Physical properties of particle-microbubble system measured at 25 ± 1 ºC.

Type of fluid-particle mixture	Concentration in water (ppm)	Density (kg/m^3)	Surface tension (mN/m)
SDS-1	5	999.73	69.00
SDS-2	10	989.76	67.00
SDS-3	15	985.79	65.20
SDS-4	20	981.02	63.00
SDS-5	30	978.84	62.00
CTAB-1	5	994.74	69.20
CTAB-2	10	989.77	66.37
CTAB-3	20	987.02	63.77
CTAB-4	50	984.84	60.75
CTAB-5	100	981.21	59.83
Tween-20-1	17	1000.08	64.03
Tween-20-2	34	999.10	57.66
Tween-20-3	69	991.028	52. 36
Tween-20-4	138	988.94	48.13
Air	-	1.18	-

The top portion of the column is made hooded for collection of froth. Both inlet and outlet of the column were at the lower end through which microbubble generator was connected. The air used to create microbubbles was supplied to the generator from a compressor controlled by a valve. The microbubble particle mixture flow rate was measured by using rotameters for which the flow was maintained by using control valves. Equal mass of fine mineral particle and silicon dioxide (10 gram each) were used a as flotation feed. The experiments were conducted at six different mixture circulation velocities (U_c) in the range of 0.24 to 0.36 m/s. The circulation velocity in the flotation column is determined by $Q_m/(A_c/2)$ where Q_m is the microbubble particle mixture volumetric flowrate measured by rotameter and A_c is the cross-sectional area of flotation column. The collected particles were dried in an oven (Model-ROV/DC, Reico Equipment and Instrument Pvt. Ltd., Kolkata India), till the equilibrium moisture content was reached and then weighed. To

minimize the error five runs were performed and the average of three was taken as a final reading. The collected samples contained both silica and the mineral particles. The amount of mineral particle from the mixture was determined by the following way:

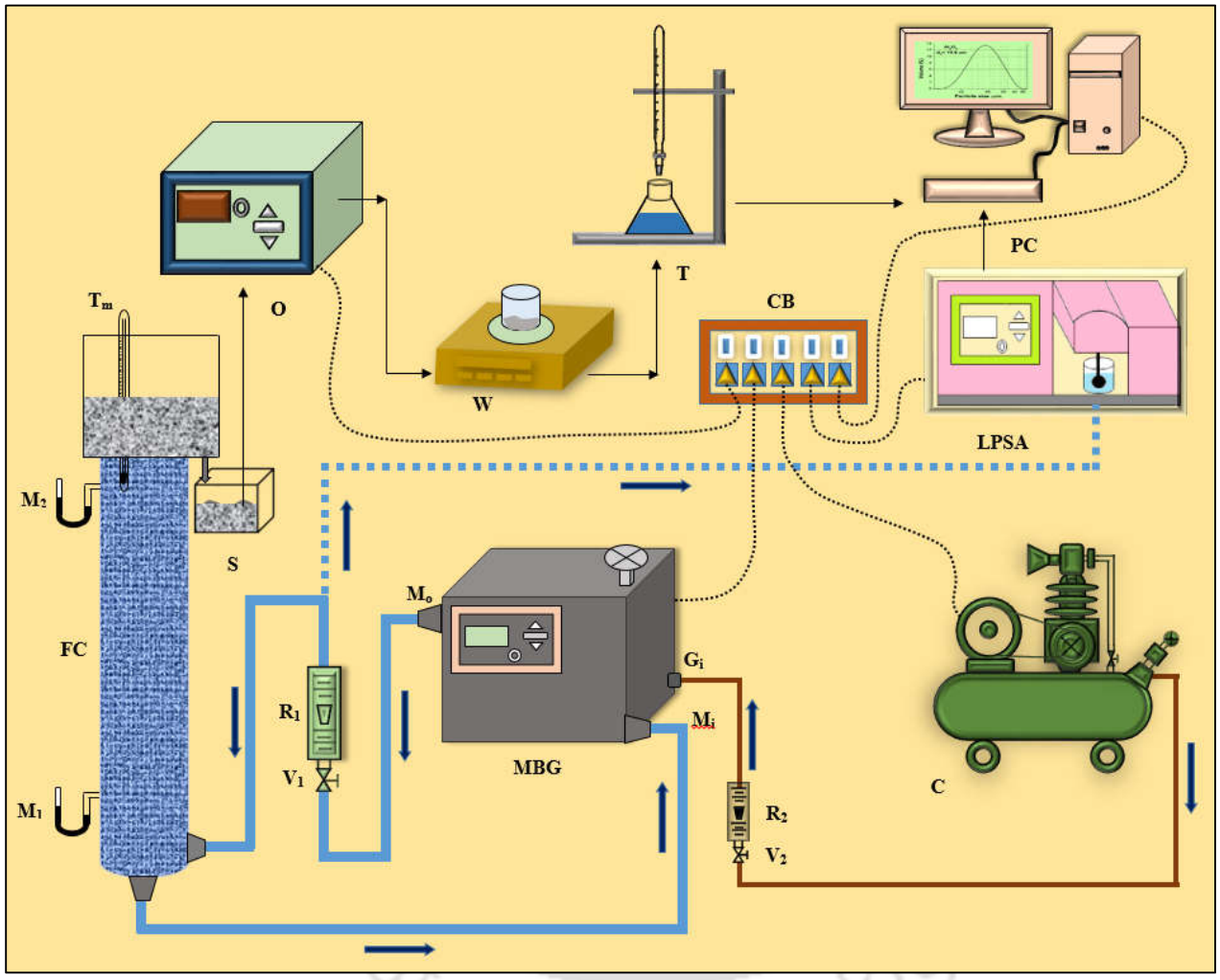

Figure 6.1: Schematic of experimental setup. Legend: - C: Air compressor; FC: Flotation column; CB: Control board; G_i: Microbubble generator gas inlet; LPSA: Laser particle size analyzer; MBG: Microbubble generator; M_o: Microbubble generator output; M_i: Microbubble generator input; M_1, M_2: Manometers; O: Electric oven; PC: Computer; R_1, R_2: Rotameters; S: Froth sample collection; T_m: Thermometer; T: Titration unit; V_1, V_2: Control valves; W: Weighing balance.

6.2.2.1 Determination of ZnO

Initially a known volume of 2N H_2SO_4 was poured in a beaker containing the dried mixture of SiO_2 and ZnO. Silicon dioxide is inert to H_2SO_4 whereas ZnO readily reacts with H_2SO_4 to form zinc sulfate and precipitates. The unreacted H_2SO_4 acid was then separated from the mixture.

$$ZnO + H_2SO_4 \rightarrow ZnSO_4 \downarrow + H_2O \quad (6.1)$$

The volume of unreacted H_2SO_4 was determined by acid base titration. The amount of ZnO in mixture was then determined from the stoichiometry analysis.

6.2.2.2 Determination of Al_2O_3 and CuO

The dried mixture of CuO/Al_2O_3 and SiO_2 was first reacted with 2N HCL. Silicon dioxide is inert to HCl whereas CuO/Al_2O_3 readily reacts with HCl to form respective chlorides and precipitates.

$$CuO + 2HCl \rightarrow CuCl_2 \downarrow + H_2O \quad (6.2)$$

$$Al_2O_3 + 6HCl \rightarrow 2AlCl_3 \downarrow + 3H_2O \quad (6.3)$$

The volume of unreacted HCl was determined by acid base titration. The amount of CuO/Al_2O_3 in mixture was determined by the stoichiometry analysis. Each experiment was replicated three times and the results showed a maximum variation of 2% of the mean value. Finally, the percentage removal efficiency or recovery *(% R_c)* was calculated as per Eq. (6.4)

$$\%R_c = \frac{M_r}{M_f} \times 100 \quad (6.4)$$

where M_r represents mass of particle recovered and M_f denotes mass of feed.

6.2.3 Estimation of Zeta Potential of Particle

The zeta-potential of particles in surfactant solution (surfactant and water) was measured using a zeta potentiometer (Model-Delsa Nano C, Beckman Coulter, Nyon, Switzerland) from the electrophoretic mobility of the particle (Tantra et al., 2010; Waters, 2008). Each data point for zeta-potential was taken as an average of three measurements at room temperature. In the present study all the experiments were conducted within the pH range 8-9. So variation of zeta potential of particles and bubble with the pH was neglected.

6.2.4 Estimation of Particle and Microbubble Size

The microbubble and particle size was calculated by laser particle size analyzer. The laser diffraction method delivers rapid bubble size distributions over milli to nanometer ranges. The particle size distributions measured by particle size analyzer is shown in Figure 6.2. The details for the measurement of microbubble size and its distribution is discussed in Chapter 3

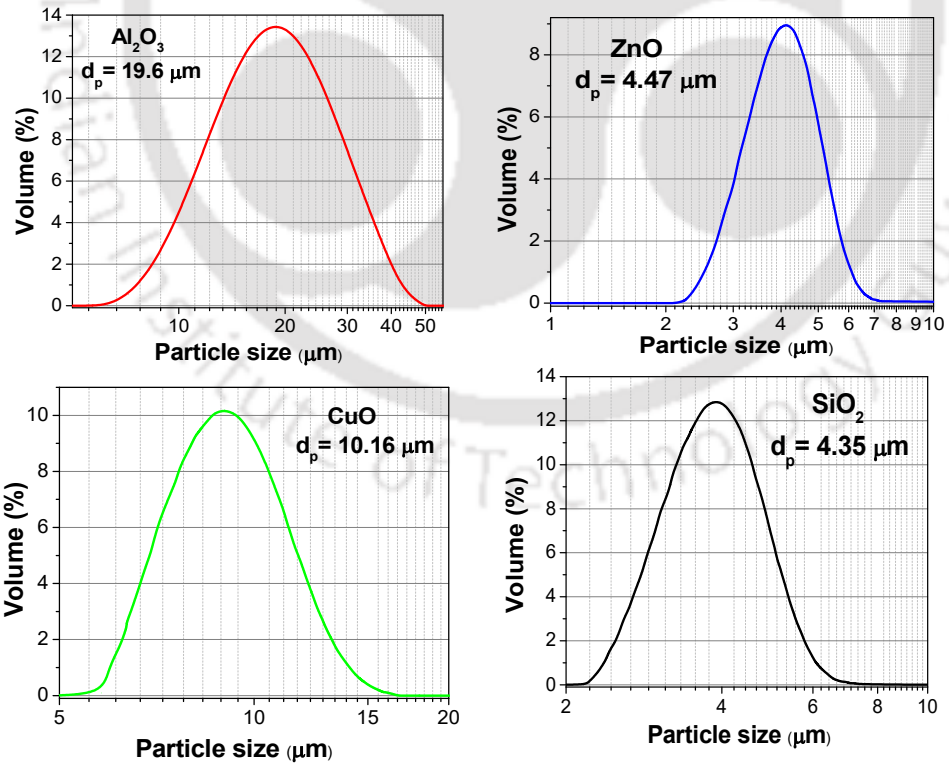

Figure 6.2: Size distributions of different mineral particles.

6.3 Results and Discussion

6.3.1 Effect of Mixture Velocity on Recovery of Mineral Particles

Flotation of fine particles by using microbubble is very complex physicochemical process. The number of variables which can affect mineral recovery may be classified broadly into the physical and the chemical. In the present work, effect of these variables are examined in details. Figure 6.3 shows the effect of mixture circulation velocity on the flotation recovery, at fixed surfactant concentration, for all the three mineral particles.

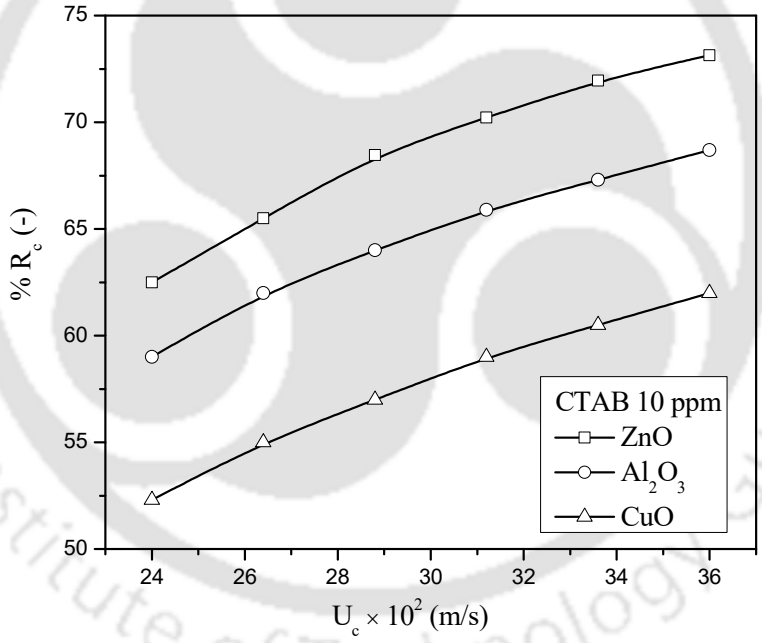

Figure 6.3: Effect of circulation velocity of mixture on the recovery of particles.

It was observed that for all the particles, the flotation recovery increased with the increase in mixture velocity. The particle microbubble collision depends on the hydrodynamics of flow, which is mainly governed by mixture velocity. The turbulence in the column increases due to increase in

mixture velocity. The mixing characteristics of microbubble-particle mixture in the column also increases with increase in turbulence in the column. Mixing increases the probability of bubble-particle collision. As the particle come nearer to the microbubbles, it colloids to the bubble. After colliding with a rising microbubble, the particle attaches on the bubble surface and forms a stable particle–bubble aggregate. However, all the particles colliding with air bubbles do not result in flotation. Only the hydrophobic particles adhere to the surface of bubbles. The attached particle on the microbubble moves upward due to buoyant force acting on the microbubble and collected from the top of the flotation column. Therefore the flotation recovery increased with increase in mixture circulation velocity. Particle detachment may also occurs when detachment forces exceed the maximum adhesive forces. One probable source of adhesive forces is bubble oscillations caused by particle and bubble which is quite often for coarse particles. It is also observed from the figure (Figure 6.3) that for same surfactant and for its same concentration, the flotation recovery is different for different particles. This is mainly due to difference in physical properties such as diameter, density, character of the surface, etc. of particles (Melo and Laskowski, 2006; Ralston, 1992; .Rahman et al., 2012). These properties affect the collision process between the particle and microbubble. Therefore the particle shows different recovery for same surfactant concentration.

6.3.2 Effects of Surfactants on Flotation Recovery of ZnO

The concentration of surfactant is another important aspect of flotation that affects flotation performance. The effect of surfactant concentration on the recovery of ZnO is shown in Figure 6.4. It is seen that with increase in surfactant concentration the ZnO recovery increases. Surfactant not only influence the density of microbubble, it also provides stability to microbubble (Feng et al., 2009). The probability of collision between a particle and a microbubble is defined as the fraction of particles that collide with a rising microbubble in its path, significantly affected by

surfactant. The probability of collision increases with increase in the particle size or decrease in the microbubble size. Addition of surfactant significantly decreases the microbubble size as described in Chapter 3.

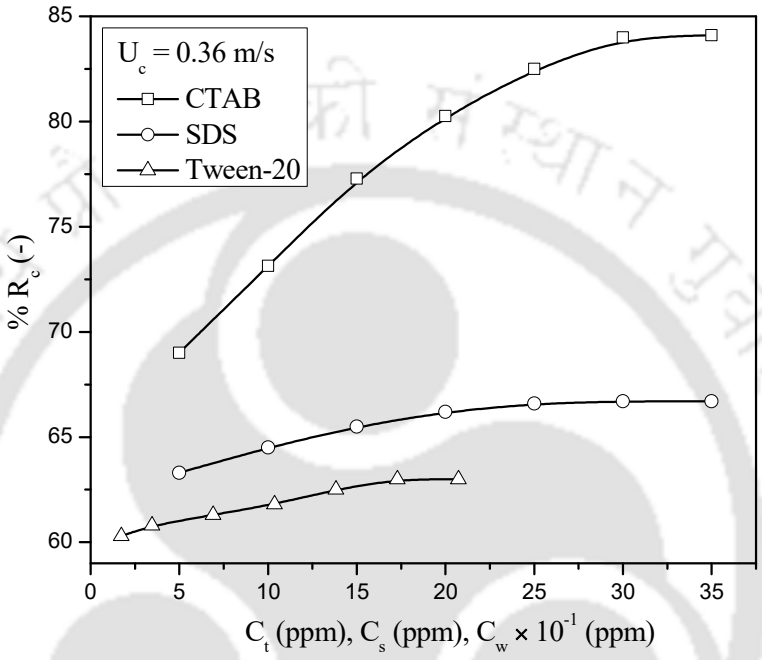

Figure 6.4: Effects of surfactants on the recovery of ZnO.

For a microbubble generated in the liquid, the probability of collision with particles is very high because of its small size, which is in part responsible for higher recovery at a given frother concentration. Addition of surfactant provides four main functions: (i) they increase the hydrophobicity of particle, which is highly desirable for high concentrate recovery; (ii) the microbubble population in flotation column significantly increases with increasing surfactant concentration, which assist to attach more particles and enhances the recovery; (iii) they reduce the microbubble size, thereby increase collision probability; (iv) the fourth important function of surfactant is that they control the surface characteristics of bubble. It is also observed from the

Figure 6.4 that the recovery of ZnO is different for different surfactants. In case of Tween-20, at fixed mixture circulation rate, the recovery of ZnO just increase from 60% to 63% as surfactant concentration increases from 0.016 ml/l to 0.18 ml/l. However a higher recovery was obtained in SDS as compared to Tween-20. As the SDS concentration increases from 5 ppm to 30 ppm the recovery increases from 63% to 68%. The maximum recovery of concentrate ($ZnO+SiO_2$) as well as Zno is obtained in case of CTAB. At a fixed circulation rate, as the surfactant concentration increases from 5 ppm to 30 pm, the recovery of ZnO increases from 69% to 84.1%. Naturally microbubbles carry negative charge on its surface (Takahashi, 2005). However this charge can be altered by adding a suitable surfactant (Yoon and Yordan, 1986). CTAB is a cationic surfactant and the microbubble formed by CTAB solution provides cationic charge on microbubbles, while SDS and Tween-20 provides anionic charge on microbubble. The ZnO particles also carry anionic charge. As the cationic microbubbles pass through the feed, oppositely charged mineral particles are attracted easily due to electrostatic forces and forms bubble-particle aggregate, stronger than the SDS and Tween-20 microbubble. This causes higher recovery of ZnO particles with CTAB as compared to SDS and Tween. The zeta potential of ZnO particle is approximately -10 mV. Addition of surfactant significantly influences the zeta potential of particle as shown in Figure 6.5. Addition of SDS and Tween-20 in the feed increases the negative charge on the ZnO surface, which is not worthwhile, as it does not create any significant attraction between the ionic microbubbles and the ZnO particles. The development of charge at the surface of particle, affects the distribution of ions in the interfacial region. Consequentially an increase in concentration of opposite ions results close to the surface. Thus an electrical double layer exists around each particle. The microbubbles formed with CTAB carry negative charge which easily attract the

opposite charged ZnO particles. Therefore the recovery of ZnO is highest with CTAB as compared to SDS and Tween-20.

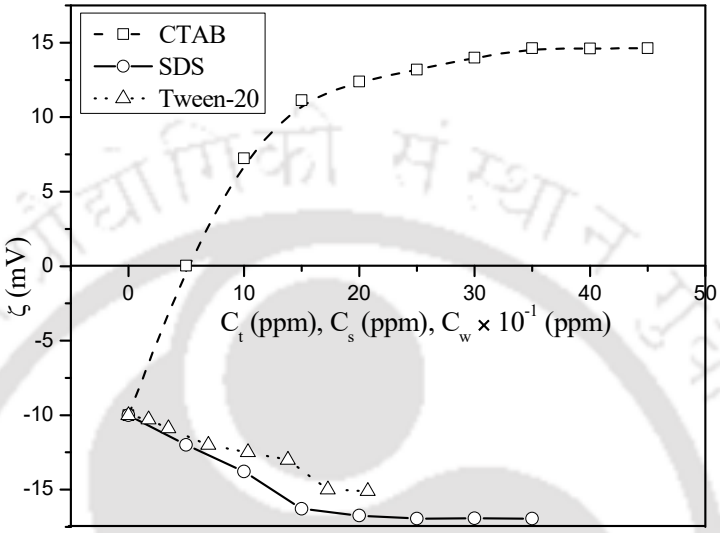

Figure 6.5: Effect of concentration of surfactants on the zeta potential of ZnO.

6.3.3 Effects of Surfactants on Flotation Recovery of CuO

The nature and magnitude of charge on the surface of particle as well as on the microbubble are significant parameters for ionic microbubble flotation. The effects of addition of different surfactants on the CuO recovery is shown in Figure 6.6. It is observed that recovery of CuO in the concentrate increases with increase in surfactant concentration, which was expected. However, the maximum recovery of copper oxide was achieved by using SDS, compared to Tween-20 and CTAB. CTAB as a cationic surfactant provides positive charge on microbubble whereas SDS and Tween-20 provide negative charges on the surface of microbubble. The zeta potential of CuO particle is positive. It is changed by addition of surfactant as shown in Figure 6.7.

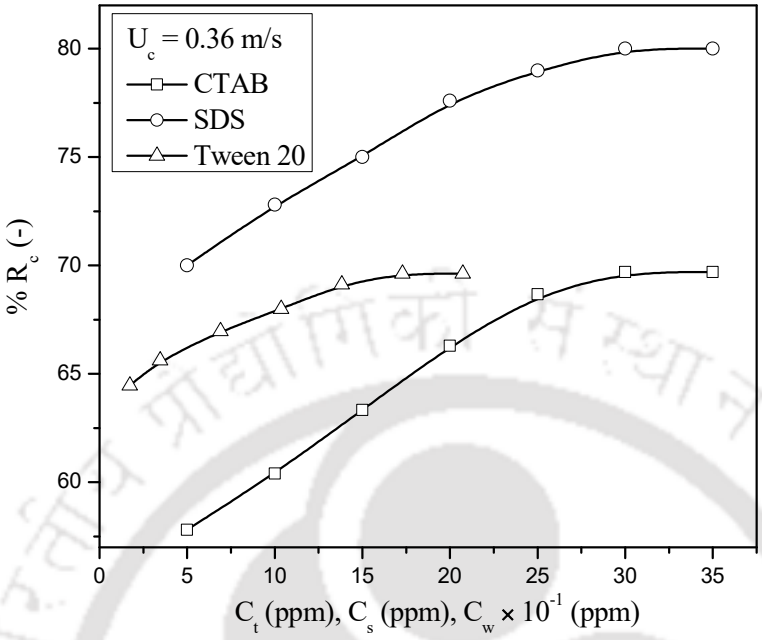

Figure 6.6: Effects of surfactants on the recovery of CuO particles.

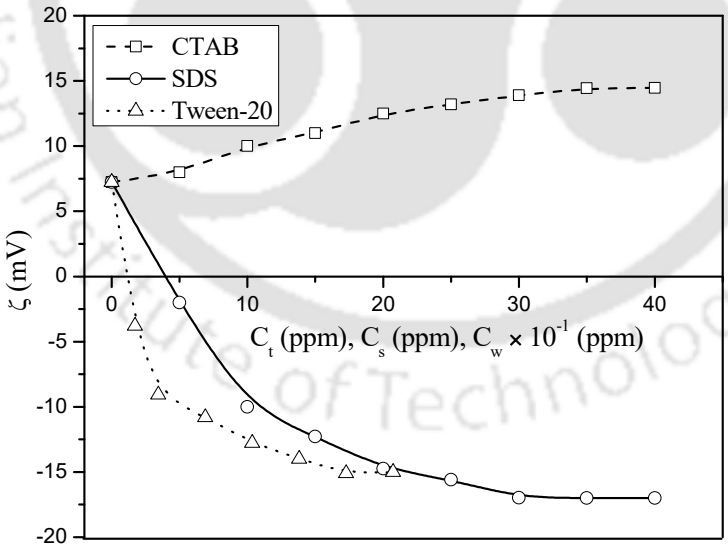

Figure 6.7: Effect of concentration of surfactants on the zeta potential of CuO particles.

Negative charged microbubble leads to high recovery of CuO particles. This high recovery indicates a higher attachment of CuO particles, and emphasizes the potential of separation using charged microbubbles. The maximum recovery of CuO with SDS is approximately 80% and the surfactant consumption of SDS up to maximum recovery is approximately 35 ppm, which is much less than the critical micelle concentration. So ionic microbubbles significantly reduces surfactant consumption. This can be associated to the increase in the contact angle and the contact area between a microbubble and a particle in the presence of microbubbles (Chipfunhu et al., 2011). Collector increases the particle hydrophobicity, thereby accelerating the liquid film drainage and particle-bubble attachment (Ralston et al., 2002). The increase in the contact angle also increases the attachment force between the microbubble and particle, leading to decreased probability of particle detachment from the bubble (Fan et al., 2010). In case of ZnO and SiO_2 mixture the concentration of concentrate (both SiO_2 and ZnO) increases with increase in CTAB concentration. However in case of CuO and SiO_2 mixture with SDS, the recovery of CuO was higher than silica. The zeta potential of silica is found to be negative as shown in Figure 6.8.

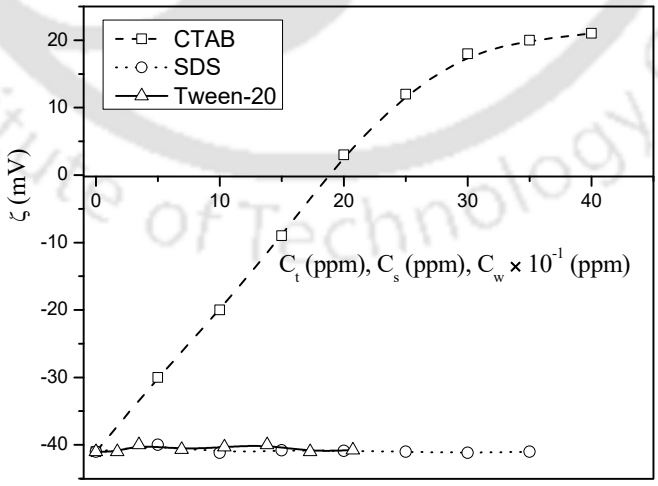

Figure 6.8: Effect of concentrations of surfactant on the zeta potential of SiO_2.

The zeta potential of silica particle in the feed mixture is approximately -41 mV. It is also seen that the zeta potential of silica did not change significantly on addition of SDS as well as Tween-20, which clearly indicates that negative charge does not adsorb on the negative silica surface. However adsorption of CTAB significantly alters the zeta potential of SiO_2. The zeta potential increases in magnitude, until there was a charge reversal after the addition of approximately 20 ppm of CTAB in feed. This indicates that the CTAB was adsorbed onto the negatively charged surface of the silica, which results in high silica recovery.

6.3.4 Effects of Surfactants on Al_2O_3 Recovery

The flotation recovery of Al_2O_3 as function of surfactant concentration is shown in Figure 6.9.

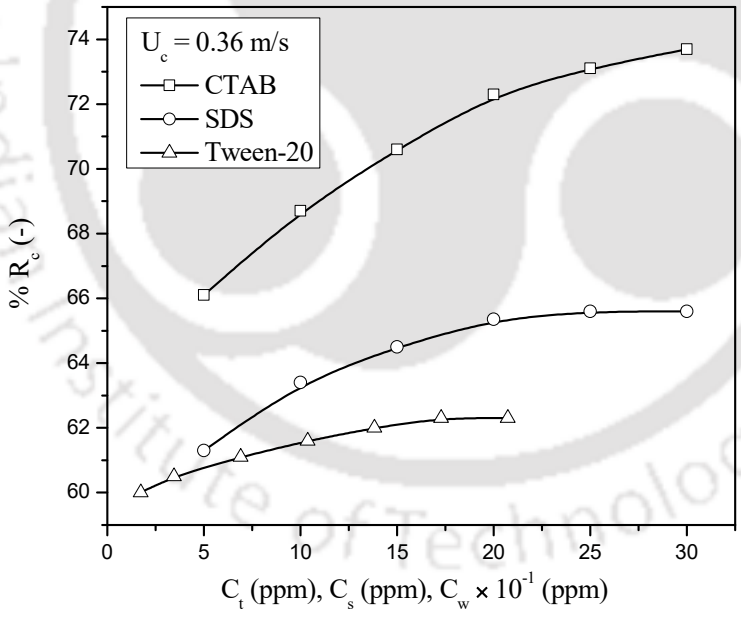

Figure 6.9: Effects of surfactants on the recovery of Al_2O_3 particles.

It is observed that the SDS and Tween-20 are found to be less effective as compared to CTAB for Al_2O_3 recovery. However, the flotation recovery in all the three surfactants increases with

increasing concentration. The maximum recovery of Al_2O_3 achieved in the present work is 73.7% with CTAB, which is less than ZnO (84.1%). There are a large number of physical variables which can affect the recovery of particles by microbubbles. The poor recovery of Al_2O_3 compared to others in the binary mixture mainly due to size of Al_2O_3 particle. The maximum recovery of particle depends upon its floatability and other physiochemical properties. The recovery reduces as the particle size increases (Trahar and Warren, 1976). In the present work the particle size of Al_2O_3 is approximate 20 µm, which is higher than CuO (10.16 µm) and ZnO (4.47 µm). As the particle size increases the probability of collision decreases, causing a low recovery. Low negative zeta potential of Al_2O_3 also affects its recovery. The zeta potential of Al_2O_3 particle is negative and has low magnitude as shown in Figure 6.10.

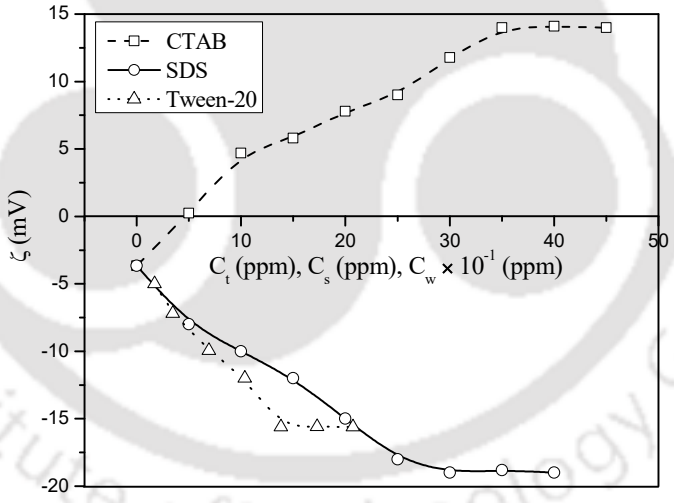

Figure 6.10: Effect of concentration of surfactants on the zeta potential of Al_2O_3.

The zeta potential of Al_2O_3 in water is approximately -3.6 mV which is low in magnitude as compared to CuO and ZnO. The attachment probability of particle depends on particle size, surface charge and surface roughness (Krasowska and Malysa, 2007). Although the electrostatic attraction

between bubbles and particles is very short range. A large difference between zeta potential values of bubble and particle can considerably increase the recovery efficiency. Collins and Jameson (1977) reported that electrostatic interactions through overlapping of diffuse double layers between microbubbles and particles affect the rate of flotation and therefore particle collection. Ralston (1983) also interpreted that surface forces has influence on particle trajectory. It is the consequence of thick wetting films stabilized on hydrophobic surfaces by long-range electrostatic forces (Ahmadi et al., 2014). These results indicate that hydrophobic as well as electrostatic forces are responsible for particle collection by ionic microbubbles.

6.3.5 Variation of Recovery of Particle with Time

It is observed that maximum fractional recovery profiles for all the three particles are quite similar to each other. A typical variation of recovery of particle with time at fixed mixture circulation velocity and surfactant concentration is shown in Figure 6.11.

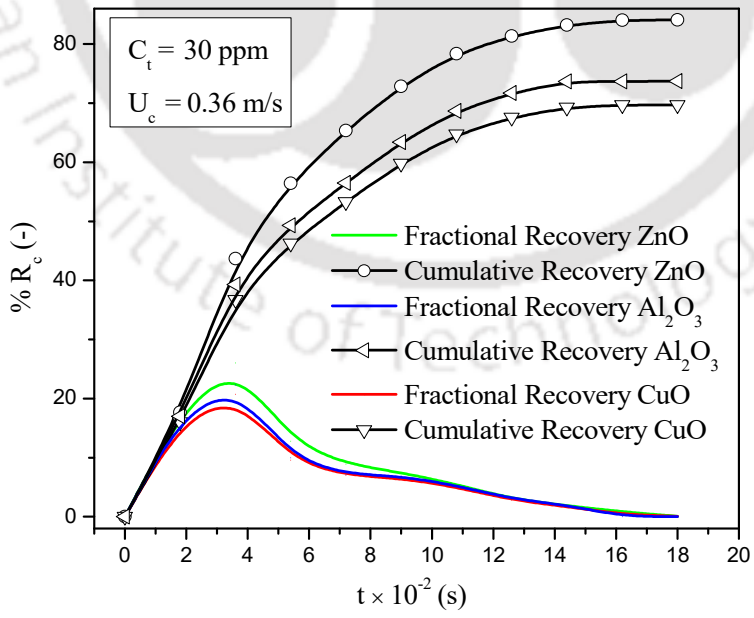

Figure 6.11: Variation of recovery of particles with time.

It is observed that approximately 60% of the particles are recovered within 11 minutes of flotation and in the later stage the fractional recovery is low. The fractional recovery decreases with time. In the initial phase the mineral particle shows a higher attraction towards the ionic microbubble than the later phase. Since the density of microbubble at high surfactant concentration is very high so it becomes very easy for the microbubble to attach the particle. In the initial phase the surface of particle is uncontaminated with adsorbed surfactant but as the time passes the opposite charged surfactant molecules adsorb on the surface of particle that causes a reduction in attraction and attachment.

6.3.6 Model for Microbubble Flotation

Flotation column operates on three main distinct processes namely: (i) aeration, where air bubbles are introduced into the flotation column; (ii) mixing, where bubbles and particles are well mixed to increase bubble–particle interaction; and finally (iii) separation, where bubbles and bubble–particle aggregates are allowed to separate from the bulk mixture and skimmed away. Many fundamental models have been developed to mark out the flotation kinetics, predominantly related to the collection zone in terms of hydrodynamics. A comprehensive description on fundamentals of the flotation process modeling for column flotation is reported by Finch and Dobby (1990), Tuteja et al. (1994) and Dai et al. (2000). Kinetic model is widely adopted for development of control strategies in flotation column. Kinetic models involve the chemical reactor analogy and consider flotation process as a reaction between bubbles and particles (Jameson et al., 1977). In the present work the flotation of fine mineral particles by microbubbles is modelled as a first-order rate process. The kinetic equation describing the rate of removal of the number of particles, for the microbubble–particle encounters can be expressed as (Bloom and Heindel, 1997)

$$\frac{dN_p}{dt} = -KN_p = ZE_cE_aE_s \tag{6.5}$$

where N_p is the number densities of floatable mineral particles available for attachment. K denotes the rate constant for particle–microbubble flotation. The parameter Z is related to the particle–microbubble collision frequency dependent on the size of the particles and microbubbles, and hydrodynamics of the flotation pulp. E_c, E_a and E_s are particle–microbubble collision, adhesion and stability efficiencies respectively. The parameter Z can be expressed as (Pyke et al., 2003)

$$Z = 5N_{mb}N_p\left(\frac{d_{mb}+d_p}{2}\right)^2\sqrt{\overline{V}_{mb}^2+\overline{V}_p^2} \tag{6.6}$$

where $\left(\overline{V}_{mb}^2\right)^{1/2}$ and $\left(\overline{V}_p^2\right)^{1/2}$ are the root mean square velocity (rms) of the particles and microbubbles relative to the fluid velocity, respectively. N_{mb} denotes microbubble density. The number density of microbubbles in the column can be calculated as

$$N_{mb} = \frac{6\varepsilon_g}{\pi d_{mb}^3} \tag{6.7}$$

where ε_g denotes the gas holdup. In the present work as the $d_{mb} >> d_p$, $\left(\overline{V}_p^2\right)^{1/2}$ can be neglected. So Eq. (6.6) becomes

$$Z = 30\frac{N_p\varepsilon_g}{\pi d_{mb}^3}\left(\frac{d_{mb}+d_p}{2}\right)^2\left(\overline{V}_{mb}^2\right)^{1/2} \tag{6.8}$$

The rms relative velocities of the microbubbles can be calculated as (Schubert, 1999)

$$\left(\overline{V}_{mb}^2\right)^{1/2} = \frac{0.33\varepsilon^{4/9}d_{mb}^{7/9}}{\nu^{1/3}}\left(\frac{\Delta\rho}{\rho_f}\right)^{2/3} \tag{6.9}$$

where $\Delta\rho$ is the density difference between the particle (ρ_p) and fluid (ρ_f), ν is kinematic viscosity of fluid and ε is the energy dissipation rate per unit mass. It can be calculated as (Wu and Patterson, 1989)

$$\varepsilon = 0.85\left(\frac{\overline{U}_{cx}^2 + \overline{U}_{cy}^2 + \overline{U}_{cy}^2}{2}\right)^{3/2} L^{-1} \tag{6.10}$$

where U_c is the microbubble-particle mixture circulation velocity. L is a measure of the flow length scale. The length scale can be taken as $0.07D_c$ (Pope, 2000).

Therefore equation (6.10) can be expressed as

$$\varepsilon = 12.143\left(\frac{\overline{U}_{cx}^2 + \overline{U}_{cy}^2 + \overline{U}_{cz}^2}{2}\right)^{3/2} D_c^{-1} \tag{6.11}$$

Thus the expression of Z of Eq. (6.8) can be written by incorporating the equation (6.9) and (9.11) as

$$Z = 30\frac{N_p\varepsilon_g}{\pi d_{mb}^3}\left(\frac{d_{mb}+d_p}{2}\right)^2 \frac{d_{mb}^{7/9}}{\nu^{1/3}}\left(\frac{\Delta\rho}{\rho_f}\right)^{2/3}\left(\left(\frac{\overline{U}_{cx}^2 + \overline{U}_{cy}^2 + \overline{U}_{cz}^2}{2}\right)^{3/2} D_c^{-1}\right)^{4/9} \tag{6.12}$$

Substituting the expression of Z from Eq. (6.12) in equation (6.5), one gets the expression of K as

$$K = 30\frac{\varepsilon_g}{\pi d_{mb}^3}\left(\frac{d_{mb}+d_p}{2}\right)^2 \frac{d_{mb}^{7/9}}{\nu^{1/3}}\left(\frac{\Delta\rho}{\rho_f}\right)^{2/3}\left(\left(\frac{\overline{U}_{cx}^2 + \overline{U}_{cy}^2 + \overline{U}_{cz}^2}{2}\right)^{3/2} D_c^{-1}\right)^{4/9} E_c E_a E_s \tag{6.13}$$

The root mean square velocity of microbubble-particle mixture is assumed to equal to circulation velocity of mixture ($U_c = \overline{U}_{cx}^2 + \overline{U}_{cy}^2 + \overline{U}_{cx}^2$), Hence the equation (6.13) becomes

$$K = 30\frac{\varepsilon_g}{\pi d_{mb}^3}\left(\frac{d_{mb}+d_p}{2}\right)^2 \frac{d_{mb}^{7/9}}{\nu^{1/3}}\left(\frac{\Delta\rho}{\rho_f}\right)^{2/3}\left(\left(\frac{U_c^2}{2}\right)^{3/2} D_c^{-1}\right)^{4/9} E_c E_a E_s \tag{6.14}$$

The percentage recovery of particle (R_c) at any time t can be expressed as

$$R_{c,t} = R_{\max}\left(1 - \exp\left(-Kt\right)\right) \tag{6.15}$$

6.3.6.1 Collision Efficiency

The collision efficiency is the ratio of the number of particles colliding with the bubble per unit time to the number of particles swept across the projected area of the bubble per unit time (Weber and Paddock, 1983). Dai et al. (2000) presented a critical review of the various models existing in the literature for the calculation of the collision efficiency between particles and single rising gas bubbles. In most particle-bubble collision models, major consideration has been given to bubbles with completely immobilized surfaces since it is believed that during flotation, the bubble surface is completely retarded by the presence of surface active impurities from the water. For mobile bubble surface, generalized Sutherland equation (GSE) and Weber and Paddock model can well predict the collision efficiency. Weber and Paddock (1983) proposed a model for the collision of spherical particles. They assumed that the particles were very small and the hydrodynamic interaction between the particles and the fluid was negligible. The streamlines of the fluid could be characterized by the Stokes stream function and the stream functions could be approximated by a Taylor series. According to them the collision efficiency can be dissected into two components: one relating to the particle settling velocity due to gravity and the other relating to the fluid velocity at the bubble surface. The former component is termed the gravitational effect and the latter is the interceptional effect. Both effects depend on the bubble Reynolds number (Re_n) and calculated by solving the Navier-Stokes equations. The collision efficiency according to Weber and Paddock model can be expressed as

$$E_c = E_{cg} + E_{ci} \tag{6.16}$$

The collision efficiency due to the gravitational effect (E_{cg}) is expressed as (Weber and Paddock, 1983)

$$E_{cg} = \frac{U_p}{1+U_p}\left(1+\left(\frac{d_p}{d_{mb}}\right)^2\right)\sin^2\theta_c \tag{6.17}$$

where U_p is particle velocity, θ_c is denoted by the maximum collision angle above which no collision is possible. The value of maximum collision angle depends on the bubble Reynolds number and can be determined by the following equations, obtained by empirical curve fitting to collision data (Woo, 1971)

$$\theta_c = 78.1 - 7.37\log(\mathrm{Re}_n) \qquad \text{For } 20 < \mathrm{Re_n} < 400 \tag{6.18}$$

$$\theta_c = 98 - 12.49\log(10\mathrm{Re}_n) \qquad \text{For } 1 < \mathrm{Re_n} < 20 \tag{6.19}$$

$$\theta_c = 90 - 2.5\log(100\mathrm{Re}_n) \qquad \text{For } 0.1 < \mathrm{Re_n} < 1 \tag{6.20}$$

where Re_n denotes the non-Newtonian Reynolds number. The non-Newtonian Reynolds number can be expressed as

$$\mathrm{Re}_n = \frac{d_{mb}^n U_c^{2-n}}{8^{n-1}K'}\left(\frac{4n}{3n+1}\right)^n \tag{6.21}$$

The collision efficiency due to the interceptional effect (E_{ci}) can be expressed as (Weber and Paddock, 1983)

$$E_{ci} = 1.5\left[1+\left(\frac{3}{16}\right)\left(\frac{\mathrm{Re}_n}{1+0.249\mathrm{Re}_n}\right)\right]\left(\frac{d_p}{d_{mb}}\right)^2 \qquad \text{For } \mathrm{Re_n} < 200 \tag{6.22}$$

6.3.6.2 Stability Efficiency

The stability efficiency addresses the stabilization/destabilization of a microbubble–particle aggregate. According to Schulze (2003), the acceleration (force) that determines the detachment of a particle from the bubble is dependent on the intensity of turbulence in the flow. The capillary and hydrostatic forces constitute the attachment forces while the forces of gravitation, buoyancy and capillary pressure in the gas bubble constitute the detachment forces. The sum of these forces is zero at equilibrium (Duan et al., 2003). The expression for stability efficiency can be written as (Schulze, 2003)

$$E_s = 1 - \exp\left(1 - \frac{\left|6\sigma \sin\omega \sin(\omega+\theta)\right|}{d_p^2\left(\Delta\rho g + \rho_p a_c\right) + 1.5 d_p (\sin\omega)^2 f(d_{mb})}\right) \tag{6.23}$$

where σ is the surface tension, ω refers to the location of a particle at the liquid– vapour interface ($\omega = 180° - \theta/2$), g is the gravitational constant and a_c is the particle centrifugal acceleration in a turbulent flow field which depends on the level of turbulence in the flotation column. The function $f(d_{mb})$ can be expresses as (Schulze, 2003)

$$f(d_{mb}) = \left(\frac{4\sigma}{d_{mb}} - d_{mb}\rho_f g\right) \tag{6.24}$$

The particle centrifugal acceleration (a_c) for the particle smaller than the microbubble can be approximated as

$$a_c = 1.9\frac{\varepsilon^{2/3}}{d_{mb}^{1/3}} \tag{6.25}$$

6.3.6.3 Attachment Efficiency

The attachment of a hydrophobic particle to a bubble is one of the significant phase of particle–bubble interaction in mineral flotation. Particle–bubble attachment occurs when the particle–bubble contact time is longer than the induction time (T_i). The induction time is defined as the time for the liquid film between the particle and the bubble to thin and rupture and for the three-phase line of contact to expand until an equilibrium value is obtained. The contact time is linked to the particle–bubble collision. If a particle impacts on the bubble surface with an adequate kinetic energy so as to cause substantial distortion of the bubble surface, the colliding particle rebounds from the deformed surface due to the elastic energy of the deformed part of the surface. The number of attachment models are limited compared to the collision models. The attachment efficiency (E_a) is defined as the fraction of all colliding particles that reside on the bubble for a time greater than the induction time (Dobby and Finch, 1987). After the collision, the particle slides over the bubble and attachment occurs when the intervening liquid film thins and ruptures (Dobby and Finch, 1987). Consequently, particles with a sliding time greater than induction time were considered to have attached on bubbles. The model of Dobby and Finch (1987) requires the knowledge of the distribution of particle on the bubble surface, particle collision angles, the maximum angle of contact between the particle and bubble and the particle sliding velocity. Later on the model was modified to improve the approach. Based on the modification, the attachment efficiency for particle-microbubble can be expressed as (Dai et al., 1999)

$$E_a = \frac{\sin^2 \theta_a}{\sin^2 \theta_t} \tag{6.26}$$

where θ_t is the maximum possible collision angle of the particle on the surface of the bubble which is given by (Dukhin, 1982)

$$\theta_t = \arcsin\left\{2\beta\left[\left(1+\beta^2\right)^{1/2} - \beta\right]\right\}^{1/2} \tag{6.27}$$

where β is dimensionless number, which is a measure of the relative importance of the interceptional and inertial contributions to the collision process in the generalized Sutherland equation and is defined as (Dai et al., 1998)

$$\beta = \frac{4E_{su}}{9K_a} \tag{6.28}$$

where E_{su} is the collision efficiency calculated by Sutherland (1948), ($E_{su}=3d_p/d_{mb}$). The parameter K_a is defined as

$$K_a = \frac{2U_c\left(\rho_p - \rho_f\right)d_p^2}{9\nu d_{mb}} \tag{6.29}$$

The parameter θ_a is the adhesion angle at which the particle collides with the bubble. Its sliding time (T_s) is equal to the induction time (Dai et al., 1998). So the angle relates the sliding time and induction time to the attachment efficiency. The adhesion angle under potential flow conditions can be expressed as (Dobby and Finch, 1987)

$$\theta_a = 2\arctan\exp\left[T_i \frac{2\left(U_{sp}+U_p\right)+U_b\left(\dfrac{d_p}{d_p+d_{mb}}\right)^3}{d_p+d_{mb}}\right] \tag{6.30}$$

In the present study, the induction time (T_i) is calculated from the best fit of Eq. (6.15) and experimental values of recoveries. Figure 6.12 represents a typical outline to estimate the induction time from the experimental values of recoveries for ZnO and SiO_2 mixture with CTAB.

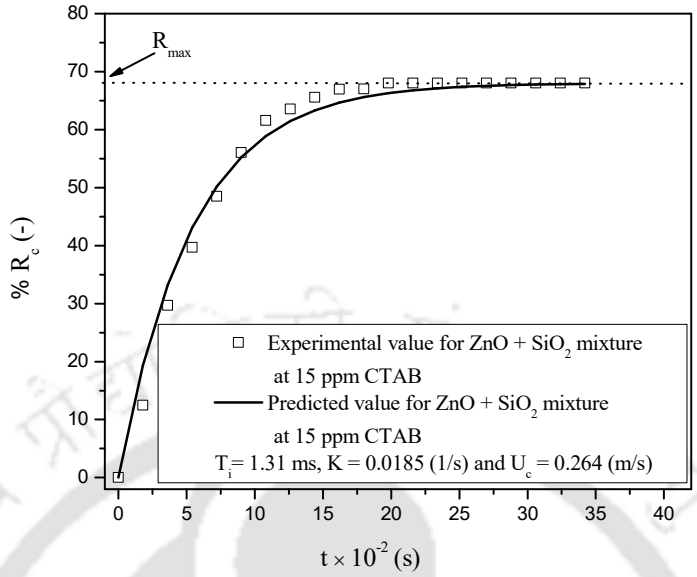

Figure 6.12: A typical outline to estimate the induction time from the experimental values of recoveries.

6.3.7 Interpretation on Induction Time

Sven-Nilsson (1935) introduced the concept of induction time who measured induction time by moving a bubble towards and then away from a flat mineral surface. The author considered induction time to be the minimum contact time for successful thinning of the intervening liquid film to critical thickness where film rupture occurs. It has been reported that induction time is a function of many physical parameters. Yoon and Yordan (1991a) observed a power law dependence between measured induction time and particle size, which was also coherent with theoretical analysis. The induction time depends not only on particle size but also on many other variables such as, the bubble size, the surface tension, disjoining pressure, and the viscosity of the continuous phase (Li et al., 1990). The present results shows that induction time depends on the concentration and type of surfactant, mineral particle as well as the mixture velocity. A typical

variation of microbubble-particle induction time with mixture circulation velocity at different surfactant concentrations for ZnO particles in CTAB is shown in Figure 6.13.

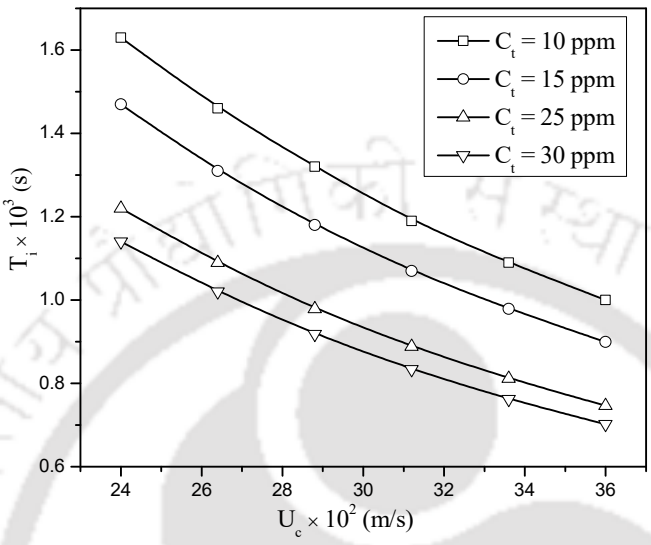

Figure 6.13: Variation of induction time of ZnO particle with mixture circulation velocity.

It is seen that induction time reduces as the mixture velocity increases. Increase in mixture velocity reduces the time for bubble-particle adhesion, leading to reduction in the induction time. Ye et al. (1989) also reported the dependency of induction on the velocities of the bubble approaching the particle. Another important conclusion that can be drawn from the Figure 6.13 is that, induction time decreases with increasing surfactant concentration, while the flotation recovery was found to be increased concomitantly. This may be attributed to increase in adsorption density at the mineral surface with increasing surfactant concentration. Both contact angle and induction time are strongly controlled by surfactant concentration. However, the contact angle is generally an equilibrium measure of hydrophobicity while the induction time is a kinetic measurement of the hydrophobicity. Particles having a shorter induction time will be more easily captured, and they are said to have a higher selectivity. Based on the present experimental data, the induction time

has been correlated in terms of the operating variables by the dimensional analysis. The correlation was made by fitting present experimental data with the help of multiple regression analysis by Microsoft Excel 2013, which can be expressed as

$$T_i = 1.98\times10^{3}\left(\frac{d_{mb}}{U_c}\right)^{1.172}\left(\frac{d_p}{d_{mb}}\right)^{-0.592} Ca^{0.405}\,\mathrm{Re}_n^{-0.434} \tag{6.31}$$

where *Ca* denotes Capillary number ($\mu_f U_c/\sigma$). The correlation coefficient and standard error of Eq. (6.31) were found to be 0.993 and 0.051 respectively. A typical parity plot for the comparison of experimental and predicted values of induction time of mixture for Al_2O_3 particles is shown in Figure 6.14. It is clear that proposed correlation can predict induction time well within the following ranges of operating variables: $4.51\times10^{-5} \le d_{mb}/U_c \le 2.33\times10^{-4}$, $8.03\times10^{-2} \le d_p/d_{mb} \le 92.20\times10^{-2}$, $3.81\times10^{-3} \le Ca \le 11.22\times10^{-3}$ and $2.47 \le Re_n \le 18.24$.

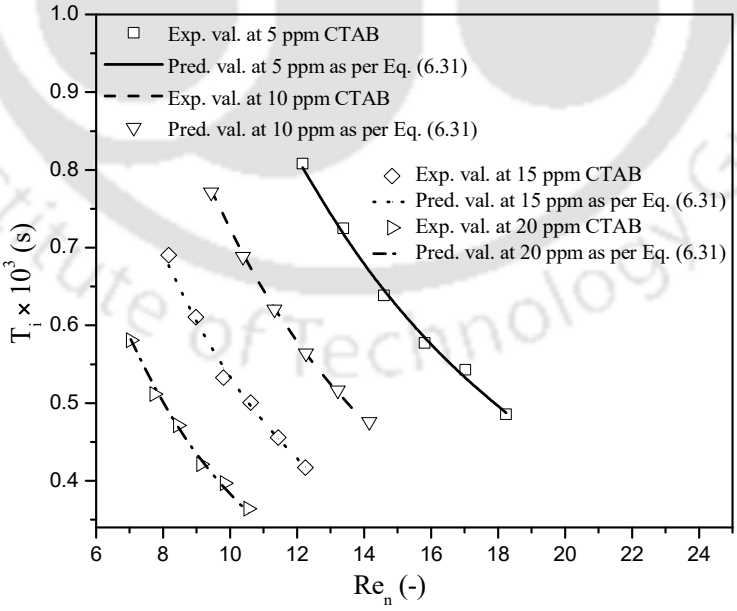

Figure 6.14: Variations of the induction with Reynolds number.

6.3.8 Interpretation on Flotation Rate Constant

The scale-up of the column requires the knowledge of flotation constant. A large number of variables may affect the ultimate performance or rate of flotation in column. Figure 6.15 shows the effect of mixture circulation velocity on flotation rate constant for the beneficiation of CuO.

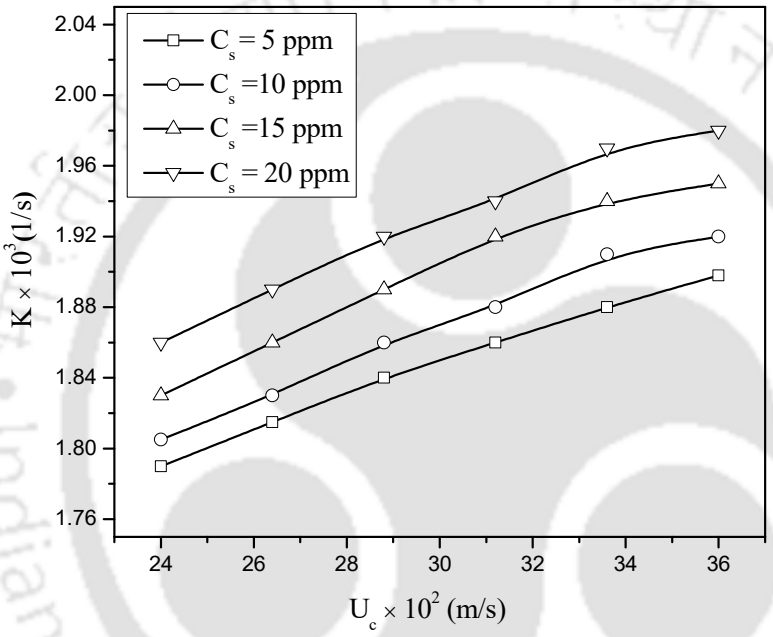

Figure 6.15: Variation of floatation rate constant of CuO particle with mixture circulation velocity.

It is seen that flotation rate constant strongly depends on the circulation velocity and surfactant concentration. Increase in the circulation velocity significantly increases the collision. It is also observed that surfactant concentration has a significant effect on the rate constant. Surfactant increases the rate constant in two ways. First, it reduces the microbubble size which helps to increase the particle-bubble collision. It also increases the ionic strength of microbubbles (Yoon and Yordan, 1986). Ionic strength has a significant role to play in determining the adsorption of

surfactant on the mineral as well as on the microbubble due to increase in electrical double-layer. Based on the present experimental data, the flotation rate constant has been correlated in terms of the affecting variables by the dimensional analysis, which can be expressed as

$$K = 5.3\times10^{-10}\left(\frac{d_{mb}}{U_c}\right)\left(\frac{d_p}{d_{mb}}\right)^{-0.064} Ca^{-1.04}\,\mathrm{Re}_n^{0.289} \tag{6.32}$$

The correlation coefficient and standard error of Eq. (6.32) were 0.989 and 0.052 respectively. A typical parity plot of the correlation proposed for the rate constant with the experimental value for the beneficiation of Al_2O_3 by CTAB is shown in Figure 6.16. It was found that the developed correlation fitted well within the ranges of variables: $4.51\times10^{-5} \le d_{mb}/U_c \le 2.33\times10^{-4}$, $8.03\times10^{-2} \le d_p/d_{mb} \le 92.20\times10^{-2}$, $3.81\times10^{-3} \le Ca \le 11.22\times10^{-3}$ and $2.47 \le Re_n \le 18.24$.

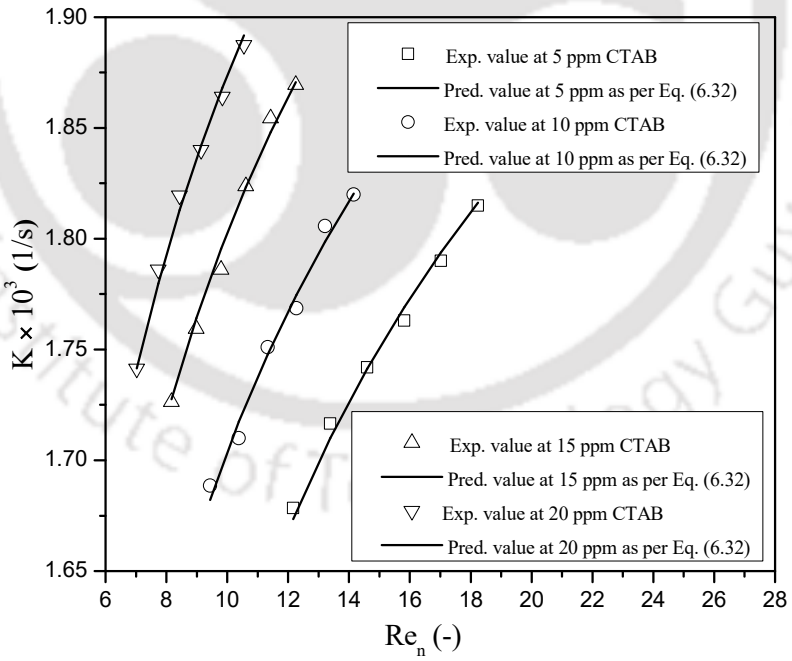

Figure 6.16. Variations of the flotation rate constant with Reynolds number at different surfactant concentrations.

6.3.9 Analysis of Efficiency of Recovery Based on Intensity of Mixing

Rice et al. (1974) was the first to apply mixing theory to flotation column. Later on Dobby and Finch (1986) developed scale-up methodology for column flotation for particle recovery efficiency that accounted for the effects of mixing. Mavros et al. (1989) also studied the effects of liquid and gas flow rates on axial dispersion and how is it related to the performance of the column for efficient particle separation. They found that an increase in gas flow rate increased mixing, while an increase in liquid flow rate reduced mixing which reduces the recovery efficiency of particle by flotation. In flotation column the dispersion parameters of the solid is of prime importance. For particles having mean diameters less than 150 μm, the solids axial dispersion coefficient has been reported equal to the axial dispersion coefficient of liquid phase which governs the degree of the recovery by flotation (Mavros, 1993; Tuteja et al., 1994). Dobby and Finch (1986) was the first to correlate the fractional recovery in the collection zone a function of the rate constant, particle residence time and degree of mixing. In their model, the recovery depends on two main factors namely, flotation kinetics and degree of mixing (axial only). The influence of radial mixing, non-uniform velocity profiles and short-circuiting on recovery was neglected. Yoon et al. (1991b) had also done research work on mathematical modelling of flotation columns for over a decade. According to Yoon et al. (1991b), the percentage recovery (R_c) of a component in a column can be expressed as a function of Bodenstein number, which is given by

$$\%R_c = \left(1 - \frac{4a \exp\left(\frac{Bo}{2}\right)}{(1+a)^2 \exp\left(\frac{aBo}{2}\right) - (1-a)^2 \exp\left(\frac{-aBo}{2}\right)} \right) \times 100 \qquad (6.34)$$

where *a* is a parameter, *Bo* is the Bodenstein number. Based on the present experimental data, a correlation for intensity of mixing was developed with the different operating variables which is represented as

$$Bo\left(=\frac{U_c L}{E_z}\right)=1.275\times10^{2}\frac{Fr^{0.209}}{\mathrm{Re}_n^{0.079}We^{0.264}} \tag{6.35}$$

The details of the experimental procedure for the calculation of Bodenstein number is discussed in Chapter 5. From experimental values of particle percentage recovery (R_c) and Bodenstein number, the parameter *a* was determined by using Matlab. The experimental value and predicted value of recovery based on the parameter *a* with axial dispersion coefficient is shown in Figure 6.17.

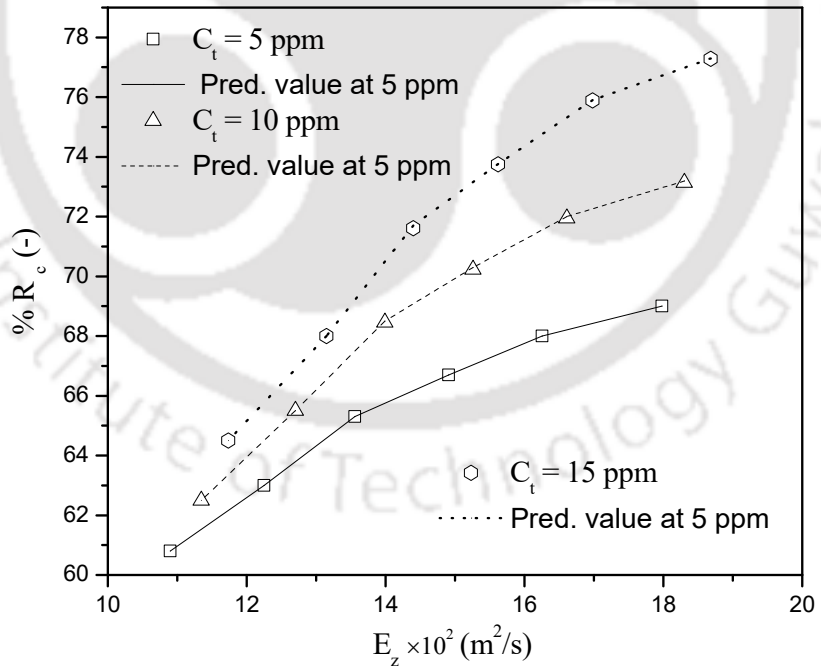

Figure 6.17: Variation of experimental and predicted recovery for ZnO with dispersion coefficient.

It is observed from the figure that the recovery increases with increase in dispersion coefficient. The parameter (a) is related to the rate constant of flotation based on mixing (K_m) which is expressed as

$$a = \sqrt{1 + \frac{4K_m t_r}{Bo}} \tag{6.36}$$

where t_r is retention time, it represents the time of particle to reach to the top from the bottom of the column. From the Eq. (6.36), the flotation rate constant based on mixing phenomena can be estimated as

$$K_m = \frac{\left(a^2 - 1\right)Bo}{4t_r} \tag{6.37}$$

The variation of rate constant based on mixing phenomena with mixture velocity is shown in Figure 6.18. It was found that the flotation rate constant based on mixing phenomena increased with increase in mixture velocity as well as surfactant concentration for all sets of experimental data. It was also found that the flotation constant based on mixing phenomena was lower than that of the values reported in earlier section interpreted based on previous model. There are many factors which may differ in the values. One on the prominent reason is that the rate constant based on mixing phenomena was calculated from the Eq. (6.34), which was developed for conventional bubbles. Another possible reason which may cause the difference is that the calculated rate constant ignores the effect of radial mixing in the system. The recovery depends on two main factors namely, flotation kinetics and degree of mixing (axial only). The influence of radial mixing, non-uniform velocity profiles and short-circuiting on recovery are neglected in model proposed by Yoon et al. (1991b). So in order to explore the technology at larger scale more detailed study is required in this field.

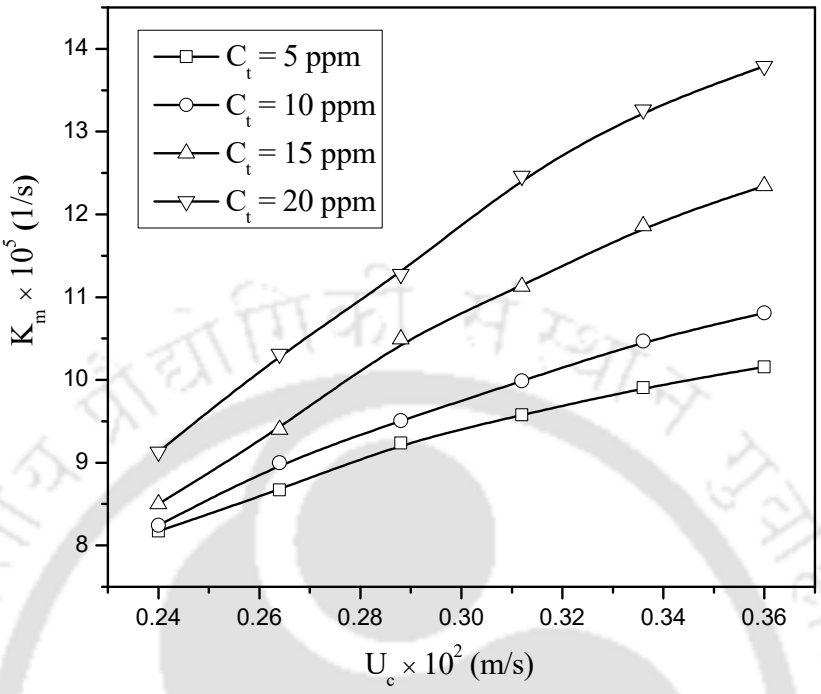

Figure 6.18: Variation of floatation rate constant based on mixing phenomena of ZnO particle with mixture circulation velocity.

6.4 Conclusion

The technical feasibility of an innovative method for fine recovery was investigated. The present chapter shows that fine particles can be significantly recovered by using microbubbles. The results revealed that the charge on the surface of microbubble is highly promising in separating opposite charged particles. The recovery of mineral particle was found to be dependent on surfactant concentration, size of microbubble and particles, zeta potential of microbubble, nature of surface potential of bubble and microbubble-particle mixture circulation velocity. It was also observed that the separation efficiency of microbubble increased with increase in mixture circulation velocity. The addition of surfactant in the mixture intensified the recovery efficiency. The recovery

of ZnO and Al_2O_3 particles was maximum with CTAB, whereas the Tween-20 and SDS were found be less effective for ZnO and Al_2O_3, due to similar surface charge. As the CTAB concentration increased from 5 ppm to 30 ppm, the recovery of ZnO increased from 69% to 84.1%, whereas for the Al_2O_3 particle the recovery increased from 66.1 to 73.7%. In case of CuO particles, the SDS and Tween-20 were found to be more effective than CTAB. The maximum recovery of CuO with SDS and Tween-20 were 80% and 60% respectively. The SDS microbubbles possessed higher magnitude of zeta potential than the Tween-20 microbubble, which caused the higher recovery. The zeta potential of SiO_2 particles was found to be independent of SDS and Tween-20 concentration within the experimental range. However in case of CTAB, a reversal of charge with increase in concentration of CTAB was observed. A flotation model that includes the contributions from the efficiencies of collision, attachment and stability between particles and microbubbles was used to calculate the flotation rate constants. It was observed that rate constant is significantly influenced by the physicochemical properties of the liquid and particles. These results clearly indicate that presence of a hydrophobic surface forces necessarily results in particle collection by a microbubble but other surface forces also contribution in fine particle separation. The flotation rate constant was also analyzed based on the mixing in the column. It was observed that the rate constant based on mixing was lower than that calculated from experiments.

Notations

A_c	Column cross-sectional area (m^2)
a	Parameter defined in Eq. (6.36)
a_c	Particle centrifugal acceleration (m^2/s)
C_t	Concentration of CTAB (ppm)

C_s	Concentration of SDS (ppm)
C_w	Concentration of Tween-20 (ppm)
D_c	Column diameter (m)
d_{mb}	Microbubble diameter (m)
d_p	Particle diameter (m)
E_c	Particle–microbubble collision efficiency (-)
E_{ci}	Collision efficiency due to the interceptional effect (-)
E_{cg}	Collision efficiency due to the gravitational effect (-)
E_a	Particle–microbubble attachment efficiency (-)
E_s	Particle–microbubble stability efficiency (-)
g	Acceleration due to gravity (m^2/s)
K'	Consistency of fluid ($Pa.s^n$)
K	Flotation rate constant (1/s)
K_a	Parameter defined in eq. (6.29)
K_m	Flotation rate constant based on mixing (1/s)
L	Turbulent macroscale length (m)
M_f	Mass of feed (kg)
M_r	Mass of particle recovered (kg)

n	Flow behavior index (-)
N_{mb}	Number density of microbubble ($1/m^3$)
N_p	Number density of particles ($1/m^3$)
Q_m	Microbubble-particle mixture flow rate (m^3/s)
r	Radius (m)
$\% R_c$	Percentage recovery (-)
R_{max}	Maximum recovery (-)
U_c	Microbubble-particle circulation velocity (m/s)
U_p	Particle velocity (m/s)
$\left(\overline{V}_{mb}^2\right)^{1/2}$	Root mean square velocity of microbubble (m/s)
$\left(\overline{V}_p^2\right)^{1/2}$	Root mean square velocity of particles (m/s)
t	Time (s)
t_r	Retention time (s)
T_i	Induction time (s)
T_s	Sliding time (s)
Z	Collision frequency per unit volume ($1/m^3.s$)

Greek letters

μ_e	Effective viscosity of mixture (kg/m.s)

v	Kinematic viscosity (m^2/s)
ε	Energy dissipation rate per unit mass (m^2/s^3)
ε_g	Gas holdup (-)
ω	Location of a particle at the gas-liquid interface (radian)
ρ_f	Density of fluid mixture (kg/m^3)
ρ_p	Density of particle (kg/m^3)
θ_c	Maximum collision angle (radian)
θ_t	Maximum possible collision angle defined in Eq. (6.27)
θ_a	Adhesion angle (radian)
β	Parameter defined in Eq. (6.28)
σ	Surface tension (N/m)
τ	Wall Shear stress (Pa)
γ_a	Apparent shear rate (1/s)
ΔP	Pressure drop (N/m^2)
θ	Contact angle (radian)

Dimensionless groups

Ca	Capillary number ($\mu_f U_c/\sigma$) (-)
Re_n	Non-Newtonian liquid Reynolds number $\left(\frac{D_c^n U_c^{2-n} \rho}{8^{n-1} K}\left(\frac{4n}{3n+1}\right)^n\right)$ (-)

Chapter-7

OVERALL CONCLUSIONS AND RECOMMENDATIONS

This chapter summarized the conclusions drawn from the present work and provides recommendation for future work.

7.1. Overall Conclusions of the Work

In this work the hydrodynamics and mineral beneficiation efficiency of ionic microbubble have been studied. From drainage curve analysis and electrical conductance method it was observed that the stability of the microbubble can be significantly enhanced by increasing surfactant concentration. The liquid drainage curves of the microbubble dispersions followed the same trend for all kind of surfactants. Microbubble drainage process found to be occurred in three distinct phases. The microbubble half-life increased with surfactant concentration. The half-life of SDS microbubbles increased from 72 s to 444 s as the SDS concentration increased from 5 ppm to 3000 ppm. For CTAB, the half-life of microbubbles increased from 101 s to 475 s as the CTAB concentration increased from 5 ppm to 500 ppm. In case of Tween-20, the half-life of microbubbles increased from 71 s to 364 s as the Tween concentration increased from 5 ppm to 100 ppm. The motion of rising microbubble was found to be significantly affected by physicochemical properties of system. The terminal rise velocity of carbon dioxide microbubble was found to be higher than air and lower than nitrogen microbubble. It was observed that the microbubble size estimated by disengagement method was lower than that predicted by particle size analyzer, while the image analysis predicted bubble size higher than the particle size analyzer. At low viscosity, the

microbubble size was found to be dependent on surface tension of liquid. The microbubble size decreased from 52 μm to 25 μm as the surface tension deceased from 72 mN/m to 57 mN/m. The bubble size distribution of microbubble suspension for different concentrations was fitted to Weibull distribution. The present study also reveals that microbubble suspensions behave as a shear-thinning non-Newtonian liquid. An increase in surfactant concentration caused a decrease in shear stress and effective viscosity with shear rate. The drag coefficient and friction factor found to be decreased inversely with the Reynolds number. The results suggested that the presence of microbubbles reduces the frictional resistance. From the present study it was found that the intensity of dispersion and mixing time of microbubble suspensions depends on the operating variables and the physicochemical properties of system. The dispersion coefficient increased with increase in surfactant concentrations whereas it decreased with increasing SCMC concentration. The value of dispersion coefficient increased from 10.9×10^{-2} m^2/s to 12.41×10^{-2} m^2/s as the SDS concentration increase from 0 ppm to 15 ppm at fixed circulation velocity. For CTAB, value of dispersion coefficient increased from 11.10×10^{-2} m^2/s to 12.10×10^{-2} m^2/s as the CTAB concentration increase from 34 ppm to 100 ppm. In case of Tween 20 dispersion coefficient increased from 11.3×10^{-2} m^2/s to 12.21×10^{-2} m^2/s as the Tween concentration increase from 0 ppm to 15 ppm at fixed circulation velocity. The effect of physicochemical properties of liquid on dispersion coefficient due to liquid circulation is also analyzed. The present study shows that fine particles can be significantly recovered by using microbubbles. The results revealed that the charge on the surface of microbubble is highly promising in separating opposite charged particles. The recovery of mineral particle was found to be dependent on surfactant concentration, size of microbubble and particles, zeta potential of microbubble, nature of surface potential of bubble and microbubble-particle mixture circulation velocity. It was also observed that the separation

efficiency of microbubble increased with increase in mixture circulation velocity. The addition of surfactant in the mixture intensified the recovery efficiency. The recovery of ZnO and Al_2O_3 particles was maximum with CTAB, whereas SDS and Tween-20 were found to be more effective than CTAB in case of CuO recovery. A maximum recovery of approximately 84 % and 72 % was obtained for ZnO and Al_2O_3 particle respectively by using CTAB. For CuO particles, maximum recovery of approximately 78 % was obtained by using SDS. A flotation model that includes the contributions from the efficiencies of collision, attachment and stability between particles and microbubbles was used to calculate the flotation rate constants. It was observed that rate constant is significantly influenced by the physicochemical properties of the liquid and particles. The flotation rate constant was also analyzed based on the mixing in the column. Correlations have been developed for the lifetime, drag coefficient, friction factor, dispersion coefficient, mixing time and rate constant. It was observed that the correlations predicts well the experimental data within the experimental range.

7.2. Recommendations for Further Work

This thesis has highlighted details of the stability characteristics, rheological characteristics, mixing characteristics and mineral beneficiation efficiency of ionic microbubble. However further work is required to have a complete idea in this field for proper design and scaling of microbubble aided processes. The possible recommendations for further research work in this field can be summarized as

- The rheological study of microbubble suspension shown in the present study is confined to two-phase system. The work can be extended to three phase system.
- The stability of microbubble is studied with only three surfactants, other surfactants may also be used to explore the research.

- The stability and dissolution characteristics of microbubble is studied at constant temperature. The work can be extended by analyzing the effect of temperature on the dissolution and stability of microbubbles.
- The mixing characteristics of microbubble suspension studied in the present work is conformed to the two-phase system only. It can be extended to three-phase system.
- For separation of fine particle, ionic microbubbles found to be very effective. In the view of industrial application, the study can be further extended by using some other surfactants and particles.
- Experiments were carried out to estimate the rise velocity of microbubble in SCMC and three surfactants. The work can be extended by investigating the rise velocity of microbubble using some other liquids.
- The effect of pollutants and contaminants on metal oxides recovery may also be studied in the future to explore the research.
- The work can be extended by comparing the experimental data with CFD simulation.

REFERENCES

- Achwal, S.K., Stepanek, J.B., 1975. An alternative method of determining hold-up in gas-liquid systems. Chemical Engineering Science 30, 1443-1444.
- Anfruns, J.F., Kitchener, J.A., 1986. Rate of capture of small particles in flotation. Mineral Processing and Extractive Metallurgy (IMM Transactions Section C) C9 86-95.
- Agarwal, A., Ng, W.J., Liu, Y., 2011. Principle and applications of microbubble and nanobubble technology for water treatment. Chemosphere 84, 1175-1180.
- Ago, K., Nagasawa, K., Takita, J., Itano, R., Morii, N., Matsuda, K., Takahashi, K., 2005. Development of an aerobic cultivation system by using a microbubble aeration technology. Journal of Chemical Engineering of Japan 38, 757-762.
- Ahmed, N., Jameson, G.J., 1989. Flotation Kinetics. Mineral processing and extractive metallurgy review 5, 77-99.
- Ahmadi, R., Khodadadi, D.A., Abdollahy, M., Fan, M., 2014. Nano-microbubble flotation of fine and ultrafine chalcopyrite particles. International Journal of Mining Science and Technology 24, 559-566.
- Al-Mashhadani, M.K.H., Bandulasena, H.C.H., Zimmerman, W.B., 2012. CO_2 Mass transfer induced through an airlift loop by microbubble cloud generated by fluidic oscillation, Industrial and Engineering Chemistry Research 51, 1864-1877.
- Al-Shamrani, A.A., James, A., Xiao, H., 2002. Separation of oil from water by dissolved air flotation. Colloids and Surfaces A: Physicochemical and Engineering Aspects 209, 15-26.

- Alves, R.W., de Souza, A.A.U., de Arruda Guelli Ulson de Souza, S.M., Jauregi, P., 2006. Recovery of norbixin from a raw extraction solution of annatto pigments using colloidal gas aphrons (CGAs). Separation and Purification Technology 48, 208-213.
- Amiri, M.C., Woodburn, E.T., 1990. A method for the characterization of colloidal gas aphron dispersions. Chemical Engineering Research and Design 68, 154-160.
- Amiri, M.C., Valsaraj, K.T., 2004. Effect of gas transfer on separation of whey protein with aphron flotation. Separation and Purification Technology 35, 161-167.
- Anastasiou, A.D., Kazakis, N.A., Mouza, A.A., Paras, S.V., 2010. Effect of organic surfactant additives on gas holdup in the pseudo-homogeneous regime in bubble columns equipped with fine pore sparger. Chemical Engineering Science 65, 5872-5880.
- Andreatta, G., Lee, L.T., Lee, F.K., Benattar J.J., 2006. Gas permeability in polymer and surfactant-stabilized bubble films. The Journal of Physical Chemistry B 110, 19537-19542.
- Aoyama, Y., Ogushi, K., Koide, K., Kubota, H., 1968. Liquid mixing in concurrent bubble columns. Journal of Chemical Engineering of Japan 1, 158-163.
- Aslan, M.M., Crofcheck, C, Tao, D, Mengüc, M.P., 2006. Evaluation of micro-bubble size and gas hold-up in two-phase gas–liquid columns via scattered light measurements. Journal of Quantitative Spectroscopy and Radiative Transfer 101, 527-539.
- Azmin, M., Mohamedi, G., Edirisinghe, M., Stride, E.P., 2012. Dissolution of coated microbubbles: The effect of nanoparticles and surfactant concentration. Materials Science and Engineering C 32, 2654-2658.
- Baarson, R.E., Ray, C.L., 1963. Precipitate flotation, a new metal extraction and concentration technique, American Institute of Mining, Metallurgical and Petroleum Engineers Symposium, Dallas, Tex.

- Bang, J.H., Jang, Y.N., Kim, W., Song, K.S., Jeon, C.W., Chae, S.C., Lee, S.W., Park, S.J., Lee, M.G., 2011. Precipitation of calcium carbonate by carbon dioxide microbubbles, Chemical Engineering Journal 174, 413-420.
- Basu, S., Malpani, P.R., 2001. Removal of methyl orange and methylene blue dye from water using colloidal gas aphron—effect of processes parameters. Separation Science and Technology 36, 2997-3013.
- Bennett, A., Goodridge, F., 1970. Hydrodynamic and mass transfer studies in packed absorption columns. Transactions of the Institution of Chemical Engineers 48, 232-244.
- Bloom, F., Heindel, T.J., 1997. Mathematical modelling of the flotation deinking process. Mathematical and Computer Modelling 25, 13-58.
- Bloom, F., Heindel, T.J., 2003. Modeling flotation separation in a semi-batch process. Chemical Engineering Science 58, 353-365.
- Boonamnuayvitaya, V., Jutaporn, P., Sae-ung, S., Jarudilokkul, S., 2009. Removal of pyrene by colloidal gas aphrons of a biodegradable surfactant. Separation and Purification Technology, 68, 411-416.
- Borden, M.A., Longo, M.L., 2002. Dissolution behaviour of lipid monolayer-coated, air-filled microbubbles: Effect of lipid hydrophobic chain length. Langmuir 18, 9225-9233.
- Borden M.A., Sirsi, S.R., Kwan. J.J., 2012. Microbubble stability and dynamics, in: Encyclopedia of Surface and Colloid Science, Taylor and Francis, USA.
- Bredwell, M.D., Worden, R.M., 1998. Mass-Transfer Properties of Microbubbles. 1. Experimental Studies. Biotechnology Progress 14, 31-38.
- Briceño, M.I., Joseph, D.D., 2003. Self-lubricated transport of aqueous foams in horizontal conduits. International Journal of Multiphase Flow 29, 1817-1831.

- Burns, L.F., Rice, R.G., 1997. Circulation in bubble columns. AIChE Journal 43, 1390-1402.
- Burns, S.E., Yiacoumi, S., Tsouris, C., 1997. Microbubble generation for environmental and industrial separations. Separation and Purification Technology 11, 221-232.
- Buwa, V.V., Ranade, V.V., 2003. Mixing in bubble column reactors: Role of unsteady flow structures. The Canadian Journal of Chemical Engineering 81, 402-411.
- Caballero, M., Cela, R., Perez-Bustamente J.A., 1989. Studies on the use of colloidal gas aphrons in coflotation and solvent sublation processes. A comparison with the conventional technique. Separation Science and Technology 24, 629-40.
- Cabezón, L.M., Caballero, M., Pérez-Bustamante J.A., 1994. Coflotation separation for the determination of heavy metals in water using colloidal gas aphrons systems. Separation Science and Technology 29, 1491-500.
- Calvert, J.R., Nezhati, K., 1986. A rheological model for a liquid-gas foam. International Journal of Heat and Fluid Flow 7, 164-168.
- Caw, W.A., Wylie, R.G., 1961. Effect of Dissolved Air on the Viscosity of Water. Nature 189, 995-996.
- Cilliers, J.J., Bradshaw, D.J., 1996. The flotation of fine pyrite using colloidal gas aphrons. Minerals Engineering 9, 235-241.
- Ciriello, S., Barnett, S.M., Deluise, F.J., 1982. Removal of Heavy Metals from Aqueous Solutions Using Microgas Dispersions. Separation Science and Technology 17, 521-534.
- Chipfunhu, D., Zanin, M., Grano, S., 2011. The dependency of the critical contact angle for flotation on particle size – Modelling the limits of fine particle flotation. Minerals Engineering 24, 50-57.

- Chhabra, R.P., Richardson, J.F., 1999. Non-Newtonian Flow in the Process Industries: Fundamentals and Engineering Applications, 1st ed. Butterworth-Heinemann, Oxford, U.K.
- Chisti, M.Y., Moo-Young, M., 1988. Gas holdup in pneumatic reactors. The Chemical Engineering Journal 38, 149-152.
- Chu, L.B., Xing, X.H., Yu, A.F., Zhou, Y.N., Sun, X.L., Jurick, B., 2007. Enhanced ozonation of simulated dyestuff wastewater by microbubbles, Chemosphere 68, 854-1860.
- Chu, L.B., Xing, X.H., Yu, A.F., Sun, X.L., Jurcik, B., 2008a. Enhanced treatment of practical textile wastewater by microbubble ozonation. Process Safety and Environmental Protection 86, 389-393.
- Clift, R., Grace, J.R., Weber, M.E., 2005. Bubbles, Drops, and Particles, 1st ed. Dover Publications, New York.
- Collins, G.L., Jameson, G.J., 1977. Double-layer effects in the flotation of fine particles. Chemical Engineering Science 32, 239-246.
- Couto, H.J.B., Nunes, D.G., Neumann, R., França, S.C.A., 2009. Micro-bubble size distribution measurements by laser diffraction technique. Minerals Engineering 22, 330-335.
- Couto, H.J., Massarani, G., Biscaia, Jr. E.C., Sant'Anna, Jr. G.L., 2009. Remediation of sandy soils using surfactant solutions and foams. Journal of Hazardous Materials 164, 1325-1334.
- Cova, D.R., 1974. Axial mixing in the liquid phase in gas-sparged columns. Industrial and Engineering Chemistry Process Design and Development 13, 292-296.

- Cubaud, T., Ho, C.M., 2004. Transport of bubbles in square microchannels. Physics of Fluids (1994-present) 16, 4575-4585.
- Dai, Z., Dukhin, S., Fornasiero, D., Ralston, J., 1998. The Inertial Hydrodynamic Interaction of Particles and Rising Bubbles with Mobile Surfaces. Journal of Colloid and Interface Science 197, 275-292.
- Dai, Z., Fornasiero, D., Ralston, J., 1999. Particle–Bubble Attachment in Mineral Flotation. Journal of Colloid and Interface Science 217, 70-76.
- Dai, Z., Fornasiero, D., Ralston, J., 2000. Particle–bubble collision models — a review. Advances in Colloid and Interface Science 85, 231-256.
- Dargar, P., Macchi, A., 2006. Effect of surface-active agents on the phase holdups of three-phase fluidized beds. Chemical Engineering and Processing: Process Intensification 45, 764-772.
- D'arrigo, J.S., Imae, T., 1992. Physical characteristics of ultrastable lipid-coated microbubbles. Journal of Colloid and interface Science 149(2), 592-595.
- Deckwer, W.D., 1992. Bubble column reactors, 1st ed. John Wiley and Sons, New York.
- Deng, X., Xu, J., Wu, Y., Luo, D., 2011. Research on the technology of oil removal by dynamic state micro-bubbles flotation. Gongye Shuichuli 31, 89-102.
- Deshpande, N.S., Barigou, M., 2001. The flow of gas–liquid foams through pipe fittings. International Journal of Heat and Fluid Flow 22, 94-101.
- Desouky, S.E.M., EL-Emam, N.A., 1989. Program designs for pseudoplastic fluids. Oil and Gas Journal 87, 48-51.

- Devatine, A., Chiciuc, I., Poupot, C., Mietton-Peuchot, M., 2007. Micro-oxygenation of wine in presence of dissolved carbon dioxide. Chemical Engineering Science 62, 4579-4588.
- Dhanuka, V.R., Stepanek, J.B., 1978. Gas and liquid hold-up and pressure drop measurements in a three-phase fluidized bed, in: Davidson, J.F., Keairns, D.L. (Eds.), Fluidization: Proceedings of the Second Engineering Foundation Conference. Cambridge University Press, Trinity College, Cambridge, England, pp. 179-183.
- Dicker, S., Mleczko, M., Schmitz, G., Wrenn, S.P., 2013. Size distribution of microbubbles as a function of shell composition. Ultrasonics 53, 1363-1367.
- Dobby, G.S., Finch, J.A., 1987. Particle size dependence in flotation derived from a fundamental model of the capture process. International Journal of Mineral Processing 21, 241-260.
- Duineveld, P.C., 1995. The rise velocity and shape of bubbles in pure water at high Reynolds number. Journal of Fluid Mechanics 292, 325-332.
- Dukhin, S.S., Derjaguin, B.V., 1974. In: matievich, E., ed. Electrokinetic Phenomena, Surface and colloidal science 7, John Willey and Sons. New York.
- Dukhin, S.S., 1982. Role of inertial forces in flotation of small particles. Kolloid. Zh. 44, 431-441.
- Duncan, P.B., Needham, D., 2004. Test of the Epstein Plesset model for gas microparticle dissolution in aqueous media: Effect of surface tension and gas undersaturation in solution. Langmuir 20, 2567-2578.
- Duan, J., Fornasiero, D., Ralston, J., 2003. Calculation of the flotation rate constant of chalcopyrite particles in an ore. International Journal of Mineral Processing 72, 227-237.

- Elmore, F.E., 1905. A process for separating certain constituents of subdivided ores and like substances, and apparatus therefore. British Patent 13578.
- Edzwald, J.K., 1995. Principles and applications of dissolved air flotation. Water Science and Technology 31, 1-23.
- Edzwald, J.K., 2010. Dissolved air flotation and me. Water research 44, 2077-2106.
- Enzendorfer, C., Harris, R.A., Valkó, P., Economides, M.J., Fokker, P.A., Davies, D.D., 1995. Pipe viscometry of foams. Journal of Rheology (1978-present) 39, 345-358.
- Epstein, P.S., Plesset, M.S., 1950. On the stability of gas bubbles in liquid-gas solutions. The Journal of Chemical Physics 18(11), 1505-1509.
- Ernest, G., David, P.E., Rene, A.K., Charles, D.A., Jeffry, G.W., 2005. Mixed gas microbubble compositions. US Patents 6953569 B2.
- Evans, G.M., Jameson, G.J., Atkinson, B.W., 1992. Prediction of the bubble size generated by a plunging liquid jet bubble column. Chemical Engineering Science 47, 3265-3272.
- Fan, L.S., Tsuchiya, K., 1990. Bubble wake dynamics in liquids and liquid-solid suspensions, 1st ed. Butterworth-Heinemann.
- Fan, M., Tao, D., Honaker, R., Luo, Z., 2010. Nanobubble generation and its application in froth flotation (part I): nanobubble generation and its effects on properties of microbubble and millimeter scale bubble solutions. Mining Science and Technology (China) 20, 1-19.
- Farook, U., Zhang, H.B., Edirisinghe, M.J., Stride, E., Saffari, N., 2007. Preparation of microbubble suspensions by co-axial electrohydrodynamic atomization. Medical Engineering and Physics 29, 749-754.

- Feng, W., Singhal, N., Swift, S., 2009. Drainage mechanism of microbubble dispersion and factors influencing its stability. Journal of Colloid and Interface Science 337, 548-554.
- Finch, J.A., Dobby, G.S., 1990. Column flotation. Pergamon Press.
- Fichera, M.A., Chudacek, M.W., 1992. Batch cell flotation models - A review. Minerals Engineering, 5, 41-55.
- Fontaine, A.A., Deutsch, S., 1992. The influence of the type of gas on the reduction of skin friction drag by microbubble injection. Experiments in Fluids 13, 128-136.
- Fuda, E., Jauregi, P., 2006. An insight into the mechanism of protein separation by colloidal gas aphrons (CGA) generated from ionic surfactants. Journal of Chromatography B 843, 317-326.
- Fuerstenau, M.C., Jameson, G., Yoon R.H., 2007. Froth Flotation: A century of innovation. Society for mining, 1st ed. Metallurgy, and Exploration Inc., Colorado, USA.
- Fuerstenau, D.W., Wayman, C.H., 1958. Minerals beneficiation - Effect of chemical reagents on the motion of single air bubbles in water. AIME Transactions 211, 694-699.
- Fujiwara, A., 2006. Generating method of microbubbles by Venturi tube. Eco Industry 11, 27-30.
- Fujikawa, S., Zhang, R., Hayama, S., Peng, G., 2003. The control of micro-air-bubble generation by a rotational porous plate. International Journal of Multiphase Flow 29, 1221-1236.
- Frumkin, A., Levich, V.G., 1947. On surfactants and interfacial motion. Zhurnal Fizicheskoi Khimii 21, 1183-1120.
- Gañán-Calvo, A.M., Gordillo, J.M., 2001. Perfectly monodisperse microbubbling by capillary flow focusing. Physical Review Letters 87, 274501.

- Gaudin, A.M., Mular, A.L., O'Connor, R.F., 1960. Separation of Microorganisms by Flotation: II. Flotation of Spores of Bacillus subtilis var. niger. Applied Microbiology 8, 91-97.
- Garabedian, P.R., 1957. On steady-state bubbles generated by Taylor instability. Proceedings of the Royal Society of London. Series A, Mathematical and Physical Sciences 241, 423-431.
- Germick, R.J., Rehill, A.S., Narsimhan, G., 1994. Experimental investigation of static drainage of protein stabilized foams–Comparison with model. Journal of Food Engineering 23, 555-578.
- Gotoh, Y., Serizawa, A., Eguchi, T., Tanaka, H., Izumi, M., 2006. Oil separation from oil polluted soil by microbubble injection and separation mechanisms. Japanese Journal of Multiphase Flow 20, 39-49.
- Haapala, A., Honkanen, M., Liimatainen, H., Stoor, T., Niinimäki, J., 2010. Hydrodynamic drag and rise velocity of microbubbles in papermaking process waters. Chemical Engineering Journal 162, 956-964.
- Haberman, W.L., Morton, R.K., (1953). An experimental investigation of the drag and shape of air bubbles rising in various liquids. Taylor Model Basin Report TMB, 802.
- Hadjiev, D., Sabiri, N.E., Zanati, A., 2006. Mixing time in bioreactors under aerated conditions. Biochemical Engineering Journal 27, 323-330.
- Han, M., Dockko, S., 1998. Zeta potential measurement of bubbles in DAF process and its effect on the removal efficiency. KSCE Journal of Civil Engineering 2, 461-466.
- Hanotu, J., Bandulasena, H.C.H., Zimmerman, W.B., 2012. Microflotation performance for algal separation. Biotechnology and Bioengineering 109, 1663-1673.

- Harnby, N., Edwards, M.F.A., Nienow, W., 1996. Mixing in the Process Industries, 2nd Ed. Butterworth-Heinemann, London, England.
- Harper, J.F., 1972. The motion of bubbles and drops through liquids, in: Chia-Shun, Y. (Ed.), Advances in Applied Mechanics. Elsevier, pp. 59-129.
- Hasegawa, H., Nagasaka, Y., Kataoka, H., 2008. Electrical potential of microbubble generated by shear flow in pipe with slits. Fluid Dynamics Research 40, 554.
- Hashim, M.A., Gupta, B.S., 1998. The application of colloidal gas aphrons in the recovery of fine cellulose fibres from paper mill wastewater. Bioresource Technology 64, 199-204.
- Hikita, H., Kikukawa, H., 1974. Liquid-phase mixing in bubble columns: Effect of liquid properties. The Chemical Engineering Journal 8, 191-197.
- Himuro, S., 207. Physicochemical characteristics of microbubbles. Kagaku Koguku 71 165-169.
- Hinze, J.O., 1955. Fundamentals of the hydrodynamic mechanism of splitting in dispersion processes. AIChE Journal 1, 289-295.
- Hughes, R.R., Gilliland, E.R., 1952. The mechanics of drops. Chemical Engineering Progress 48, 497-504.
- Hunter, R.J., 1989. Foundations of Colloid Science, 2nd ed. Oxford University Press. Oxford.
- Indrawati, L., Narsimhan, G., 2008. Characterization of protein stabilized foam formed in a continuous shear mixing apparatus. Journal of Food Engineering 88, 456-465.
- Jacobi, W.M., Woodcock, K.E., Grove, C.S., 1956. Theoretical investigation of foam drainage. Industrial and Engineering Chemistry 48, 2046-2051.

- Jamialahmadi, M., Steinhagen, H.M., 1990. Study of Gas Hold-Up in Two and Three-Phase Bubble Columns, Proceedings CHEMECA Conf., Auckland, New Zealand, 1188-1195.
- Jamialahmadi, M., Müller-Steinhagen, H., 1992. Effect of alcohol, organic acid and potassium chloride concentration on bubble size, bubble rise velocity and gas hold-up in bubble columns. The Chemical Engineering Journal 50, 47-56.
- Jameson, G.J., Nam, S., Moo Young, M., 1977. Physical factors affecting recovery rates in flotation. Mineral Science Engineering 9, 103-118.
- Jarudilokkul, S., Rungphetcharat, K., Boonamnuayvitaya, V., 2004. Protein separation by colloidal gas aphrons using nonionic surfactant. Separation and Purification Technology 35, 23-29.
- Joshi, J.B., Sharma, M.M., 1979. A circulation cell model for bubble columns. Chemical Engineering Research and Design 57A, 244-251.
- Jauregi, P., Gilmour, S., Varley, J., 1997. Characterisation of colloidal gas aphrons for subsequent use for protein recovery. The Chemical Engineering Journal and the Biochemical Engineering Journal 65, 1-11.
- Jauregi P., Dermiki, M., 2010. Separation of value-added bioproducts by colloidal gas aphrons (CGA) flotation and applications in the recovery of value-added food products. In: Rizvi, S., (Eds.), Separation, extraction and concentration processes in the food, beverage and nutraceutical industries. Elsevier, pp. 284-313.
- Johnson, B.D., Wangersky, P. J., 1987. Microbubbles: Stabilization by monolayers of adsorbed particles. Journal of Geophysical Research 92, 14641-14647.

- Johnson, D., Hilal, N., Waters, K., Hadler, K., Cilliers, J., 2009. Measurements of interactions between particles and charged microbubbles using a combined micro- and macroscopic strategy. Langmuir 25, 4880-4885.
- Jung, J.W., Jeon, H.M., Pyo, J., Lim, J.H., Weon, B.M., Yoshiki, K., Ishikawa, T., Je, J.H., 2014. Four-dimensional visualization of rising microbubbles. Scientific Reports 4(5083), 1-4.
- Jyoti, K.K., Pandit, A.B., 2004. Ozone and cavitation for water disinfection. Biochemical Engineering Journal 18, 9-19.
- Karamah, E.F., Bismo, S., Annasari, L., Widodo, W.P., 2010. Mass transfer study on micro-bubbles ozonation in a bubble column. International Journal of Chemical Engineering Research 2, 243-252.
- Kasper, C., 1940. The theory of the potential and the technical practice of electrodeposition. Transactions of the Electrochemical Society 77, 353-384.
- Kaster, J.A., Michelsen, D.L., Velander, W.H., 1990. Increased oxygen transfer in a yeast fermentation using a microbubble dispersion. Applied Biochemistry and Biotechnology 24/25, 469-484.
- Katiyar, A., Sarkar, K., Jain, P., 2009. Effects of encapsulation elasticity on the stability of an encapsulated microbubble. Journal of Colloid and Interface Science 336, 519-525.
- Katiyar, A., Sarkar, K., 2010. Stability analysis of an encapsulated microbubble against gas diffusion. Journal of Colloid and Interface Science 343, 42-47.
- Kato, Y., Nakai, T., Sato, Y., Takahashi, N., Matsuoka, I., 1993. Removal of phosphorus in wastewater by flotation method. First International Conference on Processing Materials

for Properties. Proceedings of the 1st International Conference on Processing Materials for Properties; Honolulu, HI, USA, November 7-10.

- Kato, H., Miura, K., Yamaguchi, H., Miyanaga, M., 1998. Experimental study on microbubble ejection method for frictional drag reduction. Journal of Marine Science and Technology 3, 122-129.
- Kato, H. Iwashina, T. Miyanga, M., Yamaguchi, H., 1999. Effect of microbubbles on the structure of turbulence in a turbulent boundary layer, Journal of Marine Science and Technology 4, 155-162.
- Kawahara, A., Sadatomi, M., Matsuyama, F., Matsuura, H., Tominaga, M., Noguchi, M., 2009. Prediction of micro-bubble dissolution characteristics in water and seawater. Experimental Thermal and Fluid Science 33, 883-894.
- Kawase, Y., Moo-Young, M., 1989. Mixing time in bioreactors. Journal of Chemical Technology and Biotechnology 44, 63-75.
- Kawara, Z., Yanagisawa, H., Kunugi, T., Serizawa, A., 2007. Study on flow characteristics of micro-bubble two-phase flow, in: Palma, J.M.L.M., Lopes, A.S. (Eds.), Advances in Turbulence XI. Springer Berlin Heidelberg, pp. 334-336.
- Kelkar, B.G., Shah, Y.T., 1985. Gas holdup and backmixing in bubble column with polymer solutions. AIChE Journal 31, 700-702.
- Kelsall, G.H., Tang, S., Smith, A.L., Yurdakul, S., 1996. Measurement of rise and electrophoretic velocities of gas bubbles. Journal of the Chemical Society, Faraday Transactions 92, 3879-3885.
- Khan, S.A., Armstrong, R.C., 1986. Rheology of foams: I. Theory for dry foams. Journal of Non-Newtonian Fluid Mechanics 22, 1-22.

- Khoshdast, H., Sam, A., 2011. Flotation frothers: Review of their classifications, Properties and Preparation. The Open Mineral Processing Journal 4, 25-44.
- Khuntia, S., Majumder, S.K., Ghosh, P., 2012. Microbubble-aided water and wastewater purification: a review. Reviews in Chemical Engineering 28(4-6), 191-221.
- Kobayashi, F., Hayata, Y., Ikeura H, Tamaki, M., Muto, N., Osajima, Y., 2009. Inactivation of Escherichia coliby CO_2 microbubbles at a lower pressure and near room temperature. Transactions of the American Society of Agricultural and Biological Engineers 52, 1621-1626.
- Kobayashi, F., Ikeura, H., Ohsato, S., Goto, T., Tamaki, M., 2011. Disinfection using ozone microbubbles to inactivate Fusarium oxysporum f. sp. melonisand Pectobacterium carotovorum subsp. Carotovorum. Crop Protection 30, 1514-1518.
- Kodama, Y., Kakugawa, A. Takahashi, T., Kawashima, H., 2000. Experimental study on microbubbles and their applicability to ships for skin friction reduction. International Journal of Heat and Fluid Flow, 21, 582-588.
- Kodama, Y., 2007. Reduction in ship's resistance by microbubbles. Kagaku Koguku 71, 86-188.
- Koehler, S.A., Hilgenfeldt, S., Stone, H.A., 2000. A generalized view of foam drainage: Experiment and theory. Langmuir 16, 6327-6341.
- Kommalapati, R.R., Valsaraj, K.T., Constant. W.D., Roy, D., 1998. Soilflushing using colloidal gas aphron suspensions generated from a plant-based surfactant. Journal of Hazardous Materials 60, 73-87.
- Koichi, T., Yasuyuki, S., 2007. Separation of fine particles suspended in water using microbubble flotation. Japanese Journal of Multiphase Flow 21, 77-83.

- Kramers, H., Alberda, G., 1953. Frequency response analysis of continuous flow systems. Chemical Engineering Science 2, 173-181.
- Krasowska, M., Malysa, K., 2007. Kinetics of bubble collision and attachment to hydrophobic solids: I. Effect of surface roughness. International Journal of Mineral Processing 81, 205-216.
- Kraynik, A.M., Hansen, M.G., 1987. Foam rheology: a model of viscous phenomena. Journal of Rheology (1978-present) 31, 175-205.
- Kukizaki, M., Nakashima, T., Song, J., Kohama, Y., 2004. Monodispersed nano-bubbles generated from porous glass membrane and bubble size control. Kagaku Kogaku Ronbunshu 30, 654-660.
- Kulkarni, A.A., Joshi, J.B., 2005. Bubble formation and bubble rise velocity in gas liquid systems: a review. Industrial and Engineering Chemistry Research 44, 5873-5931.
- Kumar, S.B., Devanathan, N., Moslemian, D., Dudukovic, M.P., 1994. Effect of scale on liquid in bubble columns, Chemical Engineering Science 49, 5637-5652.
- Kurup, N., Naik, P., 2010. Microbubbles: A novel delivery system. Asian Journal of Pharmaceutical Research and Health Care 2, 228-234.
- Kwan, J., Borden, M., 2010. Microbubble dissolution in a multigas environment. Langmuir 26(9), 6542-6548.
- Larmignat, S., Vanderpool, D., Lai, H.K., Pilon, L., 2008. Rheology of colloidal gas aphrons (microfoams). Colloids and Surfaces A: Physicochemical and Engineering Aspects 322, 199-210.
- Lazaridis, N.K., Matis, K.A., Stalidis, G.A., Mavros. P., 1992. Dissolved air flotation of metal ions. Separation Science and Technology 27, 1743-1758.

- Laskowski, J.S., Cho. Y.S., Ding, K., 2003. Effect of frothers on bubble size and foam stability in potash ore flotation systems. The Canadian Journal of Chemical Engineering 81, 63-69.
- Lee J.E., Lee, J.K., 2002. Effect of microbubbles and particle size on the particle collection in the column flotation. Korean Journal of Chemical Engineering 19(4), 703-710.
- Lee, S., Sutomo, W., Liu, C., Loth, E., 2005. Micro-fabricated electrolytic micro-bubblers. International Journal of Multiphase Flow 31, 706-722.
- Lehrer, I.H., 1976. A rational terminal velocity equation for bubbles and drops at intermediate and high Reynolds numbers. Journal of Chemical Engineering of Japan 9, 237-240.
- Leung, A.H.S., 1988. Microbubble flotation process for the separation of bitumen from an oil sands slurry. US Patent 4783268.
- Levich, V.G., 1962. Physicochemical hydrodynamics. 2nd ed. Prentice-Hall, Englewood Cliffs, New Jersey.
- Liang, N., Hilal, N., Langston, P., Starov, V., 2007. Interaction forces between colloidal particles in liquid: Theory and experiment. Advances in Colloid and Interface Science 134-135, 151-166.
- Li, D., Fitzpatrick, J.A., Slattery, J.C., 1990. Rate of collection of particles by flotation. Industrial and Engineering Chemistry Research 29, 955-967.
- Liu, Y., Miyoshi, H., Nakamura, M., 2006. Encapsulated ultrasound microbubbles: Therapeutic application in drug/gene delivery. Journal of Controlled Release 114, 89-99.

- Liu S., Wang Q., Ma, H., Huang, P., Li, J., Kikuchi, T., 2010. Effect of micro-bubbles on coagulation flotation process of dyeing wastewater. Separation and Purification Technology 71, 337–346.
- Llewellin, E.W., Mader, H.M., Wilson, S.D.R., 2002. The rheology of a bubbly liquid. Proceedings of the Royal Society A 458, 987-1016.
- Lochiel, A.C., Calderbank, P.H., 1964. Mass transfer in the continuous phase around axisymmetric bodies of revolution. Chemical Engineering Science. 19, 471-484.
- López, A.B., Gómez-Díaz, D., La Rubia, M.D., Navaza, J.M., 2013. Effect of carbon dioxide chemical absorption on bubble diameter and interfacial area. Chemical Engineering and Technology 36, 1968-1974.
- Lyklema, J., 2000. Fundamentals of interface and colloid science: Solid-Liquid Interfaces. Elsevier Science.
- Madavan, N.K., Deutsch, S., Merkle, C.L., 1985. Measurements of local skin friction in a microbubble modified turbulent boundary layer. Journal of Fluid Mechanics 156, 237-256.
- Madavan, N.K., Deutsch, S., Merkle, C.L., 1984. Reduction of turbulent skin friction by microbubbles. Physics of Fluids (1958-1988) 27, 356-363.
- Maeda, Y., Hosokawa, S., Baba, Y., Tomiyama, A., Ito, Y., 2015. Generation mechanism of micro-bubbles in a pressurized dissolution method. Experimental Thermal and Fluid Science 60, 201-207.
- Majumder, S.K., Kundu, G., Mukherjee, D., 2005. Mixing mechanism in a modified co-current downflow bubble column. Chemical Engineering Journal 112, 45-55.

- Majumder, S.K., Kundu, G., Mukherjee, D., 2006. Bubble size distribution and gas–liquid interfacial area in a modified downflow bubble column. Chemical Engineering Journal 122, 1-10.
- Majumder, S.K., Kundu, G., Mukherjee, D., 2007. Pressure drop and bubble–liquid interfacial shear stress in a modified gas non-Newtonian liquid downflow bubble column. Chemical Engineering Science 62, 2482-2490.
- Makuta,T., Takemura, F., Hibra, E., Matsuomoto, Shoji, Y.M., 2004. Process of uniform microbubble formation in an ultrasound field. Nihon Kikai Gakki Ronbunsho B 70, 2758-2767.
- Makuta, T., Takemura, F., Hihara, E., Matsumoto, Y., Shoji, M., 2006. Generation of micro gas bubbles of uniform diameter in an ultrasonic field. Journal of Fluid Mechanics 548, 113-131.
- Marchese, M.M., Uribe-Salas, A., Finch, J.A., 1992. Measurement of gas holdup in a three-phase concurrent downflow column. Chemical Engineering Science 47, 3475-3482.
- Marks, C.H., 1973. Measurements of the Terminal Velocity of Bubbles Rising in a Chain. Journal of Fluids Engineering 95, 17-22.
- Margaritis, A., te Bokkel, D.W., Karamanev, D.G., 1999. Bubble rise velocities and drag coefficients in non-Newtonian polysaccharide solutions. Biotechnology and Bioengineering 64, 257-266.
- Matis, K.A., 1995. Flotation science and engineering. ed., Marcel Dekker, Inc., New York.
- Matis, K.A., Mavros, P., 1991. Foam/froth flotation: Part II. Removal of particulate matter. Separation and Purification Method 20, 163.

- Matis, K.A., Mavros, P., 1991. Recovery of metals by ion flotation from dilute aqueous solutions. Separation and Purification Reviews 20, 1-48.
- Mavros, P., Lazaridis, N.K., Matis, K.A., 1989. A study and modelling of liquid-phase mixing in a flotation column. International Journal of Mineral Processing 26, 1-16.
- Mavros P., 1993. Mixing in flotation columns. Part 1: axial dispersion modelling. Minerals Engineering 6(5) 465-478.
- Mavros, P., Daniilidou, A.C., Verbeke, A., 1996. Mixing in flotation columns. IV: Effect of internal column structure on liquid-phase mixing. Minerals Engineering 9(8), 855-867.
- Maxwell, J.C., 1892. A Treatise on Electricity and Magnetism, 3rd ed. Oxford University Press, London.
- Mendelson, H.D., 1967. The prediction of bubble terminal velocities from wave theory. AIChE Journal 13, 250-253.
- Melo, F., Laskowski, J.S., 2006. Fundamental properties of flotation frothers and their effect on flotation. Minerals Engineering 19, 766-773.
- Michelsen, D.L., Smith, J.W., Suggs, J.A., 1988. Use of colloidal gas aphrons for in-situ biodegradation of contaminated water. In: The 14th Annual Research Symposium, Cincinnati, OH, May 9-11, 203-217.
- Miettinen, T., Ralston, J, Fornasiero, D., 2010. The limits of fine particle flotation. Minerals Engineering 23, 420-437.
- Mohammadi, M., Sharp K.V., 2013. Experimental techniques for bubble dynamics analysis in microchannels: A review. Journal of Fluids Engineering 135, 1-10.
- Molaei, A., Waters, K.E., 2015. Aphron applications—A review of recent and current research. Advances in Colloid and Interface Science 216, 36-54.

- Moraveji, M.K., Pasand, M.M., Davarnejad, R., Chisti, Y., 2012. Effects of surfactants on hydrodynamics and mass transfer in a split-cylinder airlift reactor. The Canadian Journal of Chemical Engineering 90, 93-99.
- Moruzzi, R.B., Reali, M.A.P., 2010. Characterization of micro-bubble size distribution and flow configuration in DAF contact zone by a non-intrusive image analysis system and tracer tests. Water Science and Technology 61(1), 253-262.
- Moriguchi, Y., Kato, H., 2002. Influence of microbubble diameter and distribution on frictional resistance reduction. Journal of Marine Science and Technology 7, 79-85.
- Moshkelani, M., Amiri, M.C., 2008. Electrical conductivity as a novel technique for characterization of colloidal gas aphrons (CGA). Colloids and Surfaces A: Physicochemical and Engineering Aspects 317, 262-269.
- Myers, D., 1991. Surfaces, Interfaces, and Colloids: Principles and Applications 2nd ed. John Wiley and Sons, Inc., New York.
- Nakano, Y., Nishijima, W., Okata, M., Fukagawa, K., 2005. Microbubble-based groundwater treatment. Groundwater treatment technology with use of activated carbon-based solvent regeneration and ozone. Environmental Solution Technology 4, 11-16.
- Nakatake, Y., Watanabe, T., Eguchi, T., 2007. Combustion improvement for diesel engines with ejector-type micro-bubble mixed fuel (Thermal Engineering). Transactions of the Japan Society of Mechanical Engineers. B 73, 2368-2374.
- Noble, M., Brown, A., Jauregi, P., Kaul, A., Varley, J., 1998. Protein recovery using gas–liquid dispersions. Journal of Chromatography B: Biomedical Sciences and Applications 711, 31-43.

- Nguyen, A.V., 2007. Flotation, in: Wilson, I.D., (Eds.), Encyclopedia of Separation Science. Academic Press, Oxford, pp. 1-27.
- Oels, U., Lücke, J., Buhholz, R., Schügerl, K., 1978. Influence of gas distributors type and composition of liquid on the behavior of bubble column reactor. German chemical engineering 1, 115-129.
- Ohnari, H., 2006. All about microbubbles. Nihin Jitsugyo Shuppanasha Co.
- Ohnari, H., 2007. Current issues in microbubble technology. Kagaku Koguku 71 154-159.
- Okada, K., Akagn, Y., 1987. Method and apparatus to measure the zeta potential of bubbles. Journal Chemical Engineering of Japan 20(1), 11-15.
- Oliveira, C., Rubio, J., 2011. Zeta potential of single and polymer-coated microbubbles using an adapted microelectrophoresis technique. International Journal of Mineral Processing 98, 118-123.
- Onoe, K., Matsumoto, M., Akiya, T., 2002. Reactive crystallization of calcium carbonate using CO_2 micro-bubbles. Bulletin of the Society of Sea Water Science, Japan 56, 357-361.
- Pallapothu, S.K., Al Taweel, A.M., 2012. Effect of contaminants on the gas holdup and mixing in internal airlift reactors equipped with microbubble generator. International Journal of Chemical Engineering 2012, 15.
- Parmar, R., Majumder, S.K., 2013. Microbubble generation and microbubble-aided transport process intensification—A state-of-the-art report. Chemical Engineering and Processing: Process Intensification 64, 79-97.
- Parkinson, L., Ralston, J., 2010. The interaction between a very small rising bubble and a hydrophilic titania surface. The Journal of Physical Chemistry C 114, 2273-2281.

- Parkinson, L., Sedev, R., Fornasiero, D., Ralston, J., 2008. The terminal rise velocity of 10–100 μm diameter bubbles in water. Journal of Colloid and Interface Science 322, 168-172.
- Peeble, F.N., Garberson, H.J., 1953. Studies on the motion of gas bubbles in liquids. Chemical Engineering Progress 49, 88-97.
- Phan, C.M., Nguyen, A.V. Miller, J.D., Evans, G.M. Jameson, G.J., 2003. Investigations of bubble–particle interactions. International Journal of Mineral Processing 72, 239-254.
- Pilhofer, T.H., Bach H, F., Mangartz K, H., 1978. Determination of Fluid Dynamic Parameters in Bubble Column Design, Chemical Reaction Engineering Houston. American Chemical Society, pp. 372-383.
- Pope, S.B., 2000. Turbulent Flows. Cambridge University Press.
- Prajapati, J.V., Agrawal, Y.K., 2012. Synthesis, characterization and application of microbubbles: a review. International Journal of Pharmaceutical Sciences and Research 3(6), 1532-1543.
- Pyke, B., Fornasiero, D., Ralston, J., 2003. Bubble particle heterocoagulation under turbulent conditions. Journal of Colloid and Interface Science 265, 141-151.
- Rahman, R.M. Ata, S., Jameson, G.J., 2012. The effect of flotation variables on the recovery of different particle size fractions in the froth and the pulp International Journal of Mineral Processing (106–109), 70-77.
- Rahman, A., Ahmad, K.D., Mahmoud, A., Maoming, F., 2014. Nano-microbubble flotation of fine and ultrafine chalcopyrite particles. International Journal of Mining Science and Technology 24, 559-566.

- Ralston, J., 1983. Thin films and froth flotation. Advances in Colloid and Interface Science 19, 1-26.
- Ralston, J., 1992. Chapter 6 - The influence of particle size and contact angle in flotation, in: Laskowski, J.S., Ralston, J. (Eds.), Developments in Mineral Processing. Elsevier, pp. 203-224.
- Ralston, J., Fornasiero, D., Hayes, R., 1999. Bubble–particle attachment and detachment in flotation. International Journal of Mineral Processing 56, 133-164.
- Ralston, J., Dukhin, S.S., Mishchuk, N.A., 2002. Wetting film stability and flotation kinetics. Advances in Colloid and Interface Science 95, 145-236.
- Raza, S.H., Marsden, S.S., 1967. The Streaming Potential and the Rheology of Foam. Society of Petroleum Engineers 7, 359-363.
- Reay, D., Ratcliff, G.A., 1973. Removal of fine particles from water by dispersed air flotation: Effects of bubble size and particle size on collection efficiency. The Canadian Journal of Chemical Engineering 51(2), 178-185
- Rice, R.G., Oliver, A.D., Newman, J.P., Wiles, R.J., 1974. Reduced dispersion using baffles in column flotation. Powder Technology 10, 201-210.
- Rice, R.G., Tupperainen, J.M.I., Hedge, R.M., 1981. Dispersion and hold-up in bubble columns—comparison of rigid and flexible spargers. The Canadian Journal of Chemical Engineering 59, 677-687.
- Rodrigue, D., De Kee, D., Fong, C.F.C.M, 1996. An experimental study of the effect of surfactants on the free rise velocity of gas bubbles. Journal of Non-Newtonian Fluid Mechanics 66, 213-232.

- Rosen, M.J., 1989. Surfactants and Interfacial Phenomena, 3rd ed. John Wiley and Sons Inc., Hoboken, New Jersey.
- Rousseau, R.W., 1987. Handbook of Separation Process Technology. 1st ed. John Wiley and Sons, New York.
- Roy, D., Valsaraj, K.T., Kottai, S.A., 1992. Separation of Organic Dyes from Wastewater by Using Colloidal Gas Aphrons. Separation Science and Technology 27, 573-588.
- Roy, D., Valsaraj, K.T., Constant, W.D., Darji, M., 1994. Removal of hazardous oily waste from a soil matrix using surfactants and colloidal gas aphron suspensions under different flow conditions. Journal of Hazardous Materials 38, 127-144.
- Roy, D., Kongara, S., Valsaraj, K.T., 1995. Application of surfactant solutions and colloidal gas aphron suspensions influshing naphthalene from a contaminated soil matrix. Journal of Hazardous Materials 42, 247-263.
- Rust, A.C., Manga, M., 2002. Effects of bubble deformation on the viscosity of dilute suspensions. Journal of Non-Newtonian Fluid Mechanics 104, 53-63.
- Ryskin, G., Leal, L.G., 1984. Numerical solution of free-boundary problems in fluid mechanics. Part 3. Bubble deformation in an axisymmetric straining flow. Journal of Fluid Mechanics 148, 37-43.
- Sadatomi, M., 2003. Microbubble producing apparatus. Japanese Patent. JP.2003-30549.A.
- Sadatomi, M., Kawahara, A., 2008. Fluids mixer and fluids mixing method. Japanese Patent, JP. 2008-173631.

- Sajjadi, B., Moraveji, M.K., Davarnejad, R., 2010. Investigation of surfactant effect on the operational characteristics of a packed bed internal loop airlift reactor. World Applied Sciences Journal 11, 1004-1014.
- Scheid, C.M., Puget, F.P., Halasz, M.R.T., Massarani, G., 1999. Fluid dynamics of bubbles in liquid. Brazilian Journal of Chemical Engineering 16, 351-358.
- Schubert, H., Bischofberger, C., 1978. On the hydrodynamics of flotation machines. International Journal of Mineral Processing 5(2), 131-142.
- Schubert, H., 1999. On the turbulence-controlled microprocesses in flotation machines. International Journal of Mineral Processing 56, 257-276.
- Schubert. H., 2008. On the optimization of hydrodynamics in fine particle flotation. Minerals Engineering 21, 930–936.
- Schügerl, K., Lücke, J., Oels, U., 1977. Bubble column bioreactors, Advances in Biochemical Engineering, Volume 7. Springer Berlin Heidelberg, pp. 1-84.
- Schulze, H.J., 1989. Hydrodynamics of bubble-mineral particle collisions. Mineral Processing and Extractive Metallurgy Review 5, 43-76.
- Schulze, H.J., 2003. Flotation as a heterocoagulation process: possibilities of calculating the probability of flotation, in: Dobias, B. (Ed.), Surfactant Science Series (Coagulation and Flocculation). Marcel Dekker, New York, pp. 321–354.
- Sebba, F. 1962. Ion Flotation, 1st ed. Elsevier Publishing Company, New York.
- Sebba, F., 1971. Microfoams—an unexploited colloid system. Journal of Colloid and Interface Science 35, 643-646.
- Sebba, F., 1985. An improved generator for micron-sized bubbles. Chemistry and Industry 4, 91-92.

- Sebba, F., 1985. Separations using aphrons. Separation and Purification Reviews 14, 127-148.
- Sebba, F., 1987. Foams and biliquid foams, aphrons, 1st ed. John Wiley & Sons New York.
- Serizawa, A., Inui, T., Yahiro, T., Kawara, Z., 2003. Laminarization of microbubble containing milky bubbly flow in a pipe. European-Japanese Two-Phase Flow Group Meeting Certosa di Pontignano, 21-27 September.
- Serizawa, A., Inui, T., Eguchi, T., 2005. Flow characteristics and pseudolaminarization of vertically upward air-water milky bubbly flow with microbubble in a pipe. Japanese Journal of Multiphase Flow 19, 335-343.
- Sevik, M., Park, S.H., 1973. The splitting of drops and bubbles by turbulent fluid flow. Journal of Fluids Engineering 95, 53-60.
- Shah, Y.T., 1979. Gas-liquid-solid reactor design, 2nd ed. McGraw-Hill Inc., New York, US.
- Shah, Y.T., Kelkar, B.G., Godbole, S.P., Deckwer, W.D., 1982. Design parameters estimations for bubble column reactors. AIChE Journal 28, 353-379.
- Shams, M.M., Dong, M., Mahinpey, N., 2014. Viscosity and rheological behavior of microbubbles in capillary tubes. AIChE Journal 60(7), 2660-2669.
- Shatat, M.M.E., Yanase, S., Takami, T., Hyakutake, T., 2009. Drag reduction effects of micro-bubbles in straight and helical pipes. Journal of Fluid Science and Technology 4, 156-167.
- Shen, M., Wheelock, T.D., 2000. Coal Agglomeration with Microbubbles. Coal Preparation 21, 277-298.

- Shen, X., Ceccio, S., Perlin, M., 2006. Influence of bubble size on micro-bubble drag reduction. Experiments in Fluids 41, 415-424.
- Shen, Y., Longo, M.L., Powell, R.L., 2008. Stability and rheological behavior of concentrated monodisperse food emulsifier coated microbubble suspensions. Journal of Colloid and Interface Science 327, 204-210.
- Shibata, E., Saito, S., Nakamura, T., 2008. Froth Separation of Ferrihydrite Slurry Using Microbubbles with Ultrasonic Irradiation. Materials Transactions 49, 1681-1687.
- Shibata, T., Ozaki, A., Takana, H., Nishiyama, H., 2011. Water treatment characteristics using activated air microbubble jet with photochemical reaction. Journal of Fluid Science and Technology 6, 242-251.
- Singhal, S., Moser, C.C., Wheatley, M.A., 1993. Surfactant-stabilized microbubbles as ultrasound contrast agents: stability study of Span 60 and Tween 80 mixtures using a Langmuir trough. Langmuir 9 (9), 2426-2429.
- Sirsi, S., Borden M., 2009. Microbubble Compositions, Properties and Biomedical Applications. Bubble Science, Engineering and Technology 1(1-2), 3-17.
- Soetanto, K., Chan, M., Okujima, M., 1997. Change in size and number of sodium laurate microbubbles with time in saline at different air concentrations. Japanese Journal of Applied Physics 36, 3238-3241.
- Solari, J.A., Gochin, R.J., 1992. Chapter 13 - Fundamental aspects of microbubble flotation processes, in: Laskowski, J.S., Ralston, J. (Eds.), Developments in Mineral Processing. Elsevier, pp. 395-418.
- Somasundaran. P., Lin, I.J., 1973. Method for Evaluating Flotation Kinetics Parameter. Society of Mining Engineers, AIME 254, 1-4.

- Spigno, G., Dermiki, M., Pastori, C., Casanova, F., Jauregi, P., 2010. Recovery of gallic acid with colloidal gas aphrons generated from a cationic surfactant. Separation and Purification Technology 71, 56-62.
- Stewart, C.W., 1969. Energy dissipation by pulsating air bubbles in a viscoelastic medium. Journal of Polymer Science Part A-2: Polymer Physics 7, 143-151.
- Stokes, G.G., 1851. On the effect of the internal friction of fluids on the motion of pendulums. Transactions of the Cambridge Philosophical Society 9, 8-106.
- Stojanović, Z., Marković, S., Uskoković, D., 2012. Determination of Particle Size Distributions by Laser Diffraction. Technics–New Materials 67, 11-20.
- Subramaniam, M.B., Blakebrough, N., Hashim, M.A., 1990. Clarification of suspensions by colloidal gas aphrons. Journal of Chemical Technology and Biotechnology 48, 41-60.
- Sutherland, K.L., 1948. Physical Chemistry of Flotation. XI. Kinetics of the Flotation Process. The Journal of Physical Chemistry 52(2), 394–425.
- Sven-Nilsson, I., 1935. Effect of contact time between mineral and air bubbles on flotation. Kolloid-Z 69, 230–232
- Szeri, A. Shahs, Y.T., Madgavkar, A.1976. Axial dispersion in two phase co-current flow with fast and instantaneous reactions. Chemical Engineering Science 31(3), 225-233.
- Takahashi, K., Weng, J.G., Tien, C.-L., 1999. Marangoni effect in microbubble systems. Microscale Thermophysical Engineering 3, 169-182.
- Takahashi, M., 2005. ζ Potential of microbubbles in aqueous solutions: Electrical properties of the gas water interface. The Journal of Physical Chemistry B 109, 21858-21864.

- Tantra, R., Schulze, P., Quincey, P., 2010. Effect of nanoparticle concentration on zeta-potential measurement results and reproducibility. Particuology 8, 279-285.
- Tao, D., 2005. Role of Bubble Size in Flotation of Coarse and Fine Particles—A Review. Separation Science and Technology 39(4), 741-760.
- Tasaki, T., Wada, T., Fujimoto, K., Kai, S., Ohe, K., Oshima, T., Baba, Y., Kukizaki, M., 2009. Degradation of methyl orange using short-wavelength UV irradiation with oxygen microbubbles, Journal of Hazardous Materials 162, 1103-1110.
- Thoma, G.J., Bowen, M.L., Hollensworth, D., 1999. Dissolved air precipitation/solvent sublation for oil-field produced water treatment. Separation and Purification Technology 16, 101-107.
- Trahar, W.J., Warren, L.J., 1976. The flotability of very fine particles — A review. International Journal of Mineral Processing 3, 103-131.
- Tsai, J., Chen, C., 2011. Boundary layer mixture model for a microbubble drag reduction technique, International Scholarly Research Network ISRN Mechanical Engineering 2011, 1-9.
- Tseng, H., Pilon, L., Warrier, G.R., 2006. Rheology and convective heat transfer of colloidal gas aphrons in horizontal minichannels. International Journal of Heat and Fluid Flow 27, 298-310.
- Tsuge, H., Hibino, S., 1972. The Motion of Gas Bubbles Generating from a Single Orifice Submerged in a Liquid. Faculty of Engineering, Keio University.
- Tsuge, H., Ogawa, T., Ohmasa, R., 2008. Microbubble formation by electrolysis using a new mixing equipment with low frequency vibratory fins. Journal of chemical engineering of japan 41, 557-561.

- Tsuge, H., 2010. Fundamentals of Microbubbles and Nanobubbles. Bulletin of the Society of Sea Water Science, Japan 64, 4-10.
- Tsuge, H., 2014. Micro and nanobubbles. Fundamentals and applications, 1st ed. CRC press, Taylor and Francis group, U.S.
- Turner, J.C.R., 1976. Two-phase conductivity: The electrical conductance of liquid-fluidized beds of spheres. Chemical Engineering Science 31, 487-492.
- Tuteja, R.K., Spottiswood, D.J., Misra, V.N., 1994. Mathematical models of the column flotation process a review. Minerals Engineering 7, 1459-1472.
- Tzounakos, A., Karamanev, D.G., Margaritis, A., Bergougnou, M.A., 2004. Effect of the surfactant concentration on the rise of gas bubbles in power-law non-Newtonian liquids. Industrial and Engineering Chemistry Research 43, 5790-5795.
- Uematsu, H., 2006. Characteristics and applications development of OHR microbubble technology. Shigen Kankyo Taisaku 42, 100-103.
- Valsaraj, K.T., Lu, X.Y., Thibodeaux, L.J., 1991. Continuous countercurrent solvent sublation for the removal of hydrophobic organics from water. Water Research 25, 1061-1072.
- Vazquez, A., Sanchez, R.M., Salinas-Rodríguez, E., Soria, A., Manasseh, R., 2005. A look at three measurement techniques for bubble size determination. Experimental Thermal and Fluid Science 30, 49-57.
- Verrelli, D.I., Koh, P.T.L., Nguyen, A.V., 2011. Particle–bubble interaction and attachment in flotation. Chemical Engineering Science 66(23), 5910-5921.
- Voncken, R.M., Holmes, D.B., Hartog, H.W.D., 1964. Fluid flow in turbine-stirred, baffled tanks—III: Dispersion during circulation. Chemical Engineering Science 19, 209-213.

- Walker, A.B., Tsouris, C., DePaoli, D.W., Thomas Klasson, K., 2001. Ozonation of Soluble Organics in Aqueous Solutions Using Microbubbles. Ozone: Science and Engineering 23, 77-87.
- Wan, J., Veerapaneni, S., Gadelle, F., Tokunag, T.K., 2001. Generation of stable microbubbles and their transport through porous media. Water Resources Research, 37(5) 1173-1183.
- Wang, W., Moser, C.C., Wheatley M.A., 1996. Trough study of surfactant mixtures used in the production of a new ultrasound contrast agent consisting of stabilized microbubbles. The Journal of Physical Chemistry 100, 13815-13821.
- Wang, Z., Narsimhan, G., 2004. Evolution of liquid holdup profile in a standing protein stabilized foam. Journal of Colloid and Interface Science 280, 224-233.
- Wang, L.K., 2006. Adsorptive bubble separation and dispersed air flotation, in: Wang, L.K., Hung, Y., Shammas, N.K. (Eds.), Hand book of Environmental Engineering, Volume 4: Advanced Physicochemical Treatment Processes. The Humana Press Inc., Totowa, New Jersey, pp. 81-122.
- Waters, K.E., Hadler, K., Cilliers, J.J., 2008. The flotation of fine particles using charged microbubbles. Minerals Engineering 21, 918-923.
- Weber, M.E., Paddock, D., 1983. Interceptional and gravitational collision efficiencies for single collectors at intermediate Reynolds numbers. Journal of Colloid and Interface Science 94, 328-335.
- Weber, J., Agblevor, F.A., 2005. Microbubble fermentation of Trichoderma reesei for cellulase production. Process Biochemistry 40, 669-676.

- Wierserna, P.H., Loeb, A.L., Overbeek, J.T.G., 1966. Calculation of the electrophoretic mobility of a spherical colloid particle. Journal of Colloid Interface Science 22, 78-98.
- Wills B.A., Munn, T.N., 2005. Froth flotation, in: Wills B.A., Munn, T.N. (Eds.), Wills' Mineral Processing Technology, Butterworth-Heinemann, Oxford, pp 267-352.
- Wilkinson, P.M., Haringa, H., Stokman, F.P.A., Van Dierendonck, L.L., 1993. Liquid mixing in a bubble column under pressure. Chemical Engineering Science 48, 1785-1791.
- Woo, S.W., 1971. Simultaneous free and forced convection around submerged cylinders and spheres. PhD. Thesis, McMaster University, Hamilton, Ontario.
- Wu, H., Patterson, G.K., 1989. Laser-Doppler measurements of turbulent-flow parameters in a stirred mixer. Chemical Engineering Science 44, 2207-2221.
- Wu, S.J., Ouyang, K., Shiah, S.W., 2008. Robust design of microbubble drag reduction in a channel flow using the Taguchi method. Ocean Engineering 35, 856-863.
- Xiaohui, D., Jingyu, X., Yingxiang, Donghong, W. L., 2011, Research on the Technology of oil removed by dynamic state micro bubble floatation, China national knowledge infrastructure. Industrial Water Treatment 04, 028.
- Xu, Q., Nakajima, M., Ichikawa, S., Nakamura, N., Shiina, T., 2008. A comparative study of microbubble generation by mechanical agitation and sonication. Innovative Food Science and Emerging Technologies 9, 489-494.
- Yamaguchi, H., Kobayashi, Y. Matsubara, D. 2001a. Behaviour of dispersed micro-bubbles in a rotating pipe section. Proceedings of the Institution of Mechanical Engineers, Part C. Journal of Mechanical Engineering Science 215, 1223-1237.
- Yamaguchi, H., Matsubara, D., Shuchi, S., 2001b. Flow characteristics and microbubble behaviour in a rotating pipe section with an abrupt enlargement. Proceedings of the

Institution of Mechanical Engineers, Part C. Journal of Mechanical Engineering Science 215, 1447-1457.

- Yamasaki, K., Uda, K., Chuhjoh, K., 2009. Wastewater Treatment Equipment and Method of Wastewater Treatment. US Patent 7578942 B2.
- Yan, Y.L., Qu, C.T., Zhang, N.S., Yang, Z.G., Liu, L., 2005. A study on the kinetics of liquid drainage from colloidal gas aphrons (CGAs). Colloids and Surfaces A: Physicochemical and Engineering Aspects 259, 167-172.
- Yasuno, M., Sugiura, S., Iwamoto, S., Nakajima, M., Shono, A., Satoh, K., 2004. Monodispersed microbubble formation using microchannel technique. AIChE Journal 50, 3227-3233.
- Yasuhiro, M., Kato, H., 2002. Influence of microbubble diameter and size distribution on frictional resistance reduction, Journal of Marine Science and Technology 7, 79-85.
- Ye, Y., Khandrika, S.M., Miller, J.D., 1989. Induction-time measurements at a particle bed. International Journal of Mineral Processing 25, 221-240.
- Yi-jun, C., Lin-ping, S., Xin-hua, Y., 2009. Research on 730 series frother for copper sulfide ore separation by cyclonic-static microbubble flotation column. Procedia Earth and Planetary Science 1, 771-775.
- Yi-jun,C,. Xia-hui, G., Zi-long, M., Xiao-xia, Y., Xiao-dong, C., Xiu-pin, Z., 2009. Process mineralogy of nickel sulphide floatation by a cyclone-static micro-bubble floatation column, Mining science and technology 19, 784-787.
- Ying, K., Al-Mashhadani M.K.H., Hanotu, J.O., 2013. Gilmour, D.J., Zimmerman, W.B. Enhanced mass transfer in microbubble driven airlift bioreactor for microalgal culture. Engineering 5, 735-743.

- Yoon, R.-H., Yordan, J.L., 1986. Zeta-potential measurements on microbubbles generated using various surfactants. Journal of Colloid and Interface Science 113, 430-438.
- Yoon, R.-H., Yordan, J.L., 1991a. Induction time measurements for the quartz—amine flotation system. Journal of Colloid and Interface Science 141, 374-383.
- Yoon, R.H., Mankosa, M.J., Luttrel, G.H. Adel, G.T., 1991b. Full-scale testing of microbubble column flotation. Volume 1, Sudbury, Canada.'
- Yoon, R.-H., 2000. The role of hydrodynamic and surface forces in bubble–particle interaction. International Journal of Mineral Processing 58, 129-143.
- Yoshida, A., Takahashi, O., Ishii, Y. Sekimoto, Y. Kurata, Y., 2008. Water purification using adsorption characteristics of microbubbles. Japanese Journal of Applied Physics 47, 6574-6577.
- Zhang J.G., 1989. Factors affecting the kinetics of froth flotation. Ph.D Thesis, Department of Mining and Mineral Engineering, University of Leeds, United Kingdom.
- Zimmerman, W.B., Tesar, V., Butler, S., Bandulasena, H.C.H., 2008. Microbubble generation. Recent Patents on Engineering 2, 1-8.
- Zouboulis, A.I., Matis, K.A., 1987. Ion flotation in environmental technology. Chemosphere 6, 623-631.
- Zouboulis, A.I., Matis, K.A., 1995. Removal of cadmium from dilute solution by flotation. Water science and technology 31, 315-326.

Appendix-I

Calculation procedure for Typical Multiple Regression

[Equation (4.40)]

The regression equation is

$$C_m = c_1\left(\frac{Z}{d_{mb}}\right)^{b_1}\left(\frac{d_t}{d_{mb}}\right)^{b_2}(We_b)^{b_3}(\mathrm{Re})^{b_4} \quad \text{(A1)}$$

Taking logarithm on both side of Equation A1, one get

$$Log(C_m) = Log(c_1) + b_1 Log\left(\frac{Z}{d_{mn}}\right) + b_2 Log\left(\frac{d_t}{d_{mb}}\right) + b_3 Log(We) + b_4 Log(\mathrm{Re}) \quad \text{(A2)}$$

The equation A2 can be written as

$$Y = b_0 + b_1X_1 + b_2X_2 + b_3X_3 + b_4X_4 + e \quad \text{(A3)}$$

where $Y = Log(C_m)$, $X_1 = Log(Z/d_{mb})$, $X_2 = Log(d_t/d_{mb})$, $X_3 = Log(We)$, $X_4 = Log(Re)$ and e is the error term which has to be minimized to estimate the regression model as

$$\hat{Y} = b_0 + b_1X_1 + b_2X_2 + b_3X_3 + b_4X_4 \quad \text{(A4)}$$

where $\hat{Y}$ is the predicted value of Y.

The intercept b_0 and the coefficients b_1, b_2, b_3 and b_4 have been estimated by multiple regression analysis by "Data Analysis Tool" of software "Microsoft Excel".

The software gives output on the basis of the following calculation

The Equation A3 can be written as matrix form for n (here n=125) and k (here k = 4) variables as

$$\begin{bmatrix} Y_1 \\ . \\ . \\ Y_n \end{bmatrix} = \begin{bmatrix} 1 & X_{11} & . & X_{1p} \\ . & . & . & . \\ . & . & . & . \\ 1 & X_{n1} & . & X_{np} \end{bmatrix} \times \begin{bmatrix} b_1 \\ . \\ . \\ b_k \end{bmatrix} + \begin{bmatrix} e_1 \\ . \\ . \\ e_n \end{bmatrix} \quad \text{(A5)}$$

$\Longrightarrow$ **Y** = **X** × **B** + **e**

Regression statistics

		Explanation
Multiple R	0.993	R = square root of R^2
R Square	0.987	R^2 = Coefficient of determination
Adjusted R Square	0.986	Adjusted R^2 used if more than one X variable
Standard Error	0.163	This is the estimate of the st. dev. of the error *e*
Observations	125	Number of observations used in the regression (n)

Analysis of variance

	Degrees of freedom	Sum of Square	Mean Sum of Square	F-stat
Regression	4	241.926	60.481	2268.792
Residual	120	3.198	0.026	
Residual	124	245.125		

Regression Sum of Square = $B'X'Y - n\bar{Y}^2$

Total Sum of Square = $Y'Y - n\bar{Y}^2$

Residual Sum of square = Total sum of square – Regression Sum of Square

$$R^2 = \frac{\text{Regression sum of square}}{\text{Residual sum of square}}$$

$$F - stat = \frac{R^2/(k-1)}{(1-R^2)/(n-k)}$$

$$Adjusted\ R^2 = 1-(1-R^2)\left(\frac{n-1}{n-k}\right)$$

$$\text{Standard Error} = \sqrt{\frac{\text{Residual Sum of Square}}{n-k}}$$

$$Y' = [Y_1 \quad Y_2 \quad Yn]$$

$$B' = [B_1 \quad B_2 \quad B_k]$$

The F-stat gives the overall F-test of null hypothesis H_0: $b_i = 0$. The F-stat gives the associated Probability value. Since it is greater than 0.05 at 5% significance level we do not reject null hypothesis for the goodness of fit.

Appendix-II

Goodness of fit for the distribution Cited in Figure: 3.6

Data points: 331
Estimates: Maximum likelihood estimates
Accuracy of Fit: 3×10^{-3}
Level of significance: 0.005

Details of the tests

Beta: Min = 23, Maxi = 68.74

Chi Square		Kolmogorov-Smirnov		Anderson-Darling	
Total class	9	K-S Stat	7.17×10^{-2}	A-D Stat	1.44
Interval type	Equal probable	p-value	6.23×10^{-2}	p-value	0.19
Degree of freedom	8	Result	Accept	Result	Accept
Chi square	0.005				
p-value	7.97×10^{-3}				
result	Reject				

Erlang: Min = 23, m = 3, $\beta = 5.186$

Chi Square		Kolmogorov-Smirnov		Anderson-Darling	
Total class	9	K-S Stat	0.112	A-D Stat	4.09
Interval type	Equal probable	p-value	4.33×10^{-3}	p-value	7.89×10^{-3}
Degree of freedom	8	Result	Reject	Result	Reject
Chi square	15.5				
p-value	1.26×10^{-3}				
result	Reject				

Logistic: $\alpha = 38.22$, $\beta = 4.181$

Chi Square		Kolmogorov-Smirnov		Anderson-Darling	
Total class	9	K-S Stat	4.13×10^{-2}	A-D Stat	0.892
Interval type	Equal probable	p-value	0.607	p-value	0.419
Degree of freedom	8	Result	Accept	Result	Accept
Chi square	15.5				
p-value	0.226				
result	Accept				

Lognormal: Min = 23, $\mu = 2.588$, $\sigma = 0.649$

Chi Square		Kolmogorov-Smirnov		Anderson-Darling	
Total class	9	K-S Stat	0.138	A-D Stat	8.55
Interval type	Equal probable	p-value	5.69×10^{-6}	p-value	0
Degree of freedom	8	Result	Reject	Result	Reject
Chi square	15.5				
p-value	2.75×10^{-10}				
result	Reject				

Weibull: Min = 23, $\alpha = 2.13$, $\beta = 17.5$

Chi Square		Kolmogorov-Smirnov		Anderson-Darling	
Total class	9	K-S Stat	6.74×10^{-2}	A-D Stat	0.968
Interval type	Equal probable	p-value	9.48×10^{-2}	p-value	0.375
Degree of freedom	8	Result	Accept	Result	Accept
Chi square	15.5				
p-value	0.217				
result	Accept				

Rayleigh: Min = 23, $\sigma = 12.22$

Chi Square		Kolmogorov-Smirnov		Anderson-Darling	
Total class	9	K-S Stat	8.65×10^{-2}	A-D Stat	1.96
Interval type	Equal probable	p-value	1.32×10^{-2}	p-value	9.61×10^{-2}
Degree of freedom	8	Result	Reject	Result	Reject
Chi square	15.5				
p-value	1.76×10^{-3}				
result	Reject				

Inverse Weibull: Min = 23, $\alpha = 1.04$, $\beta = 0.109$

Chi Square		Kolmogorov-Smirnov		Anderson-Darling	
Total class	9	K-S Stat	0.213	A-D Stat	31.6
Interval type	Equal probable	p-value	1.14×10^{-13}	p-value	0
Degree of freedom	8	Result	Reject	Result	Reject
Chi square	15.5				
p-value	0				
result	Reject				

Chi Squared: Min = 23, nu = 14.29

Chi Square		Kolmogorov-Smirnov		Anderson-Darling	
Total class	9	K-S Stat	0.138	A-D Stat	18.5
Interval type	Equal probable	p-value	5.56×10^{-6}	p-value	0
Degree of freedom	8	Result	Reject	Result	Reject
Chi square	15.5				
p-value	1.16×10^{-11}				
result	Reject				

Inverse Gaussian: Min = 23, α = 23.61, β = 15.55

Chi Square		Kolmogorov-Smirnov		Anderson-Darling	
Total class	9	K-S Stat	0.212	A-D Stat	21
Interval type	Equal probable	p-value	2.89×10^{-12}	p-value	0
Degree of freedom	8	Result	Reject	Result	Reject
Chi square	15.5				
p-value	0				
result	Reject				

The following distribution have been used to fit the experimental data in this study. Also goodness of fit has been tested by Chi Square test, Kolmogorov Smirnov test and Anderson Darling test by STAT::FIT Software. The methods of calculation for the different tests are also discussed in this section.

Beta Distribution

The Beta distribution is a continuous distribution that has both upper and lower finite bounds. The Beta distribution can approach zero or infinity at either of its bounds, with p controlling the lower bound and q controlling the upper bound (Johnson et al., 1995). It is defined as

$$F(x)=\frac{1}{B(p,q)}\frac{(x-\min)^{p-1}(\max-x)^{q-1}}{(\max-\min)^{p+q-1}}$$

where, min = minimum value of x,

max = maximum value of x

p = lower shape parameter > 0

q = upper shape parameter > 0

B(p,q) Beta Function

Erlang Distribution

The Erlang distribution is a continuous distribution bounded on the lower side (Johnson et al., 1995). It is defined as

$$F(x)=\frac{(x-\min)^{m-1}}{\beta^{m}\Gamma(m)}\exp\left(-\frac{(x-\min)}{\beta}\right)$$

where, min = minimum x

m = shape factor = positive integer

β= scale factor > 0

Logistic Distribution

The Logistic distribution is an unbounded continuous distribution which is symmetrical about its mean (Johnson et al., 1995). It is defined as

$$F(x)=\frac{\exp\left(-\frac{(x-\alpha)}{\beta}\right)}{\beta\left[1+\exp\left(-\frac{(x-\alpha)}{\beta}\right)\right]^{2}}$$

where, α= shift parameter

β= scale parameter > 0

Lognormal Distribution

The Lognormal distribution is a continuous distribution bounded on the lower side. The lognormal distribution is defined as

$$F(x)=\frac{1}{(x-\theta)\sqrt{2\pi\hat{\sigma}^{2}}}\exp\left(-\frac{[\log(x-\theta)-\hat{\mu}]^{2}}{2\hat{\sigma}^{2}}\right)$$

where, θ = minimum x

$$\hat{\mu} = \frac{\sum_{i=1}^{n} \ln(x_i)}{n}$$

$$\hat{\sigma} = \sqrt{\frac{\sum_{i=1}^{n} (\ln x_i - \hat{\mu})}{n}}$$

F(x) is always 0 at minimum x, rising to a peak that depends on both $\hat{\mu}$ and $\hat{\sigma}$, then decreasing monotonically for increasing x. By definition, the natural logarithm of a lognormal random variable is a Normal random variable. The lognormal distribution can also be used to approximate the normal distribution, for small sigma, while maintaining its strictly positive values of x (Johnson et al., 1995).

Weibull Distribution

The Weibull distribution is a continuous distribution bounded on the lower side. It provides one of the limiting distributions for extreme values (Johnson et al., 1995). It is defined as

$$F(x) = \frac{\alpha}{\beta}\left(\frac{x-\theta}{\beta}\right)^{\alpha-1} \exp\left(-\left(\frac{[x-\theta]}{\beta}\right)^{\alpha}\right)$$

where, θ = minimum x

α = shape parameter > 0

β = scale parameter > 0

F(x) has three distinct regions. For α = 1, the weibull distribution is reduced to the exponential distribution, starting at a finite value at minimum x and decreasing monotonically thereafter. For α < 1, the Weibull distribution tends to infinity at minimum x and decreases monotonically for increasing x. for α > 1, the Weibull distribution is 0 at minimum x, peaks at a value that depends on both α and β, decreasing monotonically thereafter.

Rayleigh Distribution

The Rayleigh distribution is a continuous distribution bounded on the lower side (Shooman, 1990). It is defined as

$$F(x) = \frac{(x-\theta)}{\sigma^2}\exp\left(-\frac{(x-\theta)^2}{2\sigma^2}\right)$$

where, θ = minimum x

σ = scale parameter > 0

Inverse Weibull Distribution

The Inverse Weibull distribution is a continuous distribution with a bound on the lower side. It is uniquely zero at the minimum x, and always positively skewed. In general, the Inverse weibull distributions distribution fits bounded, but very peaked, data with a long positive tail (Calabria and Pulcini, 1990). It can be expressed mathematically as

$$F(x) = \alpha\beta\left(\frac{1}{\beta(x-\theta)}\right)^{\alpha+1}\exp\left(-\left(\frac{1}{\beta(x-\theta)}\right)^{\alpha}\right)$$

where, θ= minimum x

α = shape parameter > 0

β = mixture of shape and scale > 0

Chi Squared Distribution

The Chi Squared is a bounded continuous distribution bounded on the lower side (Johnson et al., 1995). It is defined as

$$F(x) = \frac{1}{2^{\upsilon/2}\Gamma(\upsilon/2)}\exp\left(-\frac{(x-\theta)}{2}\right)(x-\theta)^{(\upsilon/2)-1}$$

where, θ= minimum x

υ = shape parameter

Inverse Gaussian Distribution

The Inverse Gaussian distribution is a continuous distribution with a bound on the lower side. It is uniquely zero at the minimum x, distributions and always positively skewed. The Inverse Gaussian distribution is also known as the Wald distribution (Johnson et al., 1994). It is defined as

$$F(x)=\left(\frac{\alpha}{2\pi(x-\theta)^3}\right)^{1//2}\exp\left[-\frac{\alpha(x-\theta-\beta)^2}{2\beta^2(x-\theta)}\right]$$

where, θ = minimum x

α = shape parameter > 0

β = mixture of shape and scale > 0

The goodness of fit for distribution

To fit a distribution with the experimental data the parameters for each distribution are calculated by using either the moment equation or the maximum likelihood equation. Finally, the test for goodness of fit are calculated for each fitted distribution in order to ascertain the relative goodness of fit (Breinam, 1973; Law and Kelton, 1991; Banks and Carson, 1984; Stuart and Ord, 1991). The tests for goodness of fit are merely comparisons of the input data to the fitted distributions in a statistically significant manner. Each test makes the hypothesis that the fit is good and calculates a test statistic for comparison to a standard. There are different types of goodness of fit tests whereas the following three teat are more useful.

1. Chi Squared test
2. Kolmogorov Smirnov test
3. Anderson Darling test

If the choice of test is uncertain, even after consulting the descriptions, Kolmogorov Smirnov test is applicable over the widest range of data and fitted parameters.

While the test statistic for the Chi Squared test can be useful, the p value is more useful in determining the goodness of fit. The p value is defined as the probability that another sample will be as unusual as the current sample given that the fit is appropriate. A small p-value indicates that the current sample is highly unlikely, and therefore, the fit should be rejected. Conversely, a high p-value indicates that the sample is likely and would be repeated, and therefore, the fit should not be rejected. Thus, the higher the p value, the more likely that the fit is appropriate. When comparing two different fitted distributions, the distribution with the higher p value is likely to be the better fit regardless of the level of significance.

Chi Squared test

The Chi Squared test is a test of the goodness of fit of the fitted density (F(x)) to the experimental data appropriately separated into different classes. Then the Chi Squared statistic for this data is calculated according to the equation:

$$\chi^2 = \sum_{i=1}^{k} \frac{(n_i - np_i)}{np_i^2}$$

where χ^2 is the Chi Squared statistic, n is the total number of data points, n_i is the number of data points in the i^{th} continuous interval or i^{th} discrete class, k is the number of intervals or classes used, and pi is the expected probability of occurrence in the interval or class for the fitted distribution. The resulting test statistic is then compared to a standard value of Chi Squared with the appropriate number of degrees of freedom and level of significance. The number of degrees of freedom is always taken to be the net number of data bins (intervals, classes) used in the calculation minus 1; because this is the most conservative test, that is, the least likely to reject the fit in error (Law and Kelton, 1991; Brunk, 1960; Stuart and Ord, 1991)

Kolmogorov Smirnov test

The Kolmogorov Smirnov test (KS) is a statistical test of the goodness of fit of the fitted cumulative distribution to the experimental data. The KS test calculates the largest absolute difference between the cumulative distributions for the experimental data and the fitted distribution according to the equations:

$$D = Max\left(D^+, D^-\right)$$

$$D^+ = Max\left(\frac{i}{n} - F(x)\right), \quad \text{i} = 1,.....\text{n}$$

$$D^- = Max\left(F(x) - \frac{i-1}{n}\right), \quad \text{i} = 1,.....\text{n}$$

where *D* is the KS statistic, *x* is the value of the i^{th} point out of n total data points, and *F(x)* is the fitted cumulative distribution. The difference is determined separately for positive and negative discrepancies on a point by point basis. The resulting test statistic is then compared to a standard value of the Kolmogorov Smirnov statistic with the appropriate number of data points and level of significance (Law and Kelton, 1991; Brunk, 1960; Stuart and Ord, 1991). The goodness of fit

view also reports a REJECT or ACCEPT decision for each KS test based on the comparison between the calculated test statistic and the standard statistic for the given level of significance.

Anderson Darling test

The Anderson Darling test (AD) is a test of the goodness of fit of the fitted cumulative distribution to the experimental data, weighted heavily in the tails of the distributions. This test calculates the integral of the squared difference between the experimental data and the fitted distribution, with increased weighting for the tails of the distribution, by the equation:

$$W_n^2 = n\int_{-\infty}^{+\infty}\frac{[F_n(x)-F(x)]^2}{F(x)(1-F(x))}dF(x)$$

where W_n^2 is the AD statistic, n is the number of data points, $F(x)$ is the fitted cumulative distribution, and $F_n(x)$ is the cumulative distribution of the input data. This can be reduced to the more useful computational equation.

$$W_n^2 = -n - \frac{1}{n}\sum_{i=1}^{n}(2i-1)[\log\mu_i + \log(1-\mu_{n-i+1})]$$

where μ_i is the value of the fitted cumulative distribution, $F(x_i)$, for the i^{th} data point ((Law and Kelton, Anderson and Darling, 1994). The resulting test statistic is then compared to a standard value of the AD statistic with the appropriate number of data points and level of significance. The goodness of fit view also reports a REJECT or ACCEPT decision for each AD test based on the comparison between the calculated test statistic and the standard statistic for the given level of significance.

References

Banks, J., Carson, J. S., 1984. Discrete-Event System Simulation, Prentice-Hall.

Breiman, L., 1973. Statistics: With a View Toward Applications, Houghton Mifflin.

Brunk, H.D., 1960. An Introduction to Mathematical Statistics, Ginn & Co.

Calabria, R., Pulcini, G., 1990. On the maximum likelihood and least-squares estimation in the Inverse Weibull Distribution, Statistica Applicata, Vol. 2, 53.

Johnson N.L., Kotz, S., Balakrishnan, N., 1995. Continuous Univariate Distributions, Volume 2, John Wiley & Sons.

Law, A.M.W., Kelton, D., 1991. Simulation Modeling & Analysis, McGraw-Hill.

Shooman, M.L., 1990. Probabilistic Reliability: An Engineering Approach, Krieger Pub Co.

Stuart, A., Ord, J. K., 1991. Kendall's Advanced Theory of Statistics, Volume 2, Oxford University Press.